The Role of Astrocytes in Brain Metastasis

Emma Rosemary O'Brien
Jesus College,
University of Oxford
2014

Thesis submitted for the degree of Doctorate of Philosophy

First and foremost, a huge thanks goes to my supervisor, Niki Sibson. I thank you so much for all your support and encouragement. You've given me so much confidence in my abilities. Additional thanks goes to Daniel Anthony, I really appreciate all your advice and humour over the years. To the entirety of the Sibson lab, past and present, thank you for driving me crazy and keeping me sane. I couldn't have asked for a better lab. Sebastien Serres, thank you so much for all your help, advice and downright cheekiness over the last 4 and half years. Manuel, the most patient man in the world, you've been so helpful and so supportive. James, thank you for knowing everything. Except for how to tell a joke. John, thank you for mopping up my tears with Belgian buns. Stavritos banana, thank you for being as caring as you are bonkers. Kleo, thank you for always offering to help and more importantly for being around to gossip with! Sasha, may your life be filled with chicken fillet burgers. Claire B, thanks for being an oasis of calm and for all your help over the years. Alastair, for Matlab, Sporkle and catch. Aisling and Clare, thanks for putting off abandoning me ;) To Yvonne, for facilitating venting, Helen, Alex and Matt. I really appreciate all your help over the years. Thank you for being as hilarious as you are judgemental…Additionally, I'd like to thank everyone in the RRI for their help and friendship, especially Karla and Magda, without whom we'd all fall apart. Veerle, John B and Sean deserve a special mention for dealing with my panic stricken use of large machines.

I have so many wonderful friends that I'd like to thank for looking out for me. Danusia and Claire. I definitely could not have done this without having you two as a bedrock of silliness. Thank you so much for all your support and understanding over the years. I am so sorry for all those visits to Oxford that involved a trip into lab! Lindsay, thank you for always being at the end of the phone, it will be so nice when we can do nothing together again! Thank you to Dominique, Ellie, Emily, Joan and Lucy, for all the years of giggling and support.

To all my friends in Oxford that have kept me jolly: Daniel, Monica, Mark, Selva and Stavritos Banana; we'll always have Dresden. Sarah, for so so much more than just the font choice. Tom, Ed Sulston, Tim, Dave, Jamie and Dan, thanks for supporting me via the medium of the pub, drawings, tea, filled pasta and more tea. Ed Owen, I couldn't have asked for a better housemate and friend, thank you

for listening to the inane details of my day and being there for me throughout. Special thanks goes to Alice and Steph. We may now be on 3 different continents but good friends are like sequined jackets; just because you can't always see them, doesn't mean they're not there. Thank you Arnaud, for asking if it's possible.

A final thanks goes to my family. To my Uncle Johnny, for always being so enthusiastic about what I have chosen to do. To my sister, Vicky, for always having more faith in me than I do in myself. Finally, to my parents, Rosemary and Alan, I can't thank you enough for all your love and support. I am so glad you encouraged me to be scientist rather than a full-time baton twirler. I have surprised myself and it turns out I am better at the former.

Abstract

Brain metastasis is a significant clinical problem, and 20-40% of cancer patients will develop metastatic spread to the brain.There remains, however, an urgent need to better understand the pathogenesis of brain metastasis and, in particular, the contribution of the tumour microenvironment. Astrocytes are activated in response to metastatic growth and *in vitro* studies suggest that this activation promotes tumour growth and invasion. However, the result of astrocyte activation has yet to be probed in relevant *in vivo* models.

The primary aim of this thesis, therefore, was to determine the role of astrocyte activation in metastatic progression. To address this question, two routes of metastatic induction were used; intracardiac and intracerebral. Astrocyte activation was demonstrated quantitatively in both models across a protracted time course, increasing both spatially and temporally. Subsequently, a CNTF-lentivirus model of chronic astrocyte activation was used to probe the effect of astrocyte activation on metastasis pathogenesis. No significant changes in either tumour seeding or growth were observed. However, based on subsequent assessment of the molecular phenotype of astrocytes incubated with either CNTF or tumour-conditioned media, I conclude that this lack of effect *in vivo* is likely to reflect the phenotypic state of the astrocytes in the CNTF-mediated model. For the converse experiment, I aimed to inhibit astrocyte activation with a targeted steroid previously shown to have anti-astrocytic effects. No significant effects on tumour burden were observed overall, although the data suggest a reduction in prefrontal areas in steroid-treated animals. *In vitro* and *ex vivo* PCR studies, together, suggested that astrocytic IL-6 may be important in metastasis progression.

Finally, in light of the robust activation of astrocytes in response to metastasis, I hypothesised that astrocyte activation could be used as a diagnostic biomarker for tumour growth, potentially facilitating diagnosis at earlier time points than currently possible. To test this hypothesis, radiolabelled small molecule ligands, targeting the translocator protein (TSPO) on activated glia, were used to image astrocyte activation with either SPECT or PET. Micrometastases were detected with both agents used, and at time points prior to that possible with current clinical methods of passive contrast enhancement across a compromised blood-brain barrier.

In conclusion, a dynamic interaction exists between astrocytes and tumour cells in brain metastases. Although the approaches used here have not yet revealed the contribution of astrocytes to metastatic growth, a framework has been established to further probe the role of astrocytes at the molecular level; *in vivo* modulation of astrocyte-derived factors will potentially yield not just mechanistic insights, but therapeutic gains. Importantly, regardless of the role of astrocytes, their robust association with tumour growth renders their activation an ideal surrogate for tumour growth.

Collaborations:

CNTF- and LacZ-lentivirus were a kind gift from Carole Escartin (MIRcen, Paris, France)

2B3-201 and empty liposomes were a kind gift from to-bbb technologies (Leiden, The Netherlands)

DPA-713 SPECT experiments were conducted in collaboration with the Chemistry Research Laboratory, University of Oxford. Particular thanks to Begona Checa for DPA-713 synthesis and Matthew Treadwell for ^{123}I labeling.

All GE-180 PET experiments were conducted in collaboration with GE Healthcare. Particular thanks to Immi Khan and for the ^{18}F labeling of GE-180.

Both nuclear imaging studies were conducted with the assistance of Veerle Kersemans, Imaging Core, Department of Oncology, Oxford.

Publications relevant to this work:

O'Brien ER, Kersemans V, Tredwell M, Checa B, Serres S, Soto MS, Gouverneur V, Leppert D, Anthony DC, Sibson NR. (2014) Glial Activation in the Early Stages of Brain Metastasis: TSPO as a Diagnostic Biomarker. *Journal of Nuclear Medicine*. **55** (2): 275-80.

Serres S, O'Brien ER, Sibson NR. (2014) Imaging angiogenesis, inflammation, and metastasis in the tumor microenvironment with magnetic resonance imaging. *Advances in Experimental Medical Biology*. **772**: 263-83.

Serres S, Martin CJ, Sarmiento Soto M, Bristow C, O'Brien ER, Connell JJ, Khrapitchev AA, Sibson NR. (2014) Structural and functional effects of metastases in rat brain determined by multimodal MRI. International Journal of Cancer. **134** (4): 885-96.

O'Brien ER, Howarth C, Sibson NR. (2013) The role of astrocytes in CNS tumors: pre-clinical models and novel imaging approaches. *Frontiers in Cellular Neuroscience*. **7** (40).

List of Abbreviations:

ACM: Astrocyte conditioned media

Ad5TNF-αm: TNF-$\alpha_{membrane}$ expressing adenovirus

ALCAM: Activated Leukocyte Cellular Adhesion Molecule

ALS: Amyotrophic Lateral Sclerosis

AMCA: Aminomethylcoumarin Acetate

Angpt2: Angiopoietin-related protein-2

ANOVA: Analysis of Variance

AP-1: Activator Protein-1

ATP: Adenosine Triphosphate

BALB/c: Bagg Albino (mouse strain)

BBB: Blood Brain Barrier

BMDC: Bone Marrow Derived Cell

CAM: Cellular Adhesion Molecule

cDNA: Complementary DNA

CHME: Cross-species Hybridisation Microarray Experiment

CNS: Central Nervous System

CNTF: Cilliary Neurotrophic Factor

CSPG: Chondroitan Sulphate Proteoglycan

CT: Computed Tomography

DAB: Diaminobenzidine

Da: Dalton

DAPI: 4,6-diamidino-2-phenylindole

DMEM: Dulbecco's Modified Eagle's Medium

DMSO: Dimethyl Sulfoxide

dn: Dominant Negative

DNA: Deoxyribonucleic Acid

DTPA: Diethylene Triamine Penta-acetic acid

EAE: Experimental Autoimmune Encephalomyelitis

ECM: Extracellular matrix

EGFR: Epidermal Growth Factor Receptor

ELISA: Enzyme-Linked Immunosorbent assay

ERK1/2: Extracellular-signal regulated kinase 1/2

ET_B: Endothelin Receptor B

FBP: Filtered Back Projection

FBS: Fetal Bovine Serum

FDG: 2-deoxy-2- (^{18}F) fluoro-D-glucose

GC: Glucocorticoid

Gd: Gadolinium

GFAP: Glial Fibrillary Acidic Protein

GFP: Green Fluorescent Protein

GLAST: Glutamate Aspartate Transporter

GLUT-1: Glucose Transporter-1

GR: Glucocorticoid Receptor

GRE: Glucocorticoid Response Element

Her2: Human epidermal growth factor receptor 2

IBA-1: Ionised calcium-Binding Adaptor molecule 1

ICAM-1: Intercelullalar CAM-1

IFN- γ: Interferon-gamma

Ig: Immunoglobulin

IκB: Inhibitor of κB

IL-: Interleukin-

iNOS: Inducible NOS

IV: Intravenous

JAG: Jagged 1

Jak: Janus Kinase

JAM: Junctional adhesion molecule

KLF2: Kruppel-like factor 2

LacZ: β-galactosidase

LFA-1: Lymphocyte function-associated antigen-1

LLC: Lewis Lung Carcinoma

LPS: Lipopolysaccharide

M1: 'Classically' activated macrophage

M2: 'Alternatively' activated macrophage

MAPK: Mitogen activated protein kinase

MMP: Matrix Metalloproteinase

MPIO: Microparticles of Iron Oxide

MPLSM: Multiphoton Laser Scanning Microscopy

MRI: Magnetic Resonance Imaging

mRNA: messenger RNA

MS: Multiple Sclerosis

MTT: (4,5-dimethylthiazol-2-yl)-2,5-diphenyltetrazolium bromide

NFκB: Nuclear Factor kappa B

NO: Nitric Oxide

NOS: Nitric Oxide Synthase

NPC: Neuronal Progenitor Cell

NSCLC: Non-Small Cell Lung Cancer

OSEM: Ordered Subsets Expectation Maximisation

PBMC: Peripheral Blood Mononuclear Cell

PBS: Phosphate Buffered Saline

PBST: PBS + Tween

PCR: Polymerisation Chain Reaction

PDGFR: Platelet Derived Growth Factor Receptor

PEG: Polyethylene Glycol

PET: Positron Emission Tomography

PFA: Paraformaldehyde

PFU: Plaque Forming Units

PKC: Protein Kinase C

PLP: Periodate Lysine PFA

PMN: Polymorphonuclear

PMT: Photomultiplier Tube

qRT-PCR: Quantitative real-time PCR

RGC: Retinal Ganglion Cell

RNA: Ribonucleic Acid

ROI: Region of Interest

ROS: Reactive Oxygen Species

SCID: Severe Combined Immunodeficiency Disease (mouse strain)

S.D: Standard Deviation

S.E.M: Standard Error of the Mean

SIC: Slow Inward Current

siRNA: Small Interfering RNA

SPECT: Single Photon Emission Computed Tomography

SRS: Stereotactic Radiosurgery

STAT: Signal Transducer and Activator of Transcription

ST6GALNAC5: (Alpha-N-Acetyl-Neuraminyl-2,3-Beta-Galactosyl-1,3)-N-Acetylgalactosaminide
Alpha-2,6-Sialyltransferase 5

T1 relaxation: Spin-lattice relaxation

T2 relaxation: Spin-spin relaxation

TAM: Tumour Associated Macrophage

TBI: Traumatic Brain Injury

TCA: Tricarboxylic Acid Cycle

TCM: Tumour conditioned media

TDSF: Tumour Derived Secreted Factor

TEER: Transendothelial electrical resistance

TGF-β: Transforming Growth Factor-β

TNF: Tumour Necrosis Factor-α

TSPO: Translocator Protein

VCAM-1: Vascular CAM-1

VEGF: Vascular Endothelial Growth Factor

VOI: Volume of Interest

WBRT: Whole Brain Radiotherapy

WT: Wild Type

Table of Contents

Chapter 1 Introduction

1.1 Cancer

Cancer is a class of diseases characterised by unregulated cellular proliferation, resulting from DNA mutagenesis. Such uncontrolled cell division leads to the formation of an abnormal mass of tissue, known as a neoplasm, or more commonly a tumour. Tumours can arise throughout the body, although cancers of the lung and colon are most common across the two sexes; breast and prostate cancer are the most common neoplasms found in women and men, respectively (Siegel et al., 2012). More than 1 in 3 people in the UK will develop cancer during their lifetime and whilst mortality rates have fallen by 20% over the last three decades, the disease still accounts for more than a quarter of deaths in the UK.

This large clinical burden has unsurprisingly resulted in a huge research investment; in 2012, $5,621 million was spent in the USA on cancer research. A seminal review in 2000 by Hanahan and Weinberg distilled the vast quantity of basic research on cancer geno- and phenotypes and proposed that all neoplasms share 6 hallmarks that drive malignant progression: evading apoptosis, self-sufficiency in growth signals, insensitivity to anti-growth signals, limitless replicative potential, angiogenesis and tissue invasion and metastasis (Hanahan and Weinberg, 2000). It is this final hallmark, the spread of cancerous cells from

a primary tumour to a distal organ that is responsible for 90% of deaths in cancer patients (Gupta and Massague, 2006) and which will be the focus of my thesis.

1.2 Metastasis

Metastasis describes the dissociation of cancer cells from a primary tumour and their spread to and growth within distal organs. The process involves dissemination of cancer cells through the blood stream or lymphatic system and their subsequent colonisation of a secondary organ, as illustrated in Figure 1.1. Environmental stress, a consequence of excessive cellular proliferation in the absence of an adequate blood supply, is thought to drive dissemination to a secondary organ. For instance, low oxygen tension, known as hypoxia, is a key factor in the progression to malignancy and the hypoxic response pathway has been implicated in mediating some of the phenotypic changes, outlined below, that drive metastasis (Lu and Kang, 2010).

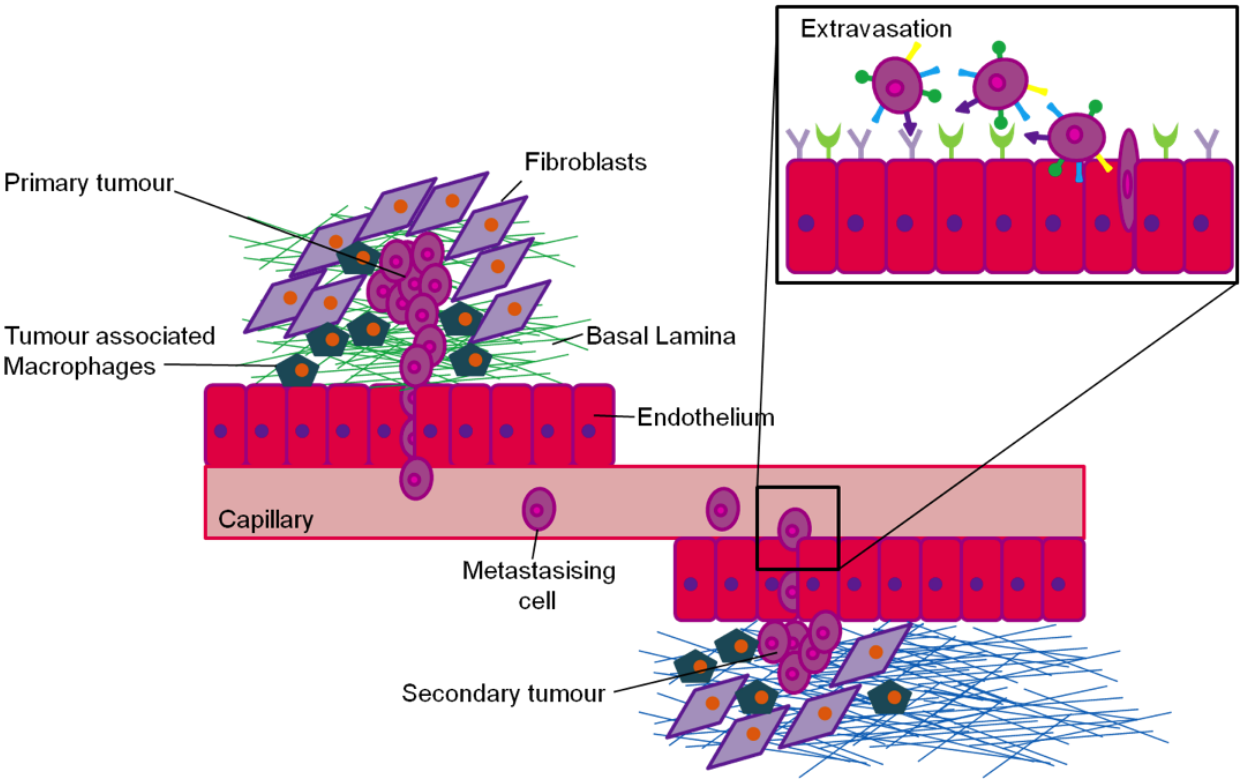

Figure 1.1: Metastasis is a multi-step process, involving interactions between many different cell types. 1) Deregulated growth leads to cellular proliferation within the extracellular matrix (ECM). The tumour microenvironment includes non-neoplastic cells, such as fibroblasts and tumour associated macrophages that may drive malignancy. 2) Metastatic tumour cells disseminate from the primary tumour and invade the local tissue, remodeling the basal lamina and ECM. 3) Cancer cells extravasate through the endothelium and enter the bloodstream. 4) Circulating cancer cells interact with cellular adhesion molecules on the luminal endothelial surface and 'roll' along the endothelium. 5) Cancer cells extravasate across the endothelium and begin to colonise the secondary site. The site of metastasis also contains its own tumour microenvironment that contributes to disease progression.

As evident in Figure 1.1, the metastatic process is comprised of multiple steps. The acquisition of a metastatic phenotype requires the loss of cell—cell and cell—matrix interactions. Cells are tethered to one another by cell adhesion molecules (CAMs) and the expression of such proteins is modulated in neoplastic disease. Perhaps the best-characterised CAM in this scenario is epithelial-cadherin (E-cadherin), an ubiquitously expressed epithelial protein. E-cadherin expression is reduced in many human cancers (Birchmeier and Behrens, 1994) and experimental models implicate its loss in facilitating invasion and metastasis (Frixen et al., 1991; Vleminckx et al., 1991). E-cadherin also acts as a signalling molecule and, therefore, modulation of its expression does not solely initiate metastasis via the disruption of cell—cell contacts (Onder et al., 2008).

Only a small proportion of cells in a primary tumour appear to be motile and they move in a linear fashion through the ECM (Farina et al., 1998). Advances in multi-photon microscopy have facilitated the observation that such cells actually track, individually, along collagen fibres (Wang et al., 2002). Progression through the ECM, with the destruction of the basement membrane, is dependent on the secretion of proteolytic enzymes. One such family of enzymes, the matrix metalloproteinases (MMPs) have been frequently linked with poor prognosis (Murray et al., 1998; Murray et al., 1996). Inhibition of members of this family have been linked to reduced invasion and metastasis in *in vitro* and *in vivo* models (Kilian et al., 2006; Liu et al., 2012; Naglich et al., 2001), however clinical trials have been disappointing with regards to reducing disease burden (Zucker and Cao, 2009). This illustrates the complex nature of the metastatic process; inhibition of just one facet alone will be unlikely to halt malignant progression.

Entry into the vasculature is often aided by the presence of neo-vessels, formed due to the tumour driven promotion of angiogenesis (Folkman et al., 1971). Such vessels are often 'leaky' and hence facilitate entry of disseminated cells into the blood stream. Survival in the vasculature appears to be dependent on coagulation, with tumour cells initiating blood clotting (Falanga et al., 2009). The formation of such microembolisms facilitates intra-vascular survival by providing protection from shear forces and immune cell destruction. Platelet aggregation has also been shown to initiate macrophage recruitment and promote neoplastic cell survival in the bloodstream (Gil-Bernabe et al., 2012).

With regards to extravasation and colonisation of the secondary organ, metastatic spread is not a random process, purely driven by the mechanical forces experienced in the vasculature (Fidler, 1978); sub-populations of cancer cells display differential organotropism. For instance, in an *in vivo* xenograft model, the human breast cancer cell line MDA-MB-231 was shown to display distinct gene signatures, encoding, in many cases, secretary or surface proteins, dictating metastasis to either lungs or bone (Minn et al., 2005). Only 6 genes were found in both signatures (Gupta et al., 2005). The same study demonstrated such gene signatures in human biopsy samples, from a cohort of 82 primary breast cancer patients. One theory suggests that the establishment of a 'pre-metastatic niche' may direct organotropism. First described in 2005, Kaplan and colleagues demonstrated that bone marrow derived cells (BMDCs) were localised at the sites of metastases prior to the arrival of metastasising cells. The location of BMDC recruitment is dictated by the primary tumour in xenograft models, and such

BMDC clusters were also observed in a spontaneous tumour model (Kaplan et al., 2005). Once at the secondary organ, BMDCs act to make the microenvironment permissive to metastatic colonisation, for example modulating the ECM and inducing immunosuppression and vascular hyperpermeability. Numerous tumour derived secreted factors (TDSFs) have been suggested to drive the formation of the pre-metastatic niche. VEGF was originally proposed to mediate BMDC recruitment (Kaplan et al., 2005), but multiple factors have been proposed (Sceneay et al., 2013), such as TGF-β and TNF (Hiratsuka et al., 2006). Whilst to date only the recruitment of BMDCs has been studied, it is plausible that TDSFs also serve to 'prime' resident cells at the secondary site of cancer growth. Clearly, there are a number of factors that are important in driving metastatic progression, most likely specific to the organ of origin. I will now consider the case of brain metastasis specifically as this is the focus of my thesis.

1.3 Brain metastasis

1.3.1 Clinical incidence, diagnosis and treatment

Metastatic spread of a primary tumour to the brain occurs in approximately 20 to 40% of cancer patients. Brain metastases are most typically derived from lung, skin or breast primary tumours (Patchell, 2003). Approximately two-thirds of patients present with neurological symptoms, typically headaches, seizures and nausea, although the nature of further symptoms are dictated by tumour size and location (Zhang et al., 2012). Metastatic colonization can occur throughout the brain, although there is a tendency for growth in the most vascularised areas (Delattre et al., 1988).

There are two key issues impeding the management of brain metastasis: (i) diagnosis and (iI) treatment options upon diagnosis. With regards to clinical diagnosis, the current gold-standard technique is contrast-enhanced magnetic resonance imaging (MRI) (Zhang et al., 2012). This technique is dependent on the breakdown of the blood-brain barrier (BBB), facilitating extravasation of contrast agents such as gadolinium, into the parenchyma. However, as I will explain later, BBB breakdown is a late event in the progression of brain metastasis. Clearly there is a need for imaging modalities that enable early detection of metastatic disease (Serres et al., 2012).

Upon diagnosis, median survival without treatment is 1 month (Patchell,2003) and chemotherapeutic options are limited owing to the presence of the BBB. Free diffusion of drugs across the BBB is dependent on lipid solubility (low number of hydrogen bonding functional groups) and a low molecular weight, typically smaller than 600 Daltons (Da) (Pardridge, 1998). In addition to these constraints, the BBB displays drug transporter membrane proteins that serve as drug efflux pumps, which actively exclude drugs from the brain in order to provide CNS protection (Girardin, F et al., 2006).

These limitations exclude the use of common chemotherapeutic agents such as cisplatin and doxorubicin. In situations where the selection of BBB permeable chemotherapeutics is possible, pharmacological treatment typically depends on the origin of the metastases. For instance, epidermal growth factor receptor (EGFR) mutations are present in up to 25% of patients with non-small cell lung

cancer (NSCLC), leading to constitutive kinase activity. Therefore Gefitinib, a tyrosine kinase inhibitor, has been trialled in conjunction with WBRT to treat brain metastases from this origin (Renfrow and Lesser, 2013). Attempts to permeabilise the BBB at sites of metastasis to facilitate drug access may provide more effective therapeutic options, as this will allow access to more targeted antibody therapies (Connell et al., 2013). For instance, Trastuzamab is a monoclonal antibody against the human epithelial growth factor receptor 2 (Her2), which is overexpressed in 20-30% breast cancer patients (Mitri et al., 2012). The antibody is used widely and successfully in the treatment of many breast cancers, thus, facilitating access of this treatment to the brain may be of considerable clinical benefit.

In light of BBB constraints, radiotherapy is the primary treatment option for patients with brain metastasis, with either whole brain radiotherapy (WBRT) or stereotactic radiosurgery (SRS) employed. Surgical resection is typically used in combination with radiotherapy, when treating up to three metastases (Renfrow and Lesser, 2013). Median survival after WBRT is of the order of 3—6 months, with the caveat of short- and long-term radiation effects, including memory loss. In the case of SRS, median survival is approximately 14 months, although almost 50% of patients will develop new metastases during this time. Thus, it is evident that there is an unmet clinical need in terms of diagnosis and treatment of brain metastasis. Through a greater understanding of the tumour microenvironment, I aim to elucidate novel methods for detecting metastatic disease at early time points, as well as inform on the molecular mechanisms of disease, which may in the future lead to novel targets for therapeutic intervention.

1.3.2 Molecular mechanisms

As discussed above, different primary tumours display different organ tropisms. In some cases, specific gene signatures have been shown to be predictive of brain metastasis (Bos et al., 2009; Harrell et al., 2012; Lee et al., 2012), with many of the genes implicated in mediating traversal of the BBB. For instance, COX2 has been shown in an *in vitro* model of the BBB, to play a role in barrier transmigration (Bos et al., 2009). Similarly, ST6GALNAC5 , a siayltransferase that catalyses the addition of sialic acid to glycoproteins and therefore facilitates cell—cell interactions, has been shown to drive brain metastasis *in vivo*; transduction of lung metastatic cells with a ST6GALNAC5 expression vector increased BBB transmigration and brain infiltration (Bos et al., 2009). In order to understand the molecular mechanisms driving brain metastasis, we must first consider the BBB.

1.3.2.1 The blood brain barrier

As illustrated in Figure 1.2, the brain is surrounded by a unique vascular compartment that places a hurdle before metastasising cells. Sophisticated imaging of fluorescent metastatic cells, using multi-photon laser scanning microscopy (MPLSM), has allowed the stages of brain metastasis to be visualized *in vivo* (Kienast et al., 2010). The tortuous nature of the cerebral micro-

vasculature enforces a reduction in the speed of circulating cells and arrest at vascular branch points is observed. Such arrested cells can reside on the luminal side of the brain endothelium for up to 5 days, in contrast to elsewhere in the body where metastasising cells rapidly extravasate within 24 hours (Lorger and Felding-Habermann, 2010). As such, the length of time for cancer cells to metastasise into the brain is considerably longer than that of other organs. In a murine *in vivo* ultrastructural study, extravasation of 3LL-HH cells, a liver cancer cell line, was first observed 48 hours after intracarotid inoculation, with 76% of metastasising cells found in an extra-capillary position at 72 hours. In contrast, extravasation at peripheral organs is much more rapid, for instance, 74% of metastasising cells were observed to have extravasated across the lung vasculature by 24 hours (Paku et al., 2000). This electron microscopy study is in agreement with fluorescent microscopic analysis of the extravasation process, demonstrating extravasation of metastatic breast cancer cells into the brain from 3 days, after introduction into the circulation via the intracarotid artery (Lorger and Felding-Habermann, 2010).

There are multiple hypotheses for the initial steps of traversal. As recently reviewed (Hamilton and Sibson, 2013), tumour cells may use similar mechanisms to those employed by immune cells, adhering to cellular adhesion molecules (CAMs). As illustrated in Figure 1.1, metastasising cells interact with receptors expressed on the endothelium and 'roll' along the luminal surface. The continuous process of forming and breaking ligand—receptor interactions leads to decreased cellular velocity, allowing more firm adhesions to form. The selectins are one such class of receptors, binding to *o*-glycosylated ligands

expressed on cancer cells. Endothelial- (E) and platelet (P)-selectin deficient mice display significantly reduced metastatic burden in a xenograft model of spontaneous metastases to the lung (Kohler et al., 2010). With regards to brain metastasis, recent work within the lab indicates that antibody mediated abrogation of the interaction between tumour cells and CAMs on the BBB, in this case vascular cellular adhesion molecule-1 (VCAM-1) and activated leukocyte cell adhesion molecule (ALCAM), attenuates brain metastatic burden *in vivo* (Soto et al., 2013).

Considering migration through the endothelium itself, two routes, analogous to leukocyte trafficking, have been proposed: paracellular and transcellular. Electron microscopy suggests that the endothelium retracts in response to cancer cell adhesion (Paku et al., 2000), perhaps facilitating traversal. An *in vitro* model of melanoma cell extravasation suggests that extravasating cells adhere at the junction between two endothelial cells and decrease trans-endothelial resistance (TEER), inducing endothelial cell apoptosis and disruption of endothelial tight-junctions, in a serine protease mediated fashion (Fazakas et al., 2011). Additionally, tumour cells have been shown to form selectin-mediated aggregates with polymorphonuclear (PMN) leukocytes (Jadhav et al., 2001), 'hijacking' immune cells to facilitate paracellular extravasation. *In vitro* work has suggested that breast cancer cells may additionally extravasate transcellularly, moving through endothelial cells, assisted via myosin contraction (Khuon et al., 2010). However, the transcellular route for metastatic cells has not been demonstrated *in vivo* (Wilhelm et al., 2013).

Upon entry to the perivascular space, it has been demonstrated that metastatic growth is dependent on contact with the abluminal endothelial membrane (Carbonell et al., 2009), as is the case in glioma (Winkler et al., 2009). Only upon growth of macrometastases, will the astrocytic end-feet component of the BBB (the glia limitans) be breached, allowing spread of metastases into the brain parenchyma (Saito et al., 2007).

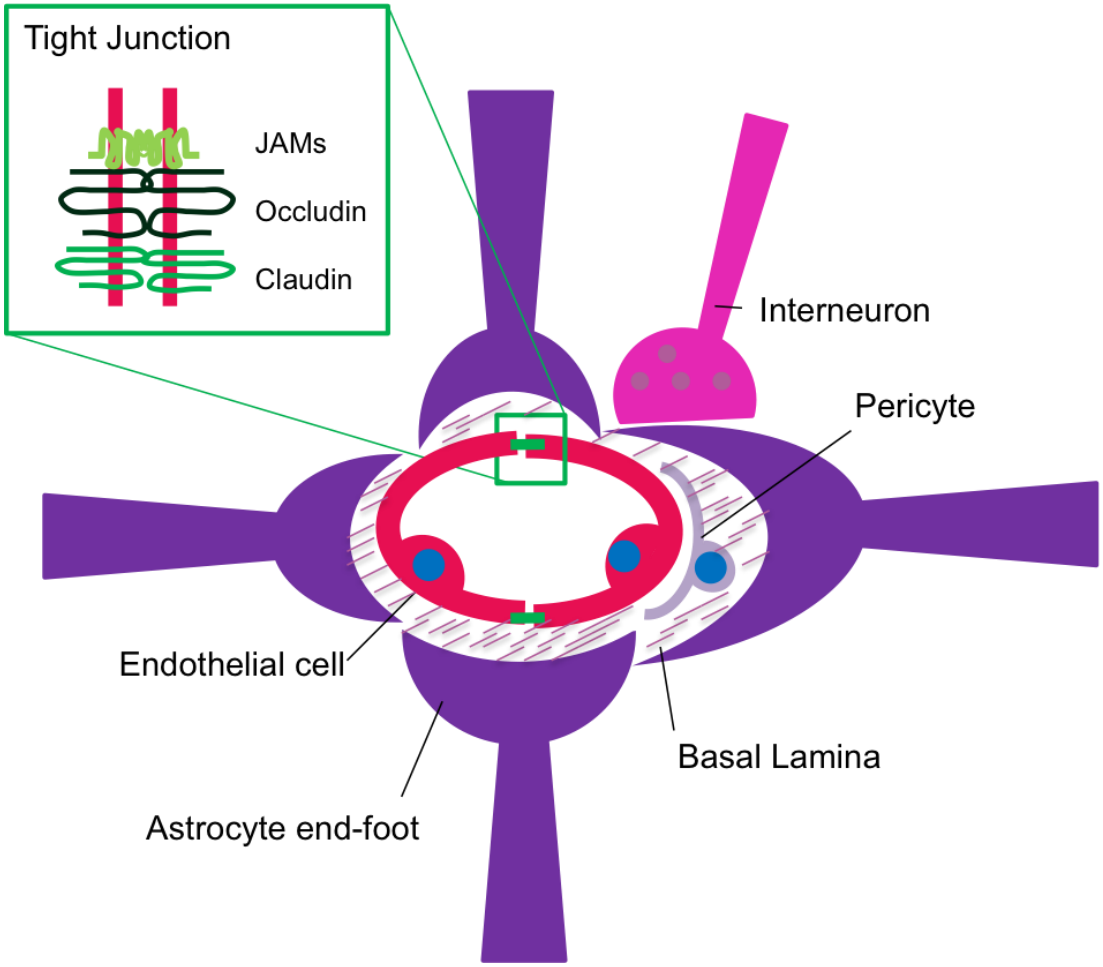

Figure 1.2: Cellular and molecular components of the blood-brain barrier. The blood-brain barrier is comprised of endothelial cells joined by specialized tight junctions, comprised of junctional adhesion molecules (JAMs), occludin and claudin. The endothelium is surrounded by basal lamina. Additionally, pericytes and astrocytic end-feet make contact with the endothelium and contribute to its integrity, both structural and metabolic. Astrocytes serve to link the endothelium with neurons.

There are contradictory reports regarding the integrity of the BBB surrounding metastases. A study by Zhang et al, using nude mice inoculated with a range of cancer cell lines demonstrated that breakdown of the BBB is well correlated with the size of the tumour, rather than location; lesions smaller than 0.2 mm^2 have an intact BBB, and the initial stages of metastasis do not induce BBB breach (Zhang et al., 1992). However a more recent *in vivo* study, using an intracardiac model of brain metastases, demonstrates that BBB permeability is heterogeneous and there is no correlation between lesion size and BBB permeability (Lockman et al., 2010). Whether these conflicting findings are due to the models used remains to be seen. Breakdown of the BBB in the peri-tumoural area of human biopsy samples can be inferred from vessel structural abnormalities. Analysis of clinical samples demonstrates the aberrant association of astrocytic processes with vessels within tumour biopsies (Nduom et al., 2013), demonstrating breach of the final component of the BBB in later disease. Such biopsies also indicate that a compromised BBB is not dependent on tumour cell contact with the vasculature, suggesting a role for tumour-derived soluble factors in modulating BBB integrity (Stewart et al., 1987).

1.4 The inflammatory microenvironment

The summary presented here, regarding the key processes involved in metastasis, has, thus far, been cancer cell centric. In a recent revision of Hanahan and Weinburg's seminal review, 'The Hallmarks of Cancer', inflammation in the tumour microenvironment was identified as an enabling characteristic; inflammation can drive the acquisition of the key features of tumourigenesis, discussed previously (Hanahan and Weinberg, 2011). This raises the important

point that cancers are not comprised of neoplastic cells alone and that the stroma, consisting of immune cells, vasculature, the ECM and non-immune stromal cells, such as fibroblasts and astrocytes,, all contribute to tumour pathogenesis. As illustrated in Figure 1.3, there are multiple components to the host inflammatory response and the balance of anti- and pro-tumourigenic factors can be modulated by the tumour itself. Here I will focus on outlining the inflammatory microenvironment at the site of metastatic colonisation specifically in the brain. I will consider systemic immune cells as well as CNS resident cell populations, namely microglia and astrocytes.

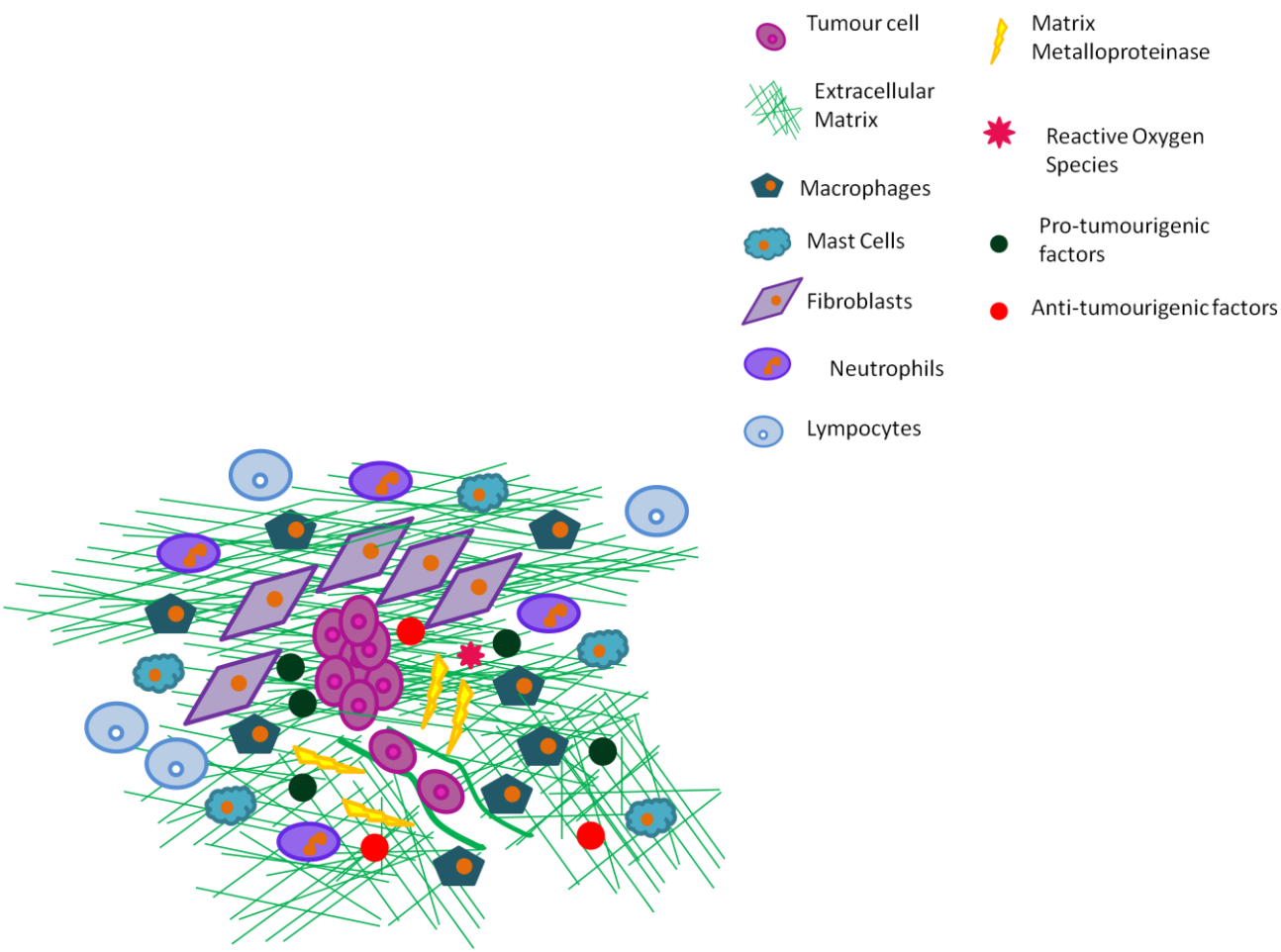

Figure 1.3: The inflammatory microenvironment. Multiple non-neoplastic stromal and immune cells may contribute to metastatic progression. Macrophages, mast cells, neutrophils and fibroblasts have all been implicated in releasing factors that may drive metastasis. When the balance of pro-tumourigenic factors outweighs the anti-tumourigenic factors present in the inflammatory milieu, then tumour growth accelerates and local invasion and metastasis can occur.

1.4.1 Systemic immune cell infiltration

As first postulated in 1986, there are striking similarities between the stromal response to tumour growth and to wounds, with a high immune cell infiltrate (Dvorak, 1986). Although the brain was originally deemed 'immuno-priviledged', immune cell recruitment is also a feature of the brain metastatic microenvironment. Inflammation has been demonstrated in the brain in response to metastasis, with an upregulation of cellular adhesion molecules present on the endothelium (Soto et al., 2013). Adhesion molecules are critical for immune cell infiltration, and such recruitment has been demonstrated in the metastatic microenvironment. Human biopsy samples show a large macrophage infiltrate in response to brain metastatic growth (Amit et al., 2013; Shinonaga et al., 1988). Similarly, T-cells are a feature of the brain metastatic niche, as has been robustly demonstrated in peripheral tumours. Interestingly, in an *in vivo* characterisation of melanoma derived brain metastases, $CD4^+$ outnumber $CD8^+$ T-cells (Amit et al., 2013). As $CD4^+$ cells co-ordinate the immunological response, whilst $CD8^+$ T-cells display cytotoxic activity, this finding implies that tumouricidal immune cells are in the minority. Neutrophil recruitment in the context of brain metastasis has not been characterized, however, extensive infiltration has been observed in human glioma, correlating with grade (Liang et al., 2014).

1.4.2 Resident macrophages

In addition to the infiltration of systemic immune cells, the brain has its own unique resident immune response. Microglia, are the brain's resident macrophages. Traditionally believed to be derived from hematopoietic stem cells

in the bone marrow before migration to, and further differentiation in, the brain, it now appears that microglia may originate in the yolk sac (Ginhoux et al., 2013) which goes on to form the brain. Microglia conduct immune surveillance via expression of a host of receptors, including Toll-like receptors. Upon activation of such receptors, microglia co-ordinate the immune response and are involved in phagocytosis and antigen-presentation to recruited T-cells. Microglia are highly plastic cells, and their response to CNS challenge can follow different pathways. As described for peripheral macrophages (Gordon, 2003), microglia can be 'classically' (M1) or 'alternatively' (M2) activated. The 'classical' pathway, mediated by cytokines such as interferon-γ (IFN-γ), initiates a pro-inflammatory response to immunogens. The 'alternative' pathway, mediated by cytokines such as IL-4, is implicated in tissue repair and regulating the immune response (Boche et al., 2013). However, one should note that there is likely to be a spectrum between the activation states, with various sub-populations (Lee et al., 2014). In the context of cancer, the established paradigm for tumour associated macrophages (TAMs) in peripheral tumours is that they display an M2 phenotype, and as such are involved in promoting tumour growth and angiogenesis (Mantovani et al., 2002). These differential activation states may also be present in response to brain metastasis.

The microglial response to metastases has been demonstrated in human biopsy samples (Berghoff et al., 2012; He et al., 2006; Zhang and Olsson, 1995) as well as in *in vitro* and *in vivo* models (Amit et al., 2013; Balathasan et al., 2013; Lorger and Felding-Habermann, 2010). Studies indicate microglia induce cellular toxicity, mediated via the production of nitric oxide (NO) (Brantley et al., 2010;

He et al., 2006; Murata et al., 1997). However, there is also evidence for differential activation of microglia, as discussed above, leading to the release of tumour trophic factors (He et al., 2006). Additionally, others have shown that microglia facilitate the initial stages of metastatic colonization. Co-culture of human breast cancer cell lines with primary mouse microglial cells leads to an increased invasion rate and organotypic slice models implicate microglia in 'pulling' tumour cells into the brain parenchyma (Pukrop et al., 2010). Again, however, this effect is microglia phenotype dependent, and skewing microglial activation to the 'classical M1 pathway' using the inflammatory challenge LPS, abrogates the ability of microglia to enhance invasion (Pukrop et al., 2010).

1.4.3 Astrocytes

Astrocytes are the most abundant member of the glial family and, although not immune cells, they do mount an inflammatory response not just to infection but also to CNS challenge, including primary and secondary brain tumours. It is this astrocytic response to tumours that my work focuses on and the subsequent sections will outline the role of astrocytes in health and disease, before focusing on evidence for a role of astrocytes in tumour pathogenesis.

Astrocytes, so called due to their stellate morphology, are found in a contiguous manner throughout the CNS, having evolved from the neuroepithelium. There are two main subtypes of astrocytes, characterised by their morphology and localisation; protoplasmic and fibrous. Whilst protoplasmic astrocytes are found in gray matter, fibrous astrocytes are found in white matter (Sofroniew and

Vinters, 2010). In the mouse brain, astrocytes outnumber neurons 4:1, with the ratio increasing with evolution, to that of the human brain, where astrocytes are typically cited to out-number neurons 10:1 throughout most brain regions. However, no primary evidence for this ratio is published, and the figure appears to be closer to 1:1, at least in the cortex (Azevedo et al., 2009). Regardless of number, astrocytes were originally believed to serve a purely structural role in the brain, supporting neurons and the BBB. However, the 'glial revolution' over the past couple of decades has seen astrocytes implicated in a whole host of CNS functions, some of which I will outline below.

1.4.3.1 Astrocytic endfeet and the blood brain barrier

As touched upon above, astrocytes are critical players in the composition of the BBB. However, astrocytes contribute not just to BBB structure, but also to its genesis, inducing tight junction formation between endothelial cells (Goldstein, 1988), and up-regulating expression of transporters such as the brain specific glucose transporter, GLUT1 (Boado and Pardridge, 1990; McAllister et al., 2001). Astrocytes also couple neural demands for increased blood supply to the vascular endothelium, releasing vasodilatory mediators such as NO, arachodonic acid (AA) and prostaglandins (PGE), as extensively reviewed elsewhere (Gordon et al., 2007). Communication with the endothelium is bi-directional, with calcium signaling also occurring between the endothelium and astrocytes (Braet et al., 2001; Leybaert et al., 1998), suggesting that endothelial changes may also have a dynamic effect on astrocyte function; this, as we will see later, has relevance for the early stages of metastatic colonisation.

1.4.3.2 Synaptic transmission

Astrocytes play a role in neuronal development and are implicated in dictating neurite extension via the formation of proteoglycan boundaries *in vitro* (Powell and Geller, 1999). Additionally, astrocytes have been shown *in vitro* to increase the number of stable neuronal synapses formed (Christopherson et al., 2005; Ullian et al., 2001). *In vivo,* at early post-natal time points, stable synapse formation occurs around the time of glial proliferation (Ullian et al., 2001), suggesting that astrocytes are critical mediators of neuronal physiology.

Besides their role in synaptogenesis, astrocytes also mediate and modulate synaptic transmission. Indeed, one of the best characterised physiological functions of astrocytes is their role in homeostasis of the neurotransmitter glutamate. Effective synaptic transmission is dependent on the maintenance of a low extracellular glutamate concentration, as compared to a high, intra-neuronal, vesicular concentration. Astrocyte processes ensheaf the synaptic cleft and take up glutamate via the glutamate transporters, GLT-1 and GLAST, which have differential regional and developmental expression profiles (Lehre et al., 1995).

Although astrocytes are not electrically excitable, they are not electrically silent; electrophysiology demonstrates that astrocytes are sensitive to neuronal activity and astrocyte signalling can modulate synaptic transmission. Astrocytes express neurotransmitter receptors and upon ligand binding, Ca^{2+} is released from intracellular stores. Thus Ca^{2+} oscillations act as a read-out for neuronal synaptic activity. However, astrocytes integrate neuronal inputs from multiple

neurotransmitters and, therefore, the read-out is not a simple summation of multiple stimulations (Perea et al., 2009). Indeed, the ligation of different neurotransmitter receptors can lead to a reduction in astrocytic Ca^{2+} oscillations in some cases (Perea and Araque, 2005). In other models, simultaneous neurotransmitter application potentiates Ca^{2+} elevations in astrocytes (Cormier et al., 2001). With regards to the physiological function of such astrocytic calcium fluctuations, modulation of neuronal transmission has been demonstrated, via the release of so called 'glial transmitters'. For instance, in hippocampal slice preparations, astrocyte Ca^{2+} elevations have been shown to cause slow inward currents (SIC) in neurons mediated by astrocytic glutamate release (Perea and Araque, 2005).

1.4.3.3 Metabolism

Astrocytes are highly metabolically active. Under normal conditions, it has been proposed that the ATP requirements of astrocytes are primarily served by glycolysis (Pellerin and Magistretti, 1994; Pellerin and Magistretti, 1997), with the end-product, lactate, extruded into the extracellular space either for uptake by neurons (Aubert et al., 2005) or clearance from the brain. However, the TCA cycle and subsequent oxidative phosphorylation within astrocytes is also a source of ATP (Serres et al., 2008), and recent transcriptome analyses of acutely isolated mouse cortical astrocytes have demonstrated elevated levels of TCA cycle enzymes as compared to neurons, combined with high mitochondrial numbers in astrocyte foot processes (Lovatt et al., 2007). Astrocytes also serve to provide

metabolic support for neurons and act as glycogen stores to sustain neuronal activity in times of hypoglycemia (Brown and Ransom, 2007).

1.4.3.4 Reactive astrocytes

In the context of this thesis, the most important role for astrocytes is that of their response to CNS challenge, in which they become 'activated' or 'reactive'. That is, they undergo a dynamic process of morphological and transcriptional changes. Glial fibrillary acidic protein (GFAP) is the archetypal astrocyte marker, first purified in 1971 from multiple sclerotic plaques (Eng et al., 2000). GFAP is an intermediate filament protein, serving a role in mediating astrocyte morphology and motility (Lepekhin et al., 2001). There are at least 8 different GFAP isoforms, the most abundant being GFAPα, with other isoforms found in specific astrocyte populations (Thomsen et al., 2013). The rapid synthesis of GFAP mediates the morphological changes observed in astrocyte activation, and anti-sense inhibition of GFAP indicates that the protein is necessary for the formation of stable astrocytic processes (Weinstein et al., 1991).

As stressed by Sofroniew & Vinters, astrocyte activation is a graded response that is dependent on the nature and the severity of the insult (Sofroniew and Vinters, 2010). Astrocytes can be activated via multiple signalling pathways and by a host of molecular triggers, including cytokines, oxidative stress, glucose deprivation and ATP released by damaged cells (Sofroniew, 2009). In turn, activated astrocytes modulate numerous pathways, including extracellular matrix and cell—cell interactions, inflammatory processes, vascular tone and energy provision. Recent studies suggest that inflammation induced astrocyte activation can also modulate electrophysiology, with an increase in voltage-dependent

currents observed in astrocytes surrounding the inflammatory lesion (Karpuk et al., 2012). Additionally, hemichannel activity is increased, thus facilitating gap junction mediated communication between astrocytes. Altered metabolic activity is a further feature of reactive astrocytes; in a ciliary neurotrophic factor (CNTF) induced model of astrocyte activation, fatty acid oxidation and ketone body metabolism are increased, whilst glycolysis is decreased (Escartin et al., 2007), conferring resistance to metabolic insults. In this same model, it also appears that astrocyte activation leads to disruption of neuro-vascular coupling (Serres, S. unpublished).

With regards to morphology, the degree of astrocyte activation can be broadly defined by cell body and process appearance (Sofroniew and Vinters, 2010). In mild to moderate astrocyte activation, cell body and process hypertrophy is observed, but there is no loss of individual glial domains. Little or no proliferation is observed. In severe diffuse astrogliosis, both cellular hypertrophy and proliferation are observed and astrocyte processes overlap. The most severe extent of astrogliosis is the formation of the glial scar. In this state, there is a loss of distinct glial domains and a deposition of extracellular matrix components, forming a border between damaged tissue and the healthy parenchyma. Ablation of reactive astrocytes, via transgenic inhibition of NFκB, led to increased inflammation and neuronal damage in a mouse model of spinal injury (Faulkner et al., 2004), suggesting a protective role for astrogliosis. Similar profiles of immune cell infiltration and neurodegeneration were observed upon astrocyte ablation in both a forebrain stab wound model (Bush et al., 1999) and traumatic brain injury (Myer et al., 2006). However, there is also evidence for deleterious

consequences of astrogliosis, such as exacerbation of inflammation in response to spinal cord injury (Brambilla et al., 2005) and EAE (Brambilla et al., 2009); inhibition of astrocyte reactivity led to improved functional outcome in both *in vivo* models. Astrocyte activation has also been implicated *in vitro* in the production of neurotoxic levels of reactive oxygen species via the upregulation of iNOS (Hamby et al., 2006). Thus, it is clear that astrocyte activation may act as a 'double-edged sword', and it is this balance that I wish to address in the context of brain metastasis.

1.5 Astrocytes in brain metastasis

As discussed above, astrocytes form an integral component of the BBB, in its development, structure and function. Calcium signalling between the endothelium and astrocytes (Braet et al., 2001; Leybaert et al., 1998) suggests that endothelial changes may also have a dynamic effect on astrocyte function. Hence, one could hypothesise that astrocytes will be activated as early as the initial steps of adhesion of metastasising cells to the vascular endothelium.

The characteristic response of astrocytes to injury, seen in numerous neuropathologies, including glioma, has also been identified as a feature of the brain metastatic microenvironment. A wall of reactive astrocytes has been reported around brain metastases in human post-mortem tissue (He et al., 2006; Zhang and Olsson, 1995), and recently there has been growing interest in establishing mouse models of brain metastasis to determine astrocyte reactivity

in vivo (Fitzgerald et al., 2008; Lorger and Felding-Habermann, 2010; Mendes et al., 2007; Mendes et al., 2005; Seike et al., 2011).

Astrocytic responses have been demonstrated in BALB/c mice in response to the syngeneic 4T1 mammary carcinoma cell line, as well as in SCID mice in response to the human MDA-MB-435 cell line, as early as 3 days post metastasis induction via intracarotid injection of tumour cells (Lorger and Felding-Habermann, 2010). Moreover, astrocyte reactivity was induced whilst the MDA-MB-435 cells were still intravascular, but in contact with the luminal endothelial membrane and qualitative assessment indicated this continued throughout extravasation and growth over a 50-day time-course. Likewise, Mendes *et al.* utilised a mammary carcinoma cell line, ENU1564, injected intracardially in rats, to demonstrate astrogliosis in response to brain metastases (Mendes et al., 2007). GFAP reactivity has also been demonstrated in an intracerebral model of brain metastasis, in which ENU1564 cells were injected into the rat thalamus (Serres et al., 2014). Gliosis is not only found in response to metastases of mammary origin; Izraely *et al* demonstrated astrocyte activation in nude mice in response to metastatic melanoma (Izraely et al., 2012) and Seike *et al.* demonstrated a wall of astrocyte reactivity in nude mice in response to the human lung cancer cell, HARA-B (Seike et al., 2011). However, the number of studies in which astrocytic responses to brain metastasis has been evaluated *in vivo* is still small. Additionally, as will be discussed below, these studies do not provide evidence for an *in vivo* role for astrocytes. Rather, molecular mechanisms have thus far been elucidated *in vitro*. As such, there is a need for *in vivo* manipulation of astrocyte reactivity to probe their role in metastatic progression.

The ‘double edged sword’ of inflammation that is so often reviewed in the literature, not just in cancer (Hagemann et al., 2007; Lin, 2010; Rizzo et al., 2011) but in other diseases such as asthma (Balhara and Gounni, 2012), stroke (Doyle and Buckwalter, 2012) and neurodegeneration (Wyss-Coray and Mucke, 2002), appears to also be a feature of the astrocytic response to brain metastasis. *In vitro* studies have shown that astrocytes produce NO, via inducible nitric oxide synthase (Simmons and Murphy, 1992), and that this has tumouricidal effects in both primary and secondary cancer cell lines (Samdani et al., 2004). Evidence that NO induces GFAP upregulation (Brahmachari et al., 2006) suggests that this may result in increased histological visualization of reactive astrocytes with disease progression.

However, a greater burden of evidence suggests a tumour-promoting role for astrocytes. Co-culture experiments between astrocytes and various tumour cell lines indicate that astrocytes release soluble factors that can enhance tumour cell growth. For instance, endothelin-1, besides its role in vasoconstriction, has also been proposed to be mitogenic (Bagnato et al., 2002; Bagnato et al., 1997; Kasuya et al., 1994), and analysis of biopsy samples suggests that endothelin-1 is expressed by astrocytes in 85% of patient cases (Zhang and Olsson, 1995). Additionally, the receptor for endothelin-1, ET_B, is upregulated in a brain-metastatic melanoma cell line over 3 fold, as compared to a non-metastatic cell line (Boukerche et al., 2004). This finding suggests that astrocytes may drive the molecular determinants of metastatic potential. Furthermore, incubation of the lung adenocarcinoma cell line PC_{14}-PE6 with an immortalised astrocytic cell line

induced cancer cell ERK1/2 phosphorylation (Langley et al., 2009), part of the MAP kinase signalling pathway heavily implicated in tumour progression. ERK1/2 phosphorylation has also been demonstrated in a metastatic mammary carcinoma cell line, ENU1564, in response to astrocyte conditioned media (Mendes et al., 2007). In this case, ERK1/2 activation was shown to increase tumour cell invasiveness *in vitro* via induction of MMP2 expression, as was also seen in astrocyte-glioma co-culture models (Le et al., 2003).

Metastatic invasion may also be facilitated by astrocyte-derived heparanase, which degrades heparin sulphate proteoglycans, a major component of the extracellular matrix. Astrocyte heparanase expression has been demonstrated in the peri-infarct regions of *in vivo* stroke models (Li et al., 2012a; Takahashi et al., 2007) and in rat astrocyte—tumour cell culture models. In the latter case, it was shown that co-culture of astrocytes with brain-metastatic melanoma cell lines led to a super-additive increase in enzyme activity, potentially through neurotrophin signalling (Marchetti et al., 2000). Treatment of melanoma cell lines with astrocyte conditioned media led to increased cell invasion, an effect which was abrogated with antibody-mediated neutralisation of heparanase. MMP production by astrocytes has also been demonstrated to drive tumour cell invasion *in vitro*, whilst inhibition of MMP activity *in vivo* was shown to reduce metastatic burden (Wang et al., 2013). Further co-culture experiments between astrocytes and several lung cancer derived cell lines indicate that astrocytes secrete IL-6, TNF and IL-1β, which stimulate tumour cell growth (Seike et al., 2011). It has also been suggested that astrocytes increase the anchorage-independent growth of cancer cell lines and that this correlates with metastatic

ability *in vivo* (Fitzgerald et al., 2008), although the mechanism has yet to be identified.

Astrocytes have also been shown to induce transcriptional changes in co-cultured tumour cells that reflect the transcriptional changes seen *in vivo* (Park et al., 2011). Here, a Competitive Hybridisation of Microarray Experiment (CHME) was used to tease apart genes upregulated in metastases as compared to the tumour microenvironment. In this case, human cancer cells were introduced into immuno-compromised mice, and differing gene signatures and methylation statuses between the cell populations were demonstrated. Subsequently, astrocytes were cultured with a breast carcinoma cell line, MDA-MB-231, and were shown to induce a similar genomic signature in the tumour cells to that seen *in vivo*, suggesting that astrocytes are mediators of tumour cell transcriptional reprogramming. For instance, brain metastatic cells were shown to upregulate genes involved in neuronal processes such as glutamate receptor signalling, axonal guidance and neurotransmission. This novel approach to probing astrocytic function in brain metastasis demonstrates the key role astrocytes play in tumour progression, but also highlights the need to determine both the mechanism and the growth advantage conferred.

Further evidence to support the hypothesis that astrocytes drive metastatic progression comes from recent work on the role of neuronal progenitor cells (NPCs). NPCs have previously been shown to migrate towards primary CNS tumours (Elvira et al., 2012; Glass et al., 2005; Tang et al., 2003) and have recently been identified in the metastatic peri-tumoural region (Neman et al.,

2013). Such cells have been shown to express SOX9, a marker for glial fate (Stolt et al., 2003), and co-culture of NPCs and the brain seeking variant of the metastatic breast cancer cell line MDA-Br-231, leads to the induction of astrocyte differentiation (Neman et al., 2013). This differentiation has been shown, in co-culture models, to shorten metastatic cell doubling time. As MDA-231 cells, which do not metastasise to the brain, do not induce NPC astrocyte differentiation, this suggests that there are genetic determinants dictating metastatic growth in the CNS.

In vitro studies suggest that astrocytes activate multiple signalling pathways in metastatic cells. Tumour conditioned media from a variety of breast cancer cell lines induces JAG1 expression in cultured rat astrocytes (Xing et al., 2013). JAG1 is a cell surface protein, which ligates Notch on neighbouring cells, eliciting downstream Notch signalling (Bash et al., 1999). The expression of JAG1 is regulated by NFκB and, in the study above it was observed that NFκB signalling was induced by IL-1β. Interestingly, brain seeking metastatic cell line variants secreted higher levels of IL-1β, and hence, induced greater astrocyte JAG1 expression, than the parental cell line (Xing et al., 2013). The subsequent interaction between astrocytic JAG1 and tumour cell Notch was shown to induce proliferation in cancer stem cells isolated from breast cancer cell lines, with inhibition of tumour derived IL-1β suppressing metastatic growth *in vivo*.

Astrocytes do not purely exert effects in the tumour microenvironment by promoting metastatic progression. Evidence is accumulating to suggest that astrocytes attenuate the effects of chemotherapeutics that cross the blood-brain

barrier. Co-culture of astrocytes and a non-small cell lung cancer cell line imparts a protective effect to rapamycin treatment (Kim et al., 2013). Further work suggests that astrocytes inhibit cancer cell apoptosis; co-culture of astrocytes with breast and lung cancer cell lines (MDA-MB-231 and $PC14Br_4$, respectively) induces up-regulation of survival genes such as *BCL2L1,* an anti-apoptotic member of the BCL-2 protein family (Kim et al., 2011). Bcl2 upregulation, along with a downregulation of Bax, the pro-apoptotic protein, has also been shown in brain-metastatic prostate cancer cells co-cultured with astrocytes (de Oliveira Barros et al., 2014). Such genes confer resistance to a range of chemotherapeutics and are absent in cell lines at secondary sites other than the brain, thus highlighting a novel role for astrocytes. Further work has shown that the mechanism of cell protection is cell contact dependent and mediated via gap junction facilitated sequestration of calcium from tumour cells (Lin et al., 2010).

Whilst the role of astrocytes in metastatic progression is yet to be fully elucidated, it is evident that astrocyte activation is a common feature of the tumour microenvironment, across metastases of different primary origins. As discussed above, diagnosis of brain metastasis is dependent on breakdown of the BBB, which occurs later in disease progression. Detecting metastases at earlier time points will aid disease management and treatment, and hopefully increase prognosis. Based on the published *in vivo* data, one would hypothesise that the astrocytic response takes place early in disease progression. Thus probing the microenvironment with molecularly targeted imaging agents may allow metastatic detection below the current diagnostic threshold. Promising *in vivo* MRI studies suggest that brain metastases can be detected based on the induced

inflammatory microenvironment (Serres et al., 2012). Thus, based on glial imaging in other neuroinflammatory conditions (Carter et al., 2012; Engler et al., 2012; Johansson et al., 2007), one would hypothesise that molecular imaging of astrocytes could be a promising diagnostic tool.

It is evident that there has been a flurry of activity in recent years with regards to the role of astrocytes in brain metastasis. Nethertheless, the vast majority of these studies are based on *in vitro* models, which can only partially reflect the *in vivo* situation or, indeed, the clinical one. Thus, the role of astrocytes has yet to be fully elucidated in an *in vivo* context. Additionally, the potential of astrocyte activation as a clinically relevant biomarker for tumour burden has yet to be explored. As such, the four primary aims of this thesis are as follows:

1. To characterise the spatial, temporal and molecular profile of astrocyte activation, in brain metastasis *in vivo*.
2. To determine the effect of astrocyte activation on tumour growth *in vivo* using a lentiviral model of chronic astrocyte activation.
3. To determine the effect of astrocyte inhibition on tumour growth *in vivo* using an astrocyte targeted steroid.
4. To determine whether astrocyte activation can be used as a biomarker for tumour growth in a diagnostic setting.

Chapter 2 Materials and Methods

The following chapter describes the materials and experimental methods used throughout this thesis. The methods are broken down into their corresponding chapters and in addition, a brief overview of the relevant techniques will be given at the beginning of each experimental chapter.

2.1The temporal and spatial profile of astrocyte activation

Two different mouse models of brain metastasis were used throughout the thesis, induced via different routes – either intracardially for hematogenous dissemination or intracerebrally for direct cerebral induction of a tumour. In both cases, 6-7 week-old female BALB/c mice, or 6-7 week-old female SCID mice (Charles River, Kent, UK) were housed under a standard 12 hour light/dark cycle and provided with food and water *ad libitum*. All procedures were carried out in accordance with the UK Animal (Scientific Procedures) Act 1986, and animals were scored for behavioural and health changes throughout.

2.1.1 Cell lines and primary cultures

2.1.1.1 Cell line culture

A mouse breast cancer cell line, 4T1, expressing green fluorescent protein (GFP, kind gift from the Muschel lab, University of Oxford), the mouse lung carcinoma

cell line, Lewis lung carcinoma (LLC, also from the Muschel lab) and the human breast cancer cell line, MDA-MB-231-Brain, expressing enhanced GFP (EGFP, kind gift of the Palmieiri lab), were each cultured in Dulbecco's Modified Eagle's Medium (DMEM, Invitrogen, UK) supplemented with 1% (v/v) 200mM glutamine (PAA, UK) and 10% (v/v) fetal bovine serum (FBS, Labtech International, UK). Cultures were typically grown in un-coated polystyrene T75 flasks (Corning, USA), unless stated otherwise, and incubated at 37°C in a water-saturated 5% CO_2 atmosphere in a HeraCell™ 150 incubator (Thermoscientific, UK). In cases where tumour conditioned media was required, media was replaced when cells were approximately 70% confluent and then harvested after 24 hours.

2.1.1.2 Cell preparation for injection

Medium was aspirated and cells were washed with sterile PBS, then incubated with 5 ml 0.05% trypsin with EDTA (LifeTechnologies, UK) for 10 minutes at 37°C. Trypsin activity was neutralised by adding 10 ml of culture medium. Cells were collected by sedimentation (250x*g*, 5 minutes, 4°C) in a Jouan CR4i centrifuge (Thermoscientific, UK). The resulting pellet was re-suspended in 1 ml of sterile PBS and cell number determined using a NucleoCounter® (Chemometec, DA), as per the manufacturer's instructions.

2.1.1.3 Primary astrocyte culture

Astrocytes were purified from pups at 3 days after birth using a procedure modified from Kim et al 2011 (Kim and Magrane, 2011). Using animals at such a young age ensures a low neuronal cell number, and reduced myelin as compared

to older animals, facilitating glial cell harvesting. Pups were killed by cranial dislocation and the cortices isolated in dissection buffer (DMEM supplemented with 10% (v/v) FBS). Tissue was mechanically dissociated with a 1mL pipette. To remove the neuronal cell population, tissue was passed through a 100μm mesh strainer (BD Biosciences, UK), with the flow-through subsequently passed through a 70 μm mesh strainer (BD Biosciences, UK). The cell suspension was plated in T75 flasks (2 brains/flask) in DMEM with 10% (v/v) FBS and 1% (v/v) Penicillin/Streptomycin (Sigma,10,000 units/mL penicillin and 10mg/mL streptomycin). The media was changed every 3 days and after 9 days, flasks were shaken at 250 RPM on a KS250 IKA Labortechnik shaker at 37°C for 12 hours, in order to remove the oligodendrocyte and microglial fractions, which are less adherent than astrocytes. The astrocyte monolayer was washed with the glial culture medium, and shaken by hand, prior to washing twice with glial culture medium to remove debris and non-adherent cells.

2.1.2 Experimental models of brain metastasis

2.1.2.1 Intracardiac model of brain metastasis

BALB/c mice were anaesthetised with 2% (v/v) isoflurane (Abbot, UK) in oxygen. Shaving and hair removal cream was used to ensure a clean ultrasound image removed hair over the thorax. Mice were maintained at 1.8% (v/v) isoflurane and placed on a heated stage. Ultrasound (Vevo770 system, VisualSonics, Canada) was used to visualise the heart and guide intracardiac injection in the left ventricle with 100μL PBS containing 10^4 4T1-GFP cells, using a 27 gauge needle (Balathasan et al., 2013). At days 10, 14, 21 and 28 post injection, animals (n=5-6 per time point) were transcardially perfusion-fixed under terminal anaesthesia

with 0.9% heparinised saline, followed by 200ml of periodate lysine paraformaldehyde (PLP) containing 0.025% (w/v) glutaraldehyde (Sigma Aldrich, UK) (PLP_{light}). Brains were removed and post-fixed for 4 h in PLP_{light} prior to cryo-protection in 30% (w/v) sucrose in water for ~24 hours. Tissue was embedded and frozen in Tissue-Tek (Bayer PLC, UK) for sectioning. 10μm-thick serial coronal sections were taken throughout the brain at a 1 in 5 sampling rate, using a cryostat (Leica, UK). Sections were mounted on Superfrost® Plus slides (Thermoscientific, UK) and allowed to dry overnight at room temperature.

2.1.2.2 Intracerebral model of brain metastasis

BALB/c mice were anaesthetised with 2% (v/v) isoflurane in a gas mix of oxygen and N_2O (30:70), and placed on ear bars in a small animal stereotactic frame (Stoetling Co., USA) under maintenance anaesthesia (1.5% (v/v) isoflurane). The skull was exposed and a small hole drilled at the injection site. Animals were injected in the left striatum (+0.5 mm from Bregma, +1.5 mm from the midline and -2.5 mm depth). Either 0.5 μl saline containing 10^7 cells/ml 4T1-GFP cells or 0.5 μl saline alone were injected using a glass micro-capillary (Clark Electromedical Instruments, UK) pulled with a single stage glass microelectrode puller (Narishige, model PP-830, Japan), heated to 72°C and cut such that the bore diameter was 75μm, as determined using a graticule. Following surgery, the skin incision was sutured using Mersilk sutures (Ethicon, Germany). At days 10, 14, 21 and 28 animals (n=5 per time point) were perfusion-fixed, and tissue processed as in section 2.1.2.1. SCID mice (n=4) were also injected with 5×10^3 MDA-Br-231-EGFP cells in 0.5 μl, and perfusion-fixed at day 14 post injection, with tissue processed as in section 2.1.2.1. In the case of the LLC model, C57 mice

(female, n=3) were injected intrastriatally with 5 x 10^3 LLC cells in 0.5 µl, and perfusion-fixed at day 14.

2.1.3 Immunohistochemistry

Throughout, antigens were revealed using an avidin-biotin-peroxidase system (Warnke & Levy, 1980). All incubations were performed at room temperature unless otherwise specified. Sections were washed in phosphate buffered saline (PBS) and quenched in methanol supplemented with 1% (v/v) H_2O_2 (30% w/w) for 20 minutes. Slides were further washed and placed in Shandon Sequenza® clips (Thermo Electron Cooperation, UK) under PBS. Sections were blocked with 10% serum derived from the same species that the secondary antibody is raised in (see Table 1) in PBS, washed (3 x 5 minutes) with PBS or PBS supplemented with 0.05% Tween20 v/v (PBS-T) if the antigen is intracellular and incubated with primary antibody overnight at 4°C as detailed in Table 1. Primary antibody binding was detected using the relevant biotinylated secondary antibody for 1 hour (See Table 1) and an ABC kit (Vector Laboratories, UK), 1:100, 45 min. Immunoreactivity was revealed using diaminobenzidine HCl (DAB) (0.016% w/v, Sigma, UK) and (0.05% v/v) H_2O_2 (30% w/v) in sodium phosphate buffer (0.1M, pH7.4) to yield an insoluble brown precipitate. Sections were counter-stained with 0.5% (w/v) cresyl violet in water, dehydrated through a series of ethanol baths at 70%, 95%, 100% and 100% (v/v) in water) and cleared in xylene (Fisher Scientific, UK). Slides were mounted using DPX mounting medium (Fisher Scientific, UK)

Antigen	Primary Antibody	Dilution	Secondary Antibody	Dilution
CXCR4	Rabbit anti-CXCR4 (AbCam)	1:100	Biotinylated anti-Rabbit IgG	1:100
GFAP	Rabbit anti-GFAP (DAKO)	1:500	Biotinylated Goat anti-Rabbit IgG	1:100
GFAP	Rat anti-GFAP (Invitrogen)	1:500	Biotinylated anti-Rat IgG	1:100
GFP	Chicken anti-GFP (AbCam)	1:1000	Biotinylated anti-Chicken IgG	1:1000
IBA-1	Goat anti-IBA-1 (AbCam)	1:500	Biotinylated anti-Goat IgG	1:100
ICAM-1	Rabbit anti-ICAM-1 (R&D systems)	1:1000	Biotinylated anti-Rabbit IgG	1:500
IL-6	Rabbit anti-IL-6 (AbCam)	1:100	Biotinylated anti-Rabbit IgG	1:100
IL-1β	Rabbit anti-IL-1β (AbCam)	1:100	Biotinylated anti-Rabbit IgG	1:100
iNOS	Rabbit anti-iNOS (AbCam)	1:50	Biotinylated anti-Rabbit IgG	1:100
OX42	Rat ant-OX42 (Serotec)	1:200	Biotinylated anti-Rat IgG	1:100
TSPO	Rabbit anti-PBR (AbCam)	1:50	Biotinylated anti-Rabbit IgG	1:100
VCAM-1	Rat anti-VCAM-1 (Southern Biotech)	1:250	Biotinylated anti-Rat IgG	1:100

Table 1: Immunohistochemistry antibody concentrations

2.1.4 Tumour and astrocyte activation quantification

Immunohistochemical slides were scanned at 200x magnification using the ScanScope CS system (Aperio, USA). In the intracardiac model, tumour area and the associated area of astrocyte activation were demarcated manually and areas calculated using ImageScope software (Aperio, USA). The area of astrocyte activation was defined as the outer limit of reactive astrocytes, visible owing to the intense staining of processes and cell bodies (as illustrated in Figure 2.1).

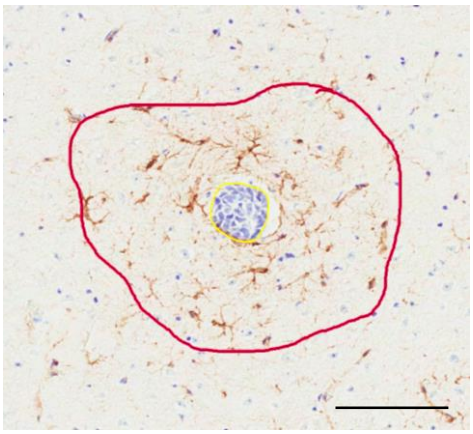

Figure 2.1: The area of astrocyte activation and tumour area was delineated using ImageScope software. Immunohistochemistry was performed as described in section 2.1.3. The area of tumour growth was demarcated using a cresyl violet counterstain (blue, yellow outline). Astrocyte reactivity was determined based on GFAP expression and stellate morphology (red outline). Scale bar= 100μm.

For the intracerebral model, sections were taken throughout the striatum. Tumour area and the associated area of astrocyte activation were demarcated as described above, on every fifth section. Tumour and astrocyte activation volume was calculated by multiplying area by the tissue section thickness (accounting for missing sections) and summing across the striatum.

2.1.5 Immunocytochemistry

Primary astrocyte cultures were passaged by washing with PBS and incubating with trypsin, as described in section 2.1.1.2. Trypsin activity was blocked with glial culture medium, and then the cells were collected by sedimentation (800x*g*, 5 minutes, 4°C). In order to confirm the presence of astrocytes in the culture, the pellet was re-suspended in glial medium and plated in a 6 well plate, containing cover slips, previously sterilised with UV light (15min each side in a CL-1000 Ultraviolet Crosslinker, UVP). After 48 hours growth, cells were removed from the incubator for fixation. All subsequent steps were performed at room temperature. Wells were washed with PBS and fixed with 4% w/v paraformaldehyde (PFA) in phosphate buffer for 10 minutes. Cells were permeabilised with PBS supplemented with 0.025% v/v Triton X-100 (10 minutes) and then washed with PBS supplemented with PBS-T (3 x 5 minutes), blocked with streptavidin solution (20 minutes) followed by biotin solution (20 minutes, Vector Laboratories, UK). Non-specific antibody binding was blocked with TNB (Tris-NaCl blocking buffer; 0.1M Tris-HCl pH7.5, 0.15M NaCl, 0.5% w/v Blocking Reagent, Perkin Elmer, UK) for 30 minutes, prior to incubation with rabbit anti-mouse GFAP (1:500, Dako) for 2 hours. Primary antibody binding was detected using a goat anti-rabbit biotinylated antibody (1:100, 30 minutes, Vector Laboratories) and streptavidin-Cy3 (1:300, 30 minutes, Invitrogen). Cover slips were mounted on Superfrost® Plus slides (Thermoscientific, UK) using DAPI mounting medium for nuclei detection (Vector Laboratories, UK). Fluorescence was visualised using a Leica DM IRBA epifluorescent microscope.

2.1.6 Astrocyte proliferation assays

2.1.6.1 In vitro MTT assay for astrocyte proliferation

Astrocytes were isolated as previously described and plated in a 6 well plate. When cells had reached approximately 50% confluence, the medium was aspirated and replaced with either tumour conditioned medium (harvested as previously described) or astrocyte culture medium. After 24 hours incubation at 37°C, 5% CO_2 the effect on cell proliferation was determined, using a colorimetric MTT dye reduction assay. Assay medium was prepared by mixing 2 volumes of culture medium with 1 volume of MTT solution (3-(4,5-dimethylthiazol-2-yl)-2,5-diphenyltetrazolium bromide, 5mg/mL). Each well had 2 mL assay medium added and was incubated for 4 hours at 37°C. The medium was then removed and replaced with 1 ml DMSO in order to dissolve the purple formazan crystals that had formed. Absorbance was measured by a photometric microplate reader (Tecan, Switzerland) at 570 nm within 30 minutes of dissolving crystals.

2.1.6.2 *In vivo* astrocyte proliferation

Female BALB/c mice were injected intracardially, as previously described, with 100μL PBS containing 1 x 10^5 4T1-GFP cells. At either day 9 (n=4) or day 20 (n=3) post tumour inoculation, mice were injected intra-peritoneally (i.p.) with 100 μL bromodeoxyuridine (BrdU, Sigma) at 100 mg/kg in saline. After 24 hours, mice were again injected i.p. with BrdU at the same dose. After a further 4 hours, animals were perfused with 4% PFA in phosphate buffer (pH 7.4) and post-fixed

over-night in 4% PFA. Tissue was processed for slicing as previously described and 10 μm sections were collected throughout the brain, at a 1 in 20 sampling rate. Immunofluoresence co-localisation was used to reveal proliferative astrocytes. A modified procedure of the basic immunohistochemistry protocol described above was required due to the nuclear localization of the antigen. Sections were washed in PBS-T (3 x 5 minutes) and then fixed for 45 minutes in 70% ethanol, diluted with 50mM glycine. After washing (3 x 5 minutes, PBS-T), slides were then incubated for 15 minutes with 0.05% trypsin-EDTA at 37°C. Subsequently, DNA was denatured with 4N HCl 20 minutes at room temperature. After washing 3 times with PBS-T to neutralise the tissue pH, endogenous streptavidin/biotin was blocked as previously described. Background staining was blocked using an incubation buffer (Roche) for 10 minutes, at room temperature. Sections were incubated with primary antibodies, 1:100 sheep anti-Brdu (AbCam) and 1:500 anti-GFAP (Invitrogen), overnight at 4°C. After incubation, sections were washed with PBS-T and incubated for 45 minutes with biotinylated anti-sheep secondary antibody (1:100, Vector Laboratories). After washing, sections were incubated with streptavidin-AMCA (1:100, Vector Laboratories) and Texas Red anti-rat (1:100, Vector Laboratories). Slides were mounted with fluorescence mounting medium (Vector Laboratories) and staining observed using an epi-fluorescence microscope. The extent of astrocyte proliferation around brain metastases ($n > 10$ per animal) was determined by quantifying the number of BrdU+/GFAP+ nuclei in the field of view surrounding a tumour.

2.1.7 RT-qPCR quantification of inflammatory markers in the tumour microenvironment

2.1.7.1 Animal models

For the intracerebral model, female SCID mice (n=5 per time point) were injected intrastriatally with 5 x 10^3 MDA-BR-231 cells in 0.5 μl saline, or with 0.5 μl saline alone (n=5) as described in section 2.1.2.2. At day 14, animals were perfused with heparinised saline. The ipsilateral striata of each of the treatment groups were dissected and snap-frozen in liquid nitrogen. Tissue was stored at -80°C prior to RNA extraction.

For the intra-cardiac model, SCID mice (n=4 per time point) were injected intracardially with 10^5 MDA-BR-231 cells as described in section 2.1.2.1. At day 14 and 21, animals were perfused with heparinised saline. The brain was dissected into 3 regions, as illustrated in Figure 2.2, and snap-frozen in liquid nitrogen. Tissue was stored at -80°C prior to RNA extraction.

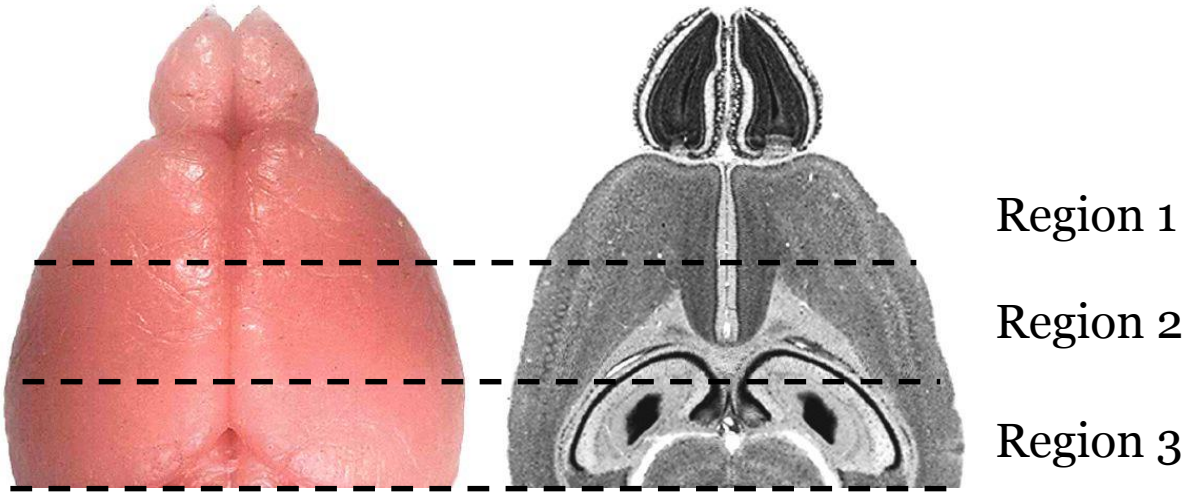

Figure 2.2: Schematic showing the dissection of the brain for RNA extraction. The cerebellum was discounted in this analysis. Tissue was processed separately to maximize RNA yield. RT-qPCR was run on brain regions in isolation, with data pooled for whole brain analysis. Figure adapted from (Airey et al., 2001).

2.1.7.2 RNA extraction

For each brain region analysed, tissue was dissected into three pieces and processed separately so as to maximize RNA extraction. RNA was then pooled at the end of the extraction protocol. RNA was extracted from mouse tissue using a Qiagen® RNeasy® Mini Kit (Qiagen, UK). β-mercaptoethanol (BME) was added to the RLT buffer (1% v/v), to inhibit endogenous ribonucleases that may be present in the sample, in order to maintain RNA integrity. Tissue samples were homogenised in RLT + BME. Buffer RLT is a lysis buffer that also enhances binding of RNA to the silica membrane in the RNeasy Mini spin column, due its guanidine isothiocycanate component. Homogenised samples were transferred to a QIAshredder column (Qiagen, UK) and centrifuged at 10000xgfor 3 minutes in a Biofuge™ Pico Heraeus™ centrifuge (Thermoscientific, UK), in order to remove

cell and extra-cellular matrix debris. The flow through was added to 70% v/v ethanol in water and inverted several times. Subsequently, the sample was transferred to an RNeasy Mini spin column in a 2ml collection tube. In the presence of ethanol, RNA precipitates, whilst protein and salts remain soluble, and hence flow through the column. The column was eluted by centrifugation (10,000xg, 15 s) and the flow-through discarded. 700µl of Buffer RW1 was subsequently added to the RNeasy spin column, and centrifuged at 10,000 RPM for 15 seconds. RW1 is a wash buffer which removes lipids, carbohydrates and protein that may have non-specifically bound to the silica membrane. Subsequently, 500 µl RPE (containing ethanol) was added. RPE is a wash buffer that removes salts from the column. The column was spun at 10000 RPM for 15 seconds, and flow through discarded. This was repeated, before changing collection tube and spinning the column spun for 2 minutes at 10000 RPM, removing ethanol contamination. The column was transferred to an Eppendorf, and 25 µl of RNase-free water was added to the membrane. After leaving to stand for 1 minute, the column was spun at 10000 RPM for 1 minute, eluting the RNA.

Contaminating genomic DNA was removed using a DNase treatment as per the manufacturer's instructions (PrimerDesign Ltd, UK). 5µl of *Precision*™ DNase reaction buffer was added per 50 µl of RNA solution, along with 1 µl of *Precision*™ DNase enzyme. The solution was incubated for 10 minutes at 30°C and subsequently the enzyme was inactivated by heating the mixture to 55°C for 5 minutes. RNA yield was calculated using a NanoDrop® Spectrophotometer ND-1000 (ThermoScientific), and samples stored at -80°C until further use.

2.1.7.3 cDNA synthesis

cDNA was reverse transcribed from RNA template using a *Precision*™ nanoScript Reverse Transcription kit (PrimerDesign Ltd, UK) as per the manufacturer's instructions. All reactions were carried out in 0.2ml PCR tubes (Starlabs). For the annealing step, per sample, typically 750 ng RNA template was combined with 1µl reverse transcription primer and the final volume made up to 10 µl using RNAse/DNAse free water. The sample was then heated to 65°C for 5 minutes to allow primer annealing, prior to immediate cooling on ice. Subsequently, for each reaction, the following master mix was made (Table 2)

Component	Per Reaction (µl)
nanoScript 10x buffer	2
dNTP mix (10mM)	1
Dithiothreitol (DTT, 100mM)	2
RNAse/DNAse free water	4
nanoScript enzyme	1
Final Volume	**10**

Table 2: Mastermix for cDNA sytnthesis

10µl was added to each of the samples on ice prior to vortexing and incubating for 20 minutes at 55°C. The reaction was subsequently heat activated by incubation at 75°C for 15 minutes. Heat incubations took place in a TC-512 termocycler (Techne, UK). cDNA was stored at -20°C until use.

2.1.7.4 RT-qPCR

RT-qPCR experiments were conducted so as to comply with MIQUE guidelines.

Housekeeper gene selection

cDNA from the striatum of SCID mice injected intracerebrally with MDA-Br-231 cells (n=3) was used to select two stable housekeeping genes. The contralateral hemispheres were used as control tissue. The cDNA was diluted to a concentration of 5ng/µl, and 5 µl added per well of a non-skirted 96 well plate (4titude, UK). Each

sample was added in duplicate, with enough wells filled to test 6 different housekeeping genes. A panel of 6 housekeeping genes (HKGs), determined to be mouse specific by PrimerDesign were trialled: zinc finger protein 91 (ZFP91), cell division cycle 40 (CDC40), β actin (ActB), glyceraldehydes 3-phosphate dehydrogenase (GAPDH), succinate dehydrogenase complex, subunit A (SDHA) and calnexin (CANX). The lyophlised primer was resuspended in 220 µl RNAse/DNAse free water and vortexed. The solution was left to stand for 5 minutes before use, prior to vortexing again. Per sample, the reaction mixture was made as detailed in Table 3. Primers were diluted to a working concentration of 300 mM in a 20 µl reaction.

Component	Per Reaction (µl)
GOI primer	1
PrimerDesign Precision 2X RT-qPCR Mastermix	10
RNAse/DNAse free water	4
Final Volume	**15**

Table 3: Mastermix for RT-qPCR

15 µl of the reaction mixture described in Table 3 was added to each well, as per a pre-defined plate layout. The plate was sealed with a PCR plate seal (4titude, UK) and spun at 250xg for 1 minute, in order to mix the sample and mastermix.

RT-PCR was performed in a Stratagene RT-qPCR machine (Agilent, UK) with MxQPCR software (Agilent, UK), using the amplification protocol detailed in Table

4. During the data collection phase, fluorogenic data was collected through the 6-carboxyfluorescein (FAM) channel, which detects Syber green. A melt curve was also required at the end of the cycling.

Step	Time	Temperature (°C)
Enzyme activation	10 minutes	95
Denaturation	15 s	95
Data collection	60s	60

Table 4: Amplification conditions for RT-qPCR. 50 cycles were performed before a melt curve was conducted (1 minute at 95°C, 30 sec at 55°C and 30 sec at 95°C).

The RT-qPCR data was analysed using qbase^{plus} software (Biogazelle, UK) as per the manufacturer's instructions, in order to determine which housekeeping gene expression levels remained most stable between treatment and control groups.

Gene of Interest RT-qPCR

9 genes of interest (GOI) were probed using qPCR. The primer sequences, along with amplicon size are defined in Table 5. Firstly, standard curves were performed in order to confirm primer efficiency. A standard curve was generated by creating a top standard, comprised of a combination of each of the samples. This top standard was then serially diluted to generate 6 standards. Each GOI was tested with a standard curve. 15 µl of mastermix, as described in Table 3, was added per well, and the plate run as described in Table 4. 100% efficient primer reactions double the amount of cDNA per qPCR cycle. This translates to a slope of -3.3 when

cycle number values (ct) are plotted against the $\log_{10}$ sample concentration, as shown in Figure 2.3.

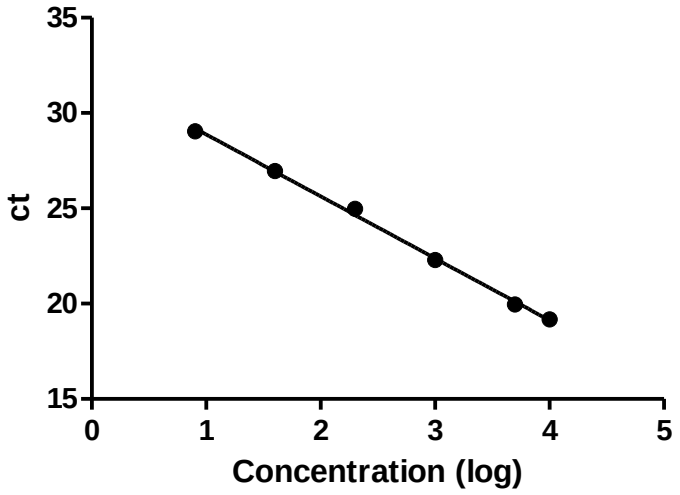

Figure 2.3: Standard curve for the HKG, CANX. The gradient is equal to -3.3, reflecting 100% primer efficiency.

Once primer efficiency was established, experimental samples analysis was performed. As comparisons in expression levels are being made across time-points, all experimental and control samples were run on the same plate, along with two housekeeping genes and one or more GOIs. As detailed for the GeNorm experiment, cDNA was diluted to 5 ng/μl and 5 μl added per well. All samples were run in duplicate for each of the GOIs/HKGs. 15 μl of mastermix, as described in Table 3, was added per well, and the plate run as described in Table 4.

GOI	Official gene symbol	Product length (bases)	Melting temperature (°C)	Sense primer	Anti-sense primer
Endothelin-1	Edn1	102	77	GGTGTTCCCTAGCCTGTCT	ATCGTGTCTCTGCTCTCTGA
Heparanase	Hpse	130	75.2	TGCCTCTTCTCTTCGTCCTT	CCTTTACCGTCATTTCCAAACC
iNOS	Nos2	105	75	GTGTTCTTTGCTTCCATGCTAAT	GTCCCTGGCTAGTGCTTCA
Interleukin-1β	Il1b	129	74.1	GCTATGGCAACTGTTCCTCAA	ACAGCCCAGGTCAAAGGTT
Interleukin-6	Il6	129	75.6	ATTCCAGAAACCGCTATGAAGT	ATCCTCTGTGAAGTCTCCTCTC
Matrix metalloproteinase2	Mmp2	84	70.9	TTAACCAGCCTTCTCCTTCAC	GTACAGTCACCTTTCTTTG
Nestin	NES	147	78.5	CCAAAGAGGTGTCCGATCATC	CTCCTTCTTCTTCATCAGCATCT
Phosphacan	Ptprz1	122	68.8	TGAATCCAGTTCTGTTATTTGTTTAC	ACATAATAAGTGAATTACAAGAAGTCA
TNF	Tnf	96	73.4	CCCACTCTGACCCCTTTACT	CCTGAGCCATAATCCCCTTTC

Table 5: Primer details for GOIs

qPCR data were analysed in terms of fold expression relative to averaged naive tissue, using the following equation:

$$\text{Fold expression} = \frac{(\text{Efficiency GOI primer})^{\text{Control GOI Ct value- Experimental GOI Ct value}}}{(\text{Efficiency HKG primer})^{\text{Control HKG Ct value- Experimental GOI Ct value}}}$$

2.1.7.5 Histological confirmation of gene of interest expression

Immunofluoresence was performed on tissue from intracerebral animals perfused at day 14 after tumour cell injection. Sections were washed with PBS-T and endogenous peroxidase activity blocked with PBS + 1% (v/v) H2O2 for 20 minutes. Streptavidin/Biotin activity was blocked with streptavidin solution (20 minutes) followed by biotin solution (20 minutes, Vector Laboratories, UK). After washing (3xPBS-T), a signal enhancer was used (Image iT FX signal enhancer, Invitrogen), incubating sections for 30 minutes. After washing (3xPBS-T), non-specific antibody binding was blocked with TNB (Tris-NaCl blocking buffer; 0.1M Tris-HCl pH7.5, 0.15M NaCl, 0.5% w/v Blocking Reagent, Perkin Elmer, UK) for 40 minutes, prior to incubation with primary antibodies (anti-GFAP and anti-IL-6, anti-IL1β and anti-iNOS), for 2 hours or overnight at 4°C, as detailed in Table 1. In the cases of IL-6, IL1β and iNOS, primary antibody binding was detected using a goat anti-rabbit biotinylated antibody (1:100, 30 minutes, Vector Laboratories), prior to streptavidin-HRP (Perkin Elmer) incubation (1:200, 30 minutes) and TSA amplification (Biotinyl tyramide reagent, Perkin Elmer, 1:100, 7 minutes). Amplification was visulaised with streptavidin-AMCA (1:100, 30 minutes). GFAP reactivity was revealed with Texas-red fluorophore (1:100, 30 minutes). Sections

were mounted with fluouresence mounting medium (Vector Laborotories) and staining visualised with a Leica epifluoresence microscope.

2.2 Modulation of brain metastatic progression by chronic astrocyte activation

2.2.1 CNTF modulation of 4T1 growth in vitro

In order to determine the effect of CNTF of 4T1 cell proliferation, an MTT assay was used to assess cellular enzyme activity. 4T1-GFP cells were plated in 6 well plates at 10% confluence and incubated for 48 hours at 37°C, 5% CO_2. 6 wells were subsequently stimulated with either human CNTF (R&D Systems) at 50 ng/ml (from a stock solution of 100 μg/ml, 0.1% w/v BSA in PBS) or the relevant concentration of BSA in PBS (n=6). The effect on cell proliferation was determined after 24 hours, using a colorimetric MTT dye reduction assay, as previously described.

2.2.2 In vivo modulation of astrocyte reactivity

The CNTF- and LacZ-lentivirus were obtained from Carole Escartin's group in Paris, synthesised as previously published (de Almeida et al., 2001). Briefly, a modified self-inactivating lentivirus was used to clone cDNA coding β-galactosidase (LacZ, control virus) or human CNTF. The viral particles were produced by transfection of 293T cells, with the supernatant collected after 48 hours. Further details regarding the viral vector can be found in Chapter 4.

2.2.2.1 Animal models

Female BALB/c mice were anaesthetised with 2% (v/v) isoflurane in a gas mix of oxygen and nitrous oxide (30:70), and placed on ear bars in a small animal stereotactic frame (Stoetling Co., USA) as described in section 2.1.2.2. Mice were injected intrastriatally (+0.5 mm Bregma, + 2 mm from the midline, - 2.5 mm depth) with 1 μl of CNTF-lentivirus, LacZ-lentivirus (both at 100 ng/μl in saline) or saline using a finely pulled capillary (Calibrated microcapillary tube, 1-5 μl, Sigma-Aldrich). Capillaries were pulled with a single stage glass microelectrode puller (Narishige, model PP-830, Japan), heated to 76°C.

2.2.2.2 MRI

In order to assess BBB integrity in response to CNTF-lentivirus, animals underwent MRI at 5 weeks post-virus injection. MRI data were acquired on a 7T magnet with a Varian Inova spectrometer (Varian), using a Rapid 26 coil. T1 weighted images (slice thickness=1mm) were acquired using a Spin Echo Multi Slice (SEMS) sequence (TR= 300ms; TE= 16.38 ms; FOV =25 x 25 mm; matrix size 256 x 256) both pre- and 5 min post-I.V. Gadolinium-DTPA (Omniscan; GE Healthcare) injection (50 μL, 0.5mmol/ml). Images were processed with VMRJ software (Varian).

2.2.2.3 Histology

5 weeks after intra-striatal injection of CNTF-, LacZ-lentivirus or saline, animals were perfusion fixed (n=4 per treatment), and tissue processed for histology, to assess astrocyte and microglial activation, as well as ICAM-1 and VCAM-1 expression, as described in section 2.1.3 and in Table 1.

Subsequently, mice from each treatment group were injected intracardially, under ultra-sound guidance, with 1 x 10^5 4T1-GFP cells in 100 μl PBS. At day 10 (n=9), 14 (n=5) and 21 (n=2) after 4T1-GFP cell injection, animals were perfusion-fixed and tissue processed for histology. 10 μm sections were taken across the striatum, with every 5^{th} section stained for GFP to reveal tumour burden following the standard immunohistochemistry protocol described above and in Table 1.

Tissue sections were scanned at 200x magnification using the ScanScope CS system (Aperio, USA) and micrometastases were delineated using ImageScope software (Aperio, USA). In order to define tumour number and volume, micrometastases or 'events' were tracked throughout the processed tissue, with continuing tumours, which may be comprised of several micrometastases, as illustrated in Figure 2.4, assigned an ID. The area and perimeter of each individual event was measured for each section on which it appeared. The data were imported into Matlab and processed using a code developed by Alastair Hamilton (Hamilton, A., DPhil thesis, 2013). In order to determine overall tumour volume, the areas of all individual events in the same tumour in a given section were summed and multiplied by 10 to give a volume (μm^3). As consecutive sections were omitted during cutting, the volumes of 'missing' sections were estimated by linear interpolation. The total tumour volume was

calculated as the sum of all the tumour volumes on each section. For each individual tumour, its hemisphere location was noted such that ipsilateral/contralateral comparisons could be made.

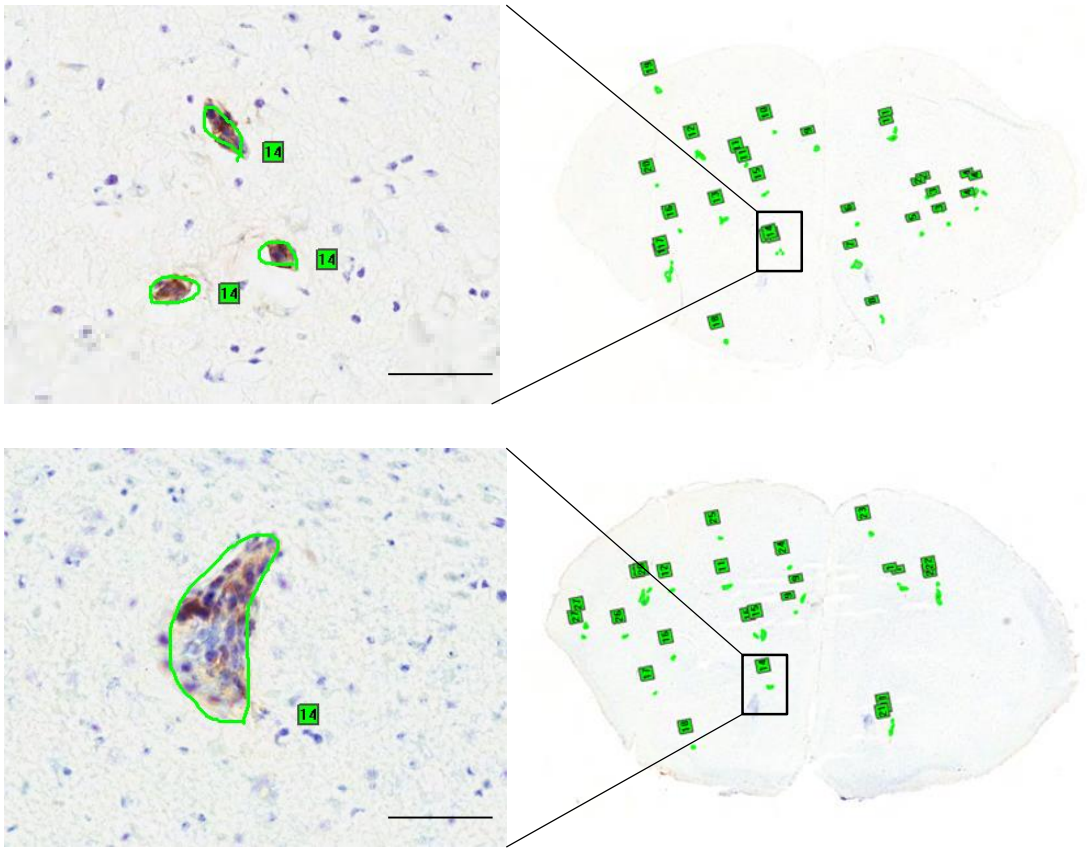

Figure 2.4: Tumour number was quantified by assigning metastatic colonies an individual ID, and tracking metastatic growth over the brain region. A) Multiple components of the same tumour are assigned the same ID (#14). B) A tumour at the same locus in the proximal section is assigned the same ID. Individual areas quantified in ImageScope (Aperio, USA), were exported to Matlab to calculate individual tumour volume and number, as described above. Scale bars = 100μm.

2.2.3 RT-qPCR quantification of factors induced by CNTF and tumour-conditioned media

In order to determine the transcriptional profile of astrocytes in response to CNTF stimulation, an astrocyte primary culture was established as described in section 2.1.1.2. Upon passaging, the pellet was re-suspended in glial culture medium and plated in T25 tissue culture flasks. At 5 days after seeding, astrocyte monolayers were treated with human CNTF (R&D Systems) at a concentration of 50 ng/μl, in glial culture media (n=3 flasks). Alternatively, astrocyte monolayers were treated with tumour-conditioned medium (n=3 flasks), derived from 4T1 cell cultures 24 hours after seeding, and sedimented by centrifugation to remove debris (250xg, 5 min, RT). Three control flasks were treated with glial culture medium alone. In all cases, astrocyte cultures were incubated for 24 hours prior to RNA extraction.

2.2.3.1 RNA isolation

In order to extract RNA from cell culture, a Qiagen® RNeasy® Mini Kit was used (Qiagen, UK) as per the manufacturer's instructions. All procedures took place on ice where possible to maintain RNA stability. Cells, treated as bove, were harvested by trypsin dissociation and collected by sedimentation (250xg, 5 min, RT). The pellet was re-suspended in 350 μl Buffer RLT and combined with 350 μl 70% ethanol, with the remainder of the protocol as described in section 2.1.7.2.

2.3 2B3-201 inhibition of astrocyte activation

2B3-201 is a liposomal-packaged steroid. Previous work within the group (Matthew Evans, DPhil thesis, 2012) suggests that this compound selectively inhibits astrocyte activation, whilst the microglial response to CNS challenge is not modulated. Therefore, the aim of this work is to ascertain whether astrocyte inhibition, using 2B3-201, alters tumour seeding and/or tumour growth.

2.3.1 Validation of 2B3-201

2.3.1.1 Animal models

In order to determine whether 2B3-201 can prophylactically inhibit astrogliosis in response to an inflammatory challenge, female BALB/c mice were injected intravenously with either 0.2 mg/kg of 2B3-201 (approximately 100 μl, n=6) or saline (n=6). After 24 hours, animals were anaesthetised and injected intrastriatally, as previously described, with 10^5 plaque forming units (PFU) of a replication-deficient adenovirus expressing membrane-bound TNF cDNA ($Ad5TNF\alpha_m$) in 0.5 μl saline. After 5 days, animals were perfusion fixed, as previously described.

In order to determine whether 2B3-201 can selectively inhibit astrogliosis after induction by an inflammatory challenge, animals were injected intrastriatally, as previously described, with 10^5 PFU TNF-Adenovirus in 0.5 μl saline. After 3 days, animals were injected intravenously with 0.2 mg/kg of 2B3-201 (n=6) or saline (n=6). At day 5 post-adenovirus injection, animals were perfusion fixed, as

previously described. In both instances, astrocyte reactivity was determined by histology, using an anti-GFAP antibody, as described in section 2.1.3.

2.3.2 Does 2B3-201 modulate tumour seeding?

In order to determine whether astrocyte inhibition alters metastatic cell colonisation, female BALB/c mice were injected with either 0.2 mg/kg 2B3-201 in approximately 100 μl saline (n=6), empty liposome solution (n=6) or saline (n=3). After 24 hours, mice were injected intracardially with 10^5 4T1-GFP cells, as previously described. After 10 days, animals were perfusion-fixed and tissue processed for histology. 10 μm sections were taken in 3 different brain regions, using a 1 in 5 sampling rate: Region 1) 3 mm to 1.3 mm, Region 2) -0.5 mm to -1.5 mm, Region 3) -4 mm to -5 mm relative to Bregma (Figure 2.5). Tumour burden was detected with GFP immunohistochemistry, as previously described. Tissue sections were scanned at 200x magnification using the ScanScope CS system (Aperio, USA) and micrometastases were delineated using ImageScope software (Aperio, USA). Tumour number was calculated as described above (section 2.2.2.3), and normalised to the volume of tissue quantified.

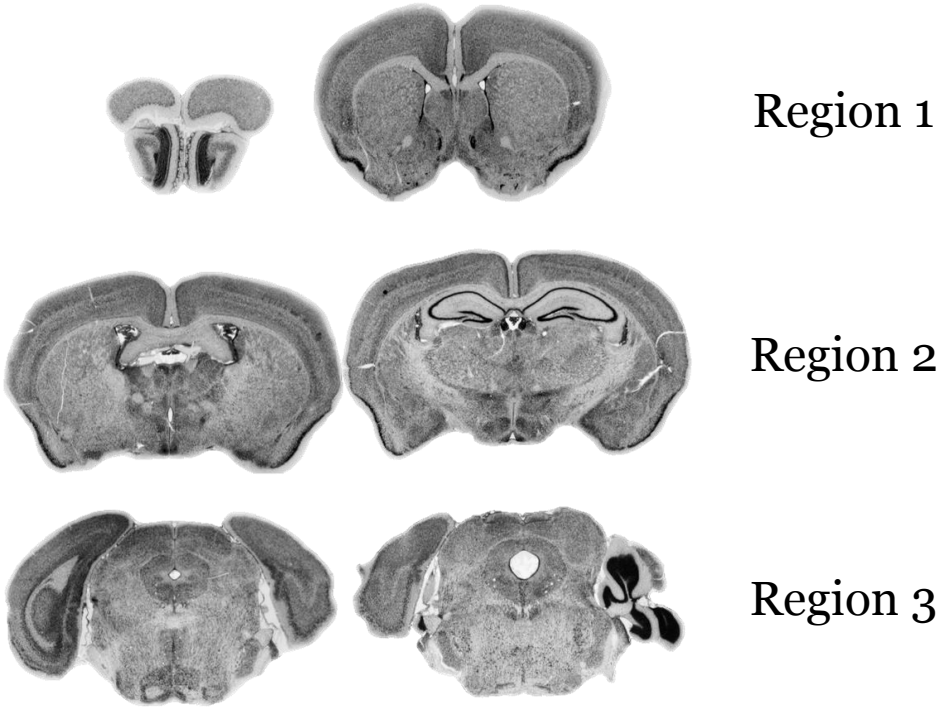

Figure 2.5: Brain regions sampled from to calculate tumour burden in the 2B3-201 studies. Region 1) 3 mm to 1.3 mm, Region 2) -0.5 mm to -1.5 mm, Region 3) -4 mm to -5 mm relative to Bregma. Image adapted from the Mouse Brain Atlas (http://www.mbl.org/mbl_main/atlas.html).

2.3.3 Does 2B3-201 modulate tumour growth?

In order to determine whether astrocyte inhibition alters metastatic growth, female BALB/c mice were injected intra-cardially with 10^5 4T1-GFP cells, as described in section 2.1.2.1. At day 7 post-tumour inoculation, animals were injected intravenously with either 0.2 mg/kg 2B3-201 in approximately 100 µl saline (n=6), empty liposome solution (n=6) or saline (n=3). This dosing was repeated at day 12 post tumour inoculation. At day 14, animals were perfusion-fixed, and brains harvested for detection of tumour burden with GFP immunohistochemistry, as

previously described. 10 μm sections were taken in 3 different brain regions, using a 1 in 5 sampling rate: Region 1) 3 mm to 1.3 mm, Region 2) -0.5 mm to -1.5 mm, Region 3) -4 mm to -5 mm relative to Bregma. Tissue sections were scanned at 200x magnification using the ScanScope CS system (Aperio, USA) and micrometastases were delineated using ImageScope software (Aperio, USA). In order to determine tumour burden, the individual micrometastatic areas were summed and normalised for the tissue area quantified.

Astrocyte activation was also assessed, using GFAP immunohistochemistry, as described in section 2.1.3. In order to quantify the extent of astrocyte activation associated with tumour burden, the area of astrocyte activation was delineated in image scope and compared to tumour area, in approximately 50 tumours per treatment group, across 3 animals.

2.4 Glial activation as a biomarker for metastatic disease

2.4.1 Immunofluorescent detection of TSPO

To determine astrocyte, microglial and 4T1 cell expression of TSPO *in vivo,* fluorescent co-localisation was used. Briefly, endogenous streptavidin and biotin were blocked as described above (SP-2002, Vector Laboratories) and then incubated with Tris-NaCl blocking buffer (TNB, PerkinElmer, UK). Sections were incubated overnight at 4°C with the appropriate primary antibody (Table 1), rinsed with PBS and incubated with biotinylated anti-rat IgG (1:100, Vector Laboratories) in TNB (30min, room temperature). Slides were washed and incubated with a

streptavidin-Cy3 fluorophore (1:300, Invitrogen) and AMCA anti-Rabbit (1:50, Vector Laboratories) for one hour. Slides were mounted using Vectashield mounting medium (Vector Laboratories).

Images were acquired using an inverted confocal microscope (LSM-710, Carl Zeiss Microimaging, Jena, Germany) or Leica DM IRBE (Leica, Germany) attached to a camera (Hamamatsu, Japan), and analysed using Zen (Carl Zeiss) or Simple PCI (Hamamatsu, Japan) software. Detection ranges were set to eliminate crosstalk between fluorophores: 409-485 nm for AMCA (TSPO visualisation), 494-553 nm for GFP (4T1 cell visualisation) and 564-712 nm for Cy3 (GFAP/OX-42 visualisation).

2.4.2 SPECT imaging of brain metastasis with 123I-DPA713

2.4.2.1 DPA713 synthesis

N,*N*-Diethyl-2-[2-(4-hydroxy-phenyl)-5,7-dimethyl-pyrazolo[1,5-*a*]pyrimidin-3-yl]-acetamide (DPA713) was synthesised as previously described (Reynolds et al., 2010) by Dr B. Checha.

2.4.2.2 ^{123}I labelling of DPA713

Radiolabeling was performed by Dr. M Tredwell, following a modified version of the procedure described by Wang *et al.* (2009). Briefly, non-carrier added ^{123}I as a 0.05M solution of NaOH (GE Healthcare, UK). One Pierce iodination bead (Thermo Scientific, UK) was added to a solution of *N*,*N*-diethyl-2-[2-(4-hydroxy-

phenyl)-5,7-dimethyl-pyrazolo[1,5-*a*]pyrimidin-3-yl]-acetamide (2 mg) in acetonitrile (0.1 mL), methanol (0.1 mL) and phosphate-buffered saline (0.1 mL). Subsequently, 260 MBq of non-carrier added [^{123}I]NaI (GE Healthcare, UK) was added. The reaction was stirred at room temperature for 90 minutes, prior to dilution with water (5 mL) and loading onto a pre-conditioned C18 Sep-Pak Light cartridge (Waters, USA). The radioactive component was eluted with diethyl ether (0.5 mL). The diethyl ether was removed under a stream of solvent and the crude reaction mixture was re-dissolved in dimethylformamide (DMF) (0.2 mL). K_2CO_3 (10 mg) and methyl iodide (30 μL of a 2M solution of Me-I in DMF) were added and the solution heated at 60°C for 60 minutes. The crude reaction mixture was purified directly by reverse phase HPLC on a Phenomenex Luna 5 μm C18 column (Phenomenex, UK). The radioactive fraction, corresponding to the desired product was collected, was diluted with water and passed through a pre-conditioned C18 Sep-Pak Light cartridge and, subsequently, eluted with ethanol (0.4 mL) to yield 96 MBq (36 % radiochemical yield) of ^{123}I-DPA713.

2.4.2.3 Animal models:

BALB/c mice were imaged 13 days after intracerebral injection of either 4T1-GFP cells (n=6) or saline (n=3), as described in section 2.1.2.2. Additionally, mice were imaged 21 days after intracardiac injection of either 10^4 4T1 GFP cells (n=5) or saline (n=3) as described in section 2.1.2.1.

2.4.2.4 MRI

24 hours prior to SPECT/CT, intracardially injected animals were imaged by MRI so as to determine areas of high metastatic burden, using BBB breakdown as a surrogate for tumour growth. MRI data were acquired on a 7T magnet with a Varian Inova spectrometer (Varian), using a Rapid 26 coil. T1 weighted images (slice thickness = 1mm) were acquired using a Spin Echo Multi Slice (SEMS) sequence (TR= 300ms; TE= 16.38 ms; FOV =25 x 25 mm; matrix size 256 x 256) both pre- and 5 min post-I.V. Gadolinium-DTPA (Omniscan; GE Healthcare) injection (50 μL).

2.4.2.5 SPECT Imaging

Animals were intravenously injected with *ca.* 20MBq ^{123}I-DPA713, 1h prior to SPECT. Mice were anaesthetised with 1.5-2.0% isoflurane in air and SPECT/CT was performed using a nanoSPECT/CT scanner (Bioscan, USA), equipped with 9-pinhole apertures (pinhole diameter of 1mm). SPECT imaging was performed using 100,000 counts/projection, 24 projections and a pitch of 1.5. CT was conducted for anatomical referencing (180 projections, 500 ms/projection, 45 kV, 177 μA). Acquisition parameters were as follows: FOV, 35.2 x 35.2 mm; data matrix, 186 x 186; acquisition time, *ca.* 1h. Data were reconstructed using InVivoScope (version 1.43, Bioscan, USA) and analysed using Inveon Research Workplace (Siemens, Germany).

2.4.2.6 SPECT analysis

For the intracerebral model, a volume of interest was drawn on coronal CT sections over the injection site, using the bore hole in the skull for reference. The corresponding internal control was delineated in the contralateral hemisphere. Mean intensity of counts per hemisphere was used to calculate the relative increase in compound binding (ipsilateral-contralateral/control x 100). For the intracardiac model, a volume of interest was drawn throughout the brain. Average intracerebral activity (KBq) over said volume, was normalised to average extracranial activity, using CT as anatomical reference.

2.4.2.7 Autoradiography

Following all SPECT imaging, animals were transcardially perfused with heparinised saline. Brains were removed and fresh-frozen in isopentane and kept on dry ice before transfer to a cryostat at the end of the imaging session. 20μm thick coronal sections were cut throughout the striatum with serial sections taken for immunohistochemistry and autoradiography. For autoradiography, slides were placed on Super Resolution Phosphor screens (Perkin Elmer, UK). Screens were held in autoradiography cassettes (Fisher Biotech, Pitsburg USA) for 36 hours at 4°C. Subsequently, the phosphor plate was developed with Perkin Elmer Cyclone Plus using OptiQuant software (Perkin Elmer, USA).

2.4.2.8 Histology

For immunohistochemistry, slides were post-fixed in 4% PFA for 30 minutes at 4°C and then underwent immunohistochemical staining as described in section 2.1.3 (for antibody concentrations see Table 1). OX-42 was used to detect activated

microglia owing to the fact that the anti-IBA-1 antibody was unsuitable for use with fresh-frozen tissue.

2.4.3 PET imaging of brain metastasis using 18F-GE180

2.4.3.1 GE180 synthesis

GE180 was synthesized by our industrial collaborators, GE Healthcare, as previously described in the literature (Wadsworth et al., 2012).

2.4.3.2 18F labeling of GE180

GE180 was labeled with ^{18}F by Immi Khan and Gareth Smith at GE Healthcare. Briefly, [^{18}F]GE180 was prepared by direct nucleophilic [^{18}F]fluorination of its corresponding mesylate precursor. The preparation was performed on a GE FASTlab™ synthesizer (Wickstrom et al., 2014) with semi-preparative HPLC purification. At the point of delivery, approximately 500 MBq activity was present.

2.4.3.3 Animal models

BALB/c mice were imaged 14 days after intracerebral injection of either 4T1-GFP cells (n=9) or saline (n=4) as described in section 2.1.2.2. Additionally, mice were imaged 21 days after intracardiac injection of either 5 x10^4 4T1 GFP cells (n=4) or saline (n=3), as described in section 2.1.2.1. 24 hours prior to PET imaging, intracardially injected animals were MR imaged, as described in section 2.4.2.4.

2.4.3.4 PET imaging

PET imaging was performed using the Inveon PET/CT system (Siemens Preclinical Solutions) equipped with a custom built mouse imaging cradle. Computed Tomography (CT) based attenuation correction was performed before each PET emission scan and was also used for anatomical referencing. Animals were

anaesthetised at 2% isofluorane in air, and a cannula, filled with saline, was inserted into the lateral tail vein. Mice were placed supine, head first, in the imaging cradle, and maintained at ~3% isofluorane in air. Following the attenuation

CT-scan, 10—50 MBq of ^{18}F-GE-180, in no more than 200 μl, was injected through the cannula. The intracerebral studies were conducted using a 30 dynamic PET minute scan, in which data were histogrammed into multiple time frames; 10 x 30 seconds, 20 x 60 seconds and 1 x 300 seconds. Due to concerns regarding the pharmacokinetics of GE-180, for the intracardiac model, a 50 minute PET acquisition times was used, with the following time frames: 12 x 10 seconds, 3 x 60 seconds and frames of 300 seconds until the end of the scan. The dynamic histograms were reconstructed using a 2-dimensional filtered back-projection (FBP) algorithm. ROI image analysis was performed using the Inveon Research Workplace software (IRW, version 2.2, Siemens Preclinical Solutions).

2.5 Statistical analysis

Throughout, statistical tests were conducted in GraphPad Prism v5.0 (GraphPad software, USA). The exact statistical tests used are defined throughout the thesis in Figure legends and in the text.

Chapter 3 Temporal and spatial profile of astrocyte activation in response to brain metastasis

3.1Introduction

As discussed in the introductory chapter, astrocyte activation has been observed in response to brain metastasis, in human biopsy samples and more recently in *in vivo* studies. However, whilst these studies suggest an involvement for astrocytes from early time points of disease, the literature does not indicate the temporal and spatial relationship between astrocytes and brain metastases. Similarly, there is little *in vivo* insight into the functional role of astrocytes in the metastatic process, with the majority of studies focusing on *in vitro* co-culture systems or conditioned media experimental schemes. As such, a host of hypotheses remain to be addressed in a relevant *in vivo* model.

3.1.1.1 Characterising the nature of astrocyte reactivity

As described in the introductory chapter, astrocyte reactivity is a graded response, with the most severe reactivity resulting in the formation of a glial scar. The glial scar is characterised by astrocyte proliferation, hypertrophy, de-differentiation and the deposition of chondroitan sulphate proteoglycans (CPSGs), resulting in re-modeling of the ECM (Sofroniew, 2009). Such a phenotype is observed in response to CNS injuries, forming a physical barrier to limit the spread of damage through the parenchyma. Based on the triggers of astrocyte proliferation, astrocytes in the tumour microenvironment might potentially be in a scar phenotype. Cytokines

typically produced by tumours (TGF-β, TNF, IL-1β and IL-6) are able to induce proliferation in astrocytes and facilitate transition to the glial scar (Karimi-Abdolrezaee and Billakanti, 2012). For instance, IL-6-like cytokines have been shown to induce astrocyte proliferation *in vitro* (Levison et al., 2000). ATP and other nucleotides have also been shown to be mitogenic in astrocyte culture models (Abbracchio et al., 1994); it is known that ATP is released by dying cells, which one would expect in a metastatic lesion. Additionally, a study has shown that fully functional cancer cells can release ATP as part of an autocrine signaling mechanism (Takai et al., 2012). As such, it is reasonable to hypothesise that the tumour microenvironment is an environment permissive to astrocyte proliferation.

The consequences of glial scar formation are varied. With regards to spinal cord injury (SCI), there are beneficial effects, namely with regards to attenuating neuronal damage, repairing a compromised BBB and limiting damaging leukocyte recruitment (Karimi-Abdolrezaee and Billakanti, 2012). However, there are also detrimental effects, which in the context of SCI, involves an inhibition of axonal regeneration. Predicting the outcome of glial scar formation in response to brain metastasis, if indeed this is the case, is difficult. Whilst the release of cytokines could lead to cellular proliferation, the deposition of CSPGs and remodeling of the ECM could limit the spread of metastatic tumours through the brain.

Whilst it is clear that there is a close association between astrocyte reactivity and tumour burden in brain metastasis (Zhang and Olsen, 1995; Mendes et al., 2007; Lorger and Felding-Habermann, 2010; Seike et al., 2011), little has been done to determine how this association changes with disease progression, both in relation

to increased tumour size and over time. The only previous studies to show that a positive correlation exists between tumour size and the extent of astrocyte activation in an *in vivo* model of brain metastasis, was published in 2011, using an intracardiac injection of a metastatic lung cell line, HARA-B (Seike et al., 2011). However, in that study, the extent of astrocyte activation was defined by the intensity of GFAP fluorescence staining, and as such, does not tease apart the spatial extent of astrocyte activation from the density of astrocytes in the vicinity. Additionally, this study did not evaluate changes in the correlation between astrocyte activation and tumour burden over time. In an earlier *in vivo* study, in which a breast cancer cell line, MDA-MB-435, was injected into the intracarotid artery, astrocyte reactivity was demonstrated from as early as day 3, and over a protracted time course of 50 days (Lorger and Felding-Habermann, 2010). However, in this study astrocyte numbers surrounding brain metastases were only quantified at a single time point (day 3). Thus, it is important to fully characterise the astrocytic response in the *in vivo* models used in this thesis, with respect to both tumour burden and time. Understanding how astrocyte reactivity may be modulated by tumour size and disease time point, may yield insights into the functional consequences of astrocyte activation. In this chapter, therefore, my primary aim is to determine the temporal and spatial profile of astrocyte activation in response to brain metastasis. Additionally, I will aim to elucidate whether astrocyte reactivity progresses to the glial scar phenotype in response to brain metastasis, by looking at astrocyte proliferation and molecular markers of the glial scar.

3.1.1 Mouse models of brain metastasis

In order to characterise the role of astrocytes in brain metastasis, it is important to select clinically relevant murine models. There is a high incidence of brain metastasis from primary breast tumours. Therefore, a mouse model of breast cancer metastasis to the brain was generated. The mouse breast cancer-cell line, 4T1-GFP, was selected for use in the majority of studies. While 4T1-GFP cells are not brain seeking *per se,* a large number of brain metastatic lesions do form with this model. As a consequence of the latter, this model shows accelerated pathology, allowing shorter time courses for animal experiments. As the 4T1-GFP cell was derived from BALB/c mice, this strain was used for the most part, in order to create a syngeneic model of brain metastasis, with an intact immune system; as there is paracrine signalling between astrocytes and immune effector cells it is important to have the full host response in order to create a clinically relevant model. In addition to 4T1-GFP cells, the brain seeking variant of the human estrogen-independent breast cancer cell line, MDA-MB-231 (Yoneda et al., 2001), was used in order to determine the clinical significance of the syngeneic model, with regards to tumour growth and astrocyte activation. Additionally, this cell-line was used in qPCR studies, in order to facilitate differentiation of the host response to metastasis from that of the tumour. As the MDA-MB-231Br cell line is of human origin, immunocompromised mice (SCIDs) were used so as not to elicit an acute phase response that would result in tumour cell destruction. The lung cancer cell line, Lewis lung carcinoma (LLC), was also used in a preliminary study demonstrating differential growth patterns of tumour cells within the brain.

There are multiple routes through which brain metastases can be induced. Injection of tumour cells via the carotid artery is frequently used as a model of brain

metastasis (Kienast et al., 2010; Kim et al., 2004a; Lorger and Felding-Habermann, 2010; Wu et al., 2012), yielding high numbers of brain metastases, with limited systemic disease (Daphu et al., 2013). However, this route is highly invasive, with extensive surgical procedures that may additionally yield systemic inflammation. Inflammation in the periphery has been correlated with CNS inflammation (Combrinck et al., 2002; Cunningham et al., 2009; Perry, 2004), a confound to be avoided due to discussion in the literature about the 'pre-metastatic niche'; it has been proposed that TDSFs, similar to those produced in response to an inflammatory challenge, may act to generate an appropriate 'soil' for secondary cancers. For example, cytokines such as IL-1β (Giavazzi et al., 1990) produced by macrophages in the periphery can lead to increased metastatic seeding (Solinas et al., 2010). Thus, it is advantageous to limit systemic inflammation to avoid potential modulation of the CNS environment prior to metastatic colonization. In contrast, intravenous injection of cancer cells is minimally invasive and does not require anaesthetic. However, this model is associated with high systemic burden (Daphu et al., 2013) and as such is not appropriate for protracted studies owing to animal welfare.

In comparison to either intracarotid or intravenous administration, the intracardiac route has a number of advantages. This route of metastatic induction enables hematogenous spread of inoculated tumour cells to the brain without the need for invasive surgery and with reduced systemic disease compared to IV delivery. In this model, tumour cells are injected directly into the left cardiac ventricle. Reports in the literature typically describe this method as being conducted 'blind'; without imaging guidance. However, work within the

department has illustrated improved CNS burden, with reduced systemic disease, if injections are ultrasound guided (Balathasan et al., 2013). Consequently, ultrasound guided intracardiac injection was used throughout this thesis to create a robust and reproducible model of brain metastasis.

Whilst the intracardiac model recapitulates the clinical scenario, with extravasation across the BBB, the nature of the technique yields disseminated disease. Thus, a more practical model must be created in order to generate focal lesions suitable for piloting imaging studies, as will be conducted in Chapter 6. Therefore, I developed an intracerebral model, in which the tumour cell line was directly injected into the striatum. The striatum was selected, as it is a self-contained brain region, with little 'spreading' of inflammation to the contralateral hemisphere. Additionally, this brain region is well characterized with regards to inflammatory response (Blond et al., 2002; Sibson et al., 2004). Whilst this model does not allow study of the extravasation process, it does facilitate observation of the parenchymal response to metastatic growth. Additionally, as shown in Chapter 6, this focal lesion model is useful when it comes to imaging studies. However, before this model could be used in imaging studies it was essential to determine whether it recapitulates the clinical situation sufficiently to be a relevant model. Thus, the second aim of this chapter was to compare the intracardiac and intracerebral model to determine the clinical relevance of intracerebral tumour injection.

3.1.2 The molecular microenvironment

Numerous *in vitro* studies suggest that astrocytes release a host of cytokines and growth factors in response to tumour cells themselves or tumour cell conditioned

media. However, few studies have looked at astrocytes *in vivo* in order to determine their role in a biologically relevant model. Additionally, those studies do not shed light on how the astrocytic transcriptional response changes with time or with proximity to the tumour; it is becoming increasingly apparent that the nature of the astrocyte response is very much dependent on the nature and intensity of the stimulus.

Astrocyte heterogeneity exists not just at a morphological level throughout the brain (Miller and Raff, 1984), but also at the molecular level in response to challenge; the transcriptional re-programming that characterizes astrocyte reactivity is both temporally and spatially heterogeneous. Comparative genomic analysis of astrogliosis in response to *in vivo* models of cerebral ischemia (middle carotid artery occlusion, MCAO) and systemic inflammation (LPS challenge), has shown that diverse molecular subtypes of astrocytes exist downstream of diverse CNS challenges (Zamanian et al., 2012). For instance nestin -a marker of glial scar formation was transiently upregulated post-MCAO, with its expression localised to the lesion core. In contrast, nestin expression was not observed at all in response to LPS challenge, suggesting that glial scar formation is not a feature of the brain's response to inflammation. Similarly, components of the antigen-presentation pathway are upregulated on astrocytes to a greater degree in response to LPS, than observed after MCAO, as one would hypothesise as LPS is a foreign challenge. An elegant transcriptional analysis of astrocyte cultures in response to TGF-β or IFN-γ and LPS stimulation also demonstrated differential gene expression profiles dependent on the nature of the challenge (Hamby et al., 2012). For instance, in response to combined stimulation with IFN-γ and LPS, a robust upregulation of

chemokines and Toll-like receptor 2 was observed, as predicted for dealing with an immune challenge. Such a transcriptional profile was not observed in astrocytes in response to TGF-β. However, there was an upregulation of the enzyme lysyl oxidase-like 1, which participates in the formation of connective tissue, consistent with the role of TGF-β in tissue repair. These findings highlight the differential responses of astrocytes to inflammatory challenges.

As evident with other non-neoplastic cells in the tumour microenvironment, such as macrophages (Allavena et al., 2008), astrocytes may also to exist in multiple phenotypes in the tumour periphery. For instance, a sub-set of peri-metastatic astrocytes have been shown to express phosphorylated-platelet derived growth facto receptor (PDGFR), in both animal models and clinical specimens (Gril et al., 2013). Phosphorylation of PDGFR can be induced in cultured astrocytes by tumour-conditioned media, although the functional consequence of this upregulation has not yet been determined. Differences in astrocytic phenotypes may also be apparent with time. I hypothesised, therefore, that the molecular phenotype of astrocytes in the metastasis microenvironment may vary temporally. To test this hypothesis, I have used qPCR to determine relative abundance of a number of factors purported in the *in vitro* literature to be produced by astrocytes in the metastasis microenvironment. Thus, the third aim of this chapter was to profile the tumour microenvironment at a molecular level, so as to determine whether in vitro models generated to date hold in relevant murine models. As both the tumour and the host may produce a number of overlapping factors involved in disease pathogenesis, I used immune-compromised mice injected with the human breast cancer cell line, MDA-Br-231 in order to be able to profile the host response

alone. PCR primers were designed against mouse mRNA in order to determine inflammatory mediators produced solely by the resident CNS cellular population. In some cases, immunofluorescence was used to confirm astrocytic expression of such factors.

In summary, therefore, the three main aims of this chapter were:

1. To determine the temporal and spatial profile of astrocyte activation in response to brain metastasis.

2. To determine whether an intracerebral model of brain metastasis recapitulates the more physiologically relevant intracardiac model.

3. To determine how the astrocyte response to brain metastasis varies over time at the molecular level.

3.2 Results

3.2.1 Astrocyte activation in response to brain metastasis; intracardiac model

The intracardiac route of tumour inoculation yields a model of disseminated brain metastases, distributed throughout the brain. Based on previous work within the lab, 10^4 4T1-GFP cells were injected into the left cardiac ventricle; this level of tumour burden allows a protracted study to be conducted without animal sickness observed. As shown in Figure 3.1, micrometastases appear to grow in the perivascular space, with mechanical disruption of the surrounding tissue away from the vasculature. The more elongated structure observed is indicative of vascular co-option. In this model, tumour growth was associated with astrocyte activation throughout the 28-day time course, as determined by GFAP immunoreactivity (Figure 3.1 A). Reactive astrocytes can be defined by their increased GFAP expression and contracted cellular processes. Quantification of the area of astrocyte activation associated with an individual metastasis (as described in Materials & Methods section 2.1.4) revealed a significant positive correlation between tumour area and the area of astrocyte activation, across the time-course (Figure 3.1 B; linear regression $y=11x + 0.006$, $r^2=0.6$, $p< 0.0001$). In order to assess the temporal profile of astrocyte activation, the ratio of astrocyte activation to tumour area was compared over time. As shown in Figure 3.1 C, there was a significant increase in this ratio over time, suggesting that the rate of astrocyte activation is faster than the rate of tumour growth (one-way ANOVA, $p=0.0187$; Tukey post-hoc test day 10 versus day 28, $p < 0.05$).

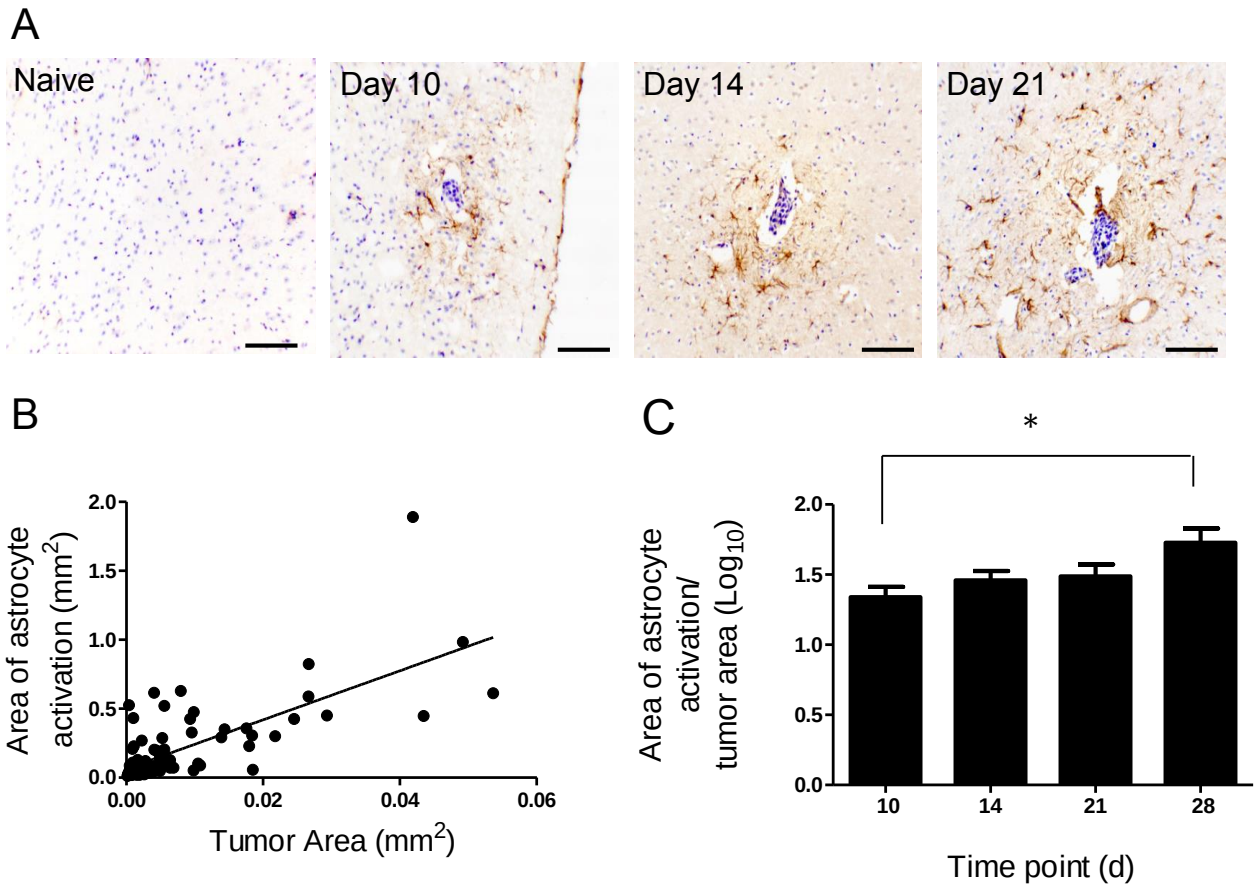

Figure 3.1: Astrocytes are activated in response to brain metastasis in an intracardiac model of the disease. (A) Photomicrographs of brain sections from a naive BALB/c mouse, and at days 10, 14 and 28 after intracardiac injection of 4T1-GFP cells (n = 5-6 per group). Reactive astrocytes were identified by GFAP immunoreactivity (brown stain) and sections were counter-stained with cresyl violet (blue). Scale bar = 100 μm. (B) A significant positive correlation was found between the extent of astrocyte activation and tumour area ($y = 11x + 0.006$; $r^2 = 0.6$; $p < 0.0001$). (C) A significant increase in the ratio of astrocyte/tumour area was found over time. Data was not normally distributed, and so data was $\log_{10}$ before parametric statistics performed. One-way ANOVA, p=0.0187; Tukey post-hoc test day 10 versus day 28, *$p < 0.05$. Data presented as mean values ± S.E.M.

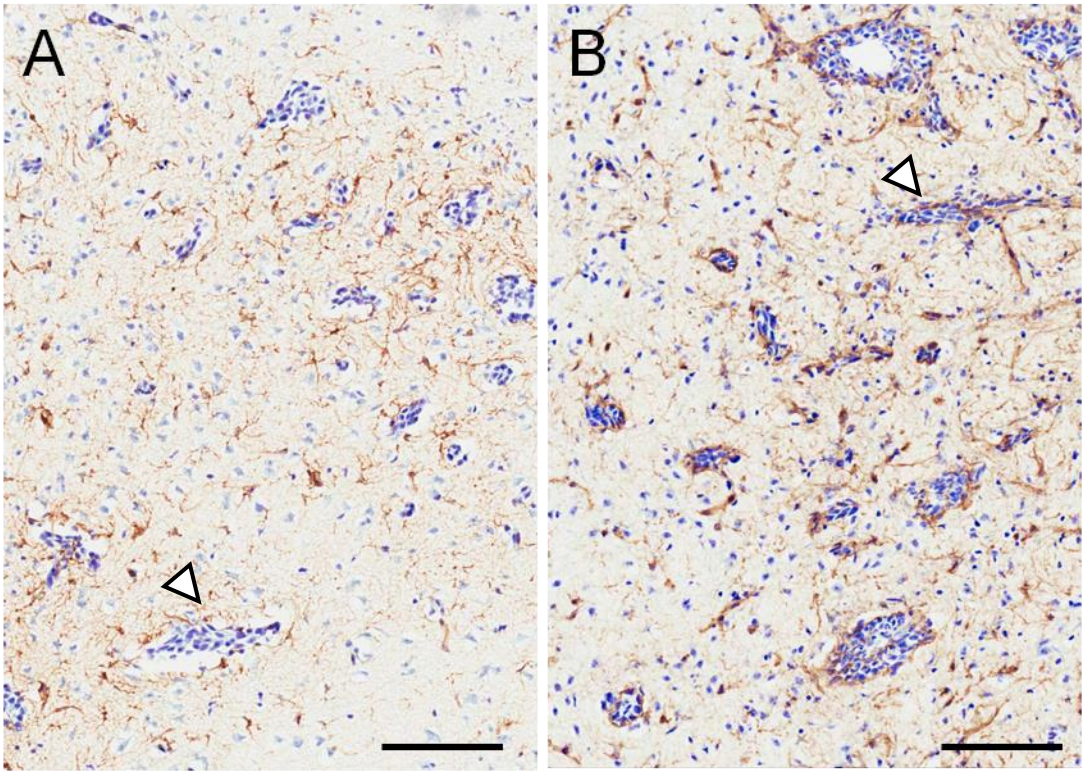

Figure 3.2: Tumour growth after intracerebral injection recapitulates that seen in the intracardiac route of tumour cell injection. (A) In the intracardiac model (day 14), micrometastases (cresyl violet nuclear counter stain, blue) proliferate in the perivascular space, associating with the microvasculature. (B) A similar pattern of growth is observed in the intracerebral model (day 14) in which an elongated phenotype (white arrows), suggesting vasculature co-option, is also apparent. In both incidences, metastases are associated with astrocyte activation (GFAP staining, brown). Scale bars = 100μm.

3.2.2 Astrocyte activation in response to brain metastasis; intracerebral model

An intracerebral model was developed to assess the astrocytic response to tumour burden in a focal lesion. As observed in Figure 3.2, the pattern of tumour growth is similar to that seen in the physiologically relevant intracardiac model; whilst the cells are initially delivered as a bolus dose, the tumour invades the local tissue and metastases appear to track along blood vessels. This pattern of growth is in contrast to that observed with intracerebral injection of the weekly-brain metastatic cell line, LLC (Balathasan et al., 2013). As shown in Figure 3.3, in that model, the bolus intracerebral cell dose does not invade the local tissue at the time point studied (day 14).

As observed in the intracardiac model, tumour growth was associated with robust astrocyte activation that persisted across a 28-day time course (Figure 3.4 A). Likewise, a significant positive correlation was also found between tumour volume and the volume of associated astrocyte activation (see Materials and Methods 2.1.4) in this model (Figure 3.4 B; linear regression $18.2x + 0.415$, $r^2 = 0.657$, $p < 0.0001$). In contrast to the intracardiac model, the ratio of astrocyte activation to tumour size did not increase across the time-course (Figure 3.4 C, one-way ANOVA $p=0.877$), suggesting that the rate of astrocyte activation increased at the same rate as tumour growth.

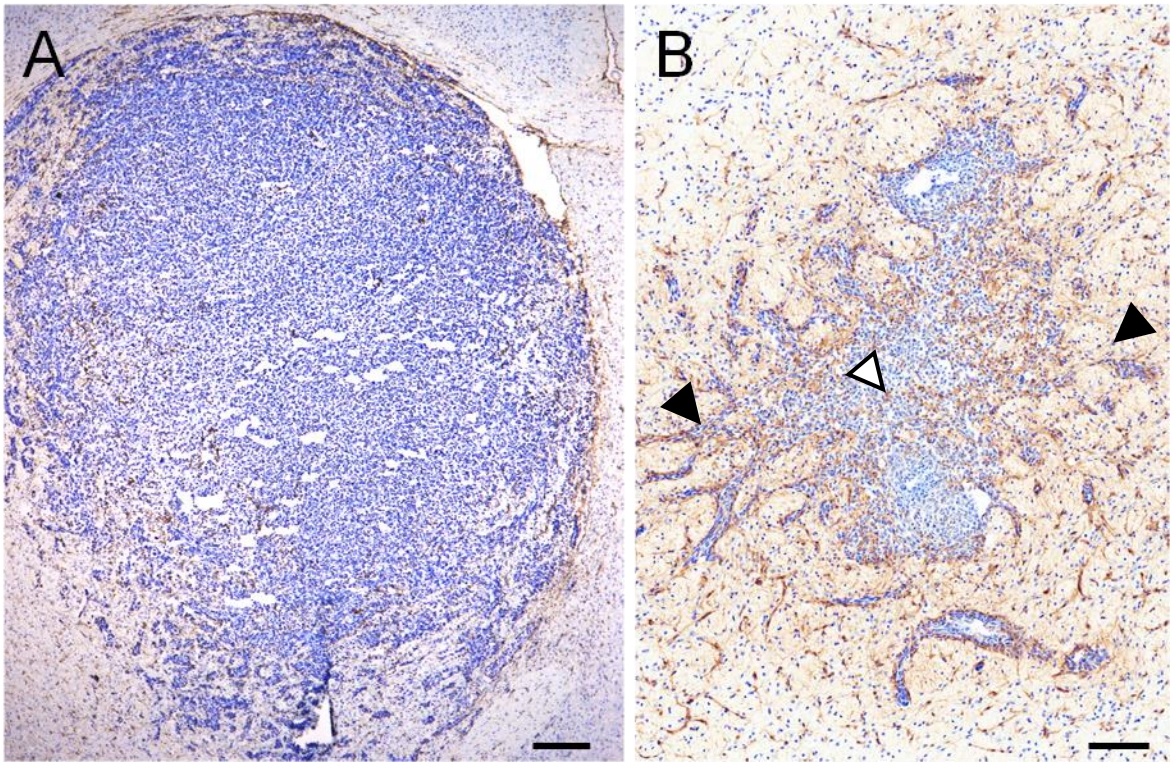

Figure 3.3: Different tumour cell lines display different patterns of tumour growth in the intracerebral model. (A) 5 x 10^3 Lewis lung cells were injected intrastriatally. At day 14, animals (n=3) were perfusion-fixed and tissue processed for histology. A cresyl counter stain (blue) indicated that little local invasion or vascular cooption occurred over the 14-day time course. (B) 5 x 10^3 4T1-GFP cells were injected intrastriatally. At day 14, animals were perfusion-fixed and tissue processed for histology. The cresyl blue counter stain suggests that although there is tumour growth *in situ* at the injection site (white arrow); there is also local invasion of the parenchyma (black arrows). Scale bars=100μm.

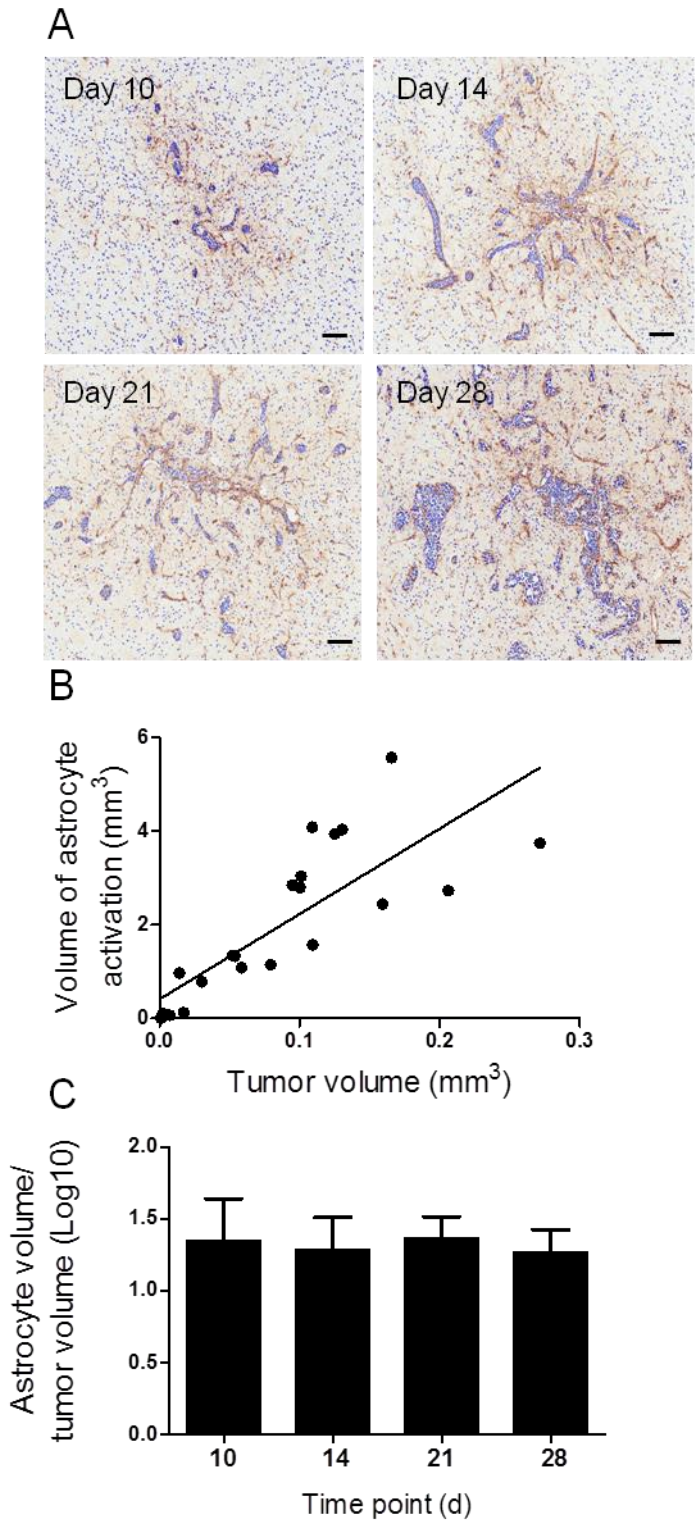

Figure 3.4: Astrocytes are activated in response to brain metastasis in an intra-cerebral model of the disease (A) Photomicrographs of brain sections from animals at days 10, 14, 21 and 28 after intra-cerebral injection of 4T1-GFP cells. Reactive astrocytes were identified by GFAP immunoreactivity (brown stain) and sections were counter-stained with cresyl violet. Scale bar = 100 μm. (B) A significant positive correlation was found between the volume of astrocyte activation and tumour volume ($y = 18.2x + 0.415$; $r^2 = 0.657$; $p < 0.0001$). (C) Data was not normally distributed, and so data was $\log_{10}$ before an ANOVA was performed. No significant differences were found in the ratio of astrocyte/tumour volume over time (one-way ANOVA, p=0.877, n = 4-5 per group). Data presented as mean values ± S.E.M.

As the intracerebral injection is an invasive procedure, quantifying the astrocyte response to vehicle injection alone was also quantified. Astrocyte activation was observed in response to saline injections, but the extent of this gliosis was significantly less than in 4T1-GFP injected animals, and decreased rapidly across the time course (Figure 3.5; Two-way ANOVA $p < 0.0001$, Bonferroni post-hoc test; treatment, $p=0.0003$).

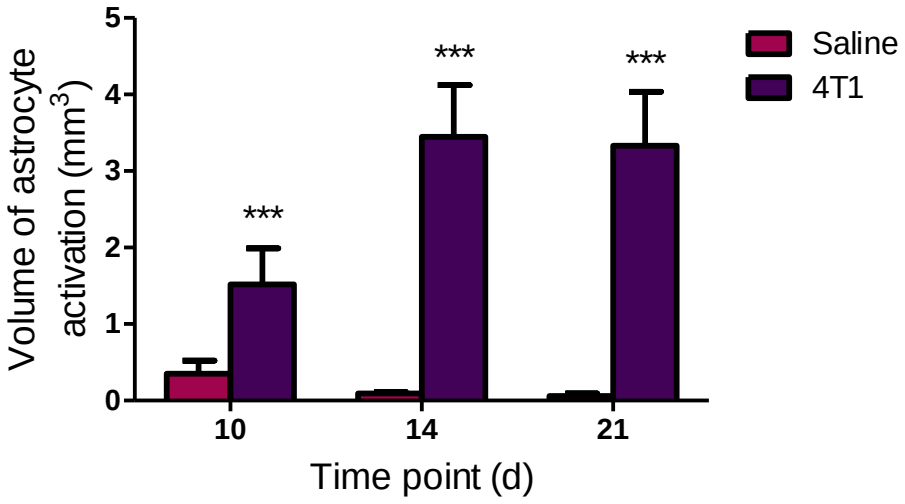

Figure 3.5: Intracerebral injection of saline elicits minimal amounts of astrocyte activation. Astrocyte activation in saline injected animals (n=3 per time-point) was significantly less than in 4T1-GFP cell injected animals (n=4-5 per time-point), and attenuated rapidly over time. Two-way ANOVA, $p< 0.0001$; Bonferroni post-hoc test treatment, ***$p=0.0003$. Data presented as mean values ± S.E.M.

In order to assess whether the astrocytic response in this intracerebral model is similar to that which would be induced by human breast cancer cells, SCID mice were injected intracerebrally with MDA-Br-231 cells. As shown in the low power histology images in Figure 3.6, the pattern of tumour growth is similar to that seen in the syngeneic 4T1-GFP, BALB/c model, although there is a trend towards lower tumour volume, presumably owing to the less aggressive nature of the MDA-Br-231 cell line. However, the ratio of astrocyte activation to tumour burden is similar to that observed in BALB/c mice in response to 4T1-GFP cells

(Figure 3.6; unpaired t-test, p=0.880).

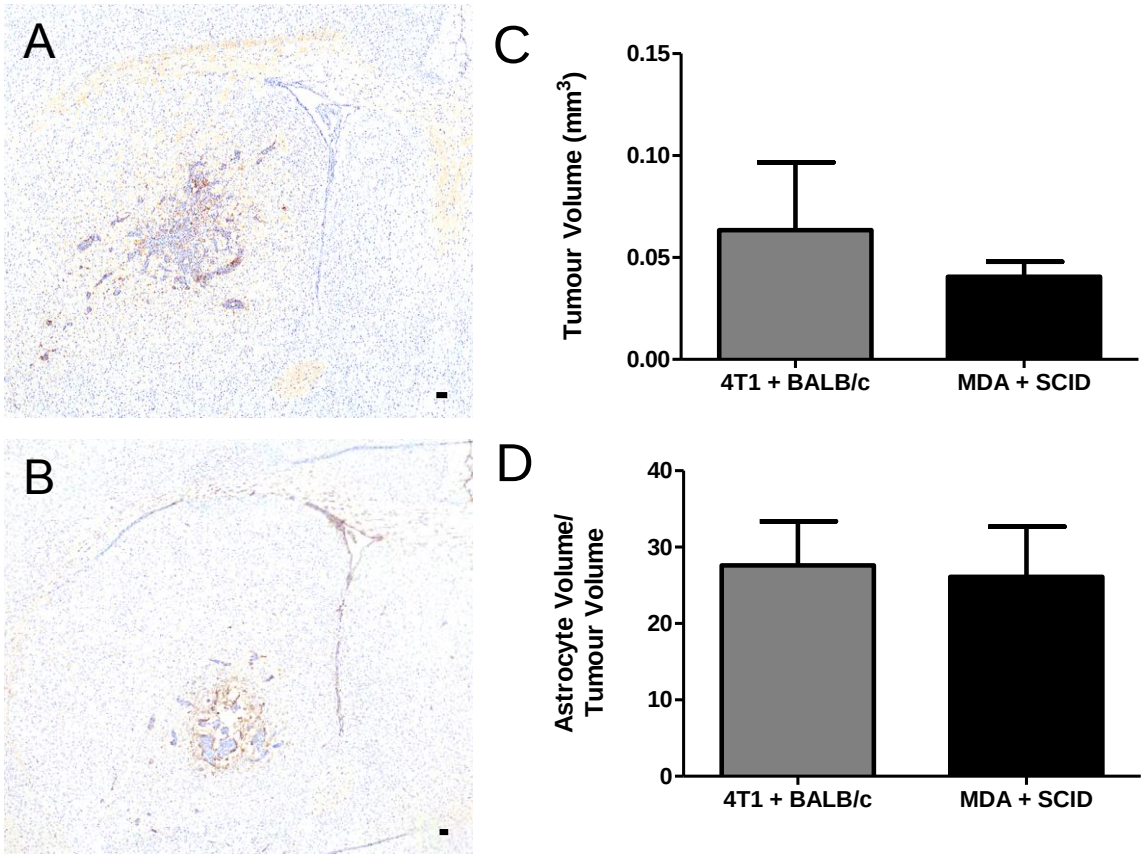

Figure 3.6: At day 14, MDA-BR-231 cells elicit a similar astrocytic response in SCID mice as compared to 4T1-GFP cells in BALB/c mice. Photomicrographs represent low magnification view of tumour growth in the intracerebral model. A) BALB/c mice were injected intracerebrally with 4T1-GFP cells as previously described (n=5). B) SCID mice were injected intracerebrally with 5 x 10^5 MDA-BR-231-EGFP cells (n=3). At day 14, animals were perfusion fixed and tissue processed for histology. Reactive astrocytes were identified by GFAP immunoreactivity (DAB, brown stain) and sections were counter-stained with cresyl violet (blue). The volumes of astrocyte activation and tumour burden were determined as previously described. C) There was a trend towards greater tumour volume at day 14 in the 4T1-GFP BALB/c model compared to the MDA-BR-231 SCID model (unpaired t-test, p=0.655). D) The ratio of astrocyte volume to tumour volume did not differ significantly between the strains and cell lines. Unpaired t-test, p=0.880. Data presented as mean values ± S.E.M. Scale bars=100μm.

3.2.3 Astrocyte proliferation

In the intracardiac model, histological analysis revealed an increase in the area of astrocyte activation with time. To determine whether this could be accounted for by an increase in GFAP reactivity or an increase in astrocyte proliferation, an *in vitro* model was used initially, with astrocytes isolated from neo-natal pups, and a primary culture generated, as shown in Figure 3.7. The presence of astrocytes was confirmed with immunocytochemistry for GFAP (Figure 3.7 A & B). Other CNS populations were also looked at, in order to confirm astrocyte purity. As shown in Figure 3.7, there was no microglial (C) or neuronal (D) contamination.

Subsequently, astrocytes were stimulated with 4T1-GFP cell-conditioned media, harvested as described in Materials & Methods (section 2.1.1). Using an *in vitro* MTT assay to quantify cellular metabolism (see Materials & Methods 2.1.6.1), commonly used as a read out for cellular viability and metabolism, it is evident, that astrocytes display increased metabolism when exposed to soluble factors released by tumour cells (Figure 3.8), although the increase in metabolic activity, as determined by absorbance, was mild.

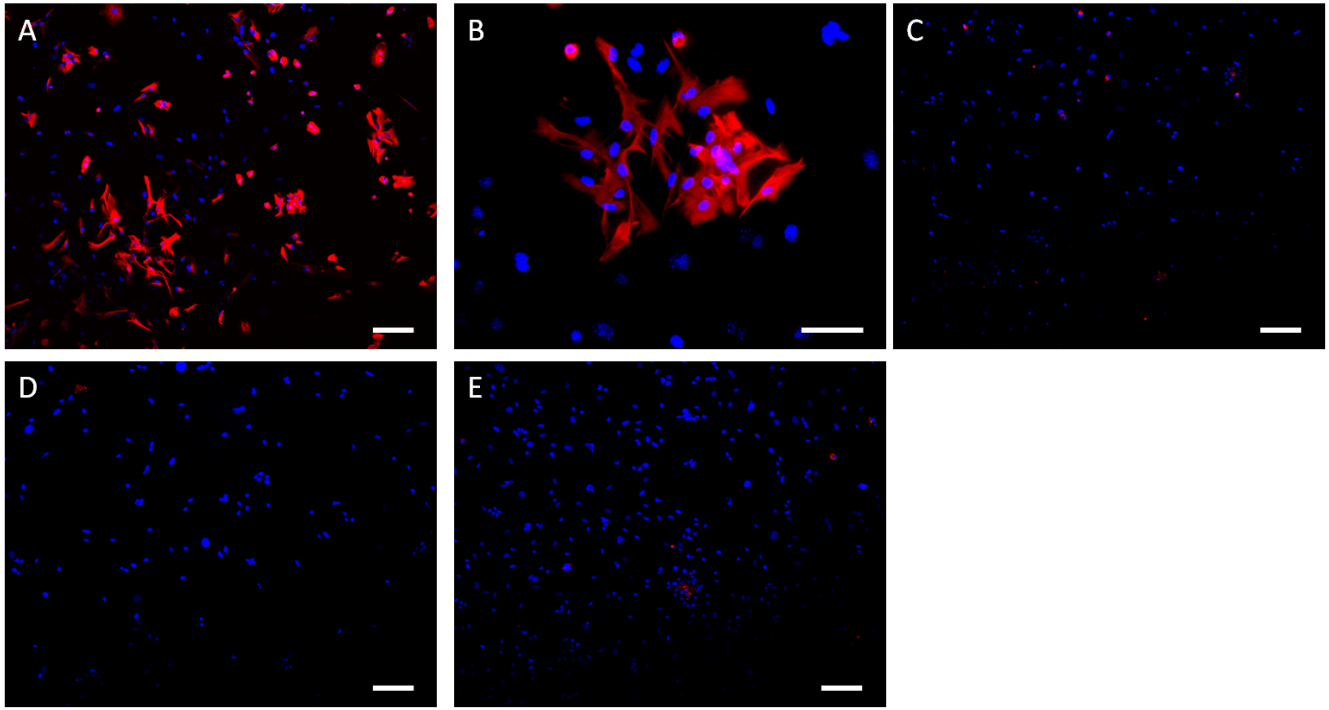

Figure 3.7: Astrocyte primary culture from p5 pups yields GFAP positive cells, with no neural or microglial contamination.

(A) Immunofluorescence image of cell nuclei (DAPI, blue) with GFAP positive cell bodies (Cy3, red). (B) GFAP reactivity at x 20 magnification. (C) Staining with IBA-1 indicates no microglial contamination. (D) Staining with NeuN indicates no neuronal contamination. (E) Negative control. Scale bars=100μm.

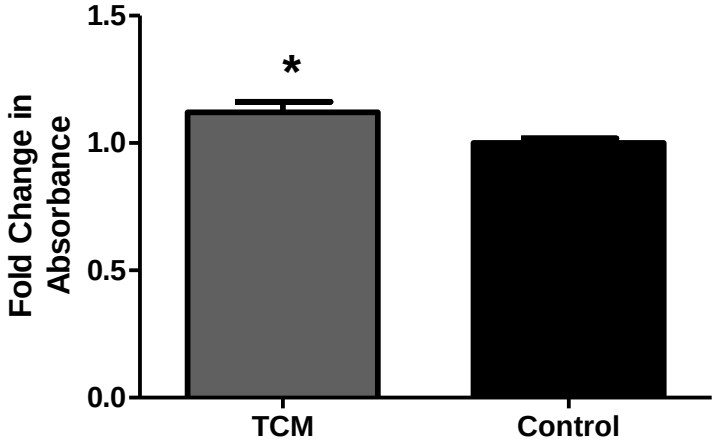

Figure 3.8: Tumour-conditioned media increases astrocyte proliferation in an *in vitro* primary culture model. Astrocytes were isolated from BALB/c pups, p5. Cultures were plated in 6 well plates and were treated with either tumour-conditioned media or control media, for 24 hours. Subsequently, astrocyte proliferation was assessed using an MTT assay. Control wells were normalised and fold change in absorbance calculated. Unpaired t-test with Welch's correction for unequal variance, p= 0.0353. Bars represent average of 6 wells ± SEM.

To translate these *in vitro* findings into the intracardiac *in vivo* model, animals were treated with BrdU prior to perfusion. BrdU is a thymidine analogue that is incorporated into replicating DNA by proliferating cells. Uptake of BrdU by cells was revealed by immunofluorescence. It was evident that whilst the tumour cells were proliferative, astrocytes in the tumour periphery were not replicating at either day 10 or day 21 post-tumour cell injection (Figure 3.9).

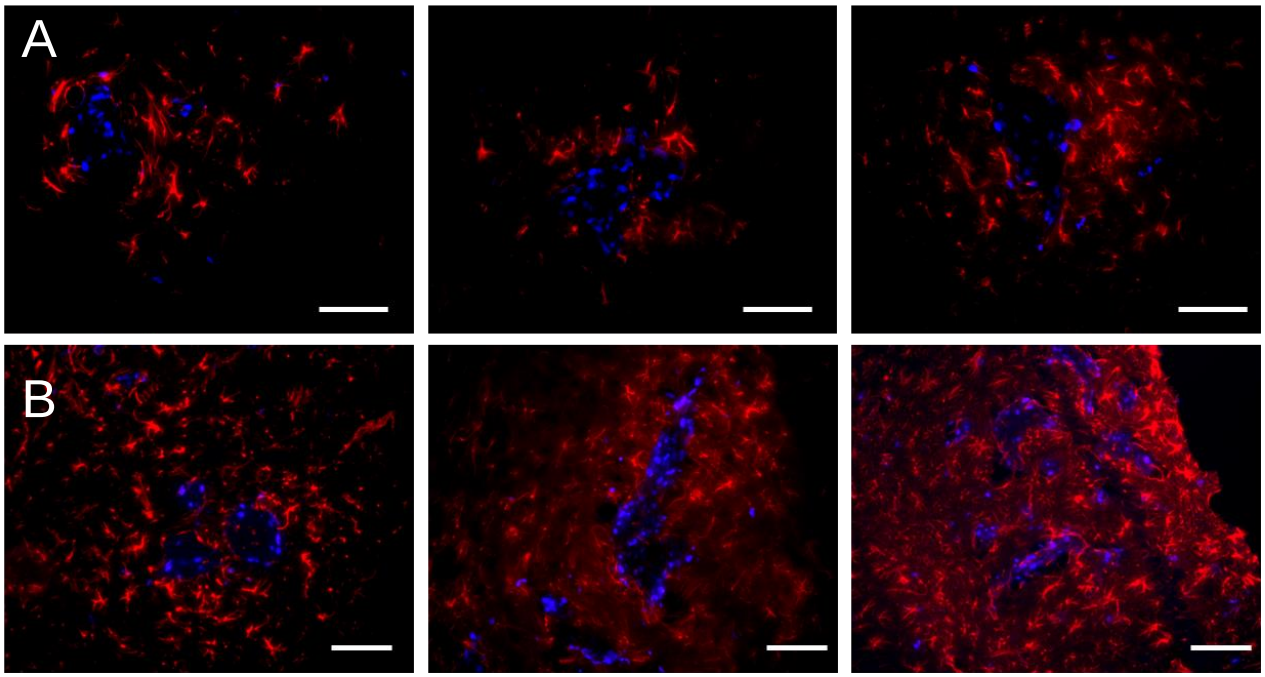

Figure 3.9: Astrocytes in the tumour microenvironment are not proliferative. Female BALB/c mice were injected intracardially with 4T1-GFP cells. In order to determine DNA replication status, mice were injected with 100 mg/kg BrdU 24 hours and 4 hours prior to perfusion-fixation at day 10 (n=4) or 21 (n=3). In order to detect BrdU incorporation, immunofluorescence was conducted with anti-BrdU alongside anti-GFAP antibodies to detect astrocyte activation. Immunocolocalisation shows that whilst astrocytes (red) are activated around proliferating cells within metastases (blue), there is no co-localisation between GFAP and BrdU positive cells at either day-10 (A) or day-21 (B) post tumour inoculation. Immunofluorescence images show representative tumours across the brain. Scale bars= 100 μm.

In addition to looking at astrocyte proliferation, typical markers of the glial scar were quantified in the intracardiac model using qPCR. SCID mice were injected intracardially with MDA-Br-231 cells and brains snap-frozen at days 14 and 21 post-tumour cell injection, prior to tissue processing for RNA extraction and qPCR. Primers specifically designed against mouse nestin and phosphacan were used, and expression levels compared to the naïve brain. A shown in Figure 3.10, there are no significant differences in the relative expression of either nestin or phosphacan across the time course in question (nestin; one-way ANOVA p=0.166, phosphacan; one-way ANOVA p=0.0535).

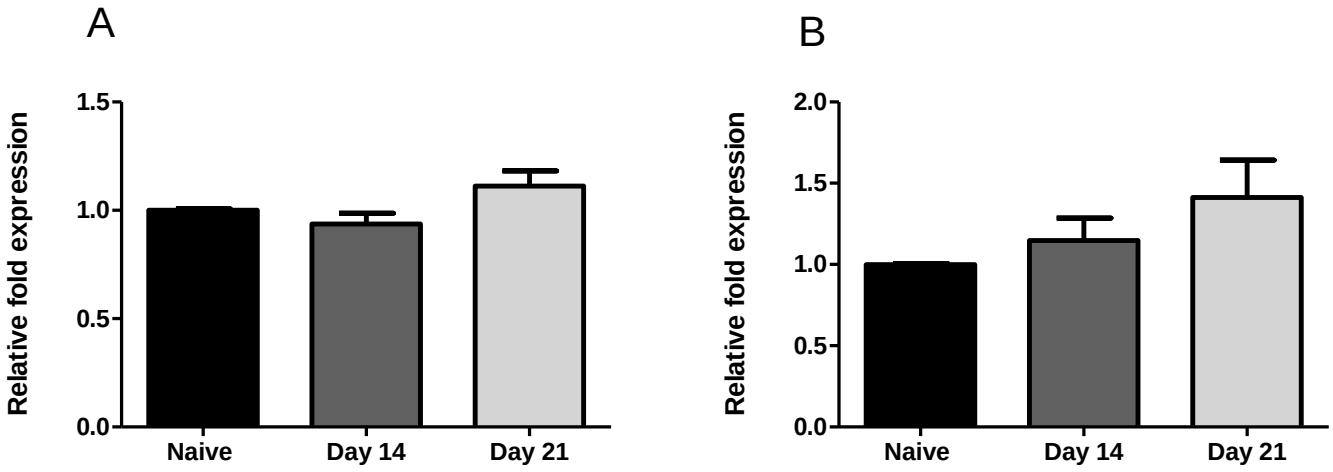

Figure 3.10: mRNA expression of phosphacan and nestin is not significantly altered across a 21-day time course by tumour burden in the intracardiac model of brain metastasis. Female SCID mice were injected intracardially with MDA-Br-231 cells. At days 14 and 21 post-tumour cell injection, animals were saline perfused (n=4 per time point) and tissue processed for RNA extraction. qPCR was performed, using primers for mouse phosphacan (A) and nestin (B). Expression levels were compared to two housekeeping genes (CANX and SDHA) and normalised to naïve tissue. One-way ANOVA (A) p=0.0535, (B) p=0.166. Data are presented as mean values ± S.E.M.

3.2.4 RT-PCR analysis of the tumour microenvironment

In order to profile the tumour microenvironment at the molecular level, qPCR was performed. To tease apart inflammatory mediators released by the CNS, as opposed to the tumour itself, SCID mice were injected with the human cell line MDA-Br-231. Thus, primers were designed specifically for mouse RNA products that would only detect host rather than tumour produced molecules. Initially, this experimental paradigm was conducted in the intracerebral model, and subsequently pursued in the intracardiac model, across two time points in order to assess the temporal profile. Genes of interest were selected based on prior literature reports on *in vitro* mediators of astrocytic function.

Evidence suggests that the archetypal housekeeping gene used in qPCR experiments, GAPDH, may not be stable across all pathologies (Glare et al., 2002; Montero-Melendez and Perretti, 2014). Additionally, MIQUE guidelines suggest that two housekeeping genes should be used to normalize expression levels (Bustin et al., 2009). To that end, a GeNorm experiment was conducted to determine the most stable housekeeping genes in my model (Vandesompele et al., 2002). As shown in Figure 3.11, CANX and SDHA were shown to be the most stable genes, and thus these were used for subsequent experiments as housekeeping controls.

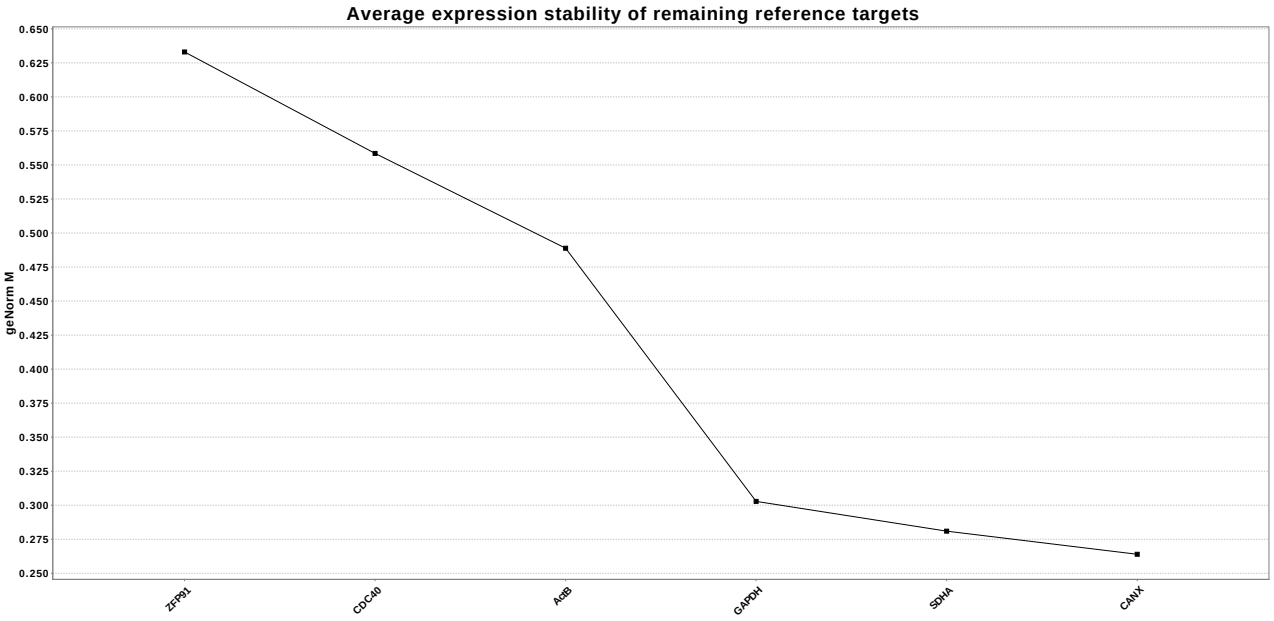

Figure 3.11: CANX and SDHA are the most stably expressed housekeeping genes as determined in a geNorm experiment. Female SCID mice were injected intracerebrally with MDA-Br-231 (n=3). At day 14, animals were saline perfused and the ipsilateral and contralateral striata removed for RNA extraction. qPCR was performed using primers for 6 different housekeeping genes, validated to be mouse specific by PrimerDesign. Biogazzelle software was used to determine which housekeeping genes remained the most stable between experimental and control tissue. In this experimental model, SDHA and CANX were the most stable genes of interest, based on their average expression stability value (M); the lower the M value, the more stable the expression level.

3.2.4.1 Intracerebral model

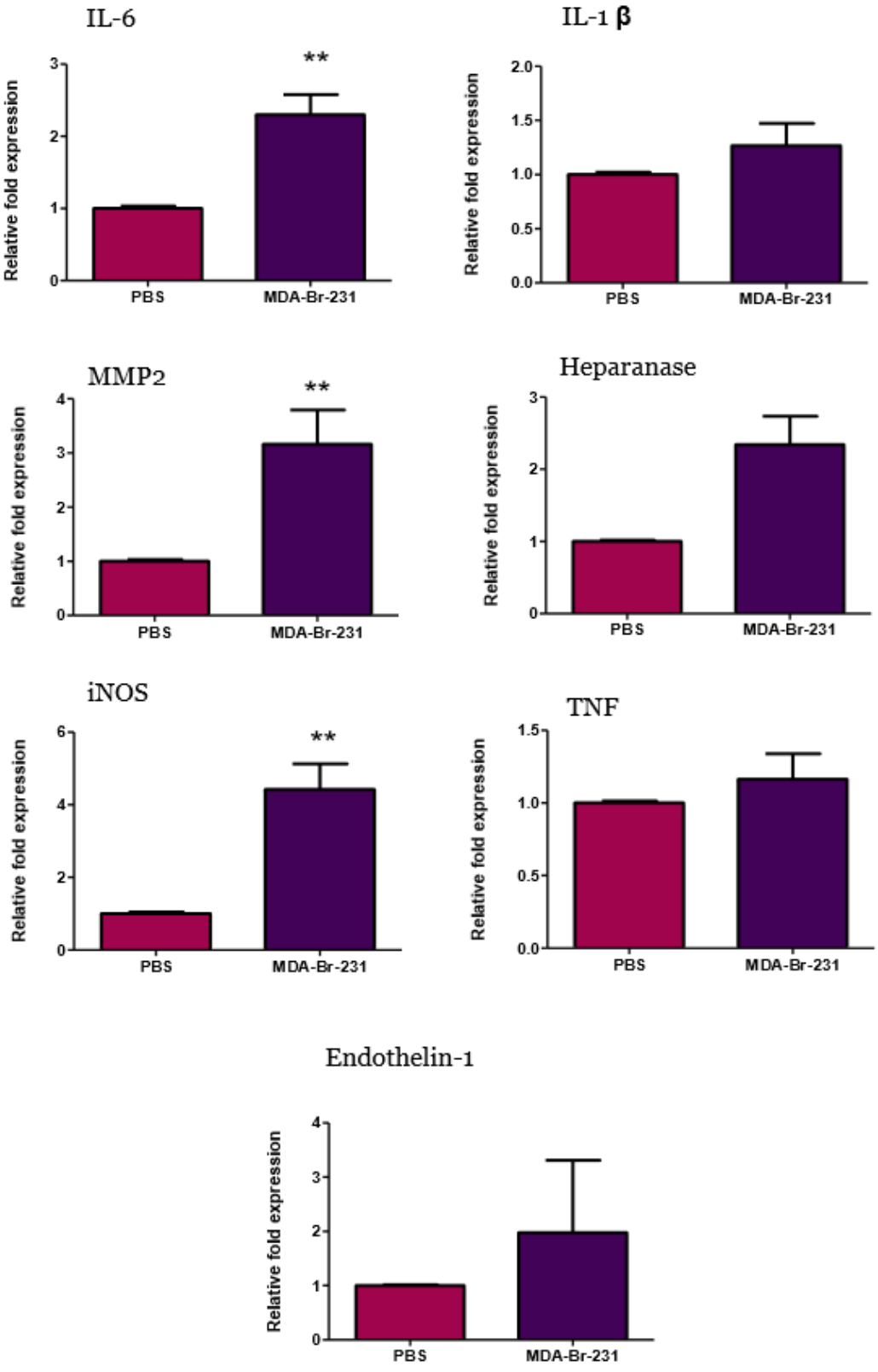

Figure 3.12: A number of inflammatory factors are expressed at the mRNA level in the intracerebral model of brain metastasis. Female SCID mice were injected intracerebrally with MDA-Br-231 cells (n=5) or PBS (n=5). At day 14 post-tumour cell injection, the striata were removed and processed for RNA extraction and cDNA synthesis. qPCR was performed, with primers designed for mouse IL-6, iNOS, IL-1β, TNF, MMP2, Heparanase and Endothelin-1. Expression levels were normalised to PBS control striata and CANX and SDHA housekeeping genes. Unpaired t-test with Welch's correction for unequal variances: *IL-6, p=0.01; iNOS, *p=0.0267; IL-1β, p=0.266; **MMP2, p=0.0083; TNF, p=0.405; Heparanase, p=0.0770; Endothelin-1, p=0.550. Data are presented as mean values ± S.E.M.

As shown in Figure 3.12, there are a host of inflammatory mediators produced at the mRNA level in the striatum, in response to MDA-Br-231 intracerebral injection. IL-6 was shown to be significantly upregulated in the striatum of mice injected with MDA-Br-231 cells, compared to PBS injected mice (unpaired t-test with Welch's correction for unequal variance, p=0.01), whilst there was no significant increase in IL-1β (unpaired t-test with Welch's correction, p=0.266). With regards to ECM remodeling, MMP2 was significantly upregulated in this intracerebral model (unpaired t-test with Welch's correction, p=0.0083). Similarly, there was a strong trend towards increased heparanase expression in response to MDA-Br-232 injection (unpaired t-test with Welch's correction, p=0.0770). iNOS expression was significantly increased compared to the PBS control striata (unpaired t-test with Welch's correction for unequal variance, p=0.0267). No significant differences were observed in the expression levels of TNF (p=0.405), or Enodthelin-1 (p=0.550) in this model.

Immunofluorescence was performed in the intracerebral model in order to determine the source of some of the factors listed above. As observed in Figure 3.13, there is widespread secretion of IL-6 in the intracerebral model and co-localisation with GFAP suggests that astrocytes are in part responsible for the production of this cytokine. Similarly, the immunofluorescence images presented in Figure 3.14 indicate that IL-1β is produced in the tumour microenvironment, again with co-localisation with astrocyte reactivity. With regards to iNOS expression, Figure 3.15 suggests that iNOS is expressed by astrocytes in the periphery, however at more removed regions, iNOS expression by astrocytes is not observed.

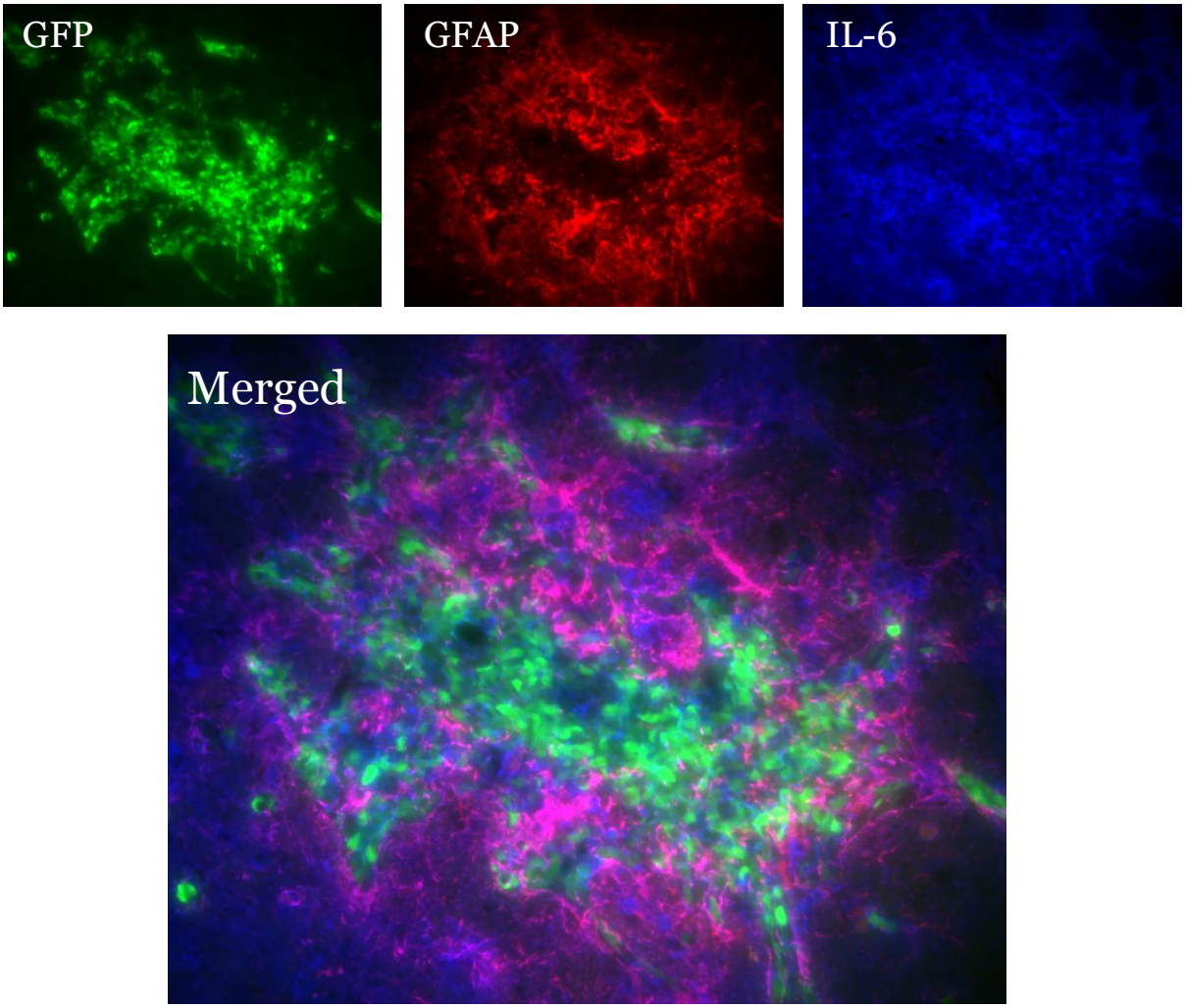

Figure 3.13: IL-6 is expressed at the protein level in the intracerebral tumour microenvironment, and its expression co-localises with activated astrocytes. Immunofluorescence was performed on sections from the 4T1-GFP intracerebral tumour model (day 14). Astrocyte reactivity was revealed using an anti-GFAP antibody in conjunction with anti-rat Texas Red fluorophore. IL-6 expression was detected using an anti-IL-6 antibody. The signal was amplified with a streptavidin-HRP detection system, and binding reveled with streptavidin-AMCA fluorophore. Tumour burden can be visualised with intrinsic GFP expression. Images show individual channels and the merged image. Pink demonstrates co-localisation between astrocyte reactivity and IL-6 expression.

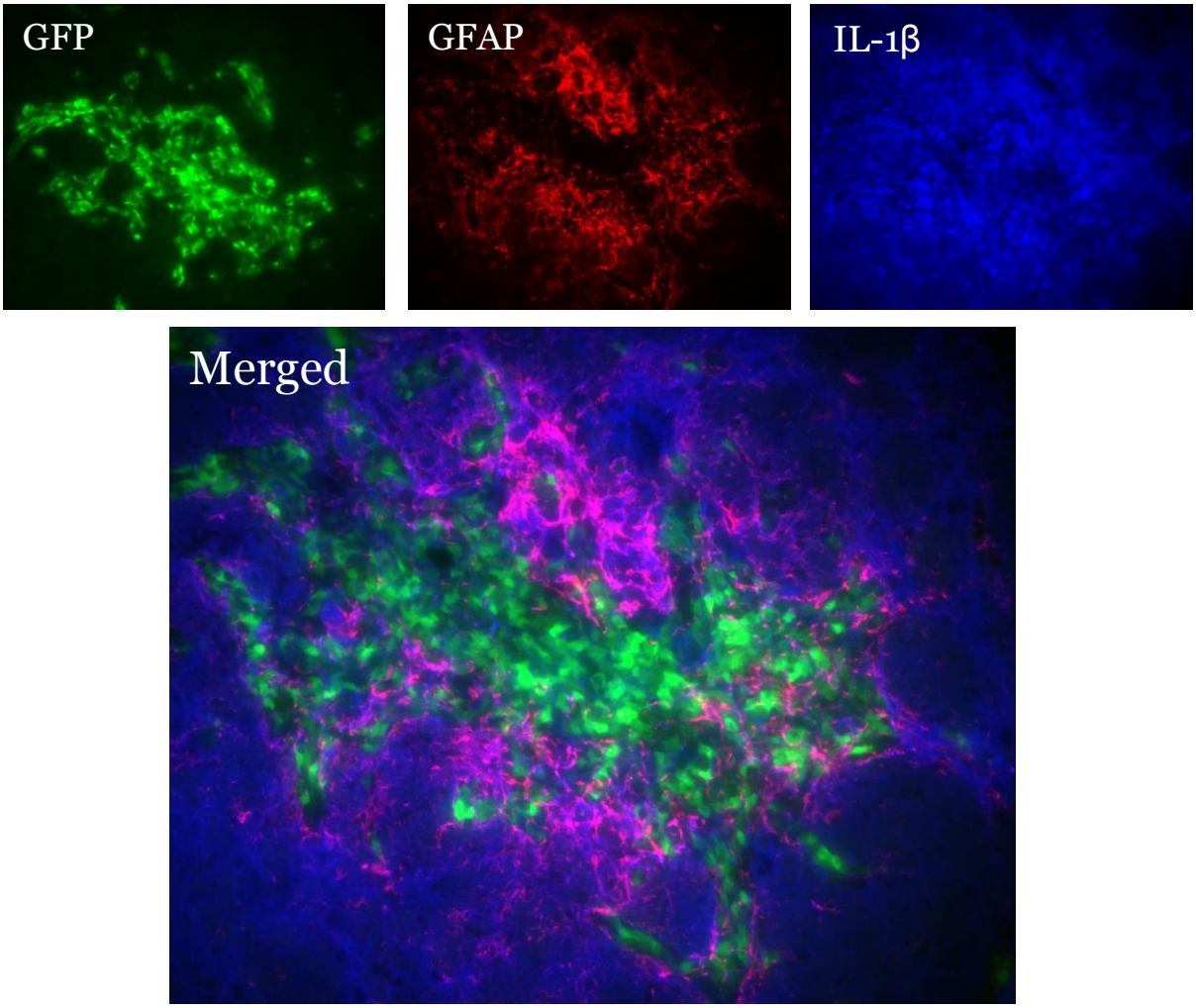

Figure 3.14: IL-1β is expressed at the protein level in the intracerebral tumour microenvironment, and its expression co-localizes with activated astrocytes. Immunofluorescence was performed on sections from the 4T1-GFP intracerebral tumour model (day 14). Astrocyte reactivity was revealed using an anti-GFAP antibody in conjunction with anti-rat Texas Red fluorophore. IL-1β expression was detected using an anti-IL-1βantibody. The signal was amplified with a streptavidin-HRP detection system, and binding reveled with streptavidin-AMCA fluorophore. Tumour burden can be visualised with intrinsic GFP expression. Images show individual channels and the merged image. Pink demonstrates co-localisation between astrocyte reactivity and IL-1β expression.

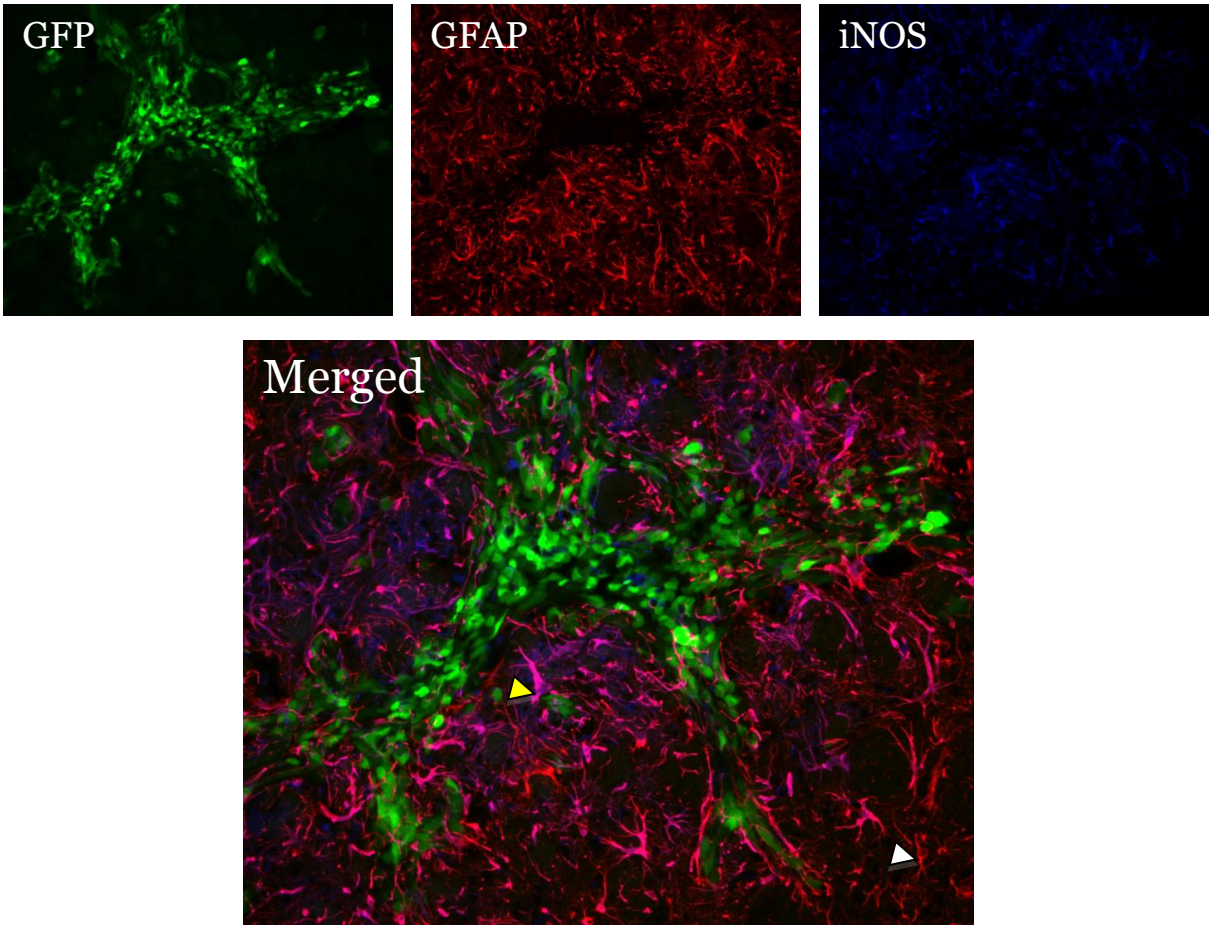

Figure 3.15: iNOS is expressed at the protein level in the intracerebral tumour microenvironment, but expression by astrocytes is limited to the tumour periphery. Immunofluorescence was performed on sections from the 4T1-GFP intracerebral tumour model (day 14). Astrocyte reactivity was revealed using a rat anti-GFAP antibody in conjunction with anti-rat Texas Red fluorophore. iNOS expression was detected using an anti-iNOS antibody. The signal was amplified with anti-rabbit biotinylated IgG and binding revealed with streptavidin-AMCA fluorophore. Tumour burden can be visualised with intrinsic GFP expression. Images show individual channels and the merged image. Pink demonstrates co-localisation between astrocyte reactivity and iNOS expression. Co-localisation is most apparent in the tumour periphery (yellow arrow), with no astrocyte-iNOS expression in the region more distal (white arrow).

3.2.4.2 Intracardiac model

In order to investigate whether there are temporal differences in the tumour microenvironment, the intracardiac model was used, with brains isolated at days 14 and 21 post-tumour inoculation and compared to naïve animals. As shown in Figure 3.13, IL-6 mRNA expression increased across the 21-day time-course, with a significant increase between naïve tissue and day 21 (one-way ANOVA, Tukey post-hoc test, $p=0.0268$, Tukey post-hoc test naïve vs day 21: $*p< 0.05$). With regards to IL-1β expression, a significant increase in expression was observed between day 14 and day 21, compared to naïve tissue (one-way ANOVA, $p=0.0185$, Tukey post-hoc test: day 14 vs day 21, $*p < 0.05$). In terms of ECM remodeling, there was no significant increase in MMP2 expression (one-way ANOVA, $p=0.483$) although there was a trend towards increased heparanase expression (one-way ANOVA, $p=0.0680$). endothelin-1; $p=0.0581$). No significant changes were observed in TNF, iNOS or endothelin-1 expression in this model (one-way ANOVA, $p=0.423$, $p=0.356$ and $p=0.0581$ respectively).

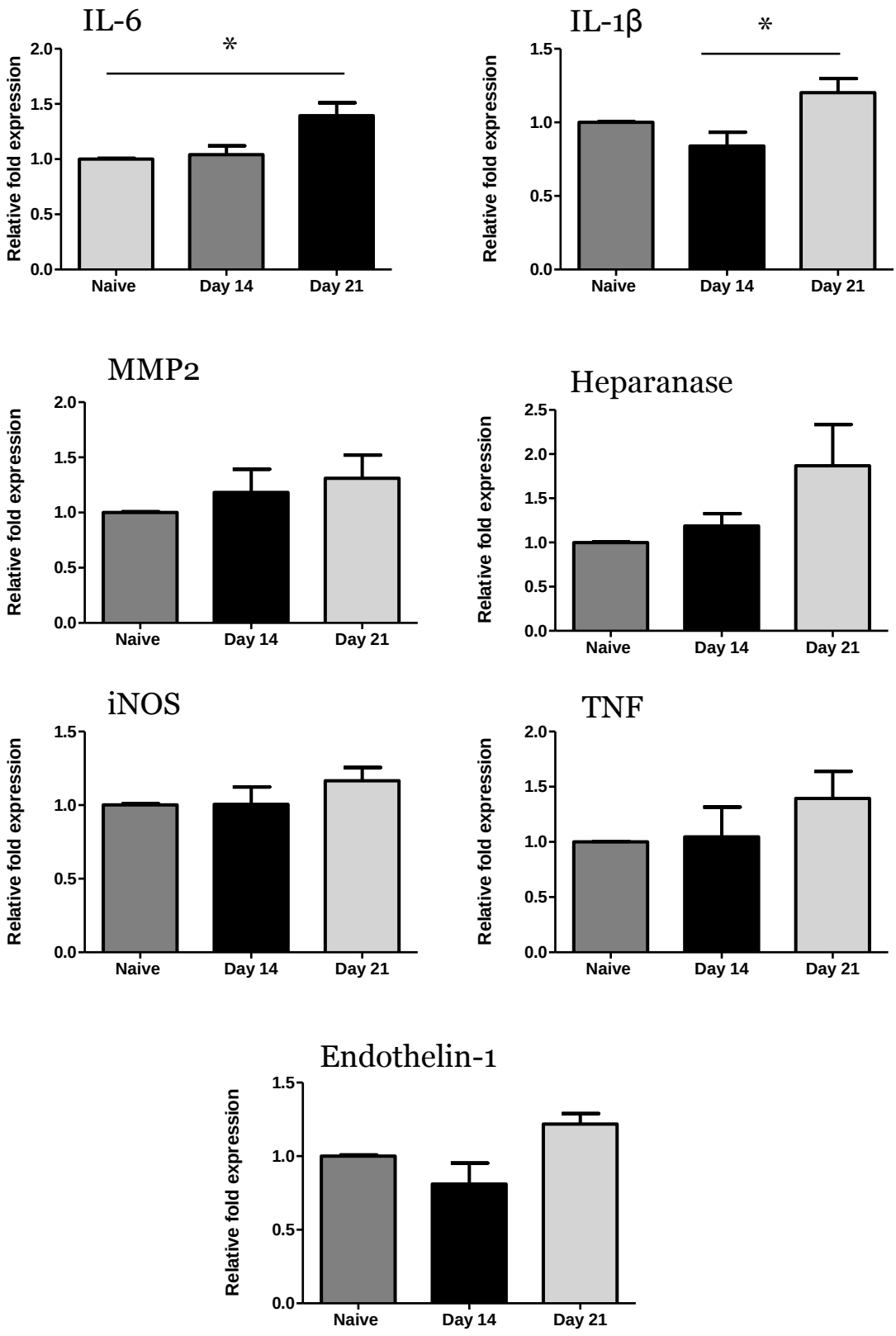

Figure 3.16: There are temporal differences in the expression profile of the tumour microenvironment. Female SCID mice were injected intracardially with MDA-BR-231 cells. At days 14 and 21 (n=4 per time point), animals were saline perfused

and tissue harvested and processed for RNA extraction as described in Methods section 2.1.7.2. . qPCR was performed, with primers designed for mouse IL-6, iNOS, IL-1β, TNF, MMP2, Heparanase and Endothelin-1. Expression levels were normalised to naïve brains and CANX and SDHA housekeeping genes. One-way ANOVA: IL-6, p=0.0268, Tukey post hoc test naïve vs. day 21 *p < 0.05; IL-1β, p=0.0185, Tukey post hoc test day 14 vs. day 21 *p < 0.05; MMP2, p=0.483; Heparanase, p=0.0680; iNOS, p=0.356; TND, p=0.423; endothelin-1, p=0.0581. Data are presented as mean ± S.E.M.

3.3 Discussion

3.3.1 Characterising the astrocyte response to brain metastasis in two in vivo models

In this chapter I have used two *in vivo* models of brain metastasis in order to investigate the role of astrocytes in metastatic disease. Whilst the intracardiac model has been published previously (Balathasan et al., 2013; Serres et al., 2012), the specific intracerebral model used here, with the use of a finely drawn microcapillary, has not been used in studies of metastasis prior to this work. The benefit of the developed technique is that CNS damage is limited by using a finely drawn glass microcapillary, rather than a Hamilton syringe with a 27-guage needle, as typically used in murine models of glioma, for example (Kaye et al., 1986). The latter has an outer diameter of ca. 400 microns as compared to the 75 microns achieved with the microcapillary. Using this method, minimal astrocyte activation was elicited in response to the injection itself, and the astrocytic response attenuated with time. In addition, it was evident that the pattern of tumour growth observed in the intracerebral model recapitulated the pattern of growth seen in the intracardiac model. Although at early time points, there was little evidence of

invasion away from the injection site, with time, apparent vessel cooption was observed. This pattern of growth, in both the intracardiac and intracerebral model was in accord with published results, indicating that rather than initiating neoangiogenesis, 4T1 cells co-opt existing vessels and grow in close association with the vasculature (Carbonell et al., 2009). This recapitulates the early stages of tumour growth in humans, with analysis of early stage biopsy samples indicating that micrometastases track along blood vessels (Carbonell et al., 2009).

In both the intracardiac and intracerebral models, brain metastases were closely associated with astrocyte activation *in vivo*, from early in disease progression and consistently throughout the 28-day time course studied. These findings are in agreement with those of Fitzgerald *et al.* (Fitzgerald et al., 2008), who showed that brain metastases are associated with reactive gliosis at 14 and 28 days post-induction in a xenograft model, in which a human breast cancer cell line was injected intracardially into immunocompromised BALB/c mice. The study presented here recapitulates and extends these findings in a syngeneic and immunocompetent mouse model of brain metastasis, both through hematogenous dissemination of tumour cells and through direct introduction into the brain. In both cases, the presence of reactive astrocytes was observed from the earliest time points studied and was considerably greater than the tumour area itself (*ca.* 25 fold for the intracerebral model, *ca.* 45 fold for the intracardiac model). Quantitatively, the area of astrocyte reactivity correlated positively with tumour growth. Similar positive correlations between astrocyte reactivity and tumour burden have been demonstrated in an *in vivo* model of lung cancer brain metastasis (Seike et al., 2011), although at a single time-point only. The work carried out here

demonstrates an association between tumour burden and astrocyte reactivity over a protracted time-course. Thus, astrocytes may be a potential target for either therapy or imaging, owing to their intimate and consistent association with tumour burden. The similarities made between the BALB/c-4T1-GFP mice and SCID mice inoculated with the human cell line MDA-BR-231-eGFP suggests that the syngeneic BALB/c-4T1-GFP model is relevant to the clinical situation. Furthermore, as BALB/c mice are immunocompetent this enables the entire host response and, therefore, paracrine signaling with astrocytes to be taken into account.

In both the intracerebral and intracardiac models used here, reactive astrocytes did not appear to form a fixed gliotic scar around the tumour, as is often seen surrounding for example, an ischemic lesion. Rather, the ratios of astrocyte activation to tumour size either remained constant (intracerebral model) or increased with time (intracardiac model). These findings suggest that the tumour continues to release astrocyte-activating factors as it grows, such that the gliosis neither resolves, nor walls off the tumour in a static rim. This concept is in accord with *in vitro* work indicating that tumour-induced astrocyte activation is not contact-dependent (Seike et al., 2011). It would be interesting to extend the time-course in this study further, in order to determine whether a scar like phenotype is present in the later stages of disease. The histological evidence from biopsy samples certainly demonstrates that astrocyte activation does not resolve at advanced stages of the disease (Zhang and Olsson, 1995).

There has been much debate regarding the nature of astrocyte reactivity in response to CNS trauma. For example, does the increase in GFAP staining

surrounding a lesion correspond solely to increased astrocyte reactivity, or is there a proliferative and migratory component? In order to determine whether the increase in GFAP staining observed with tumour size and with time was due to increased astrocyte activation, as opposed to an increase in astrocyte number, a proliferation assay was carried out, both *in vitro* and *in vivo*. Here, I have shown that in an *in vitro* setting, mouse primary cultures of astrocytes stimulated for 24 hours with 4T1-GFP cell-conditioned media undergo proliferation, as assayed using an MTT assay. The measured metabolic activity, however, was very mild, with an average of 12% increased activity compared to control wells. In contrast, in an *in vivo* model, astrocytes surrounding brain metastases were not shown to be undergoing DNA synthesis at either day 10 or day 21 post-tumour induction, as determined by a BrdU assay. The discrepancy between the *in vitro* and the *in vivo* data could be accounted for by both the different assays used and the relative developmental stage of astrocytes in the models; for the *in vitro* study, astrocytes were isolated at p5, whilst for the *in vivo* study, animals were perfused at approximately 9 weeks old. Thus, in the *in vivo* study astrocytes were more developed, and consequently, less likely to re-enter the cell cycle.

These results are discordant with the hypothesis that astrocytes in the tumor microenvironment may be proliferative, at least to a certain extent. However, the literature regarding astrocyte proliferation in neurological disease argues in both directions. In the *in vitro* situation, astrocytes can re-enter the cell cycle in response to the mitogens endothelin-1 (Gadea et al., 2008) and EGF (Levison et al., 2000), with IL6-type cytokines synergising with EGF to induce astrocyte proliferation. However, a stereological analysis of human AD brains suggests that

the apparent increased astrocyte density around Aβ plaques is due to phenotypic changes and brain atrophy, rather than an increase in astrocyte numbers (Serrano-Pozo et al., 2013). Whilst *in vivo* models of cortical stab wound do demonstrate astrocyte proliferation (Amat et al., 1996), this is only in a subset of cells and predominantly those in contact with blood vessels, proximal to the lesion (Bardehle et al., 2013). Modest astrocyte proliferation has been demonstrated at the genomic level in an *in vivo* model of stroke. However, cell-cycle regulatory genes were only transiently upregulated after MCAO, with levels returning to baseline by day 7-post-ischemic challenge (Zamanian et al., 2012). In the context of cancer, biopsy analysis of a brain metastasis of mammary origin, suggests that 20% of peri-tumoural astrocytes are proliferative, as indicated by Ki67 immunoreactivity (Neman et al., 2013). However, a recently published *in vitro* study demonstrated that a prostate cancer cell line could inhibit astrocyte proliferation and even induce cell death (de Oliveira Barros et al., 2014).

Thus, whilst many studies indicate that astrocytes do re-enter the cell cycle upon activation, only a small proportion of astrocytes, if any, in each model appears to be proliferative. The lack of astrocyte proliferation in the model used here suggests that astrocytes are moderately reactive, but they have not progressed to the formation of a glial scar (Sofroniew and Vinters, 2010). In order to confirm this, the host microenvironment was probed at the molecular level for hallmarks of the glial scar: phosphacan and nestin. Phosphacan is a CS-PG, expressed at a high level during development, where it is believed to serve a role in guiding axonal development by creating molecular barriers in the CNS. Levels decrease soon after birth, but the CS-PG is re-expressed in the glial scar. Its expression by reactive

astrocytes has been confirmed in *in vivo* models of traumatic brain injury (McKeon et al., 1999), stroke (Beck et al., 2008) and spinal cord injury (Buss et al., 2009). Nestin is an intermediate filament, absent in resting astrocytes, which has been shown to be rapidly and chronically expressed by reactive astrocytes in the glial scar, in a number of CNS pathologies including *in vivo* models of spinal cord injury (Frisen et al., 1995), CNS stab wounds (Lin et al., 1995) and stroke (Duggal et al., 1997). Neither phosphacan nor nestin was observed to be significantly upregulated at the mRNA level in the intracardiac model of brain metastasis, at either 14 or 21 days post-tumour cell injection. Thus, in conjunction with the histological data and the lack of proliferative index in astrocytes, these data indicate that a glial scar is not formed around brain metastases at these early time points. The significance of this is yet to be determined, but it would be rational to hypothesise that in the absence of ECM remodeling, the CNS is permissive to metastatic migration through the parenchyma. In this study I did not investigate the migratory pattern of astrocytes. In both the intracardiac and intracerebral models, astrocyte activation is observed surrounding the tumour, rather than astrocytes infiltrating the metastasis, indicating that astrocytes do not migrate into the tumour foci. However, in order to probe this further, an *in vitro* migration assay might be informative (Etienne-Manneville, 2006).

3.3.2 The molecular profile of the tumour microenvironment

The third aim of this chapter was to investigate whether a variety of cytokines and ECM remodeling enzymes that have been identified in astrocyte–tumour cell co-culture experiments, could also be identified in an *in vivo* model of brain metastasis. In an ideal scenario, astrocytes would be acutely isolated from the tumour microenvironment and their transcriptional profile determined with qPCR. However, the published literature regarding astrocyte isolation describes the necessity for a culturing step that would alter the transcriptional profile. Moreover, preliminary attempts to acutely isolate astrocyte by fluorescent labelling and subsequent FACS sorting were unsuccessful. Thus, a more global approach was taken, with the transcriptional profile of the CNS in response to tumour burden analysed by qPCR. In order to tease apart the host response from factors produced by the tumour itself, SCID mice were injected with the human breast cancer cell line, MDA-Br-231. To that end, primers were designed for mouse transcripts such that qPCR of the host response alone could be conducted; any tumour-derived mRNA transcripts will not be detected in this assay. Two time-points were selected, day 14 and 21, so that as assessment of temporal changes in the host response could be made. This approach does not allow confirmation of astrocytic origin of such factors and as such, immunofluorescence was used in some cases to confirm co-localisation.

Both the intracardiac and intracerebral models demonstrated an increase in IL-6 mRNA expression in the tumour microenvironment. Additionally, immunofluorescence images from the intracerebral model indicate that IL-6 is produced throughout the tumour microenvironment and that activated astrocytes are

in part responsible for this production, as indicated by the co-localisation between GFAP and IL-6 production. These results are in line with the *in vitro* publications in the literature. Previous studies using astrocyte and tumour co-culture models have suggested that IL-6 is a feature of the brain metastatic microenvironment (Seike et al., 2011). Astrocytes release IL-6 in culture and the cytokine has been implicated in driving tumour cell proliferation. Moreover, treatment with an anti-IL-6 antibody reduced cancer cell proliferation *in vitro* (Noda et al., 2012). At the same time, IL-6 receptor expression has been demonstrated in a mouse breast cancer cell line that metastasises to the brain, whilst its expression is absent in the parent cell-line that does not metastasise to the CNS (Nishizuka et al., 2002). Evidently, IL-6 plays a role in metastatic progression; however, this is the first *in vivo* study to demonstrate an increase in production of IL-6 by the brain in response to tumour burden alone, over an extended time course. Further work is necessary to determine the functional significance of IL-6 production in the tumour microenvironment, but based on the *in vitro* evidence above, one would predict that IL-6 inhibition would lead to a reduction in tumour burden. Indeed, an *in vivo* study in which mice were inoculated with the metastatic lung cell line HARA-B, demonstrated that treatment with the anti-IL-6 receptor monoclonal antibody, Tocilizumab, significantly reduced brain metastasis volume when given after the establishment of metastatic colonies (Noda et al., 2012). It would be interesting to extend this study in the models used in this thesis; IL-6 may not only play a role in tumour growth after the establishment of metastatic colonies, but in the initial colonization phase. Additionally, looking at read-outs of not only tumour volume, but how the microenvironment, particularly gliosis, is altered by IL-6 inhibition will be important.

There is much debate in the literature regarding the role of NO in tumour progression. iNOS is an inducible form of the enzymatic family that catalyses the conversion of L-arginine to nitric oxide, and it largely serves roles in the immune defense against pathogens, inducing cellular toxicity. Whilst it has been proposed that NO drives metastatic progression (Singh and Gupta, 2011), equally iNOS derived NO is tumouricidal. For instance, NO release by cytokine-stimulated endothelial cells induces cell lysis in an ovarian sarcoma cancer cell line (Li et al., 1991). Furthermore, in an *in vivo* xenograft model of Lewis Lung carcinoma, the NO donor, isosorbide 5-mononitrate, was demonstrated to reduce tumour burden (Pipili-Synetos et al., 1995). Additionally, in a well-characterised chick chorioallantoic membrane assay for angiogenesis, the NO donor was shown to reduce neo-vascularisation (Pipili-Synetos et al., 1995). In the context of brain metastasis, iNOS expression has been demonstrated *in vivo* in microglial cells, but has yet to be studied in astrocytes in the same context. iNOS expression by astrocytes has been demonstrated in several *in vitro* models. Studies suggest that IL-1β strongly induces iNOS activity in human primary astrocyte cultures (Jana et al., 2005) (Lee et al., 1993), as well as in primary cultures of rat astrocytes, where LPS and the combination of IL-1β, TNF and IFN-Ɣ was shown to induce iNOS activity and NO production (Kozuka et al., 2005). Thus, owing to the inflammatory milieu in the tumour microenvironment, iNOS expression by astrocytes would be anticipated. Indeed, in a co-culture model between astrocytes and a lung, breast and colon cell line, inflammation activated astrocytes were shown to induce tumour cell killing via an NO dependent mechanism (Samdani et al., 2004). Extending these findings to an *in vivo* model, the authors demonstrated that 'priming' the CNS with a stereotactic injection of LPS and IFN-γ lead to an upregulation of iNOS and a consequent increase in the concentration of NO. Subsequently, mice were

injected intracranially with the melanoma cell line, B16F10, and showed prolonged survival compared to mice prophylactically treated with saline. This prolonged survival was attributed to the tumouricidal actions of NO, as therapeutic effect was absent in animals treated with the iNOS inhibitor L-NAME and in iNOS knockout mice.

In this study, iNOS expression was demonstrated in the intracerebral model of brain metastasis, compared to the PBS control tissue. This expression was confirmed at the protein level with immunofluorescence. However, no significant differences were observed in the intracardiac model, although a trend towards increased iNOS expression by day 21 was apparent. This result was surprising based on the intracerebral data and the inflammatory milieu predicted to be present in the metastatic microenvironment. However, turning attention to the histological images from the intracerebral model, it is clear that only a subset of astrocytes in the tumour periphery express iNOS, and, consequently, the signal may not be great enough to detect with qPCR in the intracardiac model, where tumour burden may be less. Whilst other cell types, namely microglia and macrophages, also express iNOS, this population may also be small. These findings highlight the fact there are different astrocytic phenotypes in the microenvironment, adding to the work by Gril et al who showed that only a subset of astrocytes express PDGFR in response to tumour growth (Gril et al., 2013). Drawing parallels with the microglia/macrophage M1 versus M2 literature, the presence of iNOS on tumour-adjacent astrocytes would suggest that astrocytes in the tumour periphery display tumouricidal activity. If this is so, then paradigms to promote iNOS expression in a greater number of astrocytes may have anti-tumour potential.

A number of inflammatory cytokines were looked at in this model, based on evidence from both astrocyte—tumour co-culture models and other cancer—stroma interactions. The expression of IL-1β was probed due to contradictory evidence in the *in vitro* literature surrounding the role of astrocytes in brain metastasis. Il-1β has been proposed to induce cytotoxic effects, via its regulation of iNOS. Subsequent release of NO into the extracellular milieu has tumouricidal effects, as described above. In addition, IL-1β release has been shown to mediate cytotoxic T-cell recruitment. In astrocytes, a study suggests that stimulation with IL-1β upregulates expression of FasL and, consequently, induces apoptosis in a co-cultured lymphoblastic cell line (Choi et al., 1999). However, IL-1β has also been proposed to drive tumour progression. In the case of primary brain malignancies, the cytokine is implicated in promoting tumour invasion (Huang et al., 2009) as well as regulating angiogenesis, as demonstrated in an IL-1β knockout mouse model (Voronov et al., 2003). Regarding metastases, IL-1β production by astrocytes has been demonstrated, *in vitro,* in response to co-culture with HARA-B cells. Treatment of the lung cancer cell line with IL-1β led to increased cell proliferation (Seike et al., 2011), although this study did not look at antagonism of IL-1β action in the co-culture set-up. Thus, whilst inhibition of tumour-cell derived IL-1β reduces brain metastatic burden *in vivo* (Xing et al., 2013)*,* it has yet to be observed how modulating the host-production of IL-1β affects tumour growth in the brain.

In this study, IL-1β expression was not elevated in the intracerebral model at day 14 post-tumour injection, despite the immunofluorescence imaging suggesting that IL-1β is a feature of the tumour microenvironment. This discrepancy may be due to the

abundance of the cytokine; although expression at the protein level appears widespread in the images presented here, there may be variable amounts of expression across the tumour, resulting in a non-significant result at the mRNA level due to low target gene expression. This spatial profile throughout the tumour should be investigated more fully. Alternatively, there may be temporal differences in the expression of IL-1β at the mRNA level and at the protein level; negative transcriptional regulation may occur by this time point of the disease, whilst the protein is still present in the microenvironment. It should also be noted that the histological images are from the 4T1-GFP BALB/c model, which may also explain the discrepencies with the PCR data. Interestingly, there is an increase in IL-1β expression at the mRNA level between days 14 and 21 post-tumour cell injection in the intracardiac model and as discussed previously, the intracardiac model represents an earlier disease stage than the intracerebral model. Certainly, the increase over the time-course in the intracardiac model suggests that IL-1β plays a role in metastatic pathology, as does the histological evidence. However, in order to elucidate whether the cytokine mediates primarily tumouricidal or tumour promoting effects, inhibition studies must be performed. Neutralising IL-1β antibodies could be used. However, distribution of the antibody to the brain may be limited on account of the BBB. Thus an IL-1β receptor antagonist might provide a more appropriate means to probe the effect of inhibiting IL-1β signalling (Akeson et al., 1996). Such tools could be employed in the intracardiac model of brain metastasis, with outcomes such as brain tumour number and volume assessed. Downstream effects of IL-1β signalling such as iNOS expression and T-cell recruitment could be quantified in order to determine their contribution to disease pathogenesis. It may be that IL-1β plays different roles at various points in disease

progression. Thus, a treatment paradigm could be designed so as to look at initial colonisation and later growth independently.

TNF is an inflammatory cytokine implicated in metastatic progression. It is interesting that TNF was not shown to be present in the tumour microenvironment in these qPCR data, in either model. This finding was surprising based on *in vitro* findings demonstrating an upregulation in astrocyte-derived TNF in response to co-culture with brain metastatic cells (Seike et al., 2011). However, histological evidence from patient biopsies of lung cancer brain metastases reveals that only a small population of microglia and astrocytes in the tumour microenvironment are TNF positive. Thus, it is possible that TNF expression by the host is not as robust *in vivo* as one would expect from *in vitro* studies. Additionally, there is evidence in the literature for a negative feedback loop, initiated by microglia (Kim et al., 2002). In that *in vitro* model, rat microglia were stimulated with thrombin, a protein released after stroke or TBI. It was found that thrombin induced both TNF and the anti-inflammatory cytokine, IL-10, via different signaling pathways. IL-10 inhibited further TNF production, serving as an autocrine signal to regulate microglial inflammatory actions. Further work assessing the levels of anti-inflammatory cytokines, such as IL-10 in this model, would provide useful information as to whether this could be a reason for the apparent lack of TNF expression. There may also be negative feedback mechanisms elicited by the tumour itself, to counteract the potentially cytotoxic function of TNF. Assessment of earlier time points, prior to any negative regulatory mechanisms, may elucidate this issue further. On a separate note, the apparent lack of iNOS upregulation in the intracardiac model may be a result of a lack of one its stimulating factors, TNF.

Cytokines are not the only factors that may modulate the proliferative index of tumour cells. Endothelin-1, most commonly defined as a vasoconstrictor (Yanagisawa et al., 1988), has also been shown to be a cancer cell mitogen, produced by cancer cells and acting in an autocrine fashion by signaling via the Endothelin A receptor (Bagnato et al., 2002; Bagnato et al., 1997; Kasuya et al., 1994). Pharmacological antagonism of the endothelin receptor has been shown to attenuate growth of an ovarian cancer cell line and cervical cancer cell line, *in vitro* and *in vivo* respectively (Bagnato et al., 2002; Salani et al., 2002). Additionally, endothelin-1 has been implicated in mediating tumour invasion, decreasing gap-junction communication between ovarian cancer cells *in vitro* (Spinella et al., 2003), as well as inducing MMP secretion in a melanoma *in vitro* assay (Bagnato et al., 2004). This building paradigm for the involvement of endothelin in cancer progression (Bagnato and Natali, 2004), coupled with evidence from human autopsy samples demonstrating that endothelin-1 is expressed by astrocytes in 85% of brain metastatic cases (Zhang and Olsson, 1995), suggests that there may be paracrine signaling taking place in the tumour microenvironment that drives metastatic development. In support of this, the ET_B endothelin receptor is upregulated in a brain-metastatic melanoma cell line over 3 fold, compared to a non-metastatic cell line (Boukerche et al., 2004). Potentially, astrocyte derived endothelin-1 may in part dictate key steps in the brain metastatic cascade. To this end, expression of endothelin-1, at the mRNA level was assessed in both the intracerebral and the intracardiac models of brain metastasis.

In this model, endothelin-1 was not shown to be upregulated in the intracerebral or intracardiac models of brain metastasis, although there was a trend towards increased

endothelin-1 expression at day-21 of the intracardiac time course. These finding suggests that, in these models, endothelin-1 does not play a significant role in metastatic progression. Whilst the human pathology evidence presented above suggests that endothelin-1 is a feature of the brain metastatic microenvironment, these samples were derived from autopsies, which is likely to be a much later stage of disease than that modeled here. Thus, in order to probe the involvement of endothelin-1 further, a more protracted time-course may be required. Indeed, owing to its roles in vascular tone, perhaps endothelin-1 expression is modulated at the point of BBB breakdown, which is not be widespread at these time-points in the slower growing MDA-Br-231 model used here.

The contribution of the tumour microenvironment to metastatic progression may not purely be limited to enhanced proliferation. Enzymes that remodel the tumour microenvironment are also likely to be a feature of the CNS response. Whilst in the intracerebral model, MMP2 was significantly upregulated compared to the PBS control group, in the intracardiac model; there was no significant change in MMP2 expression over time was found, compared to the naïve control tissue. Whilst a number of studies indicate that MMP expression is elevated in response to brain metastasis, a recent *in vitro* study suggests that there may be a biphasic regulation of MMP2 expression. In tumour cells stimulated with astrocyte-conditioned media for 24 hours, an increase in MMP2 at the mRNA level was found compared to tumour cells treated with unconditioned media. At 48 hours, however, a reduction in MMP2 expression was evident compared to control (de Oliveira Barros et al., 2014). Thus, if astrocyte derived MMP2 is similarly regulated, a reduction in expression may occur at later time points. The discrepancies between the two routes of tumour injection reflect

the nature of the models; at day 14 after intrastriatal injection, the tumour 'bulk' injected is still migrating, co-opting vessels, and invading the CNS. In the intracardiac model, the colonies are more established, with minimal local invasion. In this case, a more comprehensive time-course might enable the dynamic involvement of MMP2 to be more accurately assessed.

Heparanase is an enzyme that catalyses the degradation of heparan sulphate chains, which decorate proteoglycans, and hence is involved in remodeling the ECM. Moreover, this enzyme has been suggested as a 'molecular determinant of brain metastasis' (Marchetti and Nicolson, 2001). *In vitro* studies indicate that astrocytes produce heparanase, and that astrocyte-conditioned media increases melanoma cell invasion in a tissue culture invasion assay. This enhancement of invasion has also been shown in a co-culture system between human melanoma cells and rat astrocytes (Marchetti et al., 2000). Additionally, heparanase mRNA was found in clinical samples of melanoma metastasis to the brain (Marchetti and Nicolson, 2001). Downregulation of heparanase in brain metastatic breast cancer cells with micro-RNA, reduced brain metastasis burden in an *in vivo* model, as defined by metastatic colony number (Zhang et al., 2011). Thus, potentially, heparanase plays an important role in the brain metastatic cascade, and it was hypothesized that heparanase would be upregulated in the tumour microenvironment.

In contrast to the above hypothesis, heparanase did not appear to be modulated by tumour burden in the brain, in either model, although there was a trend towards increased expression in both the intracerebral and intracardiac models. This finding may again reflect simply the limited number of time-points studied. Previous studies

suggest that the enzyme is important in the initial stages of metastatic formation (Zhang et al., 2011). Thus, the endoglycosidase may be downregulated later on in the metastatic cascade. Indeed, in a rat model of ischemic stroke, heparanase expression by astrocytes was shown in the peri-infarct region only, and enzyme expression had decreased by day 7 post-MCAO (Takahashi et al., 2007). Furthermore, heparanase expression was shown to be present in nestin positive astrocytes, which as discussed above, is not a feature of the brain metastatic environment in this model.

In order to better assess the temporal changes in the host molecular profile, it will be necessary to look at earlier time points; it is likely that the expression of ECM remodeling agents is far higher during the initial stages of colonization when extravasation across the BBB and colonisation of the perivascular space requires remodeling of the ECM. Therefore, further studies would include time-points between days 3 and 7, based on in vivo studies suggesting this time frame for the extravasation of brain metastatic cells (Lorger and Felding-Habermann, 2010). Additionally, an experimental confound here is the low copy number of inflammatory gene transcripts owing to the nature of the intracardiac model and even significant differences were very mild in this model. Therefore, increasing tumour burden by increasing the number of cells injected intracardially may enable better detection of potential genes of interest. However, caution must be taken with too high a tumour burden as the global neuroinflammation induced may be different to the clinical situation.

3.4 Conclusions and further work

In conclusion, brain metastases were associated with reactive astrocytes throughout a 28-day time course, in two *in vivo* models. A positive correlation was found between

tumour size and the extent of astrocyte activation, and this correlation persisted over time. However, rather than astrocyte reactivity progressing to a glial scar, with astrocyte proliferation and deposition of CSPGs, it was apparent that a more dynamic interaction exists between the tumour cells and surrounding glia. It will now be important to elucidate the functional significance of this relationship. Additionally, I have characterized the host response to tumour burden, *in vivo*. From these qPCR studies, I have demonstrated that there is a dynamic regulation of a number of inflammatory mediators in the tumour microenvironment. Going forward, it will be necessary to perform inhibition studies to demonstrate the relevance of each of the individual mediators, as discussed in the discussion. Overall, the work presented here provides a strong framework for further study of the role of astrocytes in brain metastasis at a molecular level.

The next step would be to characterise the transcriptional profile of astrocytes specifically. Isolation of astrocytes from the diseased brain has proved challenging, with all published work detailing an *in vitro* cell culture step, which would alter the phenotype of astrocytes surrounding metastases. However, there are multiple novel methodologies that could facilitate this. The most promising of which is the GFAP-GFP transgenic mouse, in which GFP is placed under the GFAP reporter (Zhuo et al., 1997). As such, astrocytes in the tumour periphery could be isolated from the brain using FACS, prior to qPCR. Isolation and RNA extraction from astrocytes has been successfully achieved in other pathological models using such transgenic animals (Bi et al., 2011; Katz et al., 2012) and, therefore, I believe this could be a useful and reliable tool for answering questions about the molecular contribution of astrocytes to tumour growth. At the same time, recent work by Li *et al.* (Li et al., 2012b), has shown that a

novel class of antibodies, fused with GFP, are capable of crossing the BBB and binding to GFAP. This approach would allow labeling of astrocytes *in vivo,* facilitating their subsequent isolation as described above.

Downstream of the transcriptional profiling of astrocytes, relevant factors could be modulated *in vivo* to assess effect on tumour growth. siRNA knock-down of genes of interest is now a routine technique in molecular biology. Translation to an *in vivo* setting has been more challenging, but a recent report indicates that siRNA can be delivered to the brain in liposomal packaging (Rungta et al., 2013). Such novel methodologies could really aid the understanding of astrocytic roles, in clinically relevant models. From the work presented here, I propose that IL-6 would make a promising target for tumour modulation. Further work involving either down-regulation of IL-6 at the transcriptional level with siRNA or an antibody inhibition approach could yield exciting results with clinical applications.

As touched upon, the transcriptional profile of astrocytes may be different depending on proximity to the tumour. This would be an interesting concept to pursue further. To this end, a tool that could be useful with regards to profiling the astrocytic response at different locations in the tumour microenvironment is laser capture microdissection (Emmert-Buck et al., 1996). This technique provides a rapid, sterile and precise way to remove tissue from sections, such that, for example, qPCR can be performed (Goldsworthy et al., 1999). In this manner, it would be possible to isolate the tumour microenvironment at different locations in the tumour periphery, to build up a 3D picture of the transcriptional profile surrounding the tumour. The hypothesis would

be that there are different molecular phenotypes at different regions surrounding the tumour, and techniques such as this could elucidate this further.

Whilst this study has demonstrated that there is a robust astrocytic response to brain metastasis, and illustrated that several pro-tumoural factors are upregulated in the tumour microenvironment, the role of astrocytes in metastatic progression remains unclear. Thus, the following two chapters will deal with *in vivo* manipulation of astrocyte reactivity in an attempt to determine the effect of both astrocyte activation and inhibition on tumour burden.

Chapter 4 Modulation of brain metastatic progression by chronic astrocyte activation

4.1Introduction

As demonstrated in Chapter 3, astrocyte activation is a feature of the brain metastatic stroma, throughout an extended time-course. I have shown that the relationship between tumour growth and astrocyte activation is a dynamic one, without progression to a glial scar over the time points studied. The nature of this dynamic relationship appears to be mediated by numerous inflammatory factors present in the tumour microenvironment. As the studies published to date have looked at the consequence of such a transcriptional profile *in vitro*, important questions remain to be answered in a relevant *in vivo* model. Previous *in vivo* studies have shown that astrocytes become activated by day 3 post-tumour inoculation, whilst metastasizing cells are still adhered to the luminal side of the endothelium (Lorger and Felding-Habermann, 2010). This finding suggests that astrocytes could modulate tumour cell extravasation from the earliest steps. Thus, it was hypothesised that *in vivo* manipulation of astrocyte reactivity could modulate the initial stages of metastatic seeding. In addition, the qPCR studies presented in Chapter 3 indicate that there is expression of growth factor IL-6 in the tumour microenvironment, and the bulk of *in vitro* evidence published to date suggests that astrocytes in the tumour microenvironment are in a pro-tumourigenic state, releasing growth factors and matrix metalloproteinases that may modulate tumour growth (Marchetti et al., 2000; Mendes et al., 2007; Nishizuka et al., 2002; Seike et al., 2011; Wang et al., 2013). Thus, it was hypothesised that chronic astrocyte activation would promote metastatic growth

within the CNS. The aim of this chapter, therefore, was to determine the role of chronic astrocyte activation in metastatic progression, *in vivo*. Astrocyte activation prior to tumour cell injection will enable the contribution of astrocytes to be assessed throughout the metastatic cascade.

4.1.1 Potential models of astrocyte activation

Astrocyte activation can be elicited in mice in response to multiple inflammatory challenges; it has been demonstrated that both TNF (Zhang et al., 2000) and IL-1β (Herx and Yong, 2001) induce acute astrocyte activation. However, a more sustained astrogliotic response is required to probe the role of astrocytes across the entire metastatic cascade. Whilst viral vectors could facilitate the chronic release of such inflammatory mediators into the CNS (Campbell et al., 2007; Sibson et al., 2002; Solum, 1975), cytokines are associated with a broad spectrum of CNS inflammatory processes. Thus, in order to isolate the astrocytic role in metastasis, a more targeted approach was required.

4.1.2 Ciliary Neurotrophic Factor

Ciliary Neurotrophic Factor (CNTF) is a nerve growth factor, encoded by the *CNTF* gene. The protein belongs to the IL-6 family of related cytokines, signaling via gp130 receptor subunits. Such ligand—receptor interactions lead to activation of the Jak/STAT signaling pathway, with further crosstalk to other signalling cascades (Boulton et al., 1994). CNTF was first characterised as a neuroprotective agent, in experiments demonstrating the protection of photoreceptor cells in response to constant light exposure (LaVail et al., 1992). CNTF has also been shown *in vitro* to

mediate axonal regeneration in mouse retinal ganglion cells (RGCs) (Leibinger et al., 2013). Furthermore, *in vivo* gene transfer experiments in rats indicate that CNTF can promote regeneration of adult RGCs (Leaver et al., 2006).

More recent studies suggest that the neuroprotective function of CNTF is mediated by astrocytes. Specifically, treatment of astrocytes with CNTF has been shown to reduce neuronal damage in response to excitotoxic injury *in vivo* (Bechstein et al., 2012; Beurrier et al., 2010), via an increase in astroglial glutamate transporters facilitating homeostasis of neurotransmitter concentrations(Beurrier et al., 2010). CNTF has also been shown to elicit neuroprotective effects in response to challenges such as metabolic insult (Escartin et al., 2007) and neurodegeneration (Mittoux et al., 2002). In addition to its neuroprotective role, it is known that CNTF induces astrocyte activation, both *in vitro* (Levison et al., 1998; Wu et al., 2006) and *in vivo* (Kahn et al., 1997; Levison et al., 1996; Winter et al., 1995). Multiple inflammatory pathways are initiated in response to CNTF-induced astrocyte activation, as indicated by a transcriptional profile of Müller cells in the mouse retina in which increased expression of TNF and TGF-β, along with several chemokines, was demonstrated (Xue et al., 2011).

In light of the ability of CNTF to induce astrocyte activation, it was hypothesised that such a model could be used to determine the role of astrocytes in metastatic progression. There is much discussion in the literature about the creation of a 'pre-metastatic niche' in malignancy; the formation of a suitable 'soil' at a secondary organ for the growth of metastasising primary tumour cells (Fidler, 2003). By activating astrocytes specifically, it should be possible to assess the contribution of this cell

population to tumour cell extravasation, colonization and growth; if activated astrocytes play a promoting role in brain metastasis then chronic activation will provide an environment permissive to tumour growth. Conversely, if astrocyte activation acts to inhibit metastasis development then tumour burden will be reduced.

Multiple approaches for sustained CNTF delivery to the CNS have been reported in the literature. Acute intracerebral injection of CNTF leads to sustained activation for up to 3 weeks in mice (Bechstein et al., 2012), whilst delivery using microspheres can yield sustained CNTF release for up to 70 days, although this was an *in vitro* assay and may not yield the same effects *in vivo* (Nkansah et al., 2008). For the purposes of the experimental paradigm here, I have used a lentiviral vector containing CNTF, which has been demonstrated to induce sustained astrocyte activation for at least 6 months after CNS delivery (Escartin et al., 2006). This lentiviral approach has been demonstrated previously to only induce minimal amounts of microgliosis (Lavisse et al., 2012), thus giving a model of predominantly astrocyte activation.

The overall aim of this chapter was to elucidate the consequences of astrocyte activation induced by lentiviral CNTF upregulation on the development and growth of brain metastasis. Thus, this chapter had two main aims to address:

1. To determine whether chronic astrocyte activation modulates the initial stages of tumour seeding, by quantifying differences in tumour distribution between hemispheres.

2. To test the hypothesis that chronic astrocyte activation would augment tumour growth *in vivo,* by comparing tumour volumes across an extended time-course.

4.2 Materials & Methods

Two replication-deficient viruses were used in this study, produced as published previously (Escartin et al., 2006) and kindly provided by Carole Escartin (MIRcen, Paris, France): CNTF-lentivirus and LacZ-lentivirus. The CNTF-lentivirus serves as a vector for the human CNTF gene, whilst the LacZ-lentivirus encoded bacterial β-galactosidase, to serve as a control for the administration of virus. The lentivirus can stably integrate its RNA into the host genome, in the form of cDNA. Multiple safeguards are in place to avoid the production of a replication-competent lentivirus. As shown in Figure 4.1, the HIV vector is split into 4 plasmids. Viral particles were produced by transiently transfecting a human embryonic kidney cell line (HEK293T) with the split plasmids. 48 hours after transfection the supernatant was harvested and viral titre determined as previously described (de Almeida et al., 2001).

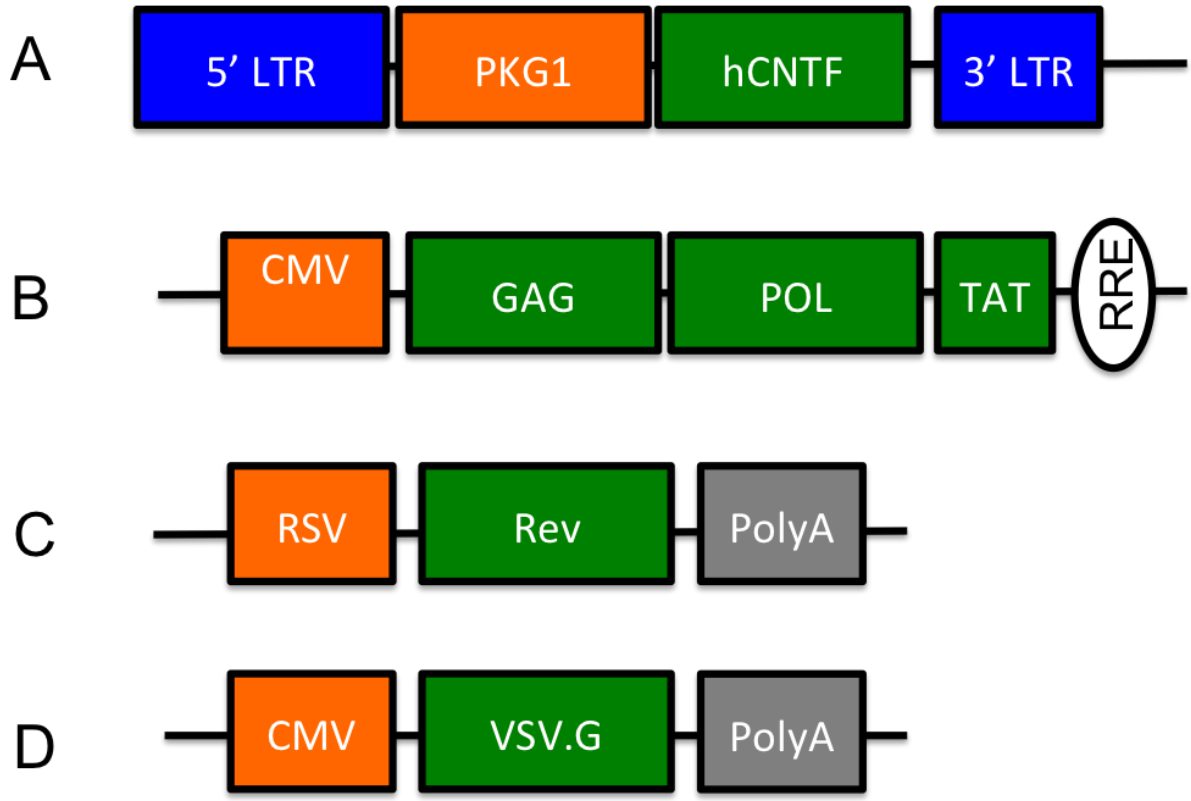

Figure 4.1: Schematic illustrating the structure of the CNTF-lentivirus. In order to improve biosafety, the lentivirus vector was divided into 4 separate constructs. A) Transfer plasmid containing human CNTF RNA/LacZ RNA, under control of the mouse phosphoglycerate kinase 1 promoter (PKG1). The 3' long terminal repeat has a large deletion, rendering the vector self-inactivating. B) Packaging plasmid containing GAG (encoding capsids that form the viral shell), POL (encoding enzymes that catalyse reverse transcription) and TAT, which regulates reverse transcription of viral RNA. The Rev response element (RRE) provides a binding site for the regulator of expression of virion proteins (Rev), which facilitates the export of viral RNA from the nucleus. These genes are under the control of the cytomegalovirus (CMV) promoter. C) A further packaging plasmid, encodes Rev under the transcriptional regulation of the RSV promoter. D) Envelope plasmid, containing vesicular stomatitis virus G-protein (VSV.G) under the CMV promoter. VSV.G confers pseudotyping, that is, it directs viral tropism towards neurons (Colin et al., 2009).

Full experimental methods are described in Materials and Methods 2.2; however the *in vivo* protocol for the following experiments is outlined in Figure 4.2.

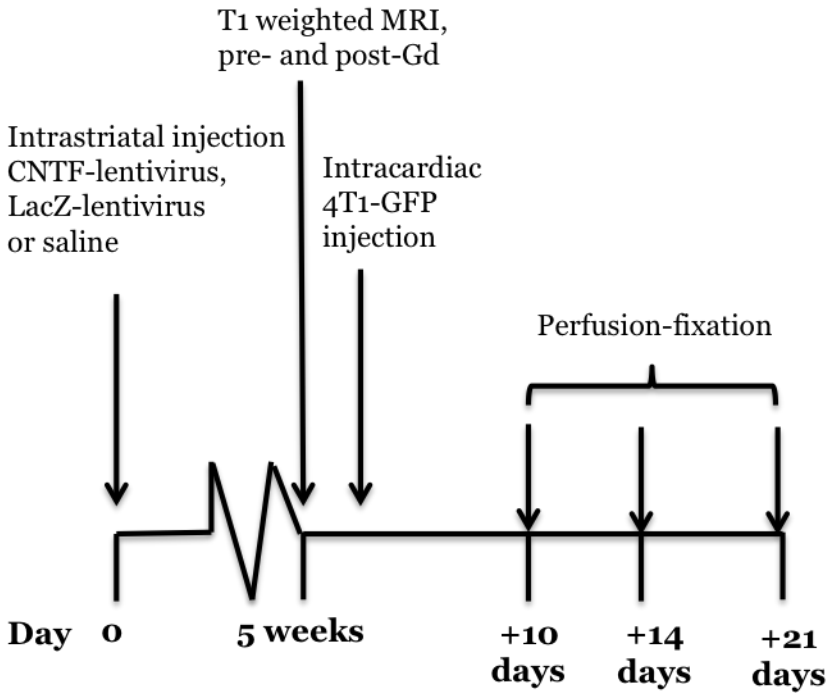

Figure 4.2: Experimental design to determine the role of CNTF activated astrocytes in brain metastasis development. Female BALB/c mice were injected intrastriatally with i) 100ng/µl CNTF-lentivirus, ii) a control LacZ-lentivirus or iii) saline as described in Materials & Methods section 2.2.2.1. After 5 weeks, animals underwent contrast-enhanced MRI (Materials & Methods section 2.2.2.2) in order to assess BBB integrity. At this point, some animals were perfused for histological profiling of the CNS response to lentivirus administration, with regards to glial reactivity and endothelial activation (Materials & Methods section 2.1.3). Further animals were injected intracardially with 10^5 4T1-GFP cells, under ultrasound guidance (Materials & Methods section 2.1.2.1). At days 10, 14 and 21 post-tumour cell injection, animals were perfusion-fixed and tissue processed for histology to quantify tumour burden (Materials & Methods section 2.1.2.1). Both tumour number and volume were analysed, to determine effects of seeding and growth respectively (Methods section 2.2.2.3).

4.2.1 Characterizing the CNS response to CNTF-lentivirus injection

As expected, intracerebral administration of CNTF-lentivirus induced astrocyte reactivity — defined by GFAP upregulation — throughout the striatum and cortex, as observed in Figure. This activation appeared to persist extensively in the anterior—posterior direction from the injection site. Thus, in studies comparing tumour burden, metastases were counted in the region spanning +1.5 mm Bregma to -1 mm Bregma. GFAP staining was also observed in response to LacZ-lentivirus injection (Figure 4.3), although to a lesser degree, indicating less robust astrocyte activation.

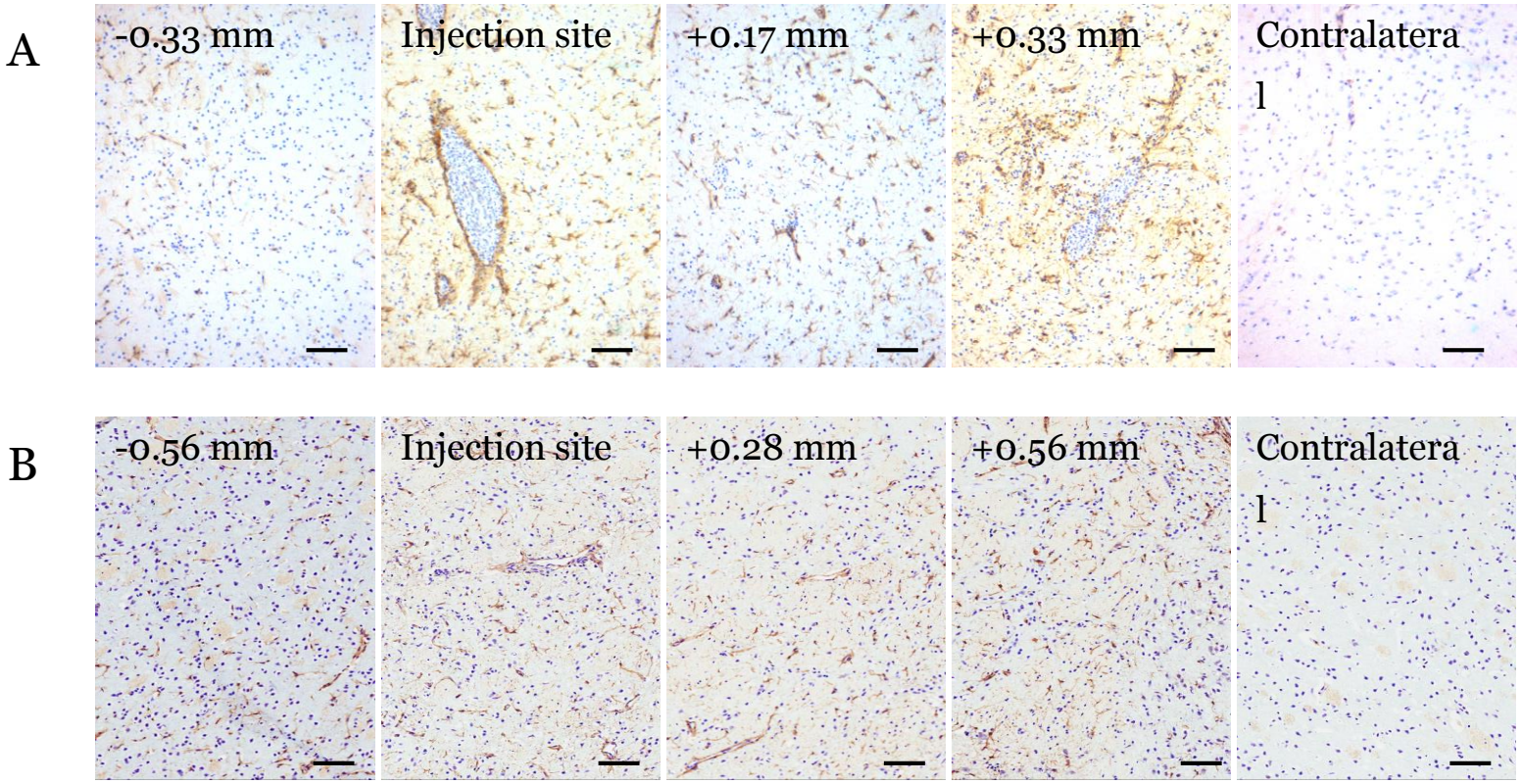

Figure 4.3: Astrocytes are activated in response to CNTF-lentivirus injection. **.** Female BALB/c mice were injected intrastriatally with CNTF-lentivirus or LacZ-lentivirus. At 5 weeks post-injection, animals were perfusion-fixed and tissue processed for histology. 10 μm sections were taken over 3mm surrounding the injection site and tissue stained for GFAP1 in order to detect astrocyte activation. Astrocyte activation was observed in response to CNTF-lentivirus (A) and to a lesser extent in response to LacZ-lentivirus (B). Astrocyte reactivity in the contralateral hemisphere is not observed in response to either virus. Sections are presented with co-ordinates from the injection site. Scale bars = 50 μm.

Although this model of astrocyte activation was purported as a 'clean' technique, eliciting little microglial activation (Lavisse et al., 2012), in our hands, the IBA-1 stain used to reveal the presence of microglia indicated that there was microglial activation in response to CNTF-lentivirus, compared to the contralateral hemisphere (Figure 4.4). This activation extended in the anterior—posterior direction away from the injection site, but the morphology of the IBA-1 positive microglia suggested strongest activation at the site of injection. Moreover, leukocyte recruitment was also observed in this region (discussed below). IBA-1 staining distal to the injection site suggested mild microgliosis, without the robust contraction of processes that characterises strong microglial activation (Kreutzberg, 1996). Microglial activation was also observed in response to the control virus injection. Again, this microglial activation extended to some degree in the anterior—posterior direction from the injection site, but could be characterised as mild activation only (Figure 4.4).

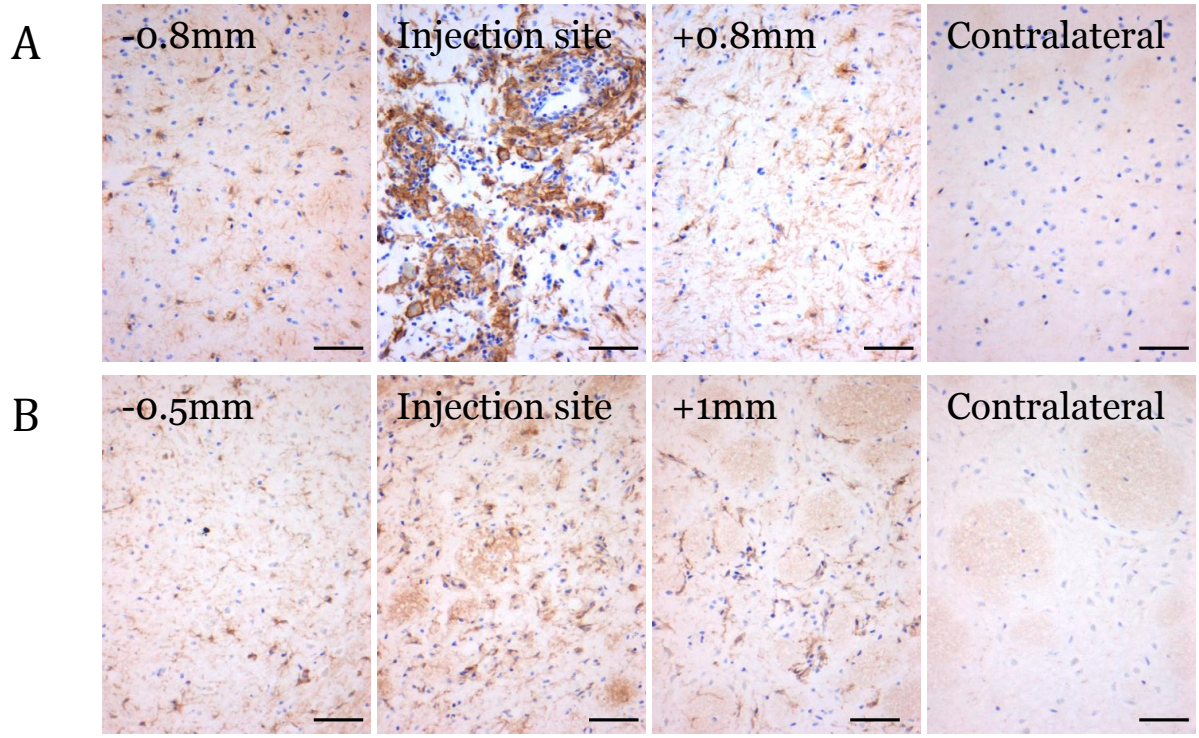

Figure 4.4: Microglia are activated in response to CNTF-lentivirus and to a lesser extent, LacZ-lentivirus. Female BALB/c mice were injected intrastriatally with CNTF-lentivirus or LacZ-lentivirus. At 5 weeks post-injection, animals were perfusion-fixed and tissue processed for histology. 10 μm sections were taken over 3mm surrounding the injection site and tissue stained for IBA-1 in order to detect microglial activation. Microglial activation was observed in response to CNTF-lentivirus (A), although this appears most robust at the site of injection. IBA-1 reactivity in the contralateral hemisphere is not observed. Microglial activation was also observed in LacZ-lentivirus animals, but this activation appeared less robust and more diffuse (B). IBA-1 reactivity in the contralateral hemisphere is not observed. Sections are presented with co-ordinates from the injection site. Scale bars = 50 μm.

Due to the intimate association between astrocytes and the BBB endothelium, mice underwent T1-weighted MRI, pre- and post-Gd-DPTA, in order to assess BBB integrity in response to chronic astrocyte activation. Focal hyperintensities were found in 41% of animals (n=17), indicating BBB permeability to the contrast agent at the site of injection (Figure 4.5). However, this region of BBB breakdown did not correlate with

increased tumour growth, as shown in the schematic in Figure 3.5, which was constructed by mapping the sites of metastatic colonization over 1 mm of brain tissue, onto the post-Gd T1 weighted MRI image. This area of BBB breakdown was associated with strong leukocyte recruitment, as observed histologically on cresyl violet stained sections proximal to the injection site (Figure 4.6). The dense, punctate staining observed was strongly suggestive of a robust infiltration of leukocytes, which on closer assessment of nuclear morphology appeared to be predominantly lymphocytes, rather than neutrophils (Anthony et al., 1997).

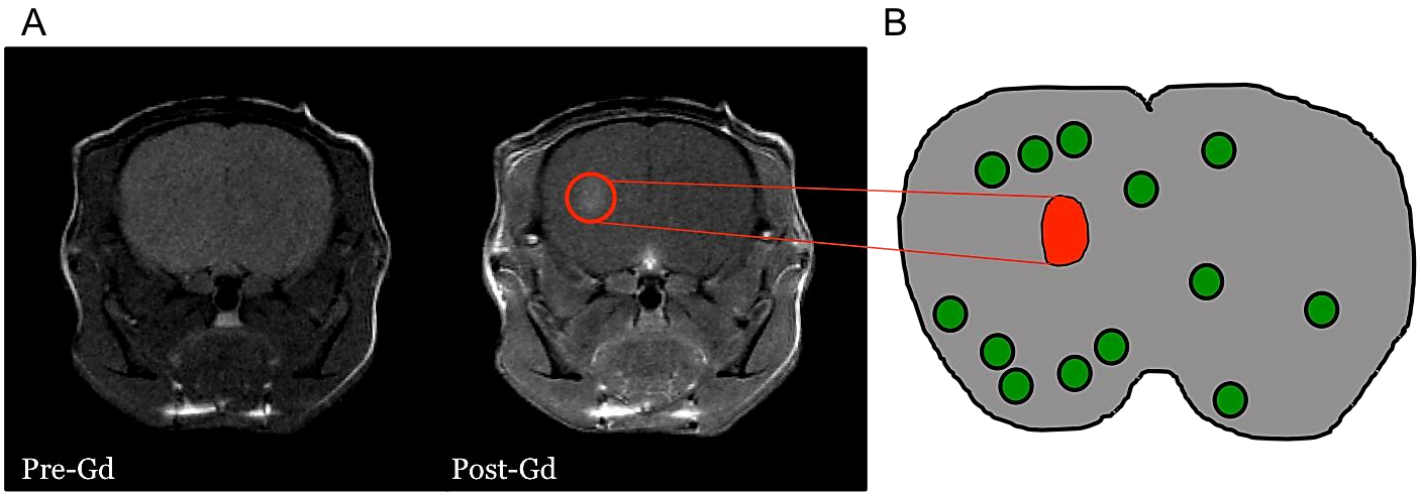

Figure 4.5: CNTF-Lentivirus injected animals display BBB breakdown, as revealed by Gadolinium enhanced MRI. (A) At 5 weeks post-lentivirus injection, were anaesthetised under 2% isofluorane in 70:30 NO2: oxygen. A cannula was placed in the lateral tail vein, and animals placed supine in a custom made cradle. Animals underwent MRI in a 7T Varian system, under maintenance anaesthesia of 1.8% isofluorane. Temperature and respiration were monitored throughout. T1 weighted imaging was performed, pre- and post-gadolinium (Gd) injection via the IV tail-line. T1 hyperintensities were observed in 41 % of animals imaged (n=17). (B) The region of BBB breakdown does not correlate with increased metastatic seeding. Schematic displays distribution of metastases (green), relative to the region of BBB breakdown (red) over 1 mm of tissue in the anterior—posterior direction, in a representative brain.

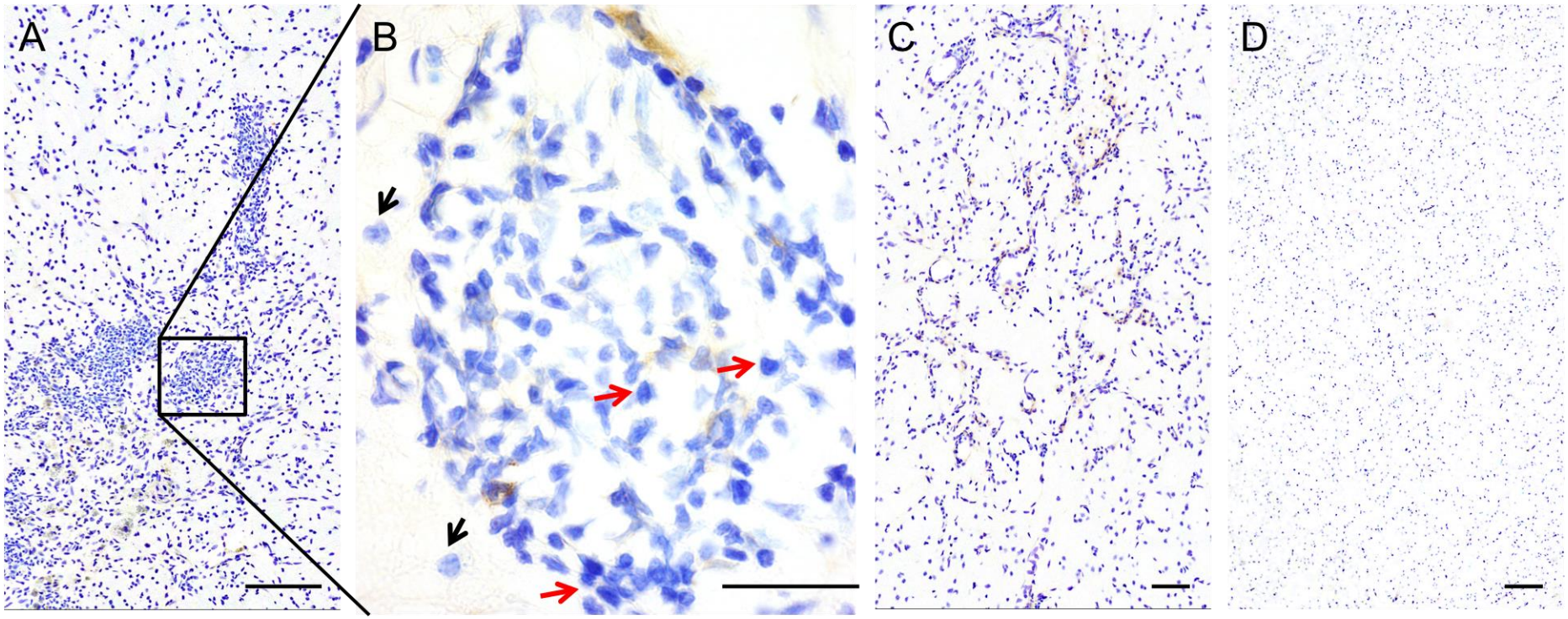

Figure 4.6: CNTF-Lentivirus injection leads to leukocyte recruitment. Intracerebral injection of CNTF-lentivirus induces immune-cell infiltration around the site of injection as revealed with a cresyl violet nuclear stain (A). (B) Photomicrograph of the infiltrate at higher-power magnification (x60) demonstrates the presence of neutrophils (black arrows) and lymphocytes (red arrows). (C) Mild leukocyte infiltration was observed in LacZ—lentivirus animals, whilst none was observed in saline injected animals (D). Scale bars denote 100 μm or 50 μm (B).

I hypothesised that astrocyte activation might lead to increased metastatic colonization through signalling with endothelial cells and endothelial activation. Therefore, the expression of cellular adhesion molecules was assessed in response to striatal injection of CNTF-lentivirus. As evident in Figure 3.7, ICAM-1 appeared to be upregulated in the injected hemisphere compared to the contralateral hemisphere. However, quantitative analysis of DAB positive pixels in the injected hemisphere compared to the contralateral hemisphere, did not reach significance (paired t-test, $p=0.1550$). VCAM-1 expression was also observed in response to the CNTF-lentivirus, although again quantitative analysis did not reveal significant increases in expression compared to the contralateral hemisphere (Figure 4.8, paired t-test, $p=0.201$). It is clear from the analysis that there is a large amount of variation between the animals, which may account for the lack of significance. In the case of ICAM-1, the cellular morphology of CAM expression suggests that this was microglial expression, rather than endothelial expression in the CNTF-lentivirus injected hemisphere. For the case of VCAM-1 the endothelial expression seemed to be primarily associated with vessels near the site of leukocyte recruitment.

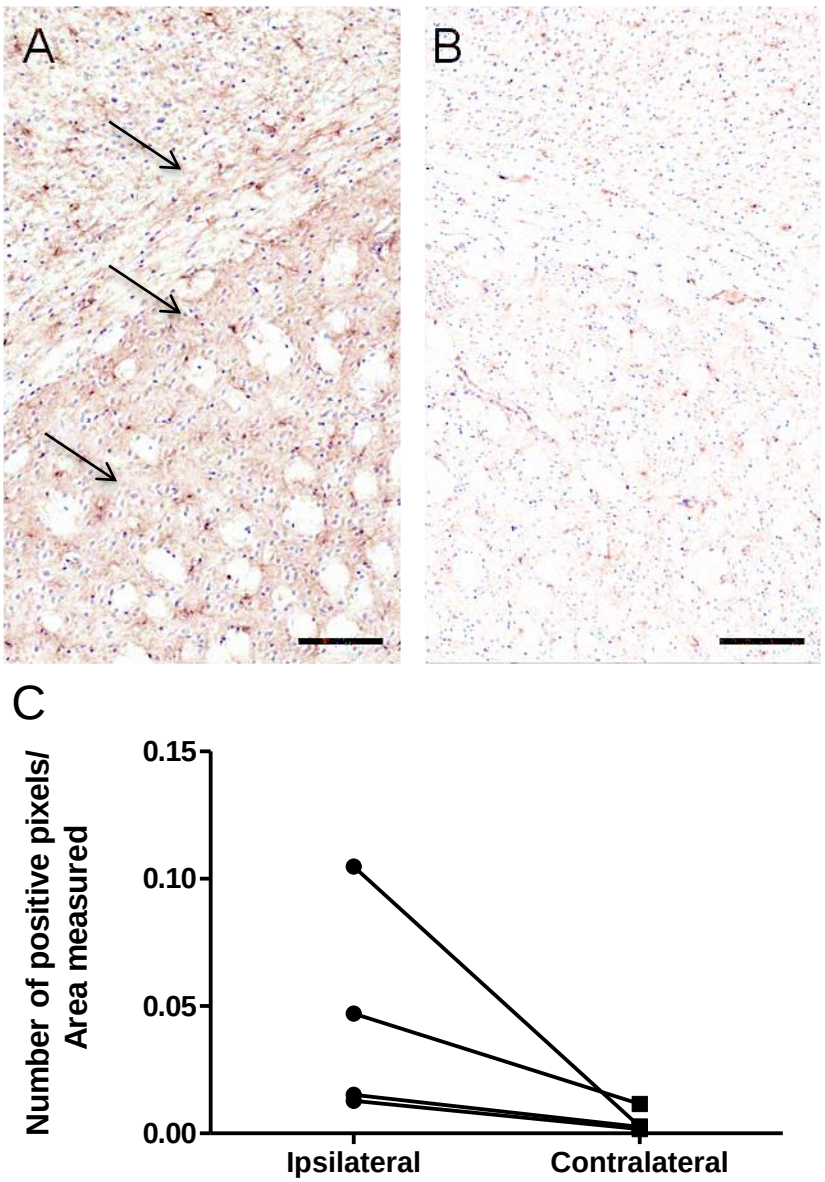

Figure 4.7: ICAM-1 is observed in response to CNTF-lentivirus mediated astrocyte activation. Female BALB/c mice were injected in the left striatum with CNTF-Lentivirus. After 5 weeks, animals were perfusion fixed (n=4) and tissue processed for histology. ICAM-1 expression was detected using immunohistochemistry, visualised with DAB (brown). ICAM-1 was upregulated in the hemisphere injected with CNTF-lentivirus (A), whilst little expression was evident in the contralateral hemisphere (B). Quantitative analysis of DAB positive pixels in both the ipsilateral and contralateral hemisphere, normalised to area measured, revealed that ICAM-1 was not significantly upregulated in response to CNTF-lentivirus (C; paired t-test p=0.155).

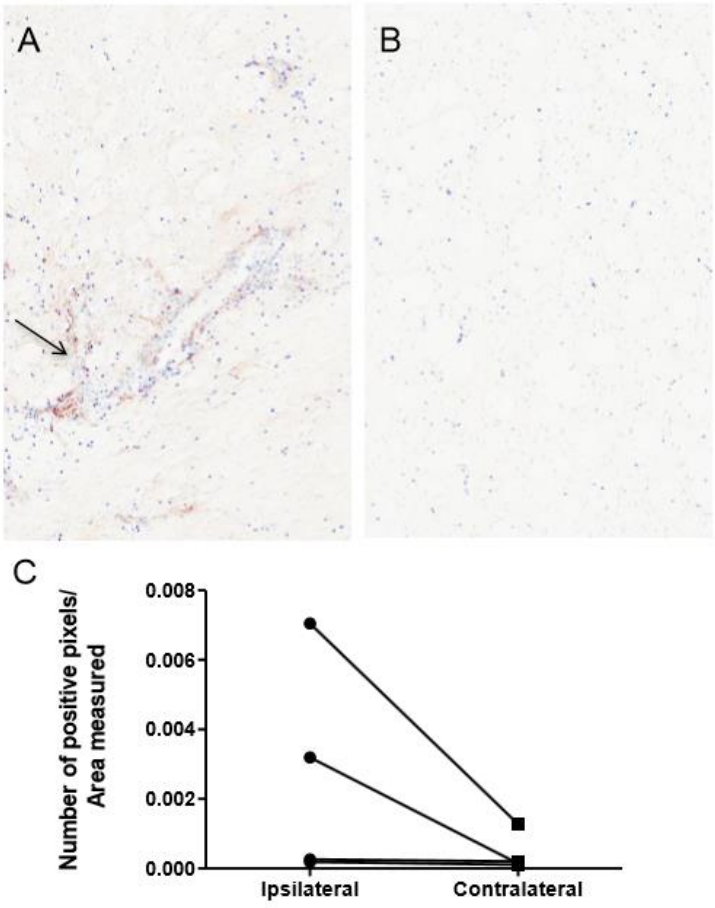

Figure 4.8: VCAM-1 is observed in response to CNTF-lentivirus mediated astrocyte activation. Female BALB/c mice were injected in the left striatum with CNTF-Lentivirus. After 5 weeks, animals were perfusion fixed (n=4) and tissue processed for histology. VCAM-1 expression was detected using immunohistochemistry, visualised with DAB (brown). VCAM-1 was upregulated in the hemisphere injected with CNTF-lentivirus (A), however, this was mainly associated with vessels around the site of leukocyte recruitment (arrows). No expression was evident in the contralateral hemisphere (B). Quantitative analysis of DAB positive pixels in both the ipsilateral and contralateral hemisphere, normalised to area measured, revealed that VCAM-1 was not significantly upregulated in response to CNTF-lentivirus (C; paired t-test p=0.201).

In addition to determining the effect of CNTF-lentivirus within the brain, the proliferative or anti-proliferative effect of CNTF on 4T1-GFP cells was also assessed. To this end, an MTT assay was conducted *in vitro*. As shown in Figure 4.9, incubation with recombinant human CNTF for 24 hours did not modulate 4T1-GFP cell metabolic activity, compared to cells treated with media alone (paired t-test $p=0.374$; $n= 18$). Thus, it is likely that any proliferative advantage (or disadvantage) conferred to tumour cells by the CNTF-lentivirus can be attributed to changes within the CNS itself.

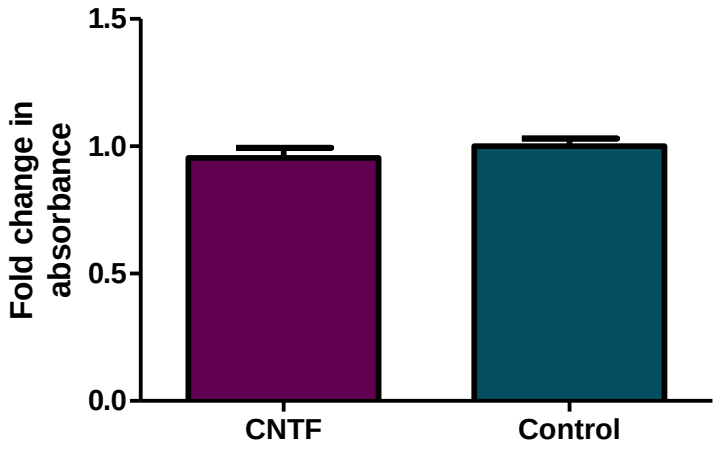

Figure 4.9: CNTF stimulation does not modulate 4T1-GFP cell metabolic activity *in vitro*. 4T1-GFP cells were seeded on a 12 well plate and treated with either CNTF at 50 ng/ml or control media. After 24 hours, an MTT assay was conducted to assess cellular metabolism. Absorbance values were normalised to baseline (control media). Paired t-test p = 0.275; n= 18. Data are given as mean ± S.E.M.

4.2.2 Chronic astrocyte activation does not alter tumour seeding

In order to determine the effect of astrocyte activation on tumour cell seeding, animals were injected intrastriatally with CNTF-lentivirus. After 5 weeks, animals were injected intracardially with 4T1-GFP cells, as described in Methods section 2.1.2.1. At 10 days post-tumour inoculation, tumour burden was quantified via GFP immunoreactivity, with the contralateral hemisphere used as an internal control for tumour seeding. As shown in Figure 4.10, in this model of astrocyte activation, there is no difference was found in the distribution of metastases between the two hemispheres (paired t-test p=0.247, n=9). As a control for both the injection of viral particles, and the injection itself, animals were injected intracerebrally with either a control virus (LacZ-lentivirus) or saline alone. In both

control experiments, no difference in tumour distribution was observed between the two hemispheres (Figure 4.10, LacZ-lentivirus; p= 0.407, n=3; saline; p=0.432, n=5).

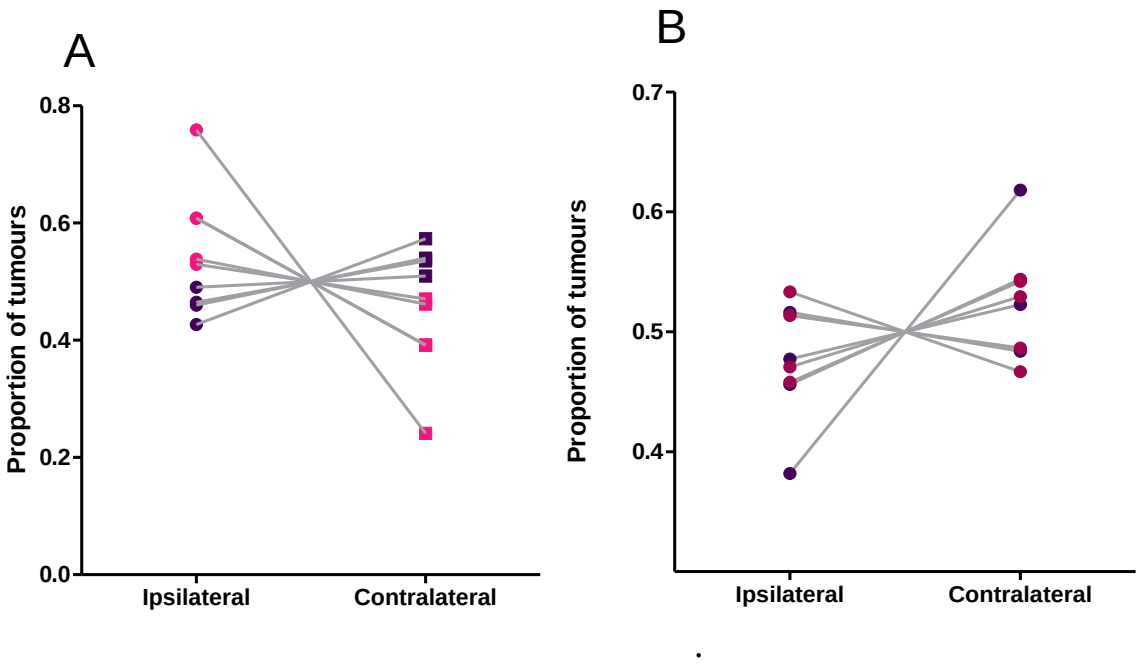

Figure 4.10: CNTF-Lentivirus mediated astrocyte activation does not modulate tumour seeding *in vivo*. Female BALB/c mice were injected in the left striatum with A) CNTF-lentivirus (100ng/μl) or B) LacZ—lentivirus or saline. After 5 weeks, animals were injected intracardially with 10^5 4T1-GFP cells. At day 10 post tumour inoculation, animals were perfusion fixed and tissue processed for histology. Tumour burden was quantified via GFP immunoreactivity and the distribution of tumour number calculated. (A) No significant difference was found in tumour distribution between the two hemispheres in animals injected with CNTF-lentivirus (paired t-test, p= 0.247, n=9). In the above plot, the pink data set represents animals in which more metastases were found in the ipsilateral hemisphere as compared to the contralateral hemispheres. The purple data sets represent the inverse. (B) No difference in tumour distribution was observed in animals injected with LacZ—lentivirus (B, purple data set) or saline (B, pink data set). Note that the y-axis starts at 0.3.

Although the proportion of tumours did not differ between the two hemispheres, it is possible that chronic astrocyte activation accelerates the extravasation process. In which case, a skew towards larger tumours in the lentivirus-injected hemisphere might be expected. However, as shown in the frequency histogram in Figure 4.11, no difference was evident in the size distribution of metastases between the two hemispheres in mice injected intracerebrally with CNTF-lentivirus.

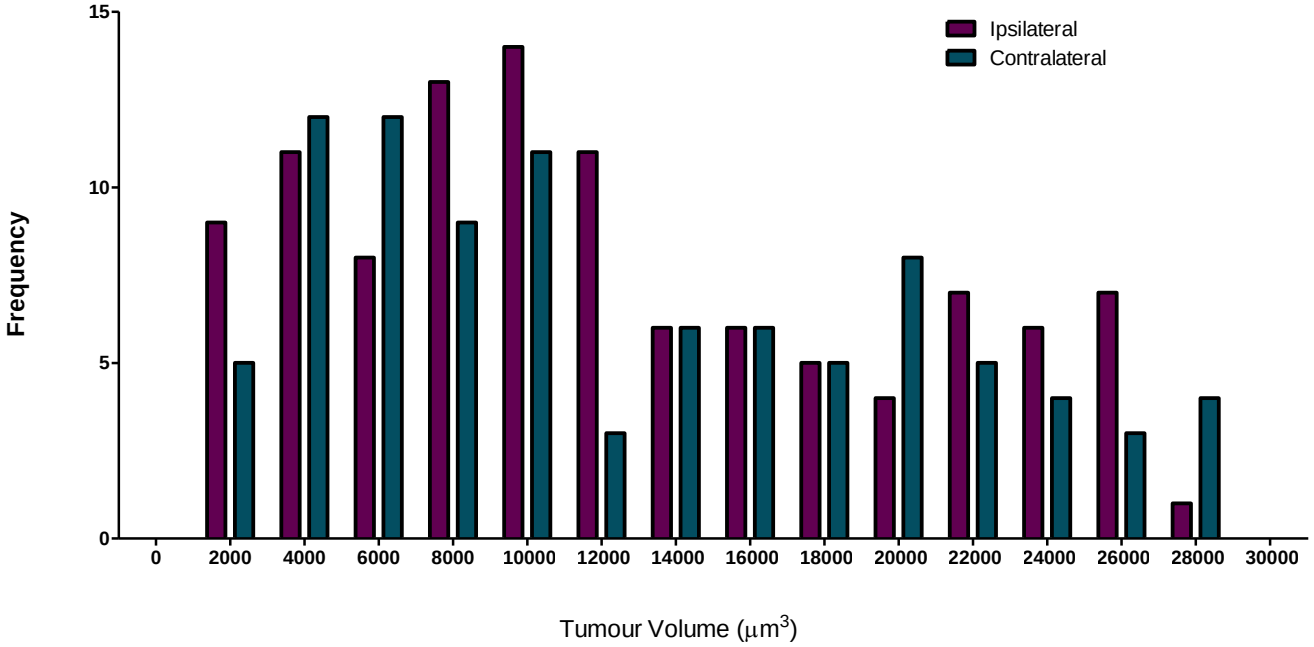

Figure 4.11: Frequency histogram of tumour volume at day 10 post-tumour inoculation. A frequency histogram was generated displaying tumour volumes below the median value. No significant difference was found in the frequency distribution of tumour volumes between the two hemispheres (Chi Squared, p= 0.675).

4.2.1 Chronic astrocyte activation does not modulate tumour growth in vivo

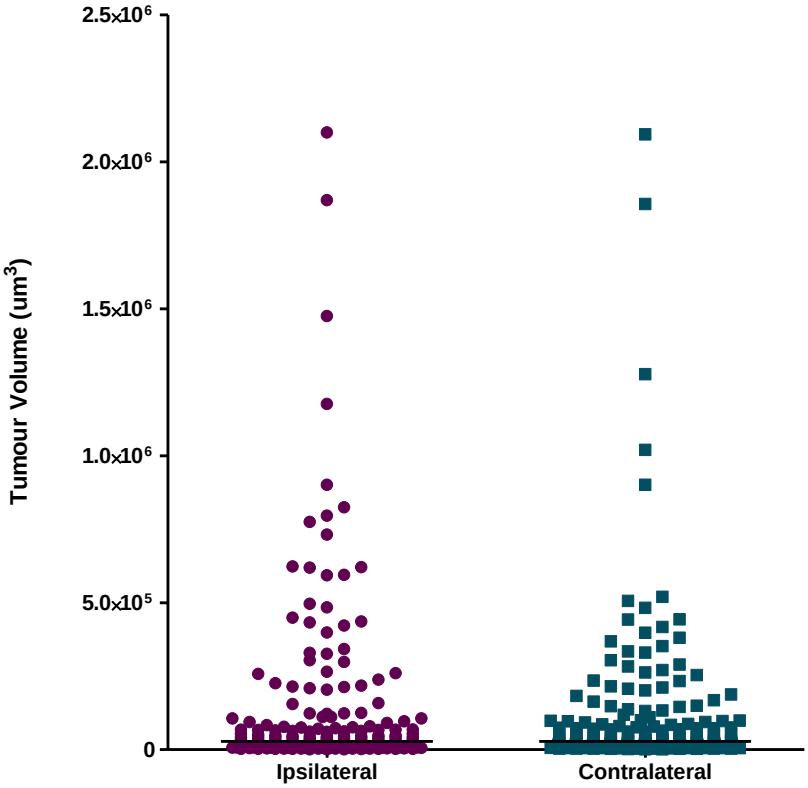

Figure 4.12: The median tumour size between hemispheres at day 10 post-tumour inoculation does not vary significantly. Tumour volumes between the two hemispheres were compared at day 10 post-tumour inoculation. As tumour sizes were not normally distributed, a Mann—Whitney test for non-parametric data was performed, revealing no significant difference in the median values (p= 0.887). Data are presented as individual points, with the black horizontal line denoting the median value.

Comparison of the median tumour volume at day 10 post-tumour inoculation did not reveal any modulation of growth by astrocyte activation (Figure 4.12, Mann—Whitney test, p=0.887). Although no alteration of tumour volume was observed in response to CNTF-induced astrocyte activation, day 10 is a relatively early time-point and an extended time-course was studied to investigate this further. To this end, tumour burden in the context of CNTF-lentivirus induced astrocyte activation was also quantified at days 14 and 21 post-tumour inoculation. As shown in Figure 4.13, no significant difference in tumour volume was found between the two hemispheres at any time point (two-way ANOVA, p=0.572). Additionally, average tumour volume across the time-course was fitted to an exponential curve to compare the rate of growth between hemispheres. Again, no significant difference was found in the rate of tumour growth between the two hemispheres (Figure 4.13, p=0.576). Thus, CNTF-mediated astrocyte activation does not appear to modulate tumour growth in this model of brain metastasis. This finding was corroborated by subsequent experiments in which direct tumour implantation into the striatum 5 weeks after CNTF-lentivirus administration did not lead to a change in tumour growth, compared to LacZ-lentivirus-injected or naïve mice (Figure 4.14 , one-way ANOVA, p= 0.366). However, there did appear to be a suggestion of increased tumour growth, subsequent to lentivirus injection in general (CNTF and LacZ) compared to naïve mice. However, large inter-animal variability meant that this difference did not reach significance (one-way ANOVA, p=0.145).

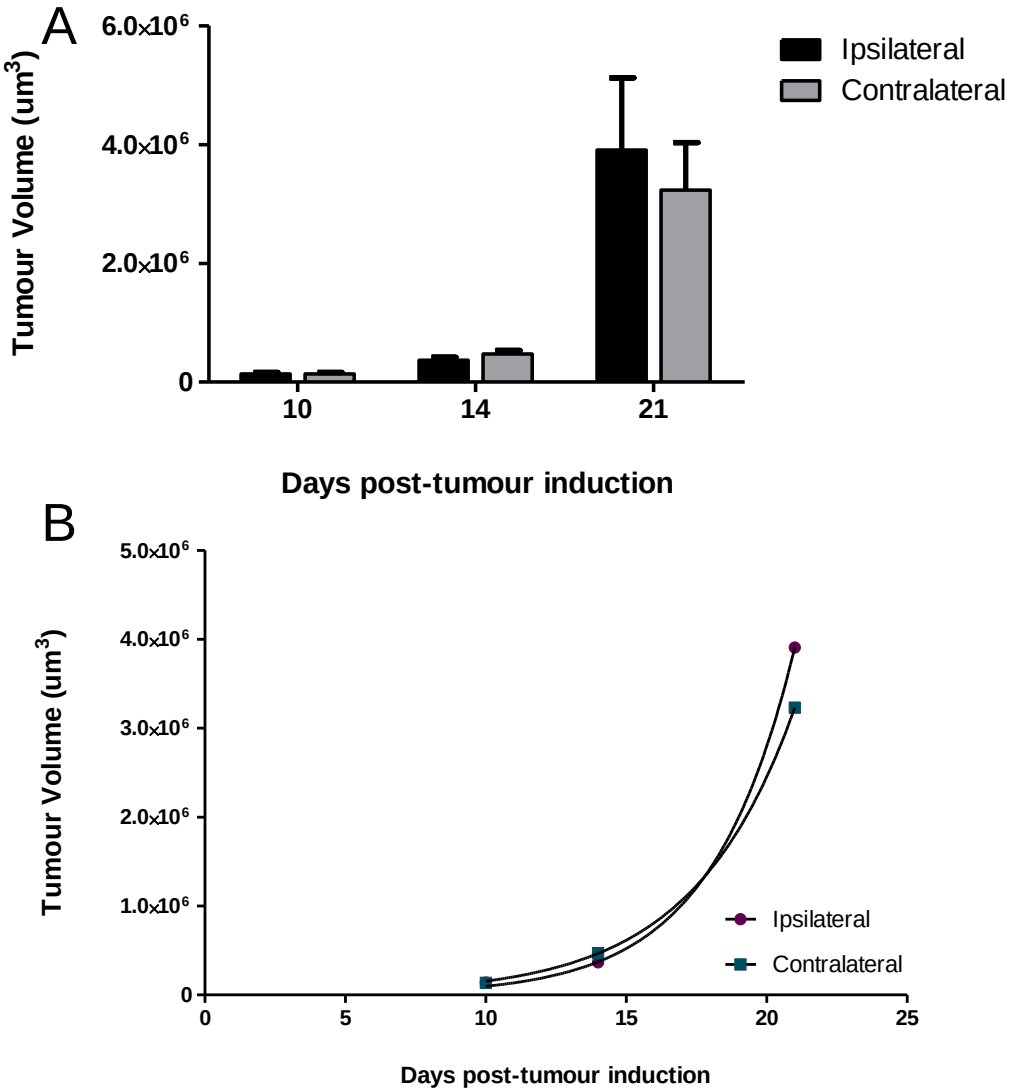

Figure 4.13: Astrocyte activation does not modulate tumour growth over a 21-day time-course. Female BALB/c mice were injected in the left striatum with CNTF-lentivirus. After 5 weeks, animals were injected intracardially with 10^5 4T1-GFP cells. At days 10, 14 and 21 post-tumour inoculation, animals were perfusion fixed and tissue processed for histology. Tumour burden was quantified via GFP immunoreactivity.
(A) Tumour volume was compared between the hemispheres (day 10; n= 155, day 14; n=361, day 21; n=142) and no significant difference was observed between hemispheres at any time-point (Two-way ANOVA; p= 0.572). Equally, there was no change in the rate of growth across time between each of the hemispheres (Two-way ANOVA; p= 0.596). Data are presented as mean values ±S.E.M. (B) Average tumour volumes across the time-course were fitted with an exponential curve. There is no significant difference between the rate of tumour growth between the ipsilateral and contralateral hemispheres (p= 0.576). Ipsilateral: Y= 3391*exp(0.336x) Contralateral: Y= 9757*exp(0.2763x).

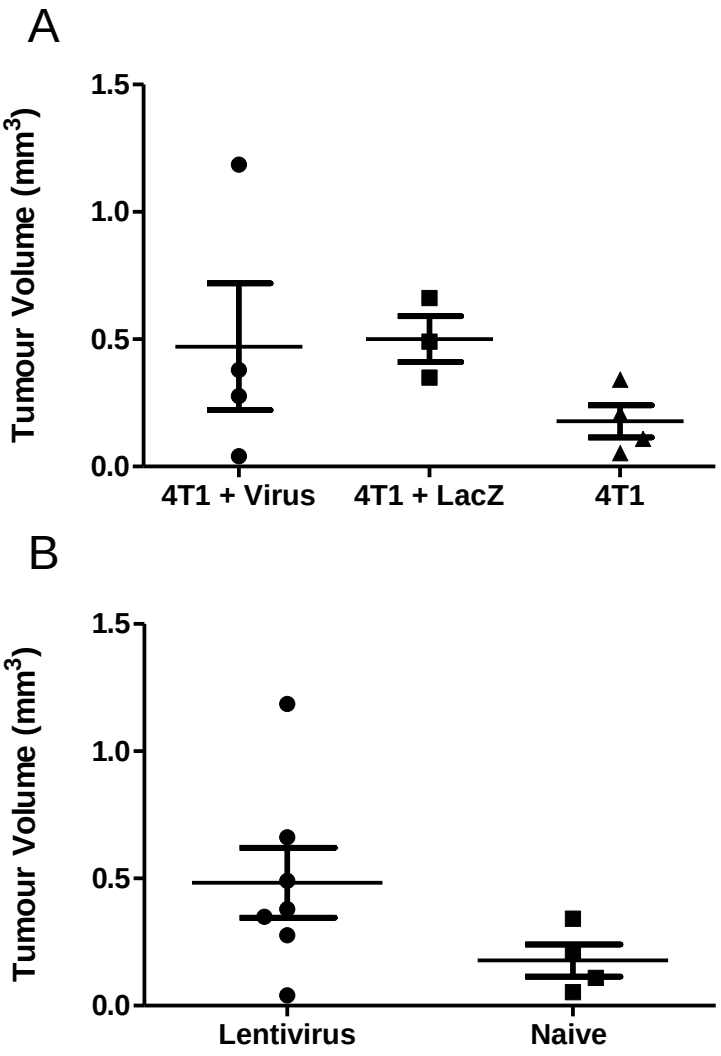

Figure 4.14: CNTF-Lentivirus does not confer a growth advantage to 4T1-GFP cells injected intracerebrally. Female BALB/c mice were injected intracerebrally with CNTF-Lentivirus (n=4) or LacZ-Lentivirus (n=3). After 5 weeks, animals were injected with 5 x 10^5 4T1-GFP cells. At 14 days post-tumour inoculation, animals were perfusion fixed and tissue processed for histology. Tumour volume was determined with GFP histology and compared to naive animals injected with 4T1-GFP cells (n=4). A) No modulation of tumour growth was seen in animals injected with either virus, compared to naive mice, injected with 4T1-GFP cells (one-way ANOVA p=0.366). B) Tumour volumes were combined for animals injected with lentivirus (CNTF and LacZ) and compared to naive mice injected with 4T1-GFP cells. Again, no significant difference was found between the groups (one-way ANOVA, p=0.145), although the data suggest a trend towards increased tumour growth in lentivirus injected animals.

4.2.2 Comparison of the transcriptional profile of astrocytes in response to CNTF and TCM

As previously discussed, astrocytes have a wide range of roles in the CNS. Consequently, it is likely that the transcriptional profile of astrocytes differs depending on the nature of the stimulus. In order to compare the astrocytic response to CNTF to that which would be elicited by the presence of tumour cells, *in vitro* qPCR experiments were conducted in primary astrocyte cultures.

Figure indicates that the transcriptional profile of astrocytes stimulated for 24 hours with human CNTF (hCNTF) is different to that of astrocytes stimulated with tumour-conditioned media (TCM), although there are some overlapping features. As demonstrated in Figure 4.15, IL-6 was significantly upregulated in response to TCM stimulation, but was unchanged in CNTF-stimulated astrocytes (one-way ANOVA, $p < 0.05$). However, IL-1β and iNOS expression was significantly reduced in response to TCM, but not significantly altered by CNTF treatment (iNOS: one-way ANOVA, $p=0.036$; IL-1β: one-way ANOVA, $p=0.0107$). With regards to similarities, in response to both CNTF and TCM, MMP-2 expression was augmented (one-way ANOVA, $p < 0.0001$). In this experimental set-up, TNF expression was not modulated by either CNTF or TCM (one-way ANOVA, $p=0.382$).

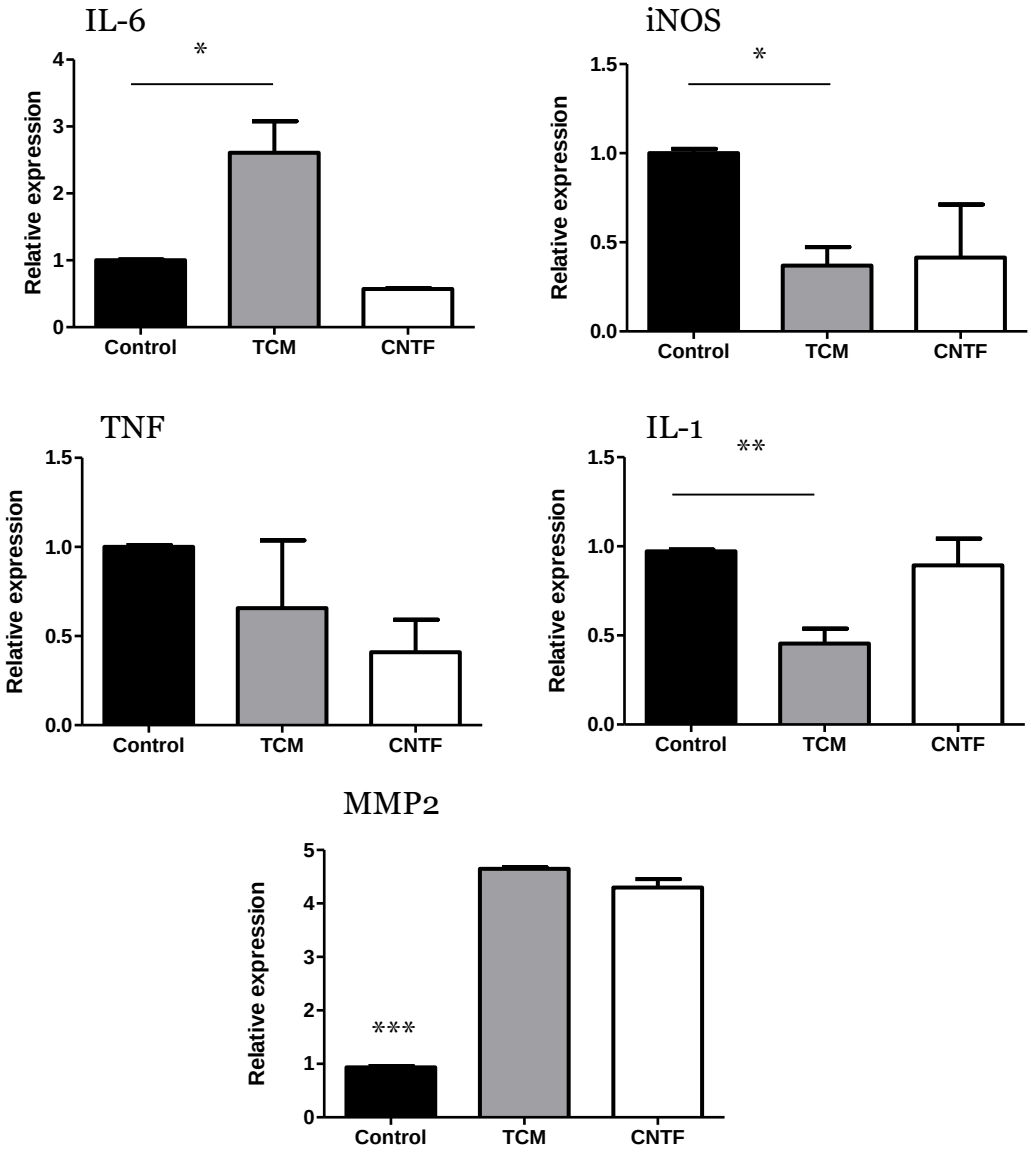

Figure 4.15: The transcriptional profile of astrocytes differs dependent on challenge. Astrocytes were isolated from mouse pups at p5. Cultures were stimulated with either tumour conditioned media (TCM) or CNTF for 24 hours (n=3), before RNA isolation. qPCR was performed, and data normalised to two housekeeping genes (CANX and SDHA) and expressed as expression relative to control wells. Post-hoc tests (Dunnett's multiple comparisons test, control vs treatment) where relevant One-way ANOVA: IL-6 $p=0.129$, TCM vs control $^{*}p < 0.05$; iNOS $p=0.0336$, TCM vs control $^{*}p < 0.05$; TNF $p=0.382$; IL-1β $p=0.0107$, $^{**}p < 0.01$; MMP2 $p < 0.0001$, TCM vs control $^{***}p < 0.0001$, CNTF vs control $^{***}p < 0.0001$. = 0.390. (C) IL-1β expression is decreased in astrocytes in response to TCM and CNTF. Data are presented as mean values ± S.E.M.

4.3 Discussion

In this chapter I used an *in vivo* model of chronic astrocyte activation to investigate the role of astrocyte activation in both metastatic seeding and tumour growth. In order to activate astrocytes over a prolonged time period, a lentivirus was used to specifically induce neurons to over-express CNTF. The chronic and elevated production of CNTF by neurons leads to sustained astrocyte activation, as previously characterized (Escartin et al., 2006; Escartin et al., 2007; Lavisse et al., 2012). In our hands, astrocyte activation was demonstrated to spread in the anterior—posterior direction from the injection site, throughout the striatum and also beyond the corpus collosum into the cortex. Microglial activation was also observed, but was largely restricted to the injection site, and only diffuse and mild at more distal locales. Whilst previous studies have indicated that significant microglial activation is not a feature of this model, in that study histological comparisons were made to the control virus, rather than naïve brain. In our hands, the LacZ-lentivirus also induced mild microglial activation, compared to the contralateral hemisphere, which may account for the discrepancy with the published literature (Lavisse et al., 2012). This microglial activation is clearly a confound in drawing any conclusion specifically about the role of astrocytes in this model. Furthermore, the apparent breakdown of the BBB in some animals indicates that this is not a 'clean' model of astrocyte activation, and other CNS responses are activated. Nevertheless, in light of the marked astrocyte activation observed, this model is still a useful tool for manipulating astrocyte reactivity over a sustained period *in vivo*.

As CNTF is a growth factor that can elicit proliferative signalling downstream of the IL-6 receptor (Schuster et al., 2003) as well as the CNTF receptor itself, the neuronal growth factor may act directly on tumour cells to induce proliferation. Indeed, there is evidence that CNTF induces cell cycle progression in hepatocellular cancer cell lines (Hu et al., 2008). Conversely, in numerous breast cancer cell lines, despite expression of the CNTF receptor, CNTF has been shown not to induce tumour cell proliferation (Douglas et al., 1997). In light of the above conflicting reports, in order to determine the effect of CNTF on 4T1-GFP cells, *in vitro* cultures were incubated with hCNTF prior to an MTT assay to assess cellular metabolism. As demonstrated, hCNTF stimulation did not induce 4T1-GFP cell proliferation. Therefore, it was concluded that in this experimental paradigm, any modulation of tumour growth is likely to be a result of astrocyte activation, rather than a direct effect of CNTF on the tumour cells.

Previous *in vivo* studies have shown that astrocytes become activated by day 3 post-tumour cell inoculation, whilst metastasising cells are still adhered to the luminal side of the endothelium (Lorger and Felding-Habermann, 2010). This finding suggests that astrocytes are activated in response to endothelial activation and that this in turn, could modulate tumour cell extravasation. However, this possibility has received little attention to date. Whilst numerous cell adhesion molecules have been implicated in mediating tumour cell extravasation across the endothelium in peripheral organs, similar routes across the BBB have yet to be fully defined. One potential mediator of tumour cell traversal is ICAM-1. ICAM-1 has been shown to interact with lymphocytes and macrophages and, thus, plays a role in transendothelial migration. Neutralising antibodies against ICAM-1 have been

shown to decrease lung cancer cell invasion in an *in vitro* Matrigel invasion assay (Yu et al., 2012). With regards to brain metastasis, ICAM-1 upregulation has been demonstrated in the tumour microenvironment (Soto et al., 2013), but no studies to date have addressed its role in tumour extravasation. The interaction between ICAM-1 and LFA-1 mediates leukocyte adhesion to the endothelium (Marlin and Springer, 1987) and *in vitro* models suggest that ICAM-1 is essential for T-cell migration across the BBB (Reiss et al., 1998). Thus, it is possible that ICAM-1 upregulation may facilitate cancer cell extravasation into the CNS. Increased VCAM-1 expression has also been shown to be correlated with brain metastatic development and, in fact, endothelial expression of VCAM-1 in response to metastatic growth can be used as a biomarker for tumour burden (Serres et al., 2012). Moreover, neutralising antibodies that ameliorate VCAM-1—VLA-4 interactions between tumour cells and the endothelium have been shown *in vivo* to reduce brain metastatic burden (Soto et al., 2013).

In the current study, despite astrocyte activation and apparent upregulation of ICAM-1 and VCAM-1, no increase in metastasis seeding was found. This finding was surprising based on studies in the lungs indicating that the induction of inflammation leads to enhanced metastatic burden (Garofalo et al., 1995; Okahara et al., 1994). However, this finding may in part reflect the observation that CAM upregulation was not robustly associated with the endothelium; ICAM-1 staining appeared to be consistent with microglial expression, whilst VCAM-1 expression seemed limited to the injection site. . Moreover, previous studies (Hamilton, A., DPhil thesis, 2013) have also shown that increased VCAM-1 expression on the CNS vasculature prior to tumour inoculation does not lead to an enhanced metastatic

burden. Additionally, it is possible that any seeding advantage conferred by astrocyte activation itself may be negated by the immune cell recruitment observed in the affected region in the model used here; no tumour growth was observed at the site of lentivirus injection, suggesting that there may be tumouricidal activity of the immune cell infiltrate. Overall, it is apparent that the model of astrocyte activation generated here does not induce a 'pre-metastatic niche' that is permissive to tumour colonisation.

In this model, astrocyte activation also did not significantly modulate tumour growth, as assessed by quantifying tumour volume over a 21-day time-course. Again, this result is surprising based on the published literature, in which the bulk of *in vitro* experimental evidence suggests that astrocyte activation leads to increased tumour cell proliferation and invasion. There may be several explanations for this finding. Firstly, the time-course of the experiment may not be appropriate. This could be argued at both ends of the time-course. It is possible that day 10 is too late to observe the effect of CNTF-induced activation alone, since activation of astrocytes by the tumour cells themselves by this time point may augment/attenuate the initial effects of CNTF. Conversely, the length of the time-course may not be sufficient to observe effects on tumour growth. In the intracardiac model, there does appear to be a trend towards increased tumour volume in response to CNTF-lentivirus at day 21 post-tumour cell injection. Moreover, taking into account the data from the intracerebral model, which represents a much later time point in disease progression, a trend towards increased tumour growth in response to CNTF-lentivirus is indicated. This exacerbation was more evident when all lentivirus-treated animals were

considered together in the intracerebral model; it should be noted that there was mild astrocyte activation was present in all such animals. Thus, extending the time-course further may tease apart differences between experimental and control hemispheres.

An alternative hypothesis would be that the 'state' of astrocyte activation induced by CNTF does not create a microenvironment appropriate for augmented tumour growth (although, equally, no inhibition of tumour growth is seen). As discussed in Chapter 3, an important consideration is the fact that astrocyte activation is a spectrum of phenotypes, and different challenges elicit distinct transcriptional profiles in astrocytes. Thus, whilst astrocyte activation induced by CNTF may not accelerate metastatic progression, other activated phenotypes may be. Indeed, whilst CNTF appears to elicit an inflammatory phenotype in Muller cells, recent qPCR analysis of the parenchyma in response to CNTF-lentivirus injection suggests that whilst TNF is upregulated, a host of other inflammatory mediators remain constant (Lavisse et al., 2012). Therefore, whilst it might be reasonable to predict that astrocytes in a neuroprotective phenotype would create a microenvironment permissive to tumour growth, this model may not provide the inflammatory environment required to drive tumour progression. Indeed, studies comparing microglial activation by CNTF and IL-6, both of which act through the same family of receptors, demonstrate different phenotypes. IL-6 was found to drive a pro-inflammatory milieu, whilst CNTF induced microglia-mediated neuroprotection (Krady et al., 2008). Supporting this, it is evident from preliminary *in vitro* experiments conducted here that the transcriptional profile induced in astrocytes by TCM differs to that induced by CNTF. Notably, IL-6

mRNA expression was induced in astrocytes stimulated with TCM, but not with CNTF. IL-6 production has previously been demonstrated in astrocytes co-cultured with a brain-metastasizing lung cancer cell line (Seike et al., 2011), and IL-6 has been implicated in promoting brain metastasis growth *in vivo* (Noda et al., 2012). Additionally, qPCR studies presented in chapter 3 indicate that IL-6 is a feature of the tumour microenvironment *in vivo*. Thus, the apparent lack of IL-6 production in CNTF-stimulated astrocytes may account in part for the lack of tumour growth modulation in the *in vivo* model, and provide further, albeit indirect, support for the tumour promoting effects of IL-6.

MMP2 expression in cultured astrocytes was induced by both TCM and CNTF. MMP2, as explained in Chapter 3, is an ECM remodeling enzyme that has been shown to be upregulated in the brain metastatic environment, as well as being released by astrocytes in response to brain metastasis (Mendes et al., 2007; Mendes et al., 2005; Wang et al., 2013). This result is in line with a recently published report that astrocyte condition media enhances invasion and migration in a range of tumour cell lines and that this phenotype is partially mediated by astrocyte-derived MMPs, including MMP2. Moreover, inhibition of MMP2 has been shown to reduce brain metastasis *in vivo* (Wang et al., 2013). In order to explore this concept further, an *in vitro* assay could be performed in which tumour cells are co-cultured with CNTF stimulated astrocytes, and the invasive nature of the metastasising cells compared to those co-cultured with unstimulated astrocytes.

The apparent reduction of astrocyte iNOS mRNA expression in response to TCM was unexpected based on the published literature. iNOS is induced by pro-inflammatory cytokines such as TNF and IL-1β, which were predicted to be present in the tumour milieu. qPCR of rat islet cells indicates that CNTF does not alter iNOS expression (Wadt et al., 1998), although no such analysis has been reported in the CNS. These *in vitro* PCR results contradict the immunofluorescence data presented in Chapter 3 that demonstrate astrocytic iNOS expression in the tumour periphery. It is possible, therefore, that astrocytic iNOS expression in response to TCM is dependent on paracrine signalling with other cells such as microglia in the microenvironment. Additionally, in this *in vitro* model, astrocytic IL-1β mRNA expression was also attenuated in response to TCM treatment. Thus, a negative feedback loop might be in place regulating iNOS expression. However, this result contradicts *in vitro* studies previously published indicating that astrocyte—tumour cell co-culture leads to an increase in astrocyte derived IL-1β (Seike et al., 2011). This discrepancy may be due to the differences in the *in vitro* system: co-culture versus treatment with conditioned media. Elevation of IL-1β may be dependent on a more sustained signal.

Some caution must be exercised with regards to the current study, in particular in relation to the dosing level of CNTF as compared to the raft of stimulatory factors in TCM. In order to more faithfully recapitulate the *in vivo* scenario, astrocytes could be co-cultured with neurons transfected with CNTF-lentivirus. Additionally, inhibition studies must be performed in order to determine the relevance of each of the secreted factors in the context of tumour growth. Nevertheless, despite these

confounds, the data observed are of value in understanding the nature of the CNTF-mediated model used and perhaps shed light on some of the *in vivo* findings.

4.4 Conclusions and further work

The results of this study suggest that the role of astrocytes in brain metastasis is likely dependent on the nature of astrocyte activation. I have demonstrated here that astrocyte activation via CNTF stimulation does not significantly modulate metastatic progression, with no difference seen in either tumour seeding or growth within the CNS. I have demonstrated, however, that the nature of astrocyte activation in response to CNTF is likely to be different to the activation state elicited in the tumour microenvironment. This work further adds to the previous chapter, highlighting the concept of astrocyte phenotypes.

The experimental model used here provides a foundation to further explore the nature of the astrocytic response to metastases. Several questions require further attention. It would be valuable to pursue the nature of signalling between astrocytes and the endothelium. The observation of BBB breakdown in the CNTF-lentivirus model demonstrates the intimate connection between astrocyte reactivity and the integrity of the BBB. In order to probe this at a molecular level, an *in vitro* model of the BBB could be used. As such, changes in tight junction proteins could be investigated in response to CNTF-stimulated astrocytes, and compared to changes observed in response to TCM-stimulated astrocytes.

As mentioned earlier, previous work within the research group has shown that certain neuroinflammatory challenges prior to tumour inoculation do not appear to modulate tumour seeding in the brain. Thus, one could conclude that unlike in the periphery, an inflammatory milieu in the CNS does not necessarily create a pro-tumourigenic environment for tumour seeding. However, that previous study did not quantify tumour growth. Therefore, perhaps a model in which chronic inflammation was initiated would shed light on whether or not, once metastases have colonised, their rate of growth can be modulated by changes in the microenvironment inflammatory profile. In the intracerebral model presented above, a trend towards increased tumour growth was found in response to lentivirus (CNTF + LacZ) injection. As there was astrocyte and microglial activation in response to LacZ injection, it could be argued that gliosis in response to viral injection alone — a more broad neuroinflammatory challenge than that mediated solely by CNTF — can promote tumour proliferation. The adenoviruses discussed earlier, driving TNF and IL-1β production in the brain, may provide a useful starting point (Campbell et al., 2007; Solum, 1975). However, the study conducted here demonstrates the difficulty in modulating cellular phenotypes in isolation *in vivo*. Going forward, in order to elucidate the role of astrocytes at the molecular level, it may be better to pharmacologically alter one or several of the factors implicated in the tumour microenvironment. Although this may not tell us solely about the contribution of astrocytes, it would give a more clinically relevant experimental paradigm, with the aim of reducing tumour burden.

A meta-analysis of clinical data, looking at the interaction between CNS pathology and incidence of brain metastasis would be a fascinating study. No such literature

exists at the moment, but this approach would allow conclusions to be drawn as to whether or not chronic CNS inflammation provides a pro-tumourigenic environment for metastatic growth. In the case of primary brain tumours, a number of longitudinal studies in various CNS pathologies have been conducted, with varied conclusions about cancer risk. In the case of MS, an increased relative risk in brain tumour occurrence was found in an analysis of patient records over a 35-year period (Fois et al., 2010) and this fits the hypothesis that CNS inflammation can contribute to tumour growth. However, no increase in relative risk was observed in another retrospective study of patient records in Denmark (Nielsen et al., 2006); the elevated relative risk observed in some studies could be accounted for by increased diagnosis due to frequent CNS scans. Additionally, no alteration of relative risk was observed in patients with either Parkinson's or motor neuron disease (Fois et al., 2010). A meta-analysis of all the published studies from different global cohorts would be incredibly useful, as well as an extension to consider metastatic disease from peripheral primary tumours.

In conclusion, CNTF-activated astrocytes did not significantly modulate brain metastasis seeding or progression. In order to determine the role of astrocytes in tumour development, an alternative approach is to consider *in vivo* astrocyte inhibition studies, as will be discussed in the following chapter.

Chapter 5 Modulation of astrocyte activation and tumour burden with glucocorticoids

In the previous chapter, I discussed the use of a lentiviral model to induce astrocyte reactivity. In that study, I found that enhanced astrocyte activation by CNTF did not significantly modulate tumour seeding or tumour growth *in vivo*. In this chapter, I will use a pharmacological agent to, conversely, inhibit astrocyte activation. Based on *in vitro* evidence in the literature, combined with trends in tumour growth observed in response to chronic astrocyte activation *in vivo*, I hypothesise that the attenuation of astrocyte activation will lead to a reduction in metastatic burden.

5.1 Introduction

As discussed in Chapters 1 and 3, there is a substantial inflammatory component to the tumour microenvironment, with the bulk of evidence suggesting that inflammation facilitates tumour progression (Hanahan and Weinberg, 2011). Thus, it seems likely that anti-inflammatory agents could modulate tumour burden. The wide range of immunomodulatory therapeutics that have been trialled pre-clinically and clinically is beyond the scope of this thesis. However, in the following sections I will discuss the use of steroids in the management of malignancy.

5.1.1 Glucocorticoids and their mechanism of action

Endogenous glucocorticoids (GCs) have roles in multiple cellular processes as extensively reviewed (Newton, 2000; Zen et al., 2011). At pharmacological concentrations, however, they primarily exert anti-inflammatory effects. As illustrated in Figure 4.1, GCs bind to the cytoplasmic glucocorticoid receptor (GR) and ligand binding induces nuclear translocation. The anti-inflammatory effects of GCs are proposed to be mediated through both transcriptional repression and transcriptional activation (Vandevyver et al., 2013). With regards to transcriptional repression, monomeric GR has been shown to interact with inflammatory transcription factors such as activator protein-1 (AP-1) and NFκB: tethering between GR and transcription factors leads to negative regulation of a raft of inflammatory mediators (Gupte et al., 2013).

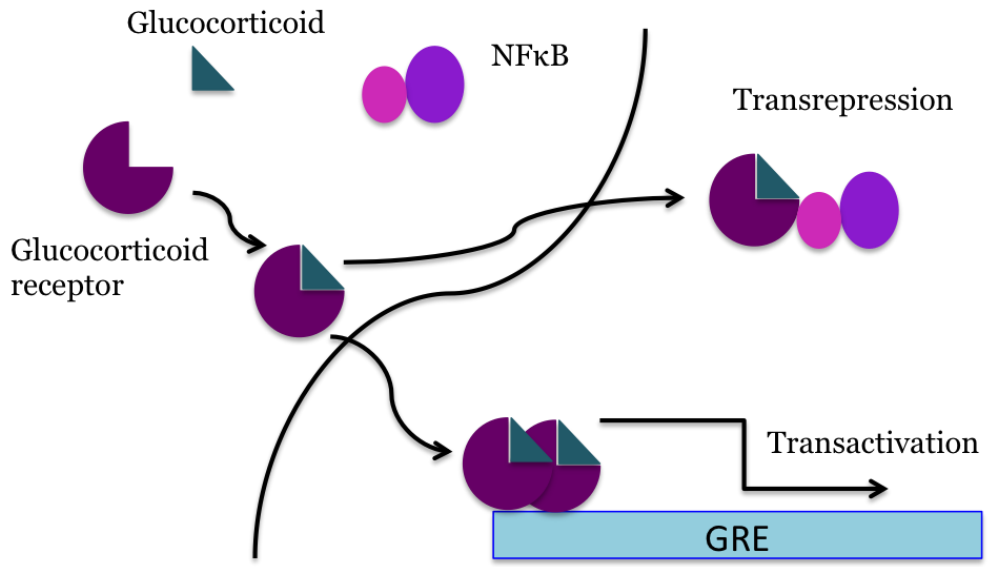

Figure 5.1: The mechanism of glucocorticoid action: Glucocorticoids (GCs) bind to the glucocorticoid receptor (GR), initiating nuclear translocation. Transrepression occurs when the monomeric GR tethers transcription factors such as NFkB. Transactivation occurs when dimeric GR binds to glucocorticoid response elements (GRE) in gene promoter sequences.

Amassing evidence also suggests that GR dimerisation and binding to glucocorticoid response elements (GREs) in promoter sequences leads to transactivation of anti-inflammatory genes. For instance, GCs can lead to the inhibition of leukocyte chemotaxis *in vitro*, via the production of thymosin β 4 sulphoxide (Young et al., 1999). The transcriptional inhibition of NFκB has also been proposed, via transcriptional activation of Kruppel-like factor (KLF2), a zinc-finger DNA binding protein.

Glucocorticoids are routinely used in the clinic as part of a disease management strategy in oncology. In the case of brain metastasis, GCs are used to reduce

vasogenic oedema and hence improve neurological symptoms (Lieberman et al., 1977). The steroid dexamethasone is typically used and therapeutic effects are seen within 24—48 hours (Vecht, 1998). However, as steroids are used in conjunction with chemotherapeutics, it is difficult to determine the clinical role of GCs alone in the modulation of tumour burden.

Brain tumour outcome in response to steroid treatment in pre-clinical models is variable. Experiments have largely been conducted in primary brain tumours, rather than in secondary metastases. A number of *in vitro* studies suggest dexamethasone is anti-proliferative. In the C6 glioma cell line, treatment with dexamethasone led to a reduction in cellular viability (Bavaresco et al., 2007). This direct effect on tumour cells by the steroid appeared to be mediated by the protein kinase c (PKC) signalling pathway, as inhibition of PKC ameliorated the anti-proliferative effect of dexamethasone. Furthermore, assays with the human astrocytoma cell line, U373 MG, suggest that dexamethasone reduces not only cellular viability, but also cellular invasion and migration, a direct effect of the steroid acting on the MAPK signalling pathway (Piette et al., 2009). In *in vivo* models of glioma, dexamethasone was shown to reduce tumour volume, reduce T-cell infiltration and decrease vascularisation, via inhibition of angiopoietin-related protein-2 (Angpt2), a member of the VEGF protein family (Villeneuve et al., 2008). This decrease in vascularisation has been observed in other studies and is associated with reduced tumour burden (Wolff et al., 1993). However, tumour burden reduction was only observed at a high dose of steroid (≥ 1 mg kg^{-1}) that was associated with chronic weight loss, and as such is not clinically relevant (Villeneuve et al., 2008). Further, in another *in vivo* glioma study, dexamethasone

did not prolong animal survival and was additionally associated with side effects such as weight loss and skin infections (Moroz et al., 2011). Regarding secondary cancers to the brain, in an intracranial model of brain metastasis, dexamethasone was shown to reduce to tumour volume compared to control animals (Lewis et al., 2013). However, assays for cellular proliferation and tumour cell apoptosis showed no differences between untreated and treated animals. Rather, the reduction in volume appeared to be an increase in cellular density, although the authors did not investigate the mechanism behind this.

When discussing the use of steroids as a chemotherapeutics, it is important to bear in mind drug interactions with other agents. Dexamethasone has been shown *in vitro* to inhibit the apoptotic action of cisplatin, 5-fluorouracil, temozolamide, taxol, doxorubicin and gemcitabine in a range of cancer cell lines (Kim et al., 2004b; Sur et al., 2005; Zhang et al., 2006). However, disease variability was demonstrated, with the steroid inducing apoptosis in lymphoid cell lines (Zhang et al., 2006). Therefore, care should be taken with treatment planning, as clearly there is variability in steroid action depending on cancer cell origin.

It is evident, from the literature, that the role of GCs alone has not been investigated in a physiologically relevant model of secondary brain cancer. Additionally, in the pre-clinical studies conducted and discussed above, it appears that peripheral toxicity has made determining the benefit of GC use impossible. Thus, using a steroid delivery system that selectively targets the brain could improve the therapeutic index.

5.1.2 2B3-201

2B3-201 is a glutathione-tagged liposome, containing the GC methylprednisolone. The various aspects of the molecule are illustrated in Figure 5.2 and will be described below.

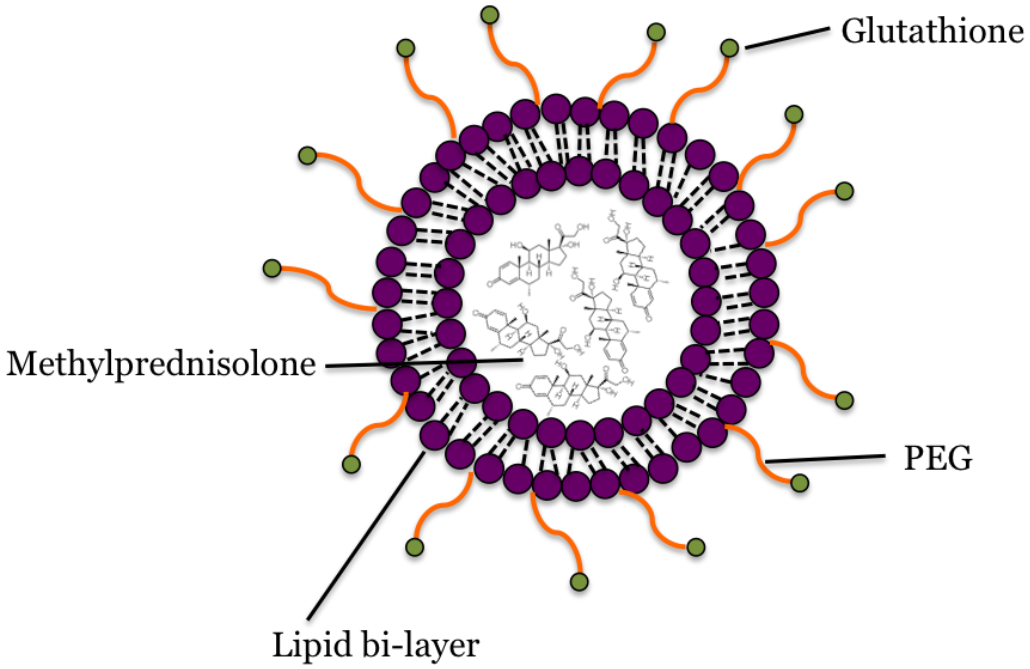

Figure 5.2: Structure of 2B3-201. 2B3-201 consists of liposome- packaged methylprednisolone. The liposomes are 'decorated' with polyethylene glycol (PEG) and glutathione.

5.1.2.1 Liposomal packaging

Glucocorticoids are rapidly cleared after IV administration and consequently, frequent dosing is required to achieve effective concentrations at inflamed sites. Due to the high toxicity profile of GCs, schemes to increase bioavailability are needed to improve the therapeutic index. Encapsulation of drugs in lipid bilayer

vesicles, also known as liposomes, increases the systemic half-life of the drug and improves tissue delivery (Metselaar et al., 2004; Metselaar et al., 2003), and numerous such agents are approved for use in the clinic, including in cancer patients (Kraft et al., 2014). Liposomes are frequently 'decorated' with polyethylene glycol (PEG) to improve pharmacokinetics further; renal clearance is inversely proportional to liposome size (Hamidi et al., 2006). Additionally, PEGylation reduces binding of plasma proteins (Ogris et al., 1999), thus decreasing clearance.

5.1.2.2 Glutathione-PEGylated liposomes

As previously discussed, the BBB prevents the access of many drugs to the CNS. Whilst liposome-packaged drugs have been developed for treatment of neurological disorders, effective CNS delivery requires receptor targeting (Lai et al., 2013). One such targeting strategy involves using the glutathione transporter. Glutathione, an endogenous antioxidant, with multiple roles in the CNS, is taken up by the cerebral microvasculature via glutathione transporters (Kannan et al., 2000; Kannan et al., 1990; Zlokovic et al., 1994). On this basis, it has recently been shown that modifying PEGylated liposomes with glutathione increases the therapeutic impact of packaged steroids in a mouse model of EAE (Gaillard et al., 2012). This increased therapeutic benefit was attributed to increased CNS uptake of steroid. Pharmacokinetic studies carried out with 2B3-201 in rats showed greater retention of the liposome-packaged steroid as compared to free methylprednisolone, 8 hours after administration, both in the plasma and the

brain (Gaillard et al., 2012). The same study showed 2B3-201 anti-inflammatory efficacy in a mouse model of MS, with improved behavioural scores compared to mice treated with free methylprednisolone. This compound is now in Phase I clinical trials in patients with MS.

5.1.2.3 Astrocyte specificity of 2B3-201

Very recently, work done in our group has suggested that 2B3-201 selectively targets inflammatory pathways in astrocytes. As touched upon, glutathione has multiple CNS roles. Astrocytes act as a glutathione pool and as such express glutathione transport mechanisms (Kannan et al., 2000). It is possible, therefore, that 2B3-201 could preferentially target astrocytes. In accord with this hypothesis, in a study utilizing 2B3-201 in a mouse transgenic model of ALS, astrocyte reactivity was shown to be attenuated, whilst microglial activation remained unaltered in response to treatment (M. Evans, in press).

A number of studies have investigated the effects of GCs on astrocytes directly. In an *in vitro* model of hypothermia, treatment with methylprednisolone reduced IL-6 secretion (Schmitt et al., 2006), a key pro-inflammatory cytokine. Methylprednisolone was also shown to reduce GFAP mRNA, as well as chondroitin sulphate proteoglycan (CSPG) expression in an *in vitro* excitotoxic model (Liu et al., 2008). Similarly, in an *in vitro* model of LPS challenge, dexamethasone was shown to reduce expression of phospholipase A2 (Oka and Arita, 1991), an enzyme involved in arachidonic acid metabolism and inflammatory pathogenesis.

Taken together, the above findings led us to hypothesise that 2B3-201 could be used to attenuate astrogliosis *in vivo,* providing another experimental paradigm to address the role of astrocytes in brain metastasis. In this chapter, I will use 2B3-201 to determine whether or not astrocyte inhibition modulates tumour seeding and, additionally, whether or not modulation of astrocyte reactivity alters tumour growth.

5.2 Materials & Methods

In order to address the hypotheses described above, two brain metastases experimental arms were conducted, as summarised in Figures 5.3 and 5.4 and detailed in Materials and Methods section 2.3.

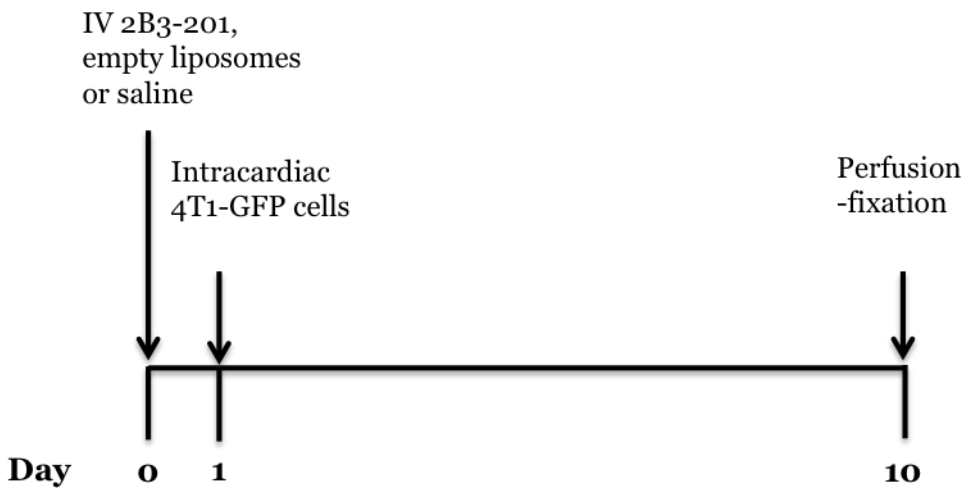

Figure 5.3: Does 2B3-201 alter tumour cell seeding? Female BALB/c mice were injected intravenously with 2B3-201 (10 mg kg^{-1}), empty liposomes or saline. After 24 hours, animals were injected with 10^5 4T1-GFP cells under ultrasound guidance. At day 10 post-tumour cell injection, animals were perfusion-fixed and tissue processed for histology as described above and in Materials & Methods.

In order to assess 2B3-201 efficacy in a focal model of neuroinflammation, a TNF-adenovirus model was used to elicit astrocyte activation, with 2B3-201/saline dosing as illustrated in Figure 5.5 and described in Materials & Methods section 2.3.,

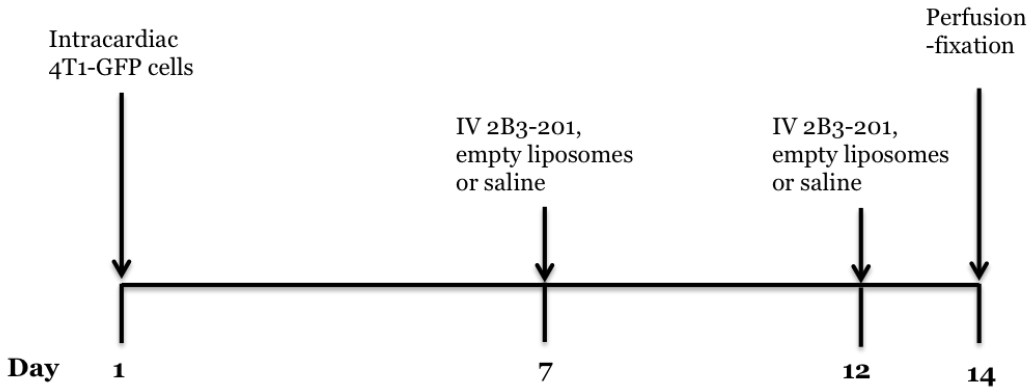

Figure 5.4: Does 2B3-201 alter tumour cell growth? Female BALB/c mice were injected intracardially with 10^5 4T1-GFP cells, under ultrasound guidance. Based on studies regarding the rate of metastatic colonisation, it was concluded that by day 7 post-tumour inoculation, micrometastases would be within the perivascular space. Thus, 2B3-201 administration at this point would affect tumour growth rather than initial colonisation. In addition, studies by to-BBB suggest that the duration of 2B3-201 action is 5 days, thus animals were re-dosed at day 12, in order to maintain the steroidal effect. Thus, at days 7 and 12 post-tumour cell injections, animals were injected intravenously with 2B3-201 (10 mg kg^{-1}), empty liposomes or saline. At day 14, animals were perfusion fixed and tissue processed for histology as described above and in Materials & Methods.

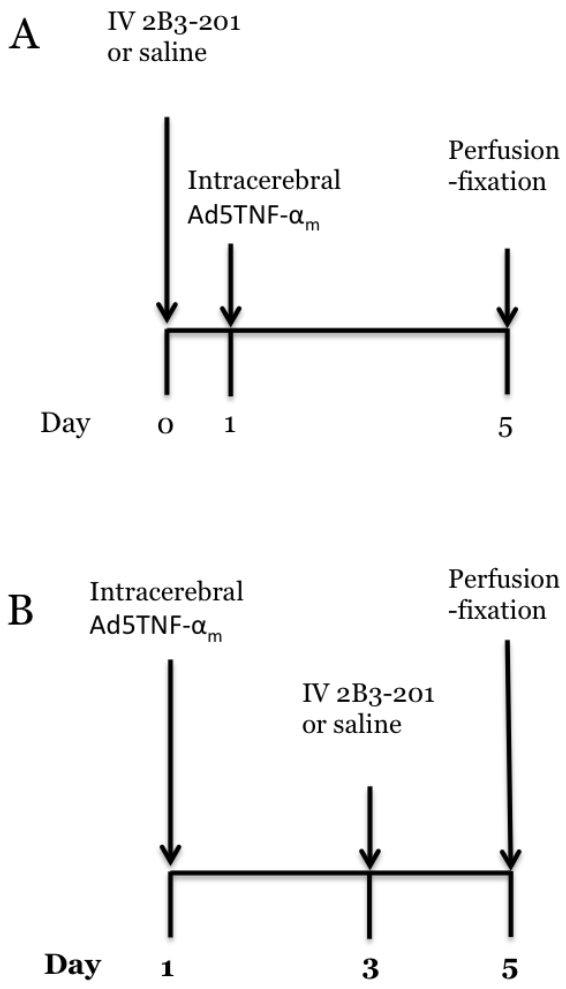

Figure 5.5: Does 2B3-201 modulate astrocyte activation in an Ad5TNF-α$_m$ model of neuroinflammation? Two experimental arms were performed. In the first (A), female BALB/c mice were injected intravenously with 2B3-201 (10 mg kg^{-1}) or saline. After 24 hours, animals were injected intrastriatally with Ad5TNF-α$_m$ and perfusion-fixed at day 5. In the second arm (B), mice were injected intrastriatally with Ad5TNF-α$_m$ and after 3 days were injected intravenously with 2B3-201 (10 mg kg^{-1}) or saline. Again, animals were perfusion fixed at day 5. In both cases, tissue was processed for histology and astrocyte reactivity quantified with regards to the volume of GFAP reactivity.

5.3 Results

5.3.1 Effect of prophylactic treatment with 2B3-201 on tumour seeding

To determine whether steroidal treatment prior to tumour induction alters metastatic seeding, animals were injected with 2B3-201 (10 mg kg^{-1}), empty liposomes or saline; after 24 hours, animals were injected intracardially with 4T1-GFP cells. Tumour number was determined at day 10 post-tumour cell injection. As shown in Figure 5.6, intravenous injection of 2B3-201 24 hours prior to tumour inoculation did not significantly alter tumour seeding, as compared to animals injected intravenously with empty liposomes (n=5—6) or saline (n=3, one-way ANOVA, p=0.0817). However, there did appear to a trend towards reduced tumour number in liposome (empty and full) animals, compared to saline controls. To determine whether or not 2B3-201 has an effect on tumour seeding with regards to the rate of metastatic colonization, tumour volume was analysed, in addition to tumour number. As shown in Figure 5.7, 2B3-201 treatment prior to tumour inoculation did not significantly modulate tumour growth compared to empty liposome control animals, as quantified at day 10 after tumour induction (unpaired t-test, p=0.577).

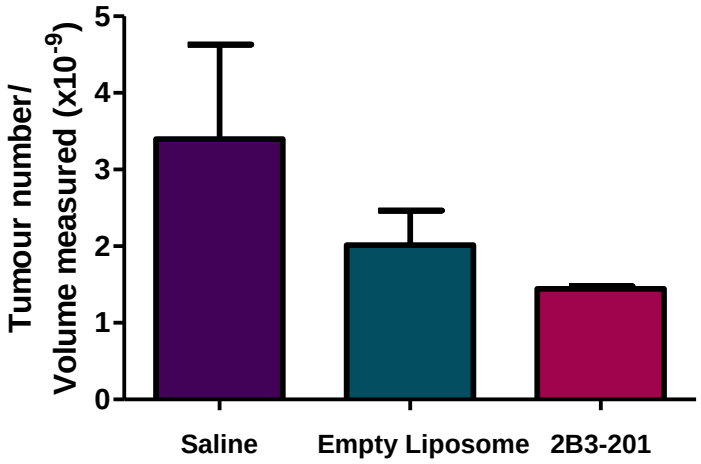

Figure 5.6: Prophylactic 2B3-201 treatment does not significantly modulate tumour seeding compared to the empty liposome control. Female BALB/c mice were injected IV with either 2B3-201 (n=6), empty liposomes (n=5) or saline (n=3). After 24 hours, animals were injected intracardially with 10^5 4T1-GFP cells. At day 10, animals were perfusion-fixed and tissue was processed for histology. Sections were stained for GFP immunoreactivity in order to visualise tumour load. Micrometastases were delineated using ImageScope and tumour number was determined. The total tumour number per animal was normalised to the brain area measured. One-way ANOVA p=0.0817. Bars represent mean ± S.E.M.

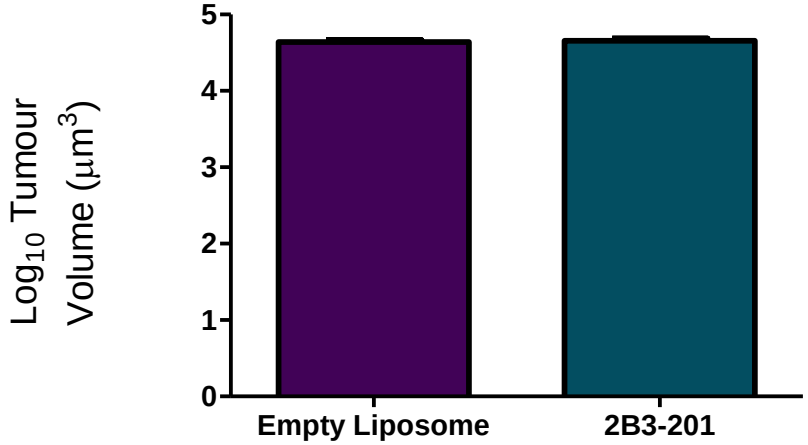

Figure 5.7: Prophylactic 2B3-201 treatment does not modulate tumour volume. Female BALB/c mice were injected IV with either 2B3-201 (n=6) or empty liposomes (n=5). After 24 hours, animals were injected intracardially with 4T1-GFP cells. At day 10, animals were perfusion fixed and tissue processed for histology. Sections were stained for GFP immunoreactivity in order to visualise tumour load. Micrometastases were delineated using ImageScope and tumour volume determined. Tumour volumes were compared between treatment and control groups (empty liposome n= 963; 2B3-201 n= 908). The data were not normally distributed, and so was normalised (log_{10}) prior to statistical analysis. Unpaired t-test, p=0.629. Bars represent mean ± S.E.M.

5.3.2 Effect of treatment of tumour-bearing animals with 2B3-201 on tumour burden

To determine whether 2B3-201 can modulate tumour growth, animals were injected intracardially with 4T1-GFP cells; 7 days after tumour inoculation, animals were injected IV with either 2B3-201, empty liposomes or saline. Animals were dosed again at day 12 after tumour inoculation and perfusion-fixed at day 14. Analysis of tumour burden, defined as the total area of tumour quantified normalised to the area of brain measured, revealed that 2B3-201 does not

significantly alter overall tumour burden within the brain when compared to the empty liposome or saline control (Figure 5.8; one-way ANOVA, p=0.612).

In order to elucidate whether methylprednisolone had an effect when distinct brain regions were considered in isolation, the tumour burden for each of the brain regions were considered separately and compared to empty liposome control animals. Three different brain regions were considered. Region 1 spanned 3 mm to 1.3 mm relative to Bregma and included structures such as the pre-limbic cortex and the anterior part of the striatum. Region 2 extended from -0.5 mm to -1.5 mm relative to Bregma and included structures such as the hippocampus and dentate gyrus. Region 3 spanned -4 mm to -5 mm relative to Bregma, and included structures such as the substantia nigra. As shown in Figure 5.9, no significant differences were found between treatment groups in any region (two way ANOVA p=0.0728). However, in region1, which includes the prefrontal cortex, there does appear to be a trend towards reduced tumour burden in the 2B3-201-treated animals. Indeed, in control animals, there is increased tumour burden in region 1 compared to regions 2 and 3 (two-way ANOVA, p=0.0009). This difference in tumour distribution is not significant in 2B3-201 treated animals.

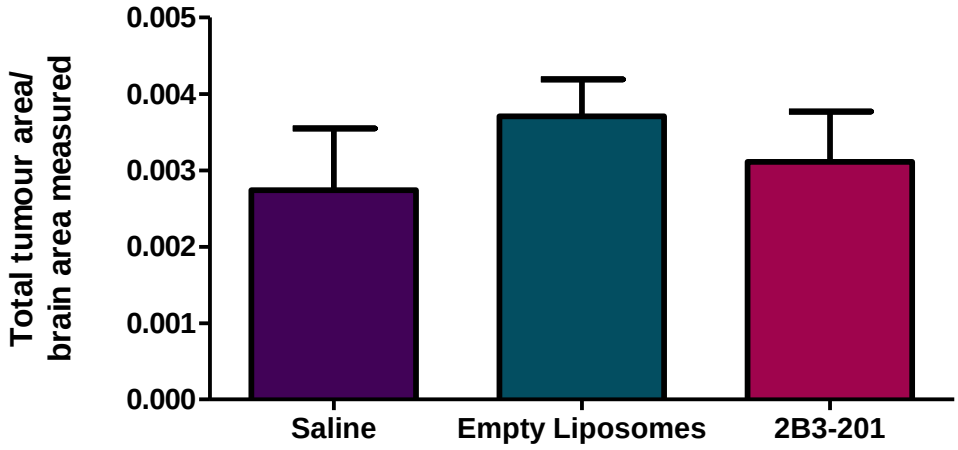

Figure 5.8: 2B3-201 does not modulate tumour burden compared to empty liposome control. Female BALB/c mice were injected intracardially with 10^5 4T1-GFP cells. At days 7 and 12, animals were injected IV with either saline (n=4), empty liposomes (n=4) or 2B3-201 (n=5). At day 14, animals were perfusion-fixed and tissue was processed for histology. Sections were stained for GFP immunoreactivity in order to visualise tumour load. Tumour burden was delineated using ImageScope. The total tumour burden per animal was normalised to the brain area measured. There was no significant difference in tumour burden between 2B3-201 treated animals and empty liposome or saline treated animals. One-way ANOVA, p=0.612. Bars represent mean ± S.E.M.

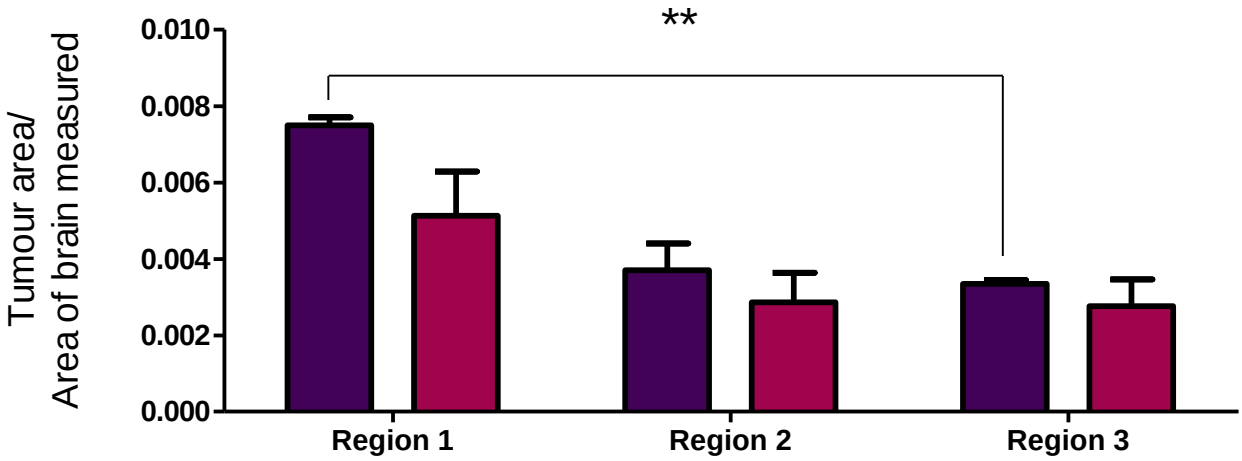

Figure 5.9: 2B3-201 treatment does not modulate tumour distribution across three distinct brain regions. Female BALB/c mice were injected intracardially with 4T1-GFP cells. At day 7 and 12 post-intracardiac injection, animals were injected IV with either empty liposomes (n=4, purple bars) or 2B3-201 (n=5, pink bars). At day 14, animals were perfusion-fixed and tissue was processed for histology. Sections were taken from three different brain regions relative to Bregma 1) 3 mm to 1.3 mm, 2) -0.5 mm to -1.5 mm, 3) -4 mm to -5 mm. Sections were stained for GFP immunoreactivity in order to visualise tumour load. Tumour burden was delineated using ImageScope and the total tumour burden per animal was normalised to the brain area measured. A two-way ANOVA did not reveal any effect of treatment on tumour burden (p=0.502). Tumour burden was not modulated by treatment in any brain region (p=0.0728), however, tumour burden was significantly different in the different brain regions; tumour burden is greatest in region 1 compared to the other regions (Tukey post-hoc test, p=0.0009). Bars represent mean ± S.E.M.

5.3.3 The effect of 2B3-201 on astrocyte activation in response to brain metastasis

As 2B3-201 did not appear to alter the progression of brain metastasis, the astrocytic response to steroid treatment was determined, via quantification of the ratio of astrocyte activation to tumour area. If 2B3-201 acted to reduce astrocyte activation, one would hypothesise that there would be a reduced area of astrocyte activation in response to brain metastasis. As shown in Figure 5.10, the ratio of astrocyte activation to tumour area was not significantly altered by 2B3-201 treatment after tumour inoculation (unpaired t-test, $p=0.429$).

As a trend towards reduced tumour burden was observed in brain region 1, GFAP reactivity was compared in this region alone in order to assess 2B3-201 effect on astrocyte activation. However, as shown in Figure 5.11, there was no significant difference in the ratio of astrocyte activation to tumour area, was evident between the two treatment groups (unpaired t-test, $p=0.361$).

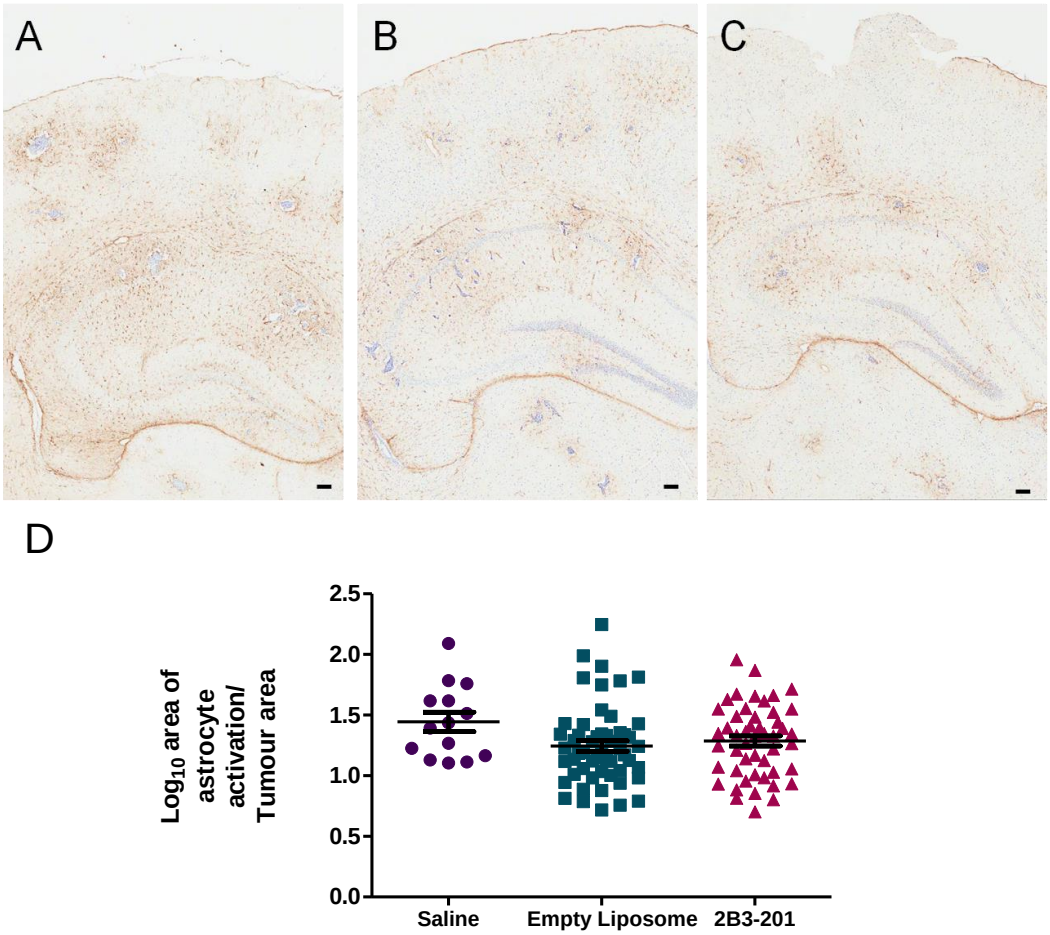

Figure 5.10: 2B3-201 does not attenuate the area of astrocyte activation in response to tumour growth. Female BALB/c mice were injected intracardially with 4T1-GFP cells. At days 7 and 12 post-tumour injection, animals were injected IV with either saline (n=4), empty liposomes (n=5) or 2B3-201 (n=6). Animals were injected once again at day 12 post intracardiac injection. At day 14, animals were perfusion-fixed and tissue was processed for histology. In three animals per treatment group, sections were stained for GFAP immunoreactivity. GFAP staining (brown) was observed surrounding metastases (blue) in saline (A), empty liposome (B) and 2B3-201 (C) treated animals. Scale bars=100μm. The area of astrocyte activation was delineated using ImageScope software, and compared to tumour area (saline: n= 16; empty liposome: n= 54; 2B3-201: n=49). The data were not normally distributed, and so were normalised (log_{10}) prior to statistical analysis. The extent of astrocyte activation was not reduced upon treatment with 2B3-201 (one-way ANOVA, p=0.139). Data are presented as individual points, with mean value ± S.E.M.

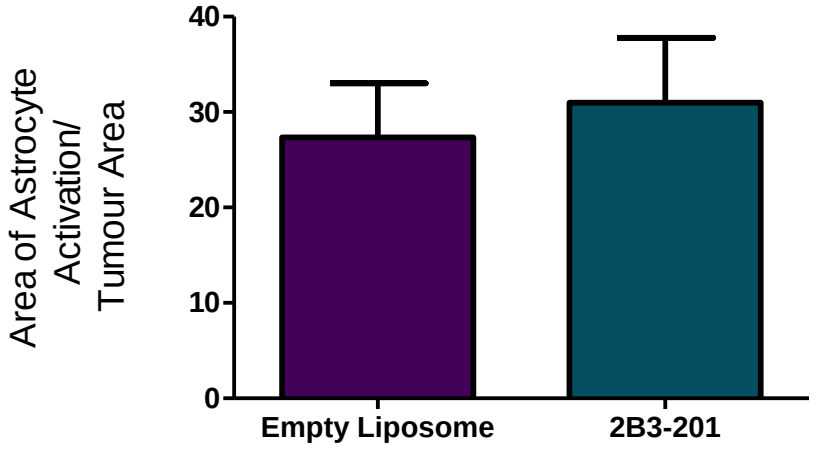

Figure 5.11: 2B3-201 does not attenuate the area of astrocyte activation in response to tumour growth in Region 1. Female BALB/c mice were injected intracardially with 4T1-GFP cells. At days 7 and 12 post-tumour injection, animals were injected IV with either empty liposomes (n=5) or 2B3-201 (n=6). At day 14, animals were perfusion-fixed and tissue was processed for histology. In three animals per treatment group, sections were stained for GFAP immunoreactivity in Region 1. The area of astrocyte activation was delineated using ImageScope software, and compared to tumour area (empty liposome: n= 16; 2B3-201: n=11). The extent of astrocyte activation was not reduced upon treatment with 2B3-201 (Mann—Whitney t-test p=0.361). Data are presented as mean values ± S.E.M.

5.3.4 Validation of 2B3-201 in a TNF-adenovirus model of neuroinflammation

In order to validate the action of 2B3-201 on astrocyte reactivity, a model of sustained neuroinflammation was generated using a replication-deficient adenovirus expressing membrane bound TNF cDNA (Ad5TNF-α_m) (Sibson et al., 2002). Animals were injected IV with 10 mg kg^{-1} 2B3-201 or saline. After 24 hours, animals were injected intracerebrally with 10^5 plaque-forming units (PFU) Ad5TNF-α_m in 0.5 µl in saline, using a finely drawn glass microcannula as previously described. At day 5, animals were perfusion-fixed and astrocyte activation quantified. As shown in Figure 5.12, prophylactic treatment with 2B3-201 did not attenuate the extent of astrocyte activation elicited by Ad5TNF-α_m (n=5, unpaired t-test, p=0.802) as quantified by the volume of GFAP immunoreactivity.

In a second experiment, animals were injected intracerebrally with 10^5 PFU Ad5TNF-α_m in 0.5 µl in saline. At day 3 post-injection, when a sustained neuroinflammatory profile was predicted based on previous work within the group, animals were injected IV with 2B3-201 or saline. At day 5, animals were perfusion-fixed and astrocyte activation quantified with GFAP staining. As shown in Figure 5.13, although there appears to be a trend towards reduced astrocyte reactivity, GFAP staining was not significantly reduced by 2B3-201 as compared to control animals (n=5—6, unpaired t-test, p=0.395).

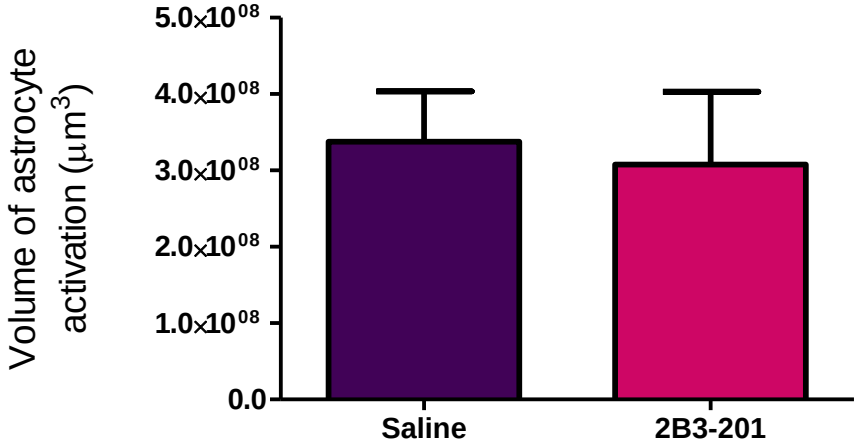

Figure 5.12: Prophylactic treatment with 2B3-201 prior to administration of Ad5TNF-α_m does not attenuate astrocyte activation. Animals (n=5 each group) were injected IV with 10 mg kg^{-1} 2B3-201 or saline. After 24 hours, animals were injected intracerebrally with 10^5 PFU Ad5TNF-α_m in 0.5 μl using the intracerebral method previously described. At day 5, animals were perfusion-fixed and brains processed for histology. The extent of astrocyte reactivity was determined by delineating GFAP staining in ImageScope and quantifying the volume of activation. Unpaired t-test p=0.802. Bars display mean ± S.E.M.

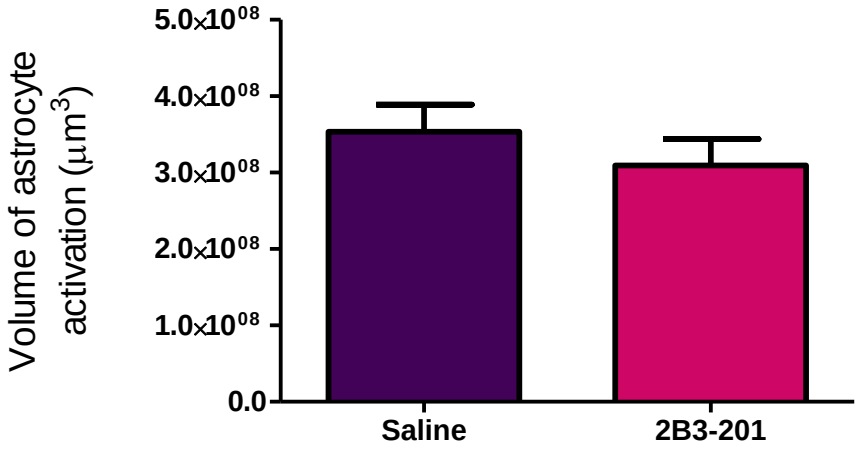

Figure 5.13: Treatment with 2B3-201 post- administration of Ad5TNF-α_m does not attenuate astrocyte activation. Animals (n=5—6 each group) were injected intracerebrally with 10^5 PFU TNF-Ad in 0.5 μl. At day 3 post-injection, when a sustained neuroinflammatory profile was predicted, animals were injected IV with 2B3-201 (10 mg kg^{-1}) or saline. At day 5, animals were perfusion-fixed and astrocyte activation quantified using GFAP staining as previously described. Unpaired t-test p=0.395. Bars display mean ± S.E.M.

5.4 Discussion

The results presented above indicate that treatment of animals with 2B3-201 does not significantly modulate metastatic progression, compared to empty liposome or saline treatment, with the dosing regimen used here. Prophylactic treatment with the liposome-packaged steroid did not alter tumour seeding, with no significant difference found in either tumour number or volume between treated and empty liposome groups. These data suggest that 2B3-201 treatment did not decelerate the rate of seeding.

Treatment of animals with 2B3-201 after tumour inoculation, in order to determine the effect of 2B3-201 on tumour growth, also did not alter total tumour burden, compared to the empty liposome or saline control groups. However, analysis of the extent of GFAP reactivity suggest that this outcome reflects the lack of anti-astrocyte activity at the doses used, since no difference in the extent of astrocyte activation between groups was observed. When looking at different brain regions in isolation, there does appear to be a trend towards reduced tumour growth in the prefrontal cortex, but this did not reach significance at the sample size used. However, analysis of the ratio of astrocyte activation to tumour area in this region alone did not reveal an effect of 2B3-201 on the extent of astrocyte activation. This finding suggests that any effect on tumour burden reflects the general anti-inflammatory effects of 2B3-201, rather than an effect on astrocytes specifically, at least by the analysis method used here. Whether this region of the brain is more susceptible to steroid intervention remains to be seen; no evidence in the literature

currently indicates regional steroid response differences. Additionally, with regards to compound uptake, no reports suggest differential regional expression of glutathione receptors on the BBB. Given the apparent lack of effect of 2B3-201 on the extent of astrocyte activation in brain metastasis, contrary to our previous findings in a mouse model of ALS, it is not possible on the basis of these data to conclude whether astrocyte downregulation alters metastasis progression.

When considering the effect of prophylactic treatment with 2B3-201 on tumour number in the brain, it is interesting that there is a trend towards decreased tumour number in both the empty liposome and 2B3-201 treated animals, compared to saline controls. Whilst this study had a low number of samples and there appears to be large variability in the saline animals, it is an interesting finding based on reports in the literature suggesting that liposomes themselves can elicit an immune response. For instance, in mice, intranasal delivery of liposomes that contained BSA, elicited elevated IgG and IgA production in the serum and saliva (Aramaki et al 1994). This antibody response was not observed in animals administered with free BSA. Murine IgG and IgA responses have also been demonstrated in response to IV administration of PEGylated liposomes (Judge et al. 2006). Thus, it is possible that the systemic immune response could be acting to clear inoculated tumour cells from the bloodstream prior to seeding in the brain. This would be an interesting avenue to pursue further, in a larger cohort and with analysis of antibody levels in the serum. Additionally, the liver could be studied in order to determine whether an acute phase response— an orchestrated immune response to challenge—has been elicited in response to liposomal delivery.

In the experimental conditions used in the brain metastasis study, astrocyte activation was not attenuated upon 2B3-201 treatment. To further examine the effect of 2B3-201 on astrocyte reactivity in a more focused model of gliosis, the compound was used in an Ad5TNF-α_m model of sustained neuroinflammation. In both experimental paradigms used, astrocyte activation, as defined by the extent of GFAP reactivity, was not significantly attenuated following treatment with 2B3-201 compared to saline control animals. Again, these findings were unexpected based on previous work in the group showing that 2B3-201 treatment attenuated astrocyte reactivity in a transgenic mouse model of ALS (Evans, M et al, unpublished). However, the experimental paradigm in that study involved repeated dosing over a protracted time-course, whilst in the work presented here, a single dose was given, before or after inflammatory challenge. Thus, the steroid dosing used here may not have been sufficient to observe an effect on astrocyte activation. Interestingly, studies conducted in the EAE rat model suggest that a single dose is sufficient to improve clinical scores. However, that study does not include histological assessment of astrocyte activation (Gaillard et al., 2012). Thus, the liposomal-packaged steroid may have improved clinical scores via mechanisms that are distinct from any astrocyte-targeted effects. In the study conducted here, although animal behavior and weight was monitored throughout the experiment, formal behavior tests were not performed, comparing experimental and control groups. Perhaps the steroid had an effect on behavioural outcomes, the mechanism of which was not observed in the histology conducted.

Based on published studies, it would be reasonable to hypothesise that GCs such as methylprednisolone would inhibit astrocyte activation. As discussed above, GCs

have multiple mechanisms of action, including transcriptional repression of NFκB target genes. NFκB activity has been demonstrated to be present in astrocytes (Moynagh et al., 1993; Moynagh et al., 1994; Sparacio et al., 1992) and a transgenic mouse model implicates NFκB in regulating astrocyte reactivity in a range of CNS challenges (Brambilla et al., 2005; Brambilla et al., 2012; Brambilla et al., 2009). As illustrated in Figure 5.1, NFκB is a heterodimer, located in the cytosol. In unstimulated cells, NFκB is inactive, bound by its cognate inhibitor, IκB. Upon stimulation, IκB is phosphorylated, flagging the protein for ubiquitination and subsequent degradation. As such, NFκB is free to translocate to the nucleus and bind the consensus sequence of target genes, of which there is a wide range, typically implicated in inflammation.

There may be multiple explanations for the lack of 2B3-201 efficacy in attenuating astrocyte activation in the both the brain metastasis and Ad5TNF-α_m models used here. Firstly, as discussed above, this could be an issue of dosing. The nature of the intracardiac model is that disseminated disease is induced and astrocyte activation is widespread in both the 2B3-201 and empty liposome treatment groups. Therefore, perhaps a greater dose is required, or more frequent dosing is necessary to see an effect on astrocytes in this model. Indeed, in a very recent study, using a rat intracerebral model of brain metastasis, a reduction in tumour volume in response to dexamethasone was shown when animals were dosed with dexamethasone at 8mg kg-1 per day (Lewis et al., 2013). It should also be noted that dexamethasone is a more potent steroid than methylprednisolone, displaying greater GR affinity and increased half-life (Hari and Srivastava, 1998). Interestingly, in that study, the authors looked at astrocyte activation in the peri-

tumoural region, and concluded that astrocyte activation was reduced in dexamethasone treated animals, compared to those treated with vehicle. However, this reduction in GFAP positive cells compared to control did not reach significance. Thus, clearly the dosing paradigm is important to see an effect on astrocyte activation. Considering the Ad5TNF-α_m model, this is a focal lesion and so the argument concerning disseminated disease does not hold here. However, perhaps just the single dose was not sufficient to modulate the strong inflammatory response elicited by TNF-alpha.

A number of studies have suggested that treatment with PEGylated liposomes may initiate an immune response that leads to enhanced clearance of subsequent liposome doses. It has been proposed that an anti-PEG IgM response is mounted in the spleen by lymphocytes. Thus, upon the second dose of PEGylated liposomes, the complement system is activated and there is increased uptake of liposomes by Kupfer cells in the liver (Ishida et al., 2007). This 'accelerated blood clearance' has also been demonstrated in rats in response to sequential liposome-packaged chemotherapeutic treatment (Yang et al., 2013). Therefore, in the brain metastasis study here, the apparent lack of astrocyte inhibition at day 14 may be due to the reduced bio-distribution of the second dose. This repeated dosing issue was not a confound in the Ad5TNF-α_m model, where just a single dose was given and still GFAP reactivity was not significantly reduced. Perhaps, as mentioned above, a single dose is not sufficient to modulate the astrocyte response elicited by TNF-α.

Alternatively, the lack of efficacy could be due to the mode of astrocyte activation. A number of mechanisms of astrocyte activation exist, some of which may be

steroid-refractory. Not all inflammatory conditions respond to steroid treatment, for example severe asthma. Cytokine activation of the MAPK pathway has been proposed as one mechanism of GC resistance. Studies on PBMCs isolated from healthy subjects showed that culture with IL-2 and IL-4 leads to p38 MAPK activation, with subsequent phosphorylation of GR, reduced GC binding affinity and nuclear translocation (Irusen et al., 2002). In *in vitro* astrocyte culture experiments, stimulation with tumour-conditioned media has been shown to activate MAPK (Mendes et al., 2007). Thus, it may be that the astrocytes in the tumour microenvironment are steroid-insensitive to some degree. Similarly, the downstream effects of Ad5TNF-α_m administration may lead to activation of multiple different pathways other than solely NFkB, especially as a range of CNS cells will have been activated in response to the inflammatory challenge, leading to paracrine signalling.

5.5 Conclusions and further work

2B3-201 is a glutathione-tagged liposome-packaged methylprednisolone molecule. Based on existing studies, it was proposed that this drug could attenuate astrocyte responses to CNS challenge. Thus, it was hypothesised that treatment of animals with 2B3-201 would alter tumour burden. There were two arms to the study. The first involved dosing prior to tumour inoculation, in order to assess the role of astrocytes in tumour seeding. The second involved drug administration after tumour inoculation in order to determine the role of astrocytes in tumour growth.

With regards to tumour seeding, 2B3-201 did not significantly alter tumour number, although there was a trend towards fewer metastatic colonies, compared to empty liposomes. Additionally, 2B3-201 was not shown to significantly reduce tumour growth, compared to empty liposome control animals, although there was a trend towards decreased tumor burden in the pre-frontal cortex. When the effect of the drug on astrocyte activation was investigated, it was found that astrocyte reactivity was not attenuated in treated animals as compared to those given empty liposomes. Thus, 2B3-201 was not an effective modulator of astrocyte activation in an *in vivo* model of brain metastasis at the dose used. Further studies are required, possibly using a more frequent dosing regimen or a stronger steroid, such as dexamethasone, in order to fully determine the use of steroids in the treatment of brain metastasis. Perhaps other mechanisms of targeting astrocytes could be investigated. Astrocyte specificity could be conferred by the lipid composition of the liposome. One study suggests that astrocytes rapidly take-up sulfocerebroside-

containing liposomes, over other lipid compositions (Suesca et al., 2013). Perhaps the liposome composition used here could be modulated accordingly.

In light of 2B3-201 being an ineffective method of astrocyte inhibition at the dosing schedule used, further studies need to be conducted in order to address the role of astrocytes in brain metastasis. With regards to pharmacological methods, arundic acid has been shown to inhibit astrocyte activation *in vivo,* with implications for neuropathology, although again dose issues will be key as will the differences in the mode of astrocyte activation (Hanada et al., 2013; Sibson et al., 2008; Tateishi et al., 2002). Perhaps, more usefully, transgenic models, such as the GFAP-IkB-dn mouse could prove valuable tools for probing the consequences of astrocyte inhibition in brain metastasis. The transgenic strain involves the overexpression of IkB, under the regulation of the GFAP promoter, thus conferring astrocyte specificity. This model has already shown the importance of astrocytes in multiple CNS pathologies (Brambilla et al., 2005; Brambilla et al., 2012; Brambilla et al., 2009; Dvoriantchikova et al., 2009), and would provide a robust mechanism of astrocyte inhibition, without direct modulation of other CNS-resident cells. This model will also be useful in order to gauge to what extent the astrocytic response to brain metastasis orchestrates the CNS response as a whole. For instance, based on what we know about astrocyte—microglia signalling, phenotypes in the tumour periphery may be influenced by the astroglial activation state. Additionally, the extent to which astrocyte activation mediates the recruitment of peripheral immune cells to the tumour microenvironment has yet to be addressed and a transgenic model such as this could be useful in answering such questions.

As discussed in Chapter 4, a more practical approach to probing the role of astrocytes in brain metastasis might be the inhibition of molecules that astrocytes secrete when activated. It would be interesting to determine how 2B3-201, once a dosing schedule has been optimised, modulates the transcriptional profile of the host microenvironment, looking at expression levels of growth factors as well as ECM remodeling enzymes. The RT-qPCR work carried out in Chapters 3 and 4 suggests a key role for IL-6 in the tumour microenvironment. Due to the effect of steroids on the transcriptional expression of inflammatory mediators, 2B3-201 may modulate IL-6 expression in brain metastasis. *In vitro,* dexamethasone treatment of a prostate cancer cell line led to a reduction in IL-6 production, via inhibition of NFkB signalling; administration of the steroid in an *in vivo* xenograft model of the same cell line led to a reduction of tumour burden (Nishimura et al., 2001). Clinically, steroid treatment has been shown to reduce IL-6 serum levels in a palliative care setting for terminally ill lung cancer patients (Yanagawa et al., 1996). Thus, it would be interesting if any reduction in tumour growth observed with steroid treatment were correlated with a reduction in IL-6 expression.

6 Glial activation in the early stages of brain metastasis as a diagnostic biomarker

6.1 Introduction

Clinical detection of brain metastases is currently performed using gadolinium-enhanced MRI (Gd-MRI). This gold standard technique is dependent on tumour induced breakdown of the BBB. As discussed in the introductory chapter, frank breakdown of the BBB does not occur until metastases are in the region of 0.5 cm in diameter; at this point the metastasis can break through the astrocytic component of the BBB and proliferate in the parenchyma. Breakdown of the BBB is not dependent on contact between tumour cells and the endothelium (Stewart et al., 1987), indicating that secreted factors play a role in BBB permeabilisation as well as mechanical disruption. As treatment options for brain metastases are limited at this advanced stage, early detection may be crucial for prolonging life expectancy. Thus, the development of novel methods for the early detection of brain metastases is of great importance.

Building on the basis of MRI, pre-clinical research suggests that the detection threshold for brain metastases can be lowered via the use of novel contrast agents that target the inflamed endothelium, rather than the tumour itself. VCAM-1 antibodies conjugated to microparticles of iron oxide (MPIO) have been used to sensitively detect micrometastases, with an estimated clinical threshold of 300—650 μm (Serres et al., 2012). Such techniques, probing the inflammatory

microenvironment, rather than the tumour *per se*, could hold great clinical potential. As there are a host of CAMs expressed on the endothelium in response to tumour growth (Soto et al., 2013), other molecular targets could also be used as biomarkers.

With regards to the inflammatory microenvironment, endothelial activation is by no means the only targetable feature. It is evident from the work carried out throughout this thesis that astrocytes play a role in the development of brain metastases. As shown in Chapter 3, the area of astrocyte activation surrounding metastases, in both the intracerebral and intracardiac model, far exceeds the size of the tumour alone. As a larger targetable region will enhance chances of tumour detection prior to BBB breakdown, targeting the glial response could enable detection of brain metastases at early time-points. Based on the success within this research group of molecular MRI in metastatic detection, one could employ a similar technique for probing reactive astrocyte-specific antigens. However, molecular MRI would be challenging in this situation, as without a patent BBB, antibodies conjugated to iron oxide particles would fail to bind parenchymal targets. Thus, one must turn to small molecule ligands—capable of crossing an intact BBB—in order to probe the glial response, and to this end, nuclear imaging could provide the appropriate modality in this instance.

Peripheral malignancies are frequently detected using 2-deoxy-2-(^{18}F)fluoro-D-glucose (FDG)-PET. FDG is a glucose analogue (Tewson et al., 1978) that is taken up by cells undergoing enhanced glycolytic metabolism, such as tumour cells (Som et al., 1980). In the clinic, FDG-PET has been shown to aid tumour staging in a

range of malignancies (Reske and Kotzerke, 2001). Whilst the high endogenous glycolytic activity of the CNS precludes the use of FDG-PET for CNS disease detection (Hicks and Hofman, 2012), the development of appropriate PET tracers could allow early detection of brain metastasis using existing clinical imaging infrastructure. In this chapter, I will briefly explain the principles of nuclear imaging, encompassing single-photon emission computed tomography (SPECT) and positron emission tomography (PET), before going on to describe how such imaging modalities could be used to detect CNS malignancies.

6.1.1 SPECT versus PET

SPECT is a nuclear imaging technique that detects γ rays emitted from radionuclides such as ^{123}Iodine (^{123}I), ^{99}Technetium (^{99}Tc) and ^{111}Indium (^{111}In). The technique allows the construction of a 3D image as a γ-camera rotates around the sample, acquiring 2D images from multiple angles, as illustrated in Figure 6.1. PET, meanwhile, detects the annihilation of positrons emitted by radionuclides such as ^{18}Fluorine (^{18}F) and ^{11}Carbon (^{11}C), as illustrated in Figure 6.2.

Since the development of commercial PET-CT systems in the early 2000s, the use of SPECT in oncology has been dwindling, on account of the higher sensitivity and greater quantitative capabilities of clinical PET-CT systems (Rahmim and Zaidi, 2008). This improved sensitivity leads to increased signal-to-noise and temporal resolution. Of considerable benefit in the clinic is the ability to perform shorter scans than with SPECT. Moreover, the enhanced temporal resolution facilitates functional studies, modelling uptake over time. Despite this, SPECT is still utilised due to lower costs and importantly the wider availability of radiotracers; tracer

synthesis is not dependent on access to a cyclotron (Hicks and Hofman, 2012). However, the success of FDG in oncology, coupled with more efficient regional distribution of radiotracers from centralised cyclotrons, has facilitated the increasing role of PET in cancer diagnosis and treatment assessment over the last decade (Hicks and Hofman, 2012). However, within the pre-clinical setting, SPECT has a host of benefits; namely, the longer half-life of radioisotopes enables more protracted studies. Additionally, multiple tracers can be used to probe different biological functions (Heiba et al., 2013; Hijnen et al., 2012), a modality impossible in PET, as emitted photons have the same energy. On account of the relative ease of the radiochemistry, SPECT was used initially in the current study to test the hypothesis that astrocyte reactivity can be probed using small molecule ligands, and that astrocyte detection can be used as a surrogate for tumour growth.

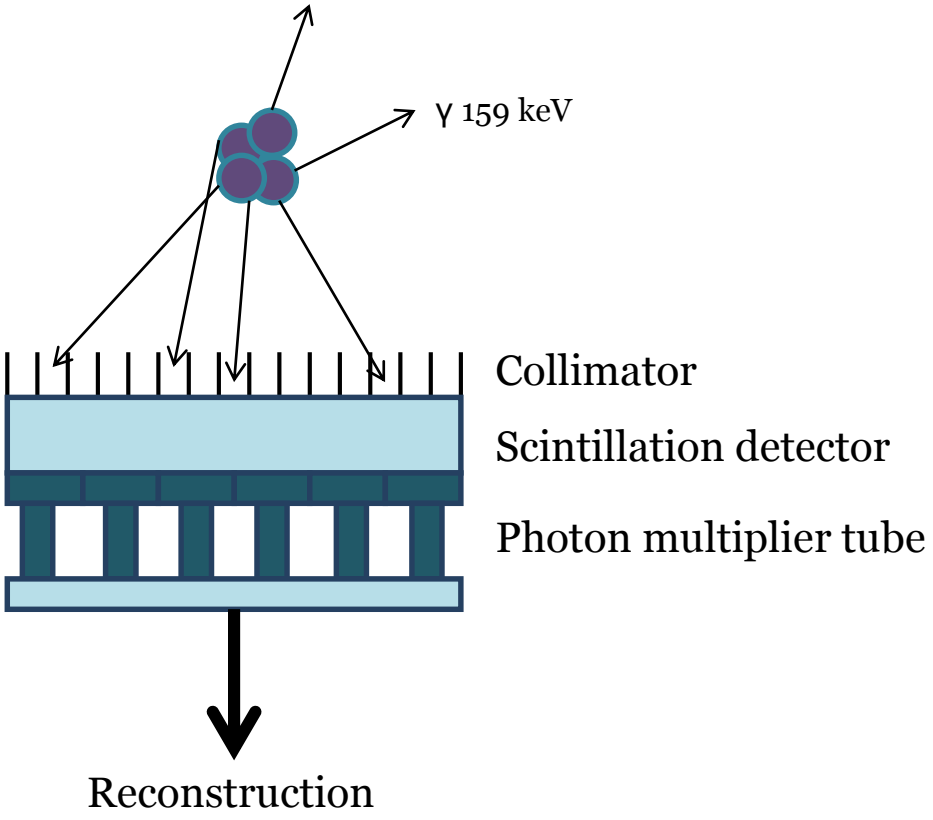

Figure 6.1: SPECT detection of gamma ray emission. Gamma ray-emitting radionuclides such as ^{123}I, are used in SPECT. Photons emitted by gamma decay that pass through a physical collimator are detected. Incident photons elicit electron excitation in the scintillation crystal, typically NaI (Tl). The subsequent emission of photons is amplified via coupling to a photon multiplier tube (PMT). The thickness of the crystal in the scintillation detector affects sensitivity and resolution. A thinner crystal yields greater spatial resolution as, amongst other reasons, multiple interactions are less likely. However, a greater crystal thickness enables enhanced detection of higher energy photons and, hence, increased sensitivity. 3D information is obtained by a rotating gantry.

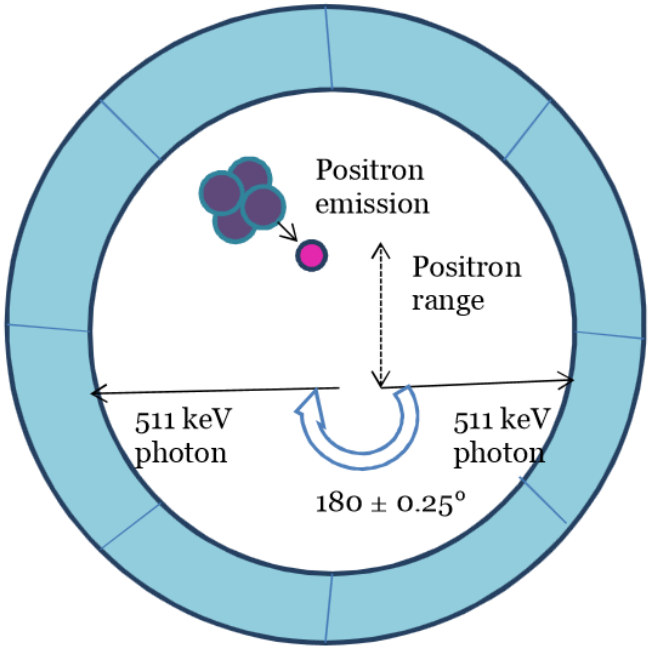

Figure 6.2: Coincidence detection in PET. Positron emitting radionuclides, such as ^{18}F, are used in PET systems. The emitted positron travels through the medium (the positron range) before annihilation with an electron. The positron range limits resolution. Upon annihilation, two photons of 511 keV are emitted, and follow trajectories 180° apart. Deviation in this angle can occur if the net momentum of the positron and electron is not zero, and as such there is inherent positional inaccuracy in the system. The annihilation events are detected electronically using coincidence detection; if two detectors are 'hit' within a short timeframe then the events are characterised as coincident. Such detection removes the need for physical collimation as spatial information can be assigned from the two relevant detectors.

6.1.2 Reconstruction techniques

In the context of nuclear medicine, a projection is a 2D image acquired by a gamma camera and projections are acquired at multiple angles so that a 3D estimation of tracer distribution can be constructed. In SPECT, the camera rotates on a gantry whilst in PET, the gamma camera is static, with detectors surrounding the subject. In order to form a 3D image, the 2D projections must be reconstructed. Filtered back projection (FBP) is the most commonly used reconstruction algorithm on account of its ease and speed, and has been used here to reconstruct data acquired with both SPECT and PET. If a projection represents the sum of all counts in a straight line through an object, the back projection redistributes the counts to their original location. Filters are applied to suppress noise and enhance signal (Lyra and Ploussi, 2011).

6.1.3 Probing CNS inflammation with radiolabelled TSPO ligands

As shown in the previous chapters, the tumour microenvironment is populated by reactive astrocytes throughout an extended time-course. Thus, developing tracers that detect astrocyte activation could provide a robust mechanism for the detection of brain metastases. A potential biomarker candidate is the translocator protein (TSPO), also known as the peripheral benzodiazepine receptor. TSPO is an outer mitochondrial membrane protein (Squires and Brastrup, 1977) and has multiple functions including cholesterol import for steroid synthesis (Hauet et al., 2005), regulation of mitochondrial metabolism (Hirsch et al., 1989) and apoptosis (Hirsch et al., 1998). These diverse functions render knockout models embryonically lethal

(Papadopoulos et al., 1997). Although TSPO was originally thought to be exclusively upregulated on microglia in disease states, studies have also demonstrated increased expression on astrocytes in humans, as well as in rodent models (Cosenza-Nashat et al., 2009; Lavisse et al., 2012). Consequently, interest has grown in the development and use of radiolabelled compounds against TSPO for imaging neuroinflammation in diverse CNS pathologies such as multiple sclerosis (Harberts et al., 2012), dementia (Cagnin et al., 2001), Alzheimer's disease (Versijpt et al., 2003) and stroke (Gulyas et al., 2012a; Gulyas et al., 2012b), as reviewed in (Ching et al., 2012). As microglial activation has been robustly identified in the brain metastatic environment (Balathasan et al., 2013; He et al., 2006; Pukrop et al., 2010), an imaging approach that targets both glial populations would presumably enhance the chances of tumour detection.

6.1.4 Small molecule TSPO ligands

The archetypal TSPO ligand is PK11195 (Le Fur et al., 1983) However, this small molecule has poor pharmacokinetic properties with regards to biodistribution. As such, a 'second generation' of TSPO ligands have been developed (Trapani et al., 2013), which also display higher TSPO affinity. In this work, two compounds have been used: DPA-713 in a SPECT system and GE-180 in a PET system. N-Diethyl-2-[2-(4-methoxy-phenyl)-5, 7-dimethylpy-razolo [1, 5-a] pyrimidin-3-yl]-acetamide (DPA713) is a TSPO ligand (Reynolds et al., 2010) that can be labelled with radionuclides to enable detection with nuclear imaging techniques (Wang et al., 2009). The compound has been used in both peripheral and CNS *in vivo* models (Chauveau et al., 2009; Doorduin et al., 2009; Foss et al., 2013) and

recently in a clinical study (Endres et al., 2012). In a comparison with PK11195, in a rat model of herpes encephalitis, DPA-713 displayed reduced nonspecific binding (Doorduin et al., 2009) and a higher TSPO affinity (4.7 nM versus 9.3 nM (Endres et al., 2009)) than PK11195. GE-180 is a further second generation TSPO ligand, more recently synthesised (Wadsworth et al., 2012). In a focal CNS inflammatory lesion model, GE-180 has been shown to outperform PK1195, with regards to compound binding the extent of gliosis (Dickens et al., 2014). GE-180 additionally displays higher TSPO affinity compared to DPA-713 (0.87 nM) (Wadsworth et al., 2012).

In light of the success of such compounds in other neuroinflammatory conditions, I hypothesised that TSPO ligands coupled with radioisotopes could be used to detect tumour burden *in vivo*. In order to test this hypothesis, I firstly used a SPECT imaging system to detect tumour burden in both intracerebral and intracardiac model of brain metastasis. The radiochemistry involved in SPECT does not necessitate a cyclotron and the isotope used (^{123}I) has a relatively long half-life (13 hours). As such, the hypothesis could be easily tested in a pre-clinical setting. Subsequently, upon finding that glial reactivity can indeed be used as a surrogate for tumour growth, the pre-clinical work was repeated in a more clinically relevant imaging modality, PET, with the rationale that greater sensitivity will allow the detection of micrometastases.

Although two different compounds will be used, it is not the aim of this chapter to directly compare the two TSPO ligands. Instead, SPECT, more practical for preliminary work, will be used to test the hypothesis prior to translation into a

more clinically relevant imaging modality, using a compound which has already progressed to clinical trials for other neuropathology.

6.2 Results

6.2.5 There is a sustained glial response to brain metastasis

As shown in Figure 6.3, astrocytes are not the only glial cell to be activated in response to brain metastases. Microglia are also activated, and unlike astrocytes, infiltrate the tumour. As quantified in Figure 6.3, microglial activation is more extensive than astrocyte activation at early time points in the intracardiac model of brain metastases (Two-way ANOVA, Bonferroni post-hoc test: day 10, $p < 0.05$; day 14, $p < 0.001$). Microglial activation plateaued by day 28 to a level comparable to that of astrocyte activation.

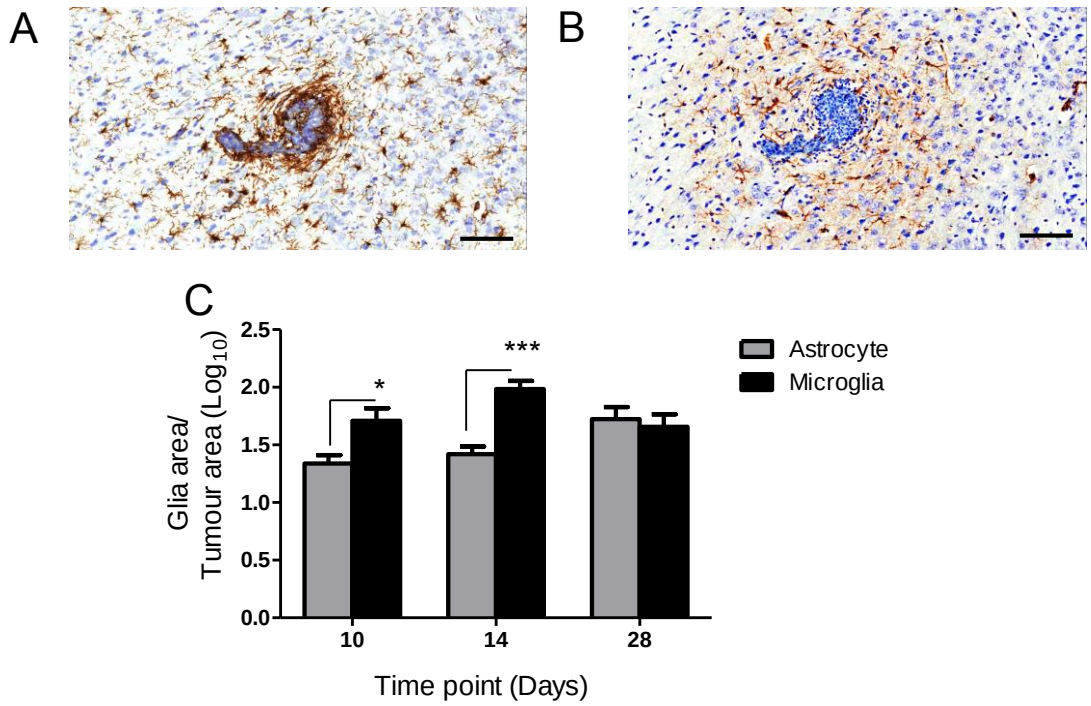

Figure 6.3: Microglia are activated in the tumour microenvironment. Female BALB/c mice were injected intracardially with 4T1-GFP cells**.** At days 10, 14 and 28 post-tumour cell injection, animals were perfusion-fixed for histology. Photomicrographs show representative images from animals at day 14 post-tumour injection, comparing microglial infiltration of metastases (blue cresyl stain), detected by Iba-1 immunoreactivity (brown stain; A), with astrocyte activation (brown stain; B). (C) Quantitation of microglial and astrocyte activation at days 10 (tumour number = 16), 14 (n = 39) and 28 (n = 7). Data was not normally distributed and so was logged_{10} before a two-way ANOVA was performed with Bonferroni post-hoc tests conducted where appropriate. * $p < 0.05$, ***$p < 0.0001$. Data presented as mean values ± S.E.M. Scale bar=100μm.

6.2.6 *TSPO is expression in the tumour microenvironment*

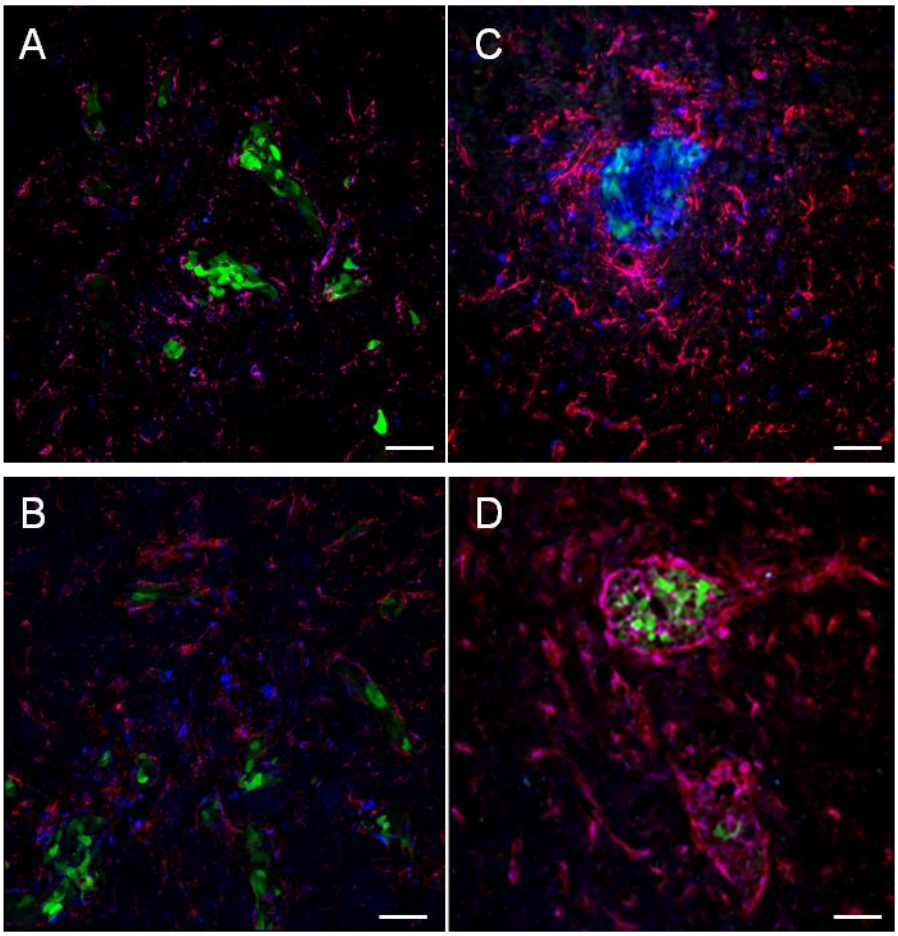

Figure 6.4: Glial TSPO expression is present in the tumour microenvironment. (A-B) Confocal microscopy images obtained from mouse brain 14 days after intrastriatal injection of 4T1-GFP cells. Astrocytes and microglia were detected with GFAP and Iba-1, respectively (red), and compared with TSPO detection (blue). Endogenous GFP expression from 4T1-GFP cells was detected (green). Merged images show co-localisation (pink) of TSPO with astrocytes (A) and microglia (B), but not 4T1-GFP cells. (C-D) Confocal microscopy images obtained from mouse brain 21 days after intracardiac injection of 10^4 4T1-GFP cells, markers as above. Merged images show co-localisation of TSPO with astrocytes (C) and microglia (D). Scale bar = 50 μm

Increased TSPO expression by both astrocytes and microglia in the tumour microenvironment was confirmed with immunofluorescence (Figure 6.4). Enhanced TSPO expression by glia was demonstrated in both the intracerebral (day 14) and intracardiac (day 21) models. Interestingly, astrocytic TSPO expression appears to be more robust in the intracerebral model, compared to microglial expression. In the intracardiac model, microglial TSPO expression is more robust.

Previous studies suggest that human breast metastatic cells, including the MDA-BR-231 cell line, express TSPO (Batarseh et al., 2012). In order to confirm the cellular origin of the TSPO signal in this model, TSPO expression in 4T1-GFP cells was investigated. As evident in Figure 6.5, 4T1-GFP cells do not express TSPO *in vitro* unlike the positive control, MDA-BR-231 cells. Co-localisation between GFP and TSPO is also not observed in the *in vivo* histology (Figure 6.4).

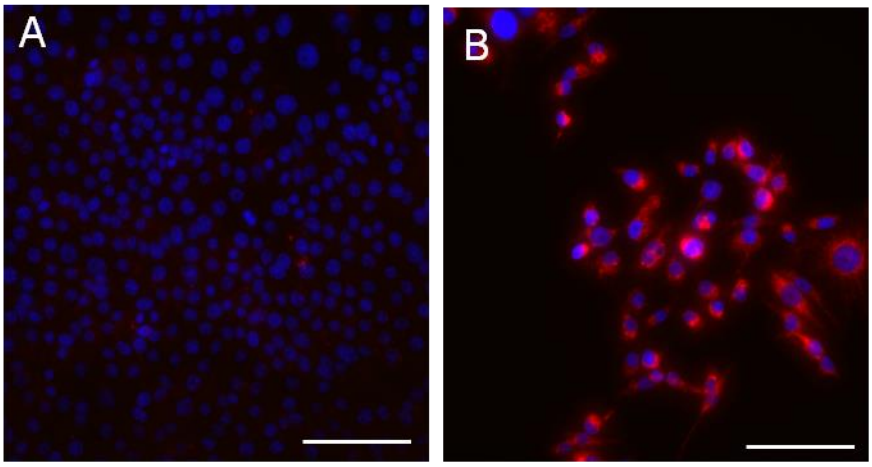

Figure 6.5: 4T1-GFP cells do not express TSPO *in vitro*. TSPO expression in 4T1-GFP and MDA231BR-GFP cells was determined *in vitro* using immunocytochemistry. Cultures, grown on coverslips, were stained for TSPO expression with anti-PBR antibodies. Primary antibody binding was revealed with Cy3 (red). Cell nuclei are stained with DAPI (blue). 4T1-GFP cells do not express TSPO (A), compared to MDA231BR-GFP cells (B). Scale bars=100 μm.

6.2.7 *^{123}I-DPA-713 detection of intracerebral tumour burden*

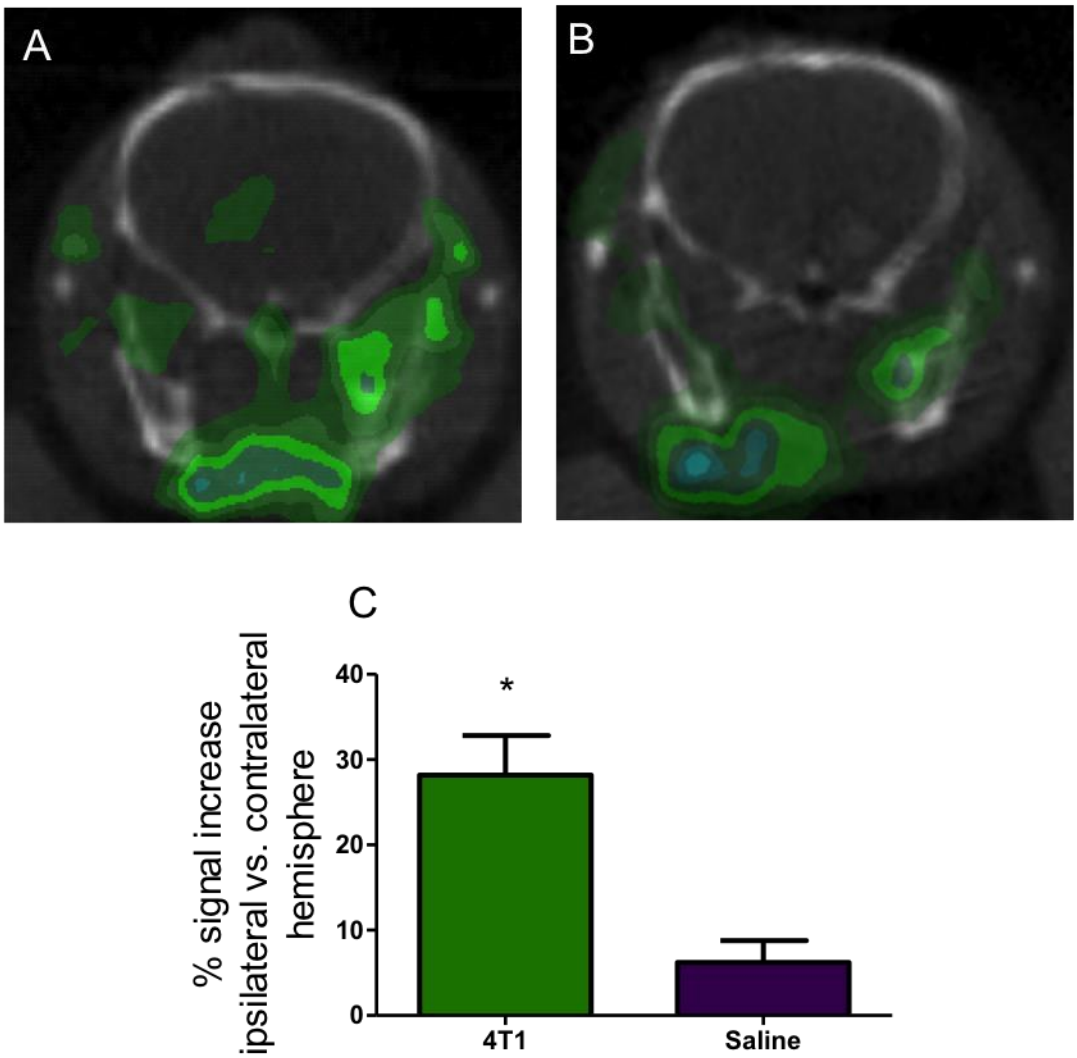

Figure 6.6: ^{123}I-DPA-713 SPECT can detect metastases induced by the intracerebral method. Female BALB/c mice were injected intrastriatally with 4T1-GFP cells or saline. At day 14 post tumour inoculation, animals were injected IV with ~20 MBq ^{123}I-DPA-713 1 hour prior to SPECT imaging. (A) Representative SPECT images at the injection site (left hemisphere) from a 4T1-GFP injected mouse and a saline injected control (B). (C) Percentage signal increase in the injected hemisphere compared to the control contralateral hemisphere for 4T1-GFP (n = 6) and saline (n = 3) injected animals. Unpaired, two-tailed t-test *p=0.0375. Data are presented as mean values ± S.E.M.

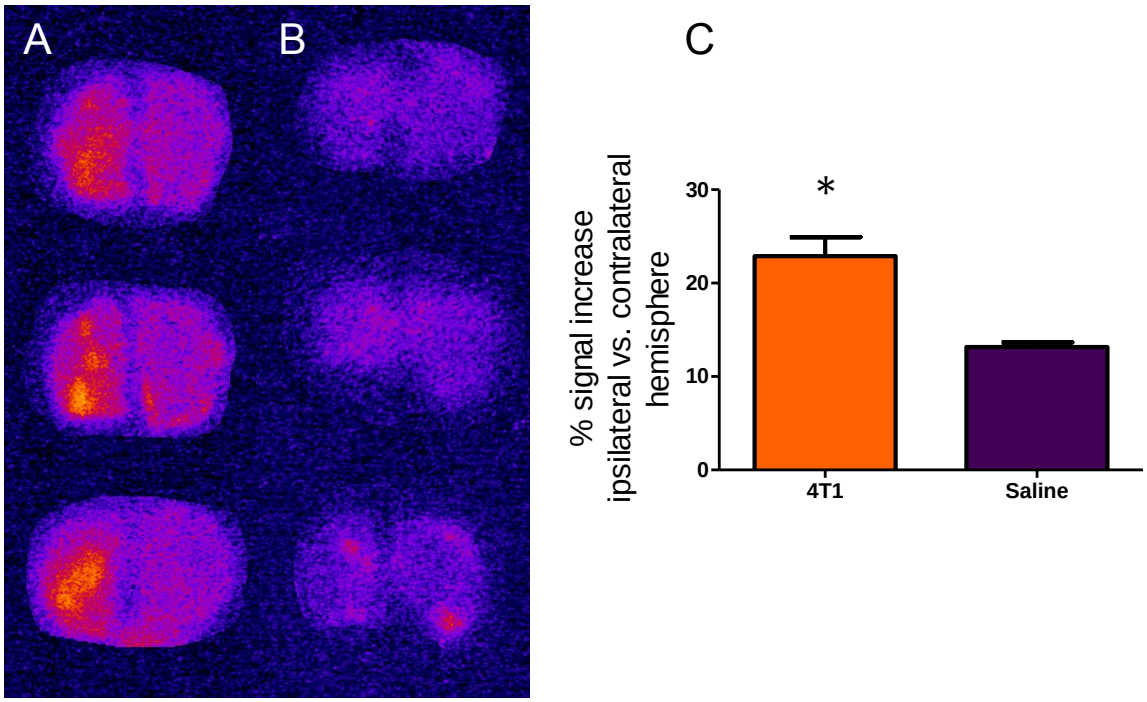

Figure 6.7: ^{123}I-DPA713 binding was confirmed by autoradiography in 4T1-GFP injected animals compared with saline injected animals. After SPECT imaging, animals were perfused with saline and brain fresh-frozen. Multiple 10 μm sections were taken through the injection site. Autoradiography was performed, incubating sections for approximately 36 hours with a phosphor plate. Representative autoradiographic images are shown from 4T1-GFP injected animals (A) and saline injected animals (B). (C) Percentage signal increase in the injected hemisphere compared to the control contralateral hemisphere for 4T1-GFP (n = 6) and saline (n = 3) injected animals. Unpaired t-test *p=0.016. Images were false-coloured in ImageJ using the 'Fire' look-up table. Data are presented as mean values ± S.E.M.

As shown in Figure 6.6, ^{123}I-DPA-713 can be used to detect tumour burden with SPECT in the intracerebral model of brain metastasis at day 14. Activity was quantified in the ROI, spanning the injection site, and compared to the contralateral hemisphere. As shown in Figure 6.6, the percentage signal increase was greater in animals injected with 4T1-GFP cells as compared to saline control animals (unpaired t-test, p =0.0375).

In order to confirm ^{123}I-DPA-713 binding rather than pooling at the site of lesion, autoradiography was performed on saline-perfused brains. As shown in Figure 6.7, ^{123}I-DPA-713 binding can be detected throughout the injection site; such enhancement of signal intensity compared to the contralateral hemisphere is absent in the saline-injected animals (unpaired t-test, p=0.016). Auto-radiography demonstrates that DPA-713 binds to areas of astrocyte activation and microglial activation at day 14 of the intracerebral model (Figure 6.8). Applying a threshold to the autoradiographic image (1 standard deviation and 1.5 standard deviations above the mean intensity) demonstrates that the areas of greatest compound binding correlate to the areas of most intense gliosis: directly within the tumour periphery, along with microglial infiltration of the tumour.

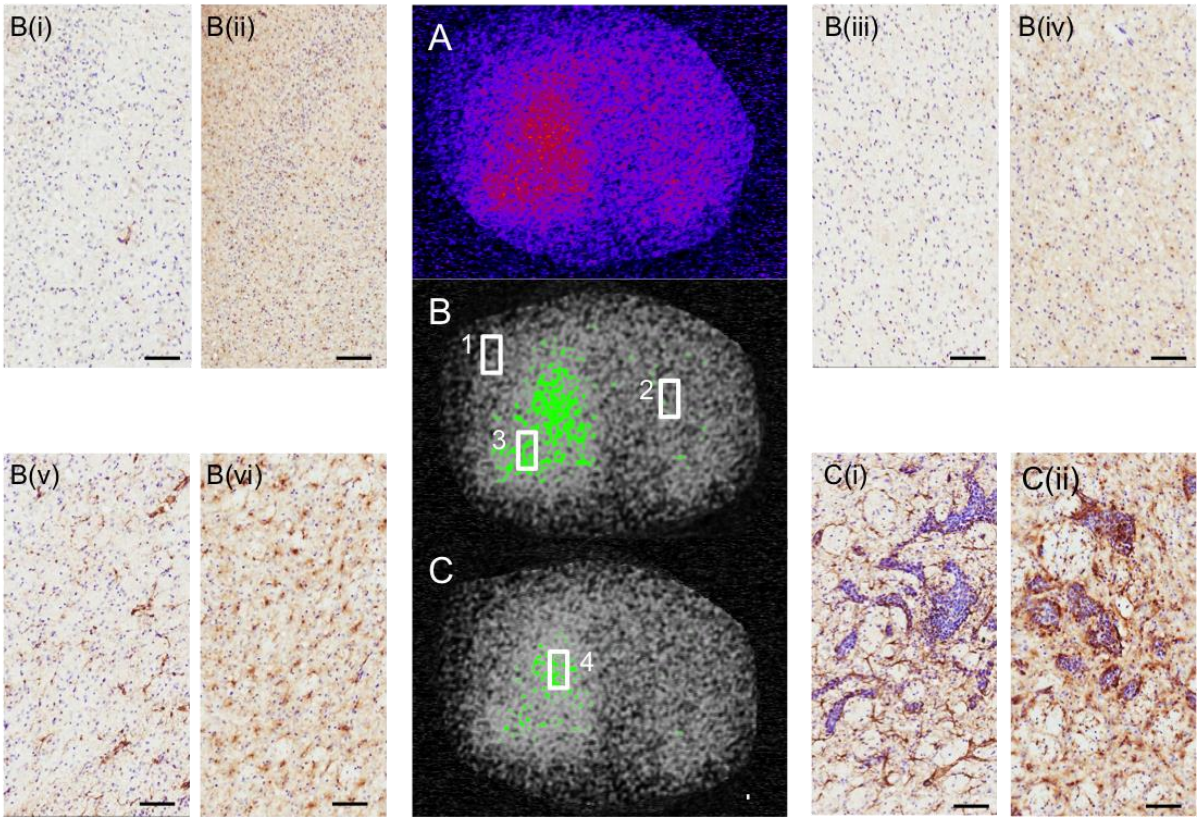

Figure 6.8: DPA-713 binding correlates with microglial and astrocyte activation. (A) Representative autoradiographic image from mouse brain injected with 4T1-GFP cells in the left striatum. (B) Thresholded autoradiographic image, highlighting areas with binding intensity of 1 S.D. above the mean. At areas distal to the most intense signal (box 1), astrocyte (Bi) and microglial (Bii) staining is low, as seen in the contralateral hemisphere (box 2; Biii and Biv, respectively). In contrast, in areas of greater binding intensity (box 3), marked astrocyte (Bv) and microglial (Bvi) activation can be seen. (C) Thresholded autoradiographic image, highlighting areas with binding intensity of 1.5 Standard deviation (SD) above the mean (i.e. maximal ^{123}I-DPA713 retention), which correspond to areas of greatest tumour burden. In these regions (box 4), strong astrocyte activation (Ci) and substantial infiltration of microglia (Cii) was evident. Reactive astrocytes and microglia were detected with GFAP and OX42 immunohistochemistry, respectively (brown stain). Scale bars = 100μm.

6.2.8 ^{123}I- DPA713 detection of intracardiac tumour burden

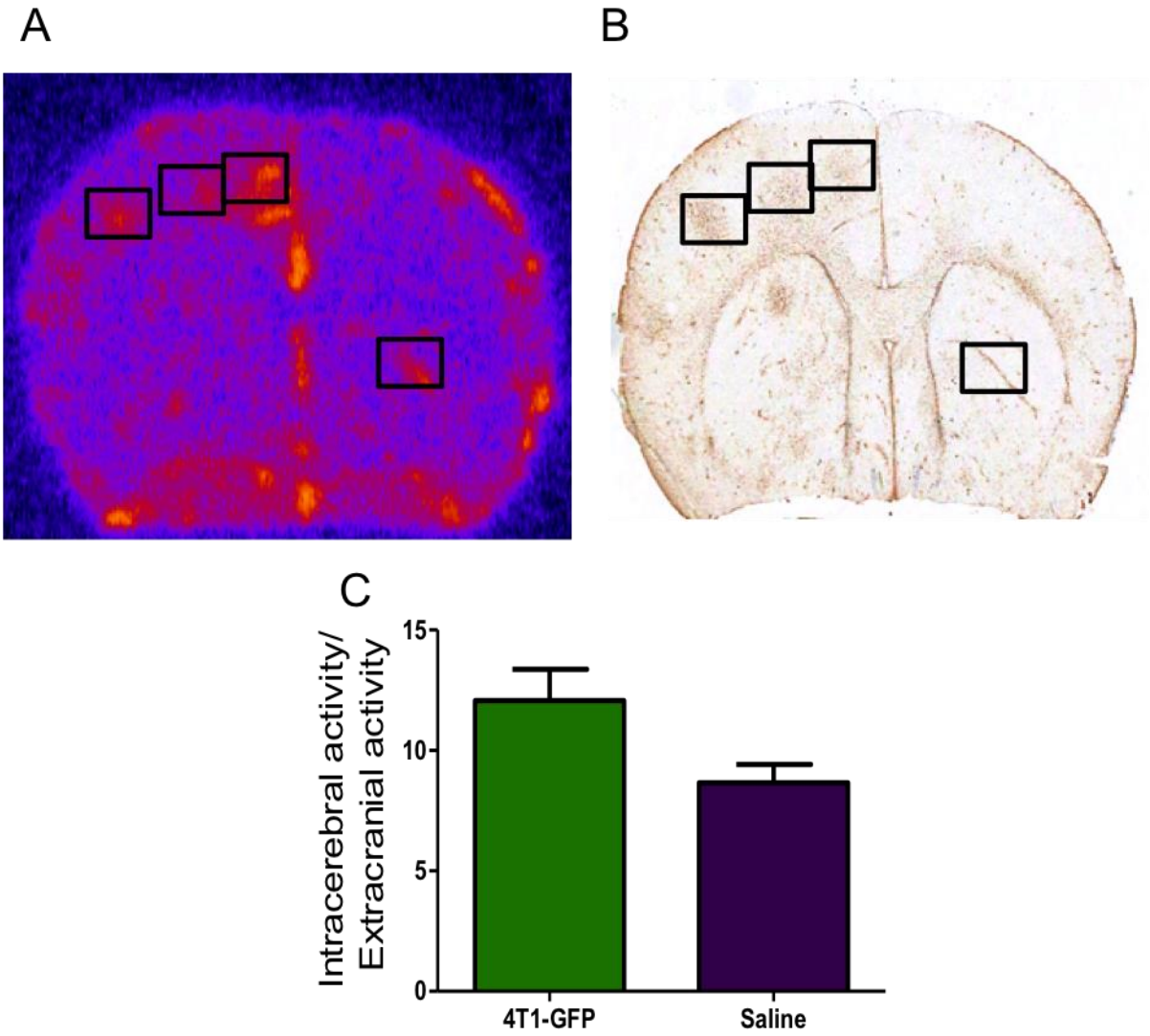

Figure 6.9: Metastases induced intracardially cannot be detected with SPECT using ^{123}I- DPA713. Animals were injected under ultra-sound guidance intracardially with 4T1-GFP cells or saline. At day 21 post tumour inoculation, animals were injected IV with ~20 Mobs ^{123}I-DPA-713 1 hour prior to SPECT imaging. (A) Representative autoradiography image; areas of increased signal correlated spatially with immunohistochemical detection of tumour burden, as seen in the immunohistochemistry image (B). (C) Quantification of ^{123}I- DPA713 binding (normalised activity), as determined by SPECT, in animals injected intracardially with either 4T1-GFP cells or saline (unpaired t-test, p=0.3942). Autoradiography images were false-coloured in ImageJ using the 'Fire' look-up table. Data are presented as mean values ± S.E.M.

In order to investigate the utility of ^{123}I-DPA-713 in detecting micrometastases in the intracardiac model, imaging was performed at day 21 in animals injected intracardially with either 4T1-GFP cells or saline. As shown in Figure 6.9, a comparison between autoradiography images and histology suggests that ligand binding occurs in regions of tumour-associated gliosis. However, comparing whole brain VOIs in 4T1-GFP injected animals and saline animals, normalising to an extra cranial reference region, revealed no significant difference was observed in uptake between the two treatment groups (unpaired t-test, p=0.394).

6.2.9 Metastatic detection with PET using ^{18}F-GE-180

Based on the success of the above experimental paradigm, with regards to detection of tumour burden in the intracerebral model, ^{18}F-GE-180 was used in conjunction with PET to detect gliosis induced by brain metastasis. Firstly, animals were injected with either 4T1-GFP cells or saline via the intracerebral route. At day 14, PET-CT was performed on the animals using a 30-minute dynamic scan. As shown in Figure 6.10, ^{18}F-GE-180 can be used to detect tumour burden in the intracerebral model of brain metastasis at day 14. Activity was quantified in the ROI, spanning the injection site and compared to the contralateral hemisphere. As shown in Figure 6.10, the percentage signal increase was greater in animals injected with 4T1-GFP cells, compared to saline control animals (unpaired t-test, p=0.0218).

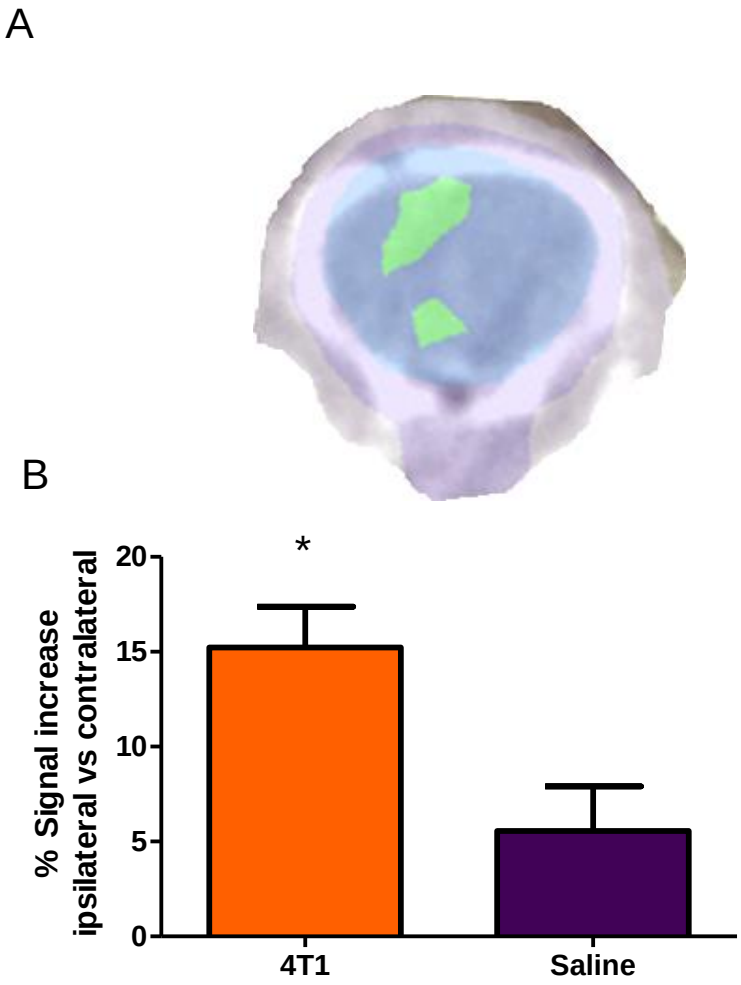

Figure 6.10: GE-180 PET can detect metastases induced via the intracerebral method. Female BALB/c mice were injected intrastriatally with 4T1-GFP cells or saline. At day 14 post tumour inoculation, animals were injected IV with ~20 MBq ^{18}F-GE-180 and a dynamic PET scan performed (A) Representative PET images at the injection site (left hemisphere) from a 4T1-GFP injected mouse. On the coronal CT section, the injection site is visible. The PET data overlay demonstrates a 'hotspot' at the sit on injection. (B) Percentage signal increase in the injected hemisphere compared to the control contralateral hemisphere for 4T1-GFP (n = 9) and saline (n = 4) injected animals. Unpaired t-test, *p=0.0218. Data are presented as mean values ± S.E.M.

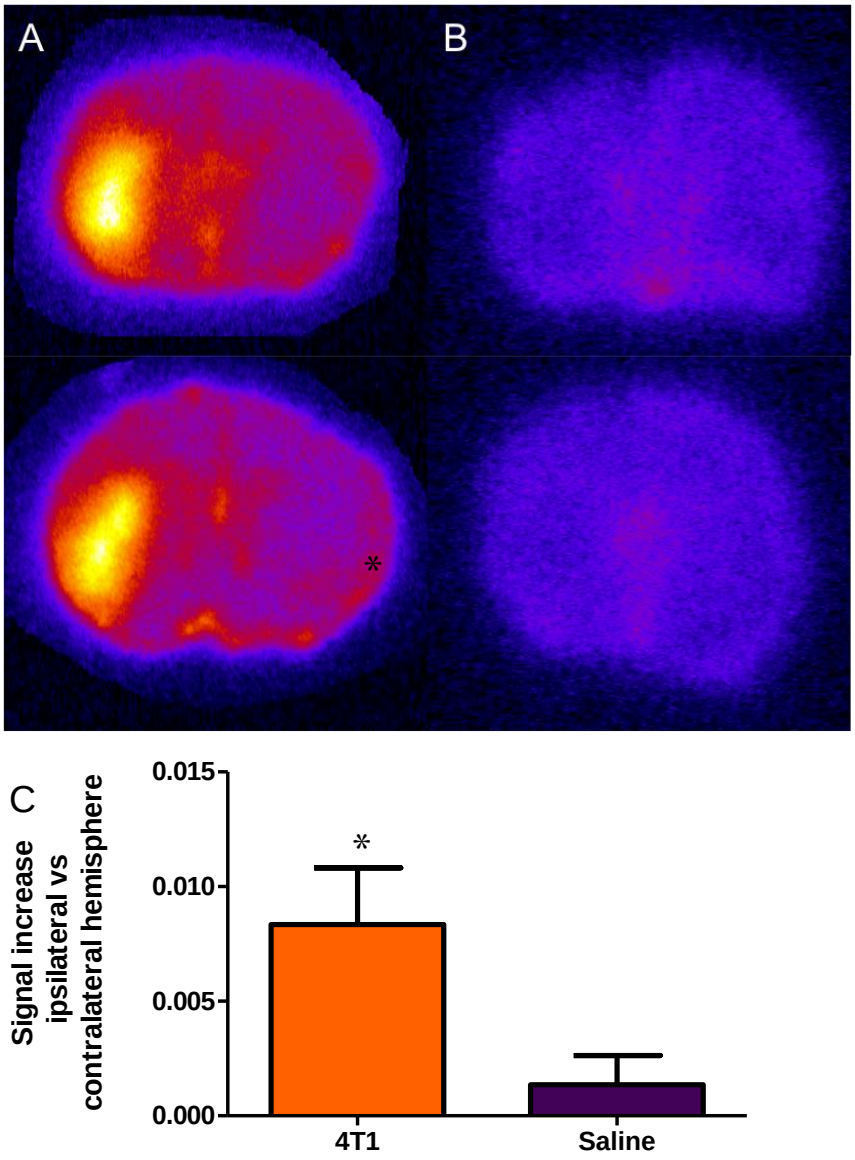

Figure 6.11: GE-180 binding was confirmed by autoradiography in 4T1-GFP injected animals as compared to saline injected animals. After PET imaging, animals were perfused with saline and brains fresh-frozen. Multiple 10 μm sections were taken through the injection site. Autoradiography was performed, incubating sections for approximately 24 hours with a phosphor plate. Representative autoradiographic images from 4T1-GFP injected animals (A) and saline injected animals (B). Images were false-coloured in ImageJ using the 'Fire' look-up table. (C) Percentage signal increase in the injected hemisphere compared to the control contralateral hemisphere for 4T1-GFP and saline injected animals, normalised for injected dose (n=4 per treatment group). Unpaired t-test, *p=0.0461.Data are presented as mean values ± S.E.M.

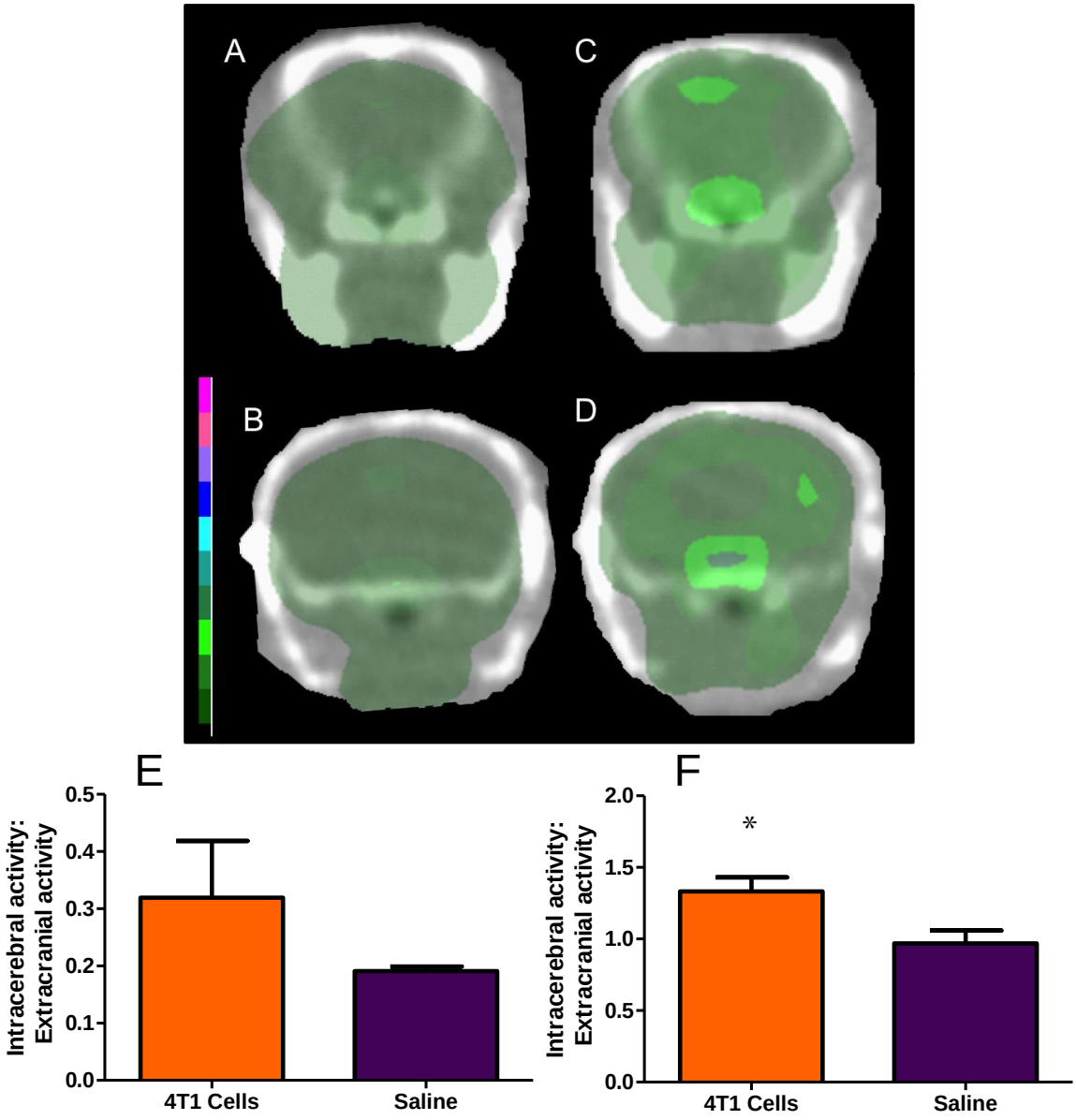

Figure 6.12: Disseminated metastatic burden can be detected with ^{18}F GE-180. At day 21 post-intracardiac tumour/saline injection, animals underwent PET-CT imaging. Representative images from saline injected animals (A&B) and 4T1-GFP injected animals (C&D), at different brain regions are displayed. The colour scale bar represents lowest activity as dark green and highest activity as pink. (E) ~ 40 MBq ^{18}F-GE-180 was injected and a dynamic scan performed for 30 minutes. A whole brain volume of interest was compared to an extracranial voxel. No significant differences were observed between 4T1-GFP injected and saline injected animals (unpaired t-test, p=0.268). (F) ~ 15 MBq ^{18}F-GE-180 was injected and a dynamic scan performed for 50 minutes. A whole brain volume of interest was compared to an extracranial voxel, looking at data collected from 25 minutes onwards. A significant difference was observed between 4T1-GFP injected and saline injected animals (unpaired t-test, p=0.0427). Data are presented as mean values ± S.E.M.

After PET-CT, animals were perfused with saline and tissue was processed for autoradiography. As shown in Figure 6.11, strong ^{18}F-GE-180 binding can be observed in the tumour-bearing hemisphere. Such signal intensity is not observed in the saline injected animals, when corrected for injected dose (unpaired t-test, p=0.0461).

In order to ascertain whether or not ^{18}F-GE-180 can be used to detect micrometastases induced by the intracardiac model, animals were imaged at 21 days post-tumour inoculation. Firstly, as with the intracerebral model, a 30-minute dynamic scan time was used. However, comparing intracranial to extracranial activity revealed no significant differences over saline injected animals (Figure 6.12 A; unpaired t-test, p=0.268). Thus, the scan time was increased on account of the compound binding kinetics; a longer scan time will increase the likelihood of capturing GE-180 binding. The dynamic scan was analysed using only frames from 25 minutes onwards. Using this experimental set-up, significant differences were revealed between treatment and control groups (Figure 6.12 B; unpaired t-test, p=0.0427).

As shown in Figure 6.13, ^{18}F-GE-180 binding in the intracardiac model was confirmed with autoradiography, with compound binding 'hotspots' clearly correlating with tumour burden. Whilst mild focal hyper intensities could be found with Gd-MRI throughout the brain at this time-point, these were not strongly enhancing (Figure 6.13 A) and did not encompass the full tumour burden. In contrast, GE-180 appears to capture a greater number of metastases. Thus, this suggests that the use of GE-180 could provide a more

sensitive mechanism of tumour detection than MRI, owing to the greater signal yielded by an increased area of compound binding.

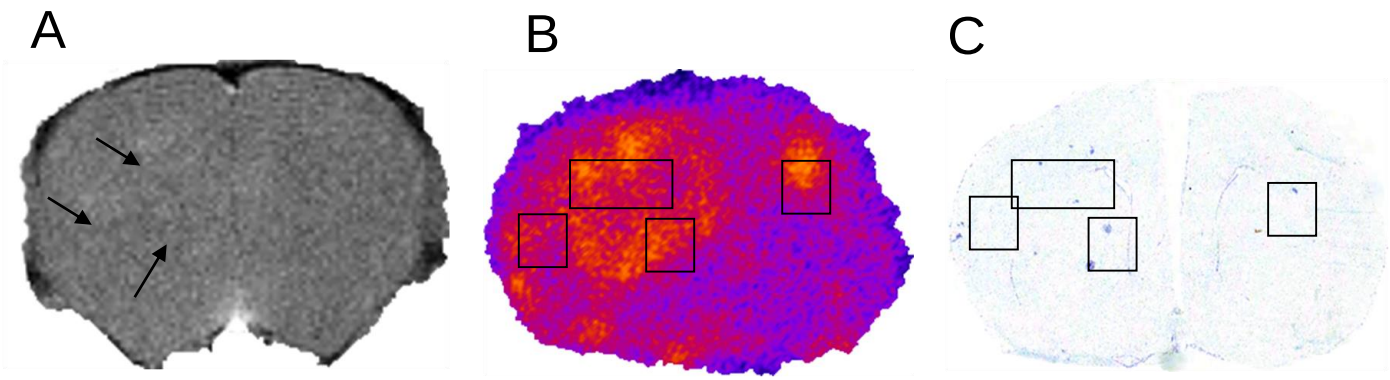

Figure 6.13: ^{18}F-GE-180 binds to areas of tumour growth facilitating more sensitive tumour detection than with Gd-MRI. Female BALB/c mice were injected intracardially with 4T1-GFP cells. At day 20 post-injection, 24 hours prior to ^{18}F-GE-180 PET, animals underwent T1 weighted MRI, pre- and post-Gd. BBB breakdown was observed at this time point, with hyper intensities observed throughout the brain. A) Representative T1 weighted MR image, post-Gd administration (1mm slice thickness). Arrows highlight hyperintensities. Animals subsequently underwent PET imaging with ^{18}F-GE-180 PET. At the end of the imaging session, animals were perfused with saline, brains fresh-frozen and processed for autoradiography. B) Autoradiography image from corresponding tissue section. 'Hot spots' in orange represent ^{18}F-GE-180 PET binding. These hotspots correlate to tumour burden shown in (C), with metastases, identified with a cresyl violet counterstain, highlighted with boxes.

6.3 Discussion

The development of techniques that enable earlier detection of brain metastases— when therapy may be more beneficial— is critical (Serres et al., 2012). In light of the robust astrocyte response to brain metastases demonstrated in Chapter 3, along with microglial response demonstrated in this chapter, a marker of gliosis could provide a useful biomarker for metastatic burden. TSPO upregulation has been demonstrated in both astrocytes and microglia when they become reactive (Cosenza-Nashat et al., 2009; Lavisse et al., 2012) and numerous studies have demonstrated the use of radiolabelled agents targeting TSPO for the detection of neuropathology (Chauveau et al., 2009; Gulyas et al., 2012a; Harberts et al., 2012; Mattner et al., 2013). Thus, such a molecular imaging approach could provide a tool for the early detection of brain metastases.

In accord with this hypothesis, increased TSPO expression was found both on astrocytes and microglia in the metastatic microenvironment, as has been reported previously in other inflammatory conditions (Cosenza-Nashat et al., 2009; Harberts et al., 2012). Interestingly, in the intracerebral model (day 14) TSPO up-regulation appeared to be more robust in reactive astrocytes than in activated microglia. Conversely, the reverse was found in the intracardiac model (day 21) with TSPO expression in astrocytes being largely restricted to the tumour periphery. These findings suggest that TSPO expression may reflect differential glial phenotypes and that induction of TSPO expression is context-dependent (Batarseh et al., 2010). Additionally, there is evidence that suggests

that TSPO expression mirrors the different activation dynamics of the glial populations. Microglia respond rapidly to challenge, whilst astrocytes are activated over a more protracted time-course (Chen and Guilarte, 2008). Thus, the reduced TSPO expression in microglia compared to astrocytes in the intracerebral model may reflect the later time-point of the disease. Nevertheless, the combined TSPO signal from both glial populations supported the concept that radiolabelled compounds targeted to TSPO could be used to image metastasis-associated gliosis.

Initial TSPO imaging work was conducted in the intracerebral model, in which the tumour cells are injected into a known location within the left striatum. ^{123}I-DPA713 accumulation was clearly evident using SPECT detection at the site of tumour cell injection, and to a significantly greater extent than was seen in saline-injected animals. Autoradiography provided higher spatial resolution, confirming ^{123}I-DPA713 binding in the tumour-bearing hemisphere, and again was greater than observed in the saline animals.

Spatial registration of the autoradiographic images with immunohistochemical staining demonstrated that radiotracer binding extended well beyond the area encompassing the metastases themselves, and correlated spatially with the overall extent of astrocyte and microglial activation. However, the greatest intensity of compound binding appeared to correlate with the metastatic foci. This is likely to be due to the strong glial activation in this region, including

dense microglial infiltration of the metastatic site and closely surrounding astrocyte activation.

Whilst the intracerebral model provides a focal lesion appropriate for trialling imaging techniques, a more physiologically relevant model should be used to demonstrate clinical potential. As such, ^{123}I-DPA-713 was used in animals at day 21 after intracardiac injection of 4T1-GFP or saline. Autoradiography data indicated that ^{123}I-DPA713 also enabled detection of astrogliosis induced by metastases in the intracardiac model. However, it appears that the spatial resolution of SPECT imaging was insufficient to enable visualisation of individual metastases at this time point *in vivo*, most likely owing to their very small size compared to the metastatic foci in the intracerebral model (*ca*. 100 μm *vs*. 600 μm diameter) and, hence, the associated area of gliosis (*ca*. 400 μm *vs*. *ca*. 1800 μm.

Taken together, the intracerebral and intracardiac ^{123}I-DPA713 SPECT data suggest a detection threshold for metastases lying between 100 and 600 μm in diameter, with an associated area of astroglial activation of 0.120 mm^2 to 120 mm^2. Whilst the spatial resolution of SPECT will not allow detection of individual metastases inducing a glial response much less than 1 mm in diameter, in addition there may be issues with compound sensitivity. Even so, this is considerably earlier than the current clinical approach of Gd-MRI, which has a detection threshold of 0.5—1.0 cm tumour diameter.

The success of this experimental paradigm in detecting tumour-induced gliosis led to progression to a PET system, with the rationale that greater sensitivity would allow detection of micrometastases in the intracardiac model.

Additionally, the acquisition of another TSPO ligand with greater receptor affinity, GE-180 (Wadsworth et al., 2012), may also facilitate enhanced tumour detection.

^{18}F-GE-180 also detects tumour burden in the intracerebral model of metastasis, as seen by autoradiography. Additionally, tumour burden can be visualised with PET using a 30-minute scan time. Volume-of-interest comparisons to a cerebral reference region (the contralateral hemisphere) indicate that PET can reliably detect tumour burden compared to saline-injected animals.

Using a 50-minute acquisition time, GE-180 can be used to detect tumour burden induced by the intracardiac model. The autoradiography data presented here demonstrate ligand binding correlating with metastatic burden. Of particular note is that the autoradiography images demonstrate that GE-180 is a more sensitive detector of tumour burden than what can be observed with Gd-enhanced MRI. Furthermore, this binding can be globally detected with PET, as demonstrated by the increased intracranial activity compared to saline-injected controls.

Going forwards with this technique, a more sophisticated analysis will be required to pull out discrete 'hotspots' in the intracardiac model, such that individual metastases can be detected; the current analysis allows global differentiation between treatment and control groups. As it stands, the data sets are very 'noisy', with a lot of background signal, even in in the saline

animals. An alternative reconstruction method could be used to remove this background. Iterative reconstruction algorithms, such as ordered subsets expectation maximisation (OSEM), are more complex than the FBP algorithm used in this thesis, but are generally considered to suppress noise to a greater extent. An image estimate is constructed, usually displaying a uniform distribution of activity. Forward projection is used to estimate a set of projection data. The estimated projections are compared to the recorded projections, with the differences used to modulate the estimated image. This process is repeated until the difference is smaller than the predefined value (Lyra and Ploussi, 2011). Once this reconstruction technique has been used, it may be possible to use cluster analysis to detect individual hotspots that correlate with tumour burden in disseminated disease. This technique has been employed in clinical analysis (Turkheimer et al., 2007), so it remains to be seen whether this can be translated into small rodent models.

This study is not a direct comparison of the two TSPO ligands. However, it does indicate that GE-180 can be used to detect tumour burden more robustly than DPA-713. Whether this is a consequence of the greater sensitivity conferred by PET over SPECT, or due to the nature of the compound itself, has not been investigated. However, greater ligand affinity could be a factor driving increased separation of experimental versus control groups.

Interestingly, very recent work has suggested the potential for imaging breast cancer metastasis to the brain on the basis of TSPO expression by the breast cancer cells themselves (Vasdev et al., 2013; Wyatt et al., 2010; Wyatt et al.,

2012); TSPO has been linked to enhanced proliferative potential (Wu and Gallo, 2013). However, the work presented here demonstrates that this approach would target not only the metastatic cells, but also the glial response. This amplified region of detection will be of critical importance for lower-resolution clinical imaging methods. Moreover, we found that the 4T1-GFP cells used here do not robustly express TSPO, in contrast to the metastatic human breast carcinoma cell line MDABR231 in which expression has previously been shown (Batarseh et al., 2012). Thus, any signal observed in this study is due to enhanced gliosis in the tumour microenvironment. These studies also suggest that not all tumour cells will be TSPO-positive, but glial activation has been found to be consistent across a number of different types of brain metastasis, making this a technique with broad clinical applications.

In the context of imaging astrocytes in primary brain tumours, numerous glioma cell lines have been shown to highly express TSPO (Winkeler et al., 2012), and recent studies in rat models of glioma suggest that this approach could be used as a clinical tool to detect metastases (Buck et al., 2011; Tang et al., 2012; Winkeler et al., 2012). These techniques are unlikely to allow differentiation of tumour growth from associated astrogliosis. However, this approach does hold potential as a surrogate biomarker for the clinical detection of CNS tumours.

In translating the above work into a clinical scenario, one should bear in mind genetic polymorphisms in the TSPO gene, which have been shown to affect

ligand binding (Guo et al., 2013; Kreisl et al., 2012; Owen et al., 2011). Additionally, there is evidence for age-related increases in TSPO ligand uptake in certain brain regions (Kumar et al., 2012), which along with age-related neuroinflammatory pathologies, may act as a confound for the detection of brain metastasis.

6.4 Conclusions and Future work

In conclusion, TSPO is expressed on both astrocytes and microglia in the tumour microenvironment. In this study, TSPO was successfully targeted with the small-molecule radiolabelled ligands, DPA-713 and GE-180. Compound binding to areas of gliosis acted as a surrogate for tumour growth in both a SPECT and PET system, with binding confirmed with autoradiography. The threshold for tumour detection was lower in the PET system, presumably as a consequence of increased sensitivity of PET over SPECT and greater TSPO affinity of GE-180 compared to DPA-713. Thus, going forward, the GE-180 PET system will be used to further test the utility of TSPO as a biomarker for tumour burden.

Attempts were made to determine, at a cellular level, the binding profile of TSPO ligands, using silver emulsion radiography. However, this approach was not successful. Thus, with regards to specific co-localisation of DPA-713 and GE-180 with astrocytes and microglia, future work could employ the use of a fluorescently labelled TSPO ligand. A fluorescently labelled analogue of DPA-713, DPA-713-IRDye680LT, has been used to demonstrate pulmonary macrophage binding in an *in vivo* model of tuberculosis: blockade of TSPO with unlabelled DPA-713 attenuates co-localisation with macrophage markers (Foss et al., 2013). Thus, using a similar strategy, one could probe the distribution of TSPO ligand binding in order to confirm astrocyte and microglial binding at a

greater spatial resolution than is achievable with autoradiography. This would have interesting implications for analysing the temporal profile of TSPO expression with disease pathogenesis and how this affects ligand binding.

With regards to early detection of disease, a longitudinal study should be conducted to define the point at which metastatic growth can be detected via TSPO imaging, and to compare this with Gd-MRI. This study would allow determination of the utility of this technique to detect neuroinflammation at time points earlier than the current clinical gold standard. As GE-180 is currently in Phase I clinical trials for Alzheimer's disease, one could envision the possibility for rapid translation to the clinic, should further pre-clinical work prove promising.

Whilst much focus has been placed on TSPO imaging, there are other markers of neuroinflammation that could be used as indicators of metastatic disease. Monoamine oxidase-B (MAO-B), like TSPO, is located on the outer mitochondrial membrane. Expression is elevated in activated astrocytes, and ligands against the enzyme have been used for PET detection in some neuropathologies (Engler et al., 2003; Johansson et al., 2007; Santillo et al., 2011). It would be interesting to investigate whether or not such ligands could be used to detect metastatic burden. With regards to the microglial response, it has been recently shown in human studies that radiolabelled ligands targeting adenosine receptor 2A (A2AR) can be used to detect the microglial response in MS (Rissanen et al., 2013). In light of the genetic polymorphisms in TSPO described above, perhaps it is wise to look at alternative tracers.

Chapter 7 Discussion and Future Directions

Over recent years there has been a flurry of activity regarding the involvement of astrocytes in brain metastases. However, functional insights into the role of astroglia have largely been limited to *in vitro* systems. The experimental work presented here is the first to manipulate astrocyte activation itself, *in vivo,* in order to attempt to elucidate its role in the progression of metastasis. Whilst an answer to the question 'What is the role of astrocytes in brain metastasis?' has yet to be fully achieved, this work has made headway in translating *in vitro* findings into relevant *in vivo* models. Not only have mechanistic insights been gained, but it is also clear that the glial response can be targeted with diagnostic imaging modalities, as a surrogate for metastatic burden.

In this thesis I have demonstrated, via two *in vivo* routes of metastatic induction, that astrocyte activation is a robust feature of the tumour microenvironment, throughout a prolonged time period. There appears to be a dynamic interaction between astrocytes and metastatic cells and, as such, astrocyte reactivity does not progress to a glial scar, as observed in other brain pathologies such as stroke and traumatic brain injury. Thus, findings in those disease states may not be translatable to the situation in brain metastasis.

In addition to demonstrating the intimate and dynamic association between astrocytes and tumour cells, I aimed to elucidate the role of astrocytes in brain metastases pathogenesis. To this end, I used two experimental paradigms. The first involved chronic activation of astrocytes using a CNTF-lentivirus. The

second, conversely, aimed to inhibit astrocytes, using a liposome-packaged steroid (2B3-201). Although no significant modulation of tumour burden was found in either model, the trends observed in both fitted with the hypothesis that astrocyte activation drives tumour progression; in the CNTF-lentivirus model there were indications towards increased tumour growth at later time points of disease, whilst in the 2B3-201 inhibition study, a trend towards decreased tumour growth was suggested, particularly in prefrontal regions.

With regards to the induction of astrocyte activation with a CNTF-lentivirus, I have demonstrated that astrocytes activated in this manner do not alter metastatic seeding or growth. Instead, I have shown that astrocytes stimulated with distinct challenges (CNTF *vs.* tumour-conditioned media) respond with different molecular phenotypes. Thus, in order to probe the effect of chronic astrocyte activation on metastatic progression, a model in which astrocytes are in a more relevant activation state may prove more useful. Perhaps 'priming' the CNS with tumour-conditioned media prior to tumour inoculation would activate astrocytes in a relevant manner. However, as manipulating the phenotype of specific cells is clearly challenging, inhibition studies may be a more practical approach. As shown in Chapter 5, attempts were made to inhibit astrocyte activation using a targeted liposomally-packaged steroid (methylprednisolone). Whilst this study did not demonstrate any significant alteration in tumour burden, this may be due to experimental design. More frequent dosing and/or a more potent steroid (e.g. dexamethasone) might be necessary to induce significant differences in astrocyte reactivity, tumour seeding and growth.

As discussed in Chapter 5, a transgenic model in which astrocyte activation is specifically inhibited, could prove a robust experimental paradigm for determining, *in vivo*, the role of astrocytes in brain metastasis. These experiments are now in progress and their outcome will have great relevance to this thesis. Although in Chapter 3 qPCR data indicated that TNF was not part of the CNS response to tumour growth, cytokine release by the tumour cells themselves has not yet been assessed. Thus, signaling via NFkB is still a relevant mechanism to probe in astrocytes, based on the experimental literature.

This thesis provides a strong framework for further studies into the role of astrocytes in metastatic progression. It is apparent that astrocytes do not exist in one phenotype surrounding the periphery of metastatic colonies. Thus, subsequent studies into modulation of the astrocytic response must take this into account. As discussed in Chapter 3, use of the transgenic mouse strain, GFAP-GFP, could prove useful for acute isolation of astrocytes from different regions around the tumour periphery, allowing a comparison of the transcriptional profile. Similarly, the novel technique of laser capture microdissection could also shed light on this issue. Utilising immunofluorescence techniques, a spatial profile of the tumour microenvironment with regards to protein expression could be achieved. As shown in Chapter 3, iNOS expression by astrocytes was only evident in the tumour periphery. It would be interesting to determine whether this spatial pattern correlates with the production of iNOS stimulating factors, such as IL-1β and whether the spatial relationship changes with time.

Moving forward, from the PCR work presented in Chapter 3 and Chapter 4, IL-6 appears to be a gene of interest for further work. As shown in Chapter 3, IL-6 expression is observed in response to tumour burden, compared to vehicle control, in the intracerebral model. Additionally, increases across the time course in the intracardiac model were observed. In the PCR study of astrocyte cultures in Chapter 4, IL-6 was differentially regulated by TCM and CNTF. Indeed, the lack of growth advantage conferred by CNTF-activated astrocytes may, in part, reflect the absence of IL-6 production. Thus, strategies to inhibit the action of IL-6 *in vivo* might prove promising for reducing brain metastatic growth. Indeed, an *in vivo* study in which mice were inoculated with the metastatic lung cell line HARA-B, demonstrated that treatment with the anti-IL-6 receptor monoclonal antibody, Tocilizumab, significantly reduced brain metastasis volume when given after the establishment of metastatic colonies (Noda et al., 2012). It would be interesting to pursue this in the models I have developed in this thesis, with a more robust quantification of tumour volume than the previous study; the authors calculated tumour volume using fluorescence and gave no indication as to whether multiple micrometastases were tracked throughout the brain. Moreover, when considering the translational potential of such a therapeutic paradigm, it is important to take in account penetration of the BBB. Whilst Tocilizumab has been demonstrated to have a good long-term peripheral safety profile in patients receiving the drug for rheumatoid arthritis (Nishimoto et al., 2009), antibodies typically do not penetrate the BBB well. Antibody delivery to the sites of metastasis could be enhanced using a novel strategy, in which a bolus intravenous injection of TNF

has been shown to induce BBB permeabilisation specifically at sites of brain metastases, facilitating antibody delivery (Connell et al., 2013). Alternatively, small molecules could be considered. For example, in an *in vivo* model of LPS induced CNS inflammation, leutolin was shown to reduce IL-6 production. Concomitant *in vitro* studies demonstrated that leutolin reduces IL-6 production in microglia (Jang et al., 2008). It would be interesting to use this small molecule in the models presented in this thesis to determine whether IL-6 production by astrocytes can be inhibited and, if so, whether that translates to a reduction in tumour burden.

Just as caution must be exercised when extrapolating *in vitro* data into an *in vivo* scenario, one must recognize the caveats of translating *in vivo* work into the clinical setting. The intracardiac model is a physiologically relevant model of hematogenous dissemination of cancer cells to the brain. However, the tumour burden induced via this method far exceeds the tumour burden typically observed in the clinic. Consequently, the neuroinflammatory response observed in these studies may not be representative of the clinical situation. Other models, such as breast cancer xenografts which spontaneously metastasise to the brain could be utilized (Daphu et al., 2013). This would also enable study of the pre-metastatic niche (Liu et al., 2013; Ramakrishna and Rostomily, 2013), allowing the contribution of astrocytes to this stage of pathogenesis to be addressed. However, such models are impractical when it comes to repeatable assessment and comparison of tumour burden as required in this study. Moreover, such models typically require resection of the primary tumour in order to allow longitudinal studies of brain metastases, whilst long-

term animal health can be a problem owing to high systemic as well as central metastatic burden. The solution, therefore, may simply be to work with fewer tumour cells introduced via the intracardiac route as described here.

Importantly, this thesis demonstrates that the astrocytic response to brain metastasis can be harnessed as a target for the early detection of brain metastasis. Glial expression of TSPO was successfully imaged using radiolabelled small molecules with both SPECT and PET modalities. As the GE-180 compound used in the PET experiments is already in clinical trials for another disease indication, this is promising for extending these *in vivo* findings to the clinic. Prior to that, however, the threshold of detection must be further defined in longitudinal studies from the point of tumour inoculation, and concurrent MRI studies employed in order to determine whether this technique can supersede the current 'gold-standard' of contrast-enhanced MRI. Additionally, as discussed above, inoculation of fewer cells may be necessary in order to more faithfully recapitulate the clinical situation.

In conclusion, astrocytes are robustly activated in response to metastatic burden. Whilst it is yet to be fully elucidated how astrocytes contribute to metastatic disease, based on the trends in both the activation and inhibition studies presented here, it appears likely that astrocytes contribute to metastatic growth. This contribution to metastatic growth may be mediated by a host of proliferative mediators, but the work described here suggests that IL-6 is a sensible candidate for future inhibition studies. Regardless of the roles of astrocytes in brain metastasis, the SPECT and PET work conducted here

demonstrate that the glial response to tumour burden is a novel mechanism for the early detection of brain metastasis. A greater understanding of the role of astrocyte reactivity, along with the ability to target gliosis as a diagnostic biomarker has great relevance for detecting and treating brain metastasis in the clinic.

Chapter 8 References

Abbracchio, M. P., Saffrey, M. J., Hopker, V., and Burnstock, G. (1994). Modulation of astroglial cell proliferation by analogues of adenosine and ATP in primary cultures of rat striatum. Neuroscience *59*, 67-76.

Airey, D. C., Lu, L., and Williams, R. W. (2001). Genetic control of the mouse cerebellum: identification of quantitative trait loci modulating size and architecture. The Journal of neuroscience : the official journal of the Society for Neuroscience *21*, 5099-5109.

Akeson, A. L., Woods, C. W., Hsieh, L. C., Bohnke, R. A., Ackermann, B. L., Chan, K. Y., Robinson, J. L., Yanofsky, S. D., Jacobs, J. W., Barrett, R. W., and Bowlin, T. L. (1996). AF12198, a novel low molecular weight antagonist, selectively binds the human type I interleukin (IL)-1 receptor and blocks in vivo responses to IL-1. J Biol Chem *271*, 30517-30523.

Allavena, P., Sica, A., Garlanda, C., and Mantovani, A. (2008). The Yin-Yang of tumor-associated macrophages in neoplastic progression and immune surveillance. Immunol Rev *222*, 155-161.

Amat, J. A., Ishiguro, H., Nakamura, K., and Norton, W. T. (1996). Phenotypic diversity and kinetics of proliferating microglia and astrocytes following cortical stab wounds. Glia *16*, 368-382.

Amit, M., Laider-Trejo, L., Shalom, V., Shabtay-Orbach, A., Krelin, Y., and Gil, Z. (2013). Characterization of the melanoma brain metastatic niche in mice and humans. Cancer Med *2*, 155-163.

Anthony, D. C., Bolton, S. J., Fearn, S., and Perry, V. H. (1997). Age-related effects of interleukin-1 beta on polymorphonuclear neutrophil-dependent increases in blood-brain barrier permeability in rats. Brain *120 (Pt 3)*, 435-444.

Aubert, A., Costalat, R., Magistretti, P. J., and Pellerin, L. (2005). Brain lactate kinetics: Modeling evidence for neuronal lactate uptake upon activation. Proc Natl Acad Sci U S A *102*, 16448-16453.

Azevedo, F. A., Carvalho, L. R., Grinberg, L. T., Farfel, J. M., Ferretti, R. E., Leite, R. E., Jacob Filho, W., Lent, R., and Herculano-Houzel, S. (2009). Equal numbers of neuronal and nonneuronal cells make the human brain an isometrically scaled-up primate brain. J Comp Neurol *513*, 532-541.

Bagnato, A., Cirilli, A., Salani, D., Simeone, P., Muller, A., Nicotra, M. R., Natali, P. G., and Venuti, A. (2002). Growth inhibition of cervix carcinoma cells in vivo by endothelin A receptor blockade. Cancer Res *62*, 6381-6384.

Bagnato, A., and Natali, P. G. (2004). Targeting endothelin axis in cancer. Cancer Treat Res *119*, 293-314.

Bagnato, A., Rosano, L., Spinella, F., Di Castro, V., Tecce, R., and Natali, P. G. (2004). Endothelin B receptor blockade inhibits dynamics of cell interactions and communications in melanoma cell progression. Cancer Res *64*, 1436-1443.

Bagnato, A., Tecce, R., Di Castro, V., and Catt, K. J. (1997). Activation of mitogenic signaling by endothelin 1 in ovarian carcinoma cells. Cancer Res *57*, 1306-1311.

Balathasan, L., Beech, J. S., and Muschel, R. J. (2013). Ultrasonography-Guided Intracardiac Injection: An Improvement for Quantitative Brain Colonization Assays. Am J Pathol.

Balhara, J., and Gounni, A. S. (2012). The alveolar macrophages in asthma: a double-edged sword. Mucosal Immunol *5*, 605-609.

Bardehle, S., Kruger, M., Buggenthin, F., Schwausch, J., Ninkovic, J., Clevers, H., Snippert, H. J., Theis, F. J., Meyer-Luehmann, M., Bechmann, I.*, et al.* (2013). Live imaging of astrocyte responses to acute injury reveals selective juxtavascular proliferation. Nat Neurosci *16*, 580-586.

Bash, J., Zong, W. X., Banga, S., Rivera, A., Ballard, D. W., Ron, Y., and Gelinas, C. (1999). Rel/NF-kappaB can trigger the Notch signaling pathway by inducing the expression of Jagged1, a ligand for Notch receptors. EMBO J *18*, 2803-2811.

Batarseh, A., Barlow, K. D., Martinez-Arguelles, D. B., and Papadopoulos, V. (2012). Functional characterization of the human translocator protein (18kDa) gene promoter in human breast cancer cell lines. Biochim Biophys Acta *1819*, 38-56.

Batarseh, A., Li, J., and Papadopoulos, V. (2010). Protein kinase C epsilon regulation of translocator protein (18 kDa) Tspo gene expression is mediated through a MAPK pathway targeting STAT3 and c-Jun transcription factors. Biochemistry *49*, 4766-4778.

Bavaresco, L., Bernardi, A., Braganhol, E., Wink, M. R., and Battastini, A. M. (2007). Dexamethasone inhibits proliferation and stimulates ecto-5'-nucleotidase/CD73 activity in C6 rat glioma cell line. J Neurooncol *84*, 1-8.

Bechstein, M., Haussler, U., Neef, M., Hofmann, H. D., Kirsch, M., and Haas, C. A. (2012). CNTF-mediated preactivation of astrocytes attenuates neuronal damage and epileptiform activity in experimental epilepsy. Exp Neurol *236*, 141-150.

Beck, H., Semisch, M., Culmsee, C., Plesnila, N., and Hatzopoulos, A. K. (2008). Egr-1 regulates expression of the glial scar component phosphacan in astrocytes after experimental stroke. Am J Pathol *173*, 77-92.

Berghoff, A. S., Lassmann, H., Preusser, M., and Hoftberger, R. (2012). Characterization of the inflammatory response to solid cancer metastases in the human brain. Clinical & experimental metastasis.

Beurrier, C., Faideau, M., Bennouar, K. E., Escartin, C., Kerkerian-Le Goff, L., Bonvento, G., and Gubellini, P. (2010). Ciliary neurotrophic factor protects striatal neurons against excitotoxicity by enhancing glial glutamate uptake. PLoS One *5*, e8550.

Bi, B., Salmaso, N., Komitova, M., Simonini, M. V., Silbereis, J., Cheng, E., Kim, J., Luft, S., Ment, L. R., Horvath, T. L.*, et al.* (2011). Cortical glial fibrillary acidic protein-positive cells generate neurons after perinatal hypoxic injury. J Neurosci *31*, 9205-9221.

Birchmeier, W., and Behrens, J. (1994). Cadherin expression in carcinomas: role in the formation of cell junctions and the prevention of invasiveness. Biochim Biophys Acta *1198*, 11-26.

Blond, D., Campbell, S. J., Butchart, A. G., Perry, V. H., and Anthony, D. C. (2002). Differential induction of interleukin-1beta and tumour necrosis factor-alpha may account for specific patterns of leukocyte recruitment in the brain. Brain Res *958*, 89-99.

Boado, R. J., and Pardridge, W. M. (1990). The brain-type glucose transporter mRNA is specifically expressed at the blood-brain barrier. Biochem Biophys Res Commun *166*, 174-179.

Boche, D., Perry, V. H., and Nicoll, J. A. (2013). Review: activation patterns of microglia and their identification in the human brain. Neuropathol Appl Neurobiol *39*, 3-18.

Bos, P. D., Zhang, X. H., Nadal, C., Shu, W., Gomis, R. R., Nguyen, D. X., Minn, A. J., van de Vijver, M. J., Gerald, W. L., Foekens, J. A., and Massague, J. (2009). Genes that mediate breast cancer metastasis to the brain. Nature *459*, 1005-1009.

Boukerche, H., Su, Z. Z., Kang, D. C., and Fisher, P. B. (2004). Identification and cloning of genes displaying elevated expression as a consequence of metastatic progression in human melanoma cells by rapid subtraction hybridization. Gene *343*, 191-201.

Boulton, T. G., Stahl, N., and Yancopoulos, G. D. (1994). Ciliary neurotrophic factor/leukemia inhibitory factor/interleukin 6/oncostatin M family of cytokines induces tyrosine phosphorylation of a common set of proteins overlapping those induced by other cytokines and growth factors. J Biol Chem *269*, 11648-11655.

Braet, K., Paemeleire, K., D'Herde, K., Sanderson, M. J., and Leybaert, L. (2001). Astrocyte-endothelial cell calcium signals conveyed by two signalling pathways. Eur J Neurosci *13*, 79-91.

Brahmachari, S., Fung, Y. K., and Pahan, K. (2006). Induction of glial fibrillary acidic protein expression in astrocytes by nitric oxide. J Neurosci *26*, 4930-4939.

Brambilla, R., Bracchi-Ricard, V., Hu, W. H., Frydel, B., Bramwell, A., Karmally, S., Green, E. J., and Bethea, J. R. (2005). Inhibition of astroglial nuclear factor kappaB reduces inflammation and improves functional recovery after spinal cord injury. J Exp Med *202*, 145-156.

Brambilla, R., Dvoriantchikova, G., Barakat, D., Ivanov, D., Bethea, J. R., and Shestopalov, V. I. (2012). Transgenic inhibition of astroglial NF-kappaB protects from optic nerve damage and retinal ganglion cell loss in experimental optic neuritis. J Neuroinflammation *9*, 213.

Brambilla, R., Persaud, T., Hu, X., Karmally, S., Shestopalov, V. I., Dvoriantchikova, G., Ivanov, D., Nathanson, L., Barnum, S. R., and Bethea, J. R. (2009). Transgenic inhibition of astroglial NF-kappa B improves functional outcome in experimental autoimmune encephalomyelitis by suppressing chronic central nervous system inflammation. J Immunol *182*, 2628-2640.

Brantley, E. C., Guo, L., Zhang, C., Lin, Q., Yokoi, K., Langley, R. R., Kruzel, E., Maya, M., Kim, S. W., Kim, S. J.*, et al.* (2010). Nitric oxide-mediated tumoricidal activity of murine microglial cells. Transl Oncol *3*, 380-388.

Brown, A. M., and Ransom, B. R. (2007). Astrocyte glycogen and brain energy metabolism. Glia *55*, 1263-1271.

Buck, J. R., McKinley, E. T., Hight, M. R., Fu, A., Tang, D., Smith, R. A., Tantawy, M. N., Peterson, T. E., Colvin, D., Ansari, M. S.*, et al.* (2011). Quantitative, preclinical PET of translocator protein expression in glioma using 18F-N-fluoroacetyl-N-(2,5-dimethoxybenzyl)-2-phenoxyaniline. Journal of nuclear medicine : official publication, Society of Nuclear Medicine *52*, 107-114.

Bush, T. G., Puvanachandra, N., Horner, C. H., Polito, A., Ostenfeld, T., Svendsen, C. N., Mucke, L., Johnson, M. H., and Sofroniew, M. V. (1999). Leukocyte infiltration, neuronal degeneration, and neurite outgrowth after ablation of scar-forming, reactive astrocytes in adult transgenic mice. Neuron *23*, 297-308.

Buss, A., Pech, K., Kakulas, B. A., Martin, D., Schoenen, J., Noth, J., and Brook, G. A. (2009). NG2 and phosphacan are present in the astroglial scar after human traumatic spinal cord injury. BMC Neurol *9*, 32.

Bustin, S. A., Benes, V., Garson, J. A., Hellemans, J., Huggett, J., Kubista, M., Mueller, R., Nolan, T., Pfaffl, M. W., Shipley, G. L.*, et al.* (2009). The MIQE guidelines: minimum information for publication of quantitative real-time PCR experiments. Clin Chem *55*, 611-622.

Cagnin, A., Brooks, D. J., Kennedy, A. M., Gunn, R. N., Myers, R., Turkheimer, F. E., Jones, T., and Banati, R. B. (2001). In-vivo measurement of activated microglia in dementia. Lancet *358*, 461-467.

Campbell, S. J., Deacon, R. M., Jiang, Y., Ferrari, C., Pitossi, F. J., and Anthony, D. C. (2007). Overexpression of IL-1beta by adenoviral-mediated gene transfer in the rat brain causes a prolonged hepatic chemokine response, axonal injury and the suppression of spontaneous behaviour. Neurobiol Dis *27*, 151-163.

Carbonell, W. S., Ansorge, O., Sibson, N., and Muschel, R. (2009). The vascular basement membrane as "soil" in brain metastasis. PLoS One *4*, e5857.

Carter, S. F., Scholl, M., Almkvist, O., Wall, A., Engler, H., Langstrom, B., and Nordberg, A. (2012). Evidence for astrocytosis in prodromal Alzheimer disease provided by 11C-deuterium-L-deprenyl: a multitracer PET paradigm combining 11C-Pittsburgh compound B and 18F-FDG. Journal of nuclear medicine : official publication, Society of Nuclear Medicine *53*, 37-46.

Chauveau, F., Van Camp, N., Dolle, F., Kuhnast, B., Hinnen, F., Damont, A., Boutin, H., James, M., Kassiou, M., and Tavitian, B. (2009). Comparative evaluation of the translocator protein radioligands 11C-DPA-713, 18F-DPA-714, and 11C-PK11195 in a rat model of acute neuroinflammation. Journal of nuclear medicine : official publication, Society of Nuclear Medicine *50*, 468-476.

Chen, M. K., and Guilarte, T. R. (2008). Translocator protein 18 kDa (TSPO): molecular sensor of brain injury and repair. Pharmacology & therapeutics *118*, 1-17.

Ching, A. S., Kuhnast, B., Damont, A., Roeda, D., Tavitian, B., and Dolle, F. (2012). Current paradigm of the 18-kDa translocator protein (TSPO) as a molecular target for PET imaging in neuroinflammation and neurodegenerative diseases. Insights Imaging *3*, 111-119.

Choi, C., Park, J. Y., Lee, J., Lim, J. H., Shin, E. C., Ahn, Y. S., Kim, C. H., Kim, S. J., Kim, J. D., Choi, I. S., and Choi, I. H. (1999). Fas ligand and Fas are expressed constitutively in human astrocytes and the expression increases with IL-1, IL-6, TNF-alpha, or IFN-gamma. J Immunol *162*, 1889-1895.

Christopherson, K. S., Ullian, E. M., Stokes, C. C., Mullowney, C. E., Hell, J. W., Agah, A., Lawler, J., Mosher, D. F., Bornstein, P., and Barres, B. A. (2005). Thrombospondins are astrocyte-secreted proteins that promote CNS synaptogenesis. Cell *120*, 421-433.

Colin, A., Faideau, M., Dufour, N., Auregan, G., Hassig, R., Andrieu, T., Brouillet, E., Hantraye, P., Bonvento, G., and Deglon, N. (2009). Engineered lentiviral vector targeting astrocytes in vivo. Glia *57*, 667-679.

Combrinck, M. I., Perry, V. H., and Cunningham, C. (2002). Peripheral infection evokes exaggerated sickness behaviour in pre-clinical murine prion disease. Neuroscience *112*, 7-11.

Connell, J. J., Chatain, G., Cornelissen, B., Vallis, K. A., Hamilton, A., Seymour, L., Anthony, D. C., and Sibson, N. R. (2013). Selective Permeabilization of the Blood-Brain Barrier at Sites of Metastasis. J Natl Cancer Inst.

Cormier, R. J., Mennerick, S., Melbostad, H., and Zorumski, C. F. (2001). Basal levels of adenosine modulate mGluR5 on rat hippocampal astrocytes. Glia *33*, 24-35.

Cosenza-Nashat, M., Zhao, M. L., Suh, H. S., Morgan, J., Natividad, R., Morgello, S., and Lee, S. C. (2009). Expression of the translocator protein of 18 kDa by microglia, macrophages and astrocytes based on immunohistochemical localization in abnormal human brain. Neuropathol Appl Neurobiol *35*, 306-328.

Cunningham, C., Campion, S., Lunnon, K., Murray, C. L., Woods, J. F., Deacon, R. M., Rawlins, J. N., and Perry, V. H. (2009). Systemic inflammation induces acute behavioral and cognitive changes and accelerates neurodegenerative disease. Biol Psychiatry *65*, 304-312.

Daphu, I., Sundstrom, T., Horn, S., Huszthy, P. C., Niclou, S. P., Sakariassen, P. O., Immervoll, H., Miletic, H., Bjerkvig, R., and Thorsen, F. (2013). In vivo animal models for studying brain metastasis: value and limitations. Clinical & experimental metastasis *30*, 695-710.

de Almeida, L. P., Zala, D., Aebischer, P., and Deglon, N. (2001). Neuroprotective effect of a CNTF-expressing lentiviral vector in the quinolinic acid rat model of Huntington's disease. Neurobiol Dis *8*, 433-446.

de Oliveira Barros, E. G., Palumbo, A., Jr., Mello, P. L., de Mattos, R. M., da Silva, J. H., Pontes, B., Viana, N. B., do Amaral, R. F., Lima, F. R., da Costa, N. M.*, et al.* (2014). The reciprocal interactions between astrocytes and prostate cancer cells represent an early event associated with brain metastasis. Clinical & experimental metastasis.

Delattre, J. Y., Krol, G., Thaler, H. T., and Posner, J. B. (1988). Distribution of brain metastases. Arch Neurol *45*, 741-744.

Dickens, A. M., Vainio, S., Marjamaki, P., Johansson, J., Lehtiniemi, P., Rokka, J., Rinne, J., Solin, O., Haaparanta-Solin, M., Jones, P. A.*, et al.* (2014). Detection of Microglial Activation in an Acute Model of Neuroinflammation Using PET and Radiotracers 11C-(R)-PK11195 and 18F-GE-180. Journal of nuclear medicine : official publication, Society of Nuclear Medicine.

Doorduin, J., Klein, H. C., Dierckx, R. A., James, M., Kassiou, M., and de Vries, E. F. (2009). [11C]-DPA-713 and [18F]-DPA-714 as new PET tracers for TSPO: a

comparison with [11C]-(R)-PK11195 in a rat model of herpes encephalitis. Mol Imaging Biol *11*, 386-398.

Douglas, A. M., Goss, G. A., Sutherland, R. L., Hilton, D. J., Berndt, M. C., Nicola, N. A., and Begley, C. G. (1997). Expression and function of members of the cytokine receptor superfamily on breast cancer cells. Oncogene *14*, 661-669.

Doyle, K. P., and Buckwalter, M. S. (2012). The double-edged sword of inflammation after stroke: what sharpens each edge? Ann Neurol *71*, 729-731.

Duggal, N., Schmidt-Kastner, R., and Hakim, A. M. (1997). Nestin expression in reactive astrocytes following focal cerebral ischemia in rats. Brain Res *768*, 1-9.

Dvorak, H. F. (1986). Tumors: wounds that do not heal. Similarities between tumor stroma generation and wound healing. N Engl J Med *315*, 1650-1659.

Dvoriantchikova, G., Barakat, D., Brambilla, R., Agudelo, C., Hernandez, E., Bethea, J. R., Shestopalov, V. I., and Ivanov, D. (2009). Inactivation of astroglial NF-kappa B promotes survival of retinal neurons following ischemic injury. Eur J Neurosci *30*, 175-185.

Elvira, G., Garcia, I., Benito, M., Gallo, J., Desco, M., Penades, S., Garcia-Sanz, J. A., and Silva, A. (2012). Live imaging of mouse endogenous neural progenitors migrating in response to an induced tumor. PLoS One *7*, e44466.

Emmert-Buck, M. R., Bonner, R. F., Smith, P. D., Chuaqui, R. F., Zhuang, Z., Goldstein, S. R., Weiss, R. A., and Liotta, L. A. (1996). Laser capture microdissection. Science *274*, 998-1001.

Endres, C. J., Coughlin, J. M., Gage, K. L., Watkins, C. C., Kassiou, M., and Pomper, M. G. (2012). Radiation dosimetry and biodistribution of the TSPO ligand 11C-DPA-

713 in humans. Journal of nuclear medicine : official publication, Society of Nuclear Medicine *53*, 330-335.

Endres, C. J., Pomper, M. G., James, M., Uzuner, O., Hammoud, D. A., Watkins, C. C., Reynolds, A., Hilton, J., Dannals, R. F., and Kassiou, M. (2009). Initial evaluation of 11C-DPA-713, a novel TSPO PET ligand, in humans. Journal of nuclear medicine : official publication, Society of Nuclear Medicine *50*, 1276-1282.

Eng, L. F., Ghirnikar, R. S., and Lee, Y. L. (2000). Glial fibrillary acidic protein: GFAP-thirty-one years (1969-2000). Neurochem Res *25*, 1439-1451.

Engler, H., Lundberg, P. O., Ekbom, K., Nennesmo, I., Nilsson, A., Bergstrom, M., Tsukada, H., Hartvig, P., and Langstrom, B. (2003). Multitracer study with positron emission tomography in Creutzfeldt-Jakob disease. Eur J Nucl Med Mol Imaging *30*, 85-95.

Engler, H., Nennesmo, I., Kumlien, E., Gambini, J. P., Lundberg, P., Savitcheva, I., and Langstrom, B. (2012). Imaging astrocytosis with PET in Creutzfeldt-Jakob disease: case report with histopathological findings. Int J Clin Exp Med *5*, 201-207.

Escartin, C., Brouillet, E., Gubellini, P., Trioulier, Y., Jacquard, C., Smadja, C., Knott, G. W., Kerkerian-Le Goff, L., Deglon, N., Hantraye, P., and Bonvento, G. (2006). Ciliary neurotrophic factor activates astrocytes, redistributes their glutamate transporters GLAST and GLT-1 to raft microdomains, and improves glutamate handling in vivo. J Neurosci *26*, 5978-5989.

Escartin, C., Pierre, K., Colin, A., Brouillet, E., Delzescaux, T., Guillermier, M., Dhenain, M., Deglon, N., Hantraye, P., Pellerin, L., and Bonvento, G. (2007). Activation of astrocytes by CNTF induces metabolic plasticity and increases resistance to metabolic insults. J Neurosci *27*, 7094-7104.

Etienne-Manneville, S. (2006). In vitro assay of primary astrocyte migration as a tool to study Rho GTPase function in cell polarization. Methods Enzymol *406*, 565-578.

Falanga, A., Panova-Noeva, M., and Russo, L. (2009). Procoagulant mechanisms in tumour cells. Best Pract Res Clin Haematol *22*, 49-60.

Farina, K. L., Wyckoff, J. B., Rivera, J., Lee, H., Segall, J. E., Condeelis, J. S., and Jones, J. G. (1998). Cell motility of tumor cells visualized in living intact primary tumors using green fluorescent protein. Cancer Res *58*, 2528-2532.

Faulkner, J. R., Herrmann, J. E., Woo, M. J., Tansey, K. E., Doan, N. B., and Sofroniew, M. V. (2004). Reactive astrocytes protect tissue and preserve function after spinal cord injury. J Neurosci *24*, 2143-2155.

Fazakas, C., Wilhelm, I., Nagyoszi, P., Farkas, A. E., Hasko, J., Molnar, J., Bauer, H., Bauer, H. C., Ayaydin, F., Dung, N. T.*, et al.* (2011). Transmigration of melanoma cells through the blood-brain barrier: role of endothelial tight junctions and melanoma-released serine proteases. PLoS One *6*, e20758.

Fidler, I. J. (1978). Tumor heterogeneity and the biology of cancer invasion and metastasis. Cancer Res *38*, 2651-2660.

Fidler, I. J. (2003). The pathogenesis of cancer metastasis: the 'seed and soil' hypothesis revisited. Nat Rev Cancer *3*, 453-458.

Fitzgerald, D. P., Palmieri, D., Hua, E., Hargrave, E., Herring, J. M., Qian, Y., Vega-Valle, E., Weil, R. J., Stark, A. M., Vortmeyer, A. O., and Steeg, P. S. (2008). Reactive glia are recruited by highly proliferative brain metastases of breast cancer and promote tumor cell colonization. Clinical & experimental metastasis *25*, 799-810.

Fois, A. F., Wotton, C. J., Yeates, D., Turner, M. R., and Goldacre, M. J. (2010). Cancer in patients with motor neuron disease, multiple sclerosis and Parkinson's disease: record linkage studies. J Neurol Neurosurg Psychiatry *81*, 215-221.

Folkman, J., Merler, E., Abernathy, C., and Williams, G. (1971). Isolation of a tumor factor responsible for angiogenesis. J Exp Med *133*, 275-288.

Foss, C. A., Harper, J. S., Wang, H., Pomper, M. G., and Jain, S. K. (2013). Noninvasive Molecular Imaging of Tuberculosis-Associated Inflammation With Radioiodinated DPA-713. J Infect Dis.

Frisen, J., Johansson, C. B., Torok, C., Risling, M., and Lendahl, U. (1995). Rapid, widespread, and longlasting induction of nestin contributes to the generation of glial scar tissue after CNS injury. J Cell Biol *131*, 453-464.

Frixen, U. H., Behrens, J., Sachs, M., Eberle, G., Voss, B., Warda, A., Lochner, D., and Birchmeier, W. (1991). E-cadherin-mediated cell-cell adhesion prevents invasiveness of human carcinoma cells. J Cell Biol *113*, 173-185.

Gadea, A., Schinelli, S., and Gallo, V. (2008). Endothelin-1 regulates astrocyte proliferation and reactive gliosis via a JNK/c-Jun signaling pathway. J Neurosci *28*, 2394-2408.

Gaillard, P. J., Appeldoorn, C. C., Rip, J., Dorland, R., van der Pol, S. M., Kooij, G., de Vries, H. E., and Reijerkerk, A. (2012). Enhanced brain delivery of liposomal methylprednisolone improved therapeutic efficacy in a model of neuroinflammation. J Control Release *164*, 364-369.

Garofalo, A., Chirivi, R. G., Foglieni, C., Pigott, R., Mortarini, R., Martin-Padura, I., Anichini, A., Gearing, A. J., Sanchez-Madrid, F., Dejana, E., and et al. (1995). Involvement of the very late antigen 4 integrin on melanoma in interleukin 1-augmented experimental metastases. Cancer Res *55*, 414-419.

Giavazzi, R., Garofalo, A., Bani, M. R., Abbate, M., Ghezzi, P., Boraschi, D., Mantovani, A., and Dejana, E. (1990). Interleukin 1-induced augmentation of experimental metastases from a human melanoma in nude mice. Cancer Res *50*, 4771-4775.

Gil-Bernabe, A. M., Ferjancic, S., Tlalka, M., Zhao, L., Allen, P. D., Im, J. H., Watson, K., Hill, S. A., Amirkhosravi, A., Francis, J. L., *et al.* (2012). Recruitment of monocytes/macrophages by tissue factor-mediated coagulation is essential for metastatic cell survival and premetastatic niche establishment in mice. Blood *119*, 3164-3175.

Glare, E. M., Divjak, M., Bailey, M. J., and Walters, E. H. (2002). beta-Actin and GAPDH housekeeping gene expression in asthmatic airways is variable and not suitable for normalising mRNA levels. Thorax *57*, 765-770.

Glass, R., Synowitz, M., Kronenberg, G., Walzlein, J. H., Markovic, D. S., Wang, L. P., Gast, D., Kiwit, J., Kempermann, G., and Kettenmann, H. (2005). Glioblastoma-induced attraction of endogenous neural precursor cells is associated with improved survival. J Neurosci *25*, 2637-2646.

Goldstein, G. W. (1988). Endothelial cell-astrocyte interactions. A cellular model of the blood-brain barrier. Ann N Y Acad Sci *529*, 31-39.

Goldsworthy, S. M., Stockton, P. S., Trempus, C. S., Foley, J. F., and Maronpot, R. R. (1999). Effects of fixation on RNA extraction and amplification from laser capture microdissected tissue. Mol Carcinog *25*, 86-91.

Gordon, G. R., Mulligan, S. J., and MacVicar, B. A. (2007). Astrocyte control of the cerebrovasculature. Glia *55*, 1214-1221.

Gordon, S. (2003). Alternative activation of macrophages. Nat Rev Immunol *3*, 23-35.

Gril, B., Palmieri, D., Qian, Y., Anwar, T., Liewehr, D. J., Steinberg, S. M., Andreu, Z., Masana, D., Fernandez, P., Steeg, P. S., and Vidal-Vanaclocha, F. (2013). Pazopanib Inhibits the Activation of PDGFRbeta-Expressing Astrocytes in the Brain Metastatic Microenvironment of Breast Cancer Cells. Am J Pathol.

Gulyas, B., Toth, M., Schain, M., Airaksinen, A., Vas, A., Kostulas, K., Lindstrom, P., Hillert, J., and Halldin, C. (2012a). Evolution of microglial activation in ischaemic core and peri-infarct regions after stroke: a PET study with the TSPO molecular imaging biomarker [((11))C]vinpocetine. J Neurol Sci *320*, 110-117.

Gulyas, B., Toth, M., Vas, A., Shchukin, E., Kostulas, K., Hillert, J., and Halldin, C. (2012b). Visualising neuroinflammation in post-stroke patients: a comparative PET study with the TSPO molecular imaging biomarkers [11C]PK11195 and [11C]vinpocetine. Curr Radiopharm *5*, 19-28.

Guo, Q., Colasanti, A., Owen, D. R., Onega, M., Kamalakaran, A., Bennacef, I., Matthews, P. M., Rabiner, E. A., Turkheimer, F. E., and Gunn, R. N. (2013). Quantification of the Specific Translocator Protein Signal of 18F-PBR111 in Healthy Humans: A Genetic Polymorphism Effect on In Vivo Binding. Journal of nuclear medicine : official publication, Society of Nuclear Medicine.

Gupta, G. P., and Massague, J. (2006). Cancer metastasis: building a framework. Cell *127*, 679-695.

Gupta, G. P., Minn, A. J., Kang, Y., Siegel, P. M., Serganova, I., Cordon-Cardo, C., Olshen, A. B., Gerald, W. L., and Massague, J. (2005). Identifying site-specific metastasis genes and functions. Cold Spring Harb Symp Quant Biol *70*, 149-158.

Gupte, R., Muse, G. W., Chinenov, Y., Adelman, K., and Rogatsky, I. (2013). Glucocorticoid receptor represses proinflammatory genes at distinct steps of the transcription cycle. Proc Natl Acad Sci U S A *110*, 14616-14621.

Hagemann, T., Balkwill, F., and Lawrence, T. (2007). Inflammation and cancer: a double-edged sword. Cancer Cell *12*, 300-301.

Hamby, M. E., Coppola, G., Ao, Y., Geschwind, D. H., Khakh, B. S., and Sofroniew, M. V. (2012). Inflammatory mediators alter the astrocyte transcriptome and calcium signaling elicited by multiple G-protein-coupled receptors. J Neurosci *32*, 14489-14510.

Hamby, M. E., Hewett, J. A., and Hewett, S. J. (2006). TGF-beta1 potentiates astrocytic nitric oxide production by expanding the population of astrocytes that express NOS-2. Glia *54*, 566-577.

Hamidi, M., Azadi, A., and Rafiei, P. (2006). Pharmacokinetic consequences of pegylation. Drug Deliv *13*, 399-409.

Hamilton, A., and Sibson, N. R. (2013). Role of the systemic immune system in brain metastasis. Mol Cell Neurosci *53*, 42-51.

Hanada, M., Shinjo, R., Miyagi, M., Yasuda, T., Tsutsumi, K., Sugiura, Y., Imagama, S., Ishiguro, N., and Matsuyama, Y. (2013). Arundic acid (ONO-2506) inhibits secondary injury and improves motor function in rats with spinal cord injury. J Neurol Sci.

Hanahan, D., and Weinberg, R. A. (2000). The hallmarks of cancer. Cell *100*, 57-70.

Hanahan, D., and Weinberg, R. A. (2011). Hallmarks of cancer: the next generation. Cell *144*, 646-674.

Harberts, E., Datta, D., Chen, S., Wohler, J. E., Oh, U., and Jacobson, S. (2012). Translocator Protein 18 kDa (TSPO) Expression in Multiple Sclerosis Patients. J Neuroimmune Pharmacol.

Hari, P., and Srivastava, R. N. (1998). Pulse corticosteroid therapy with methylprednisolone or dexamethasone. Indian J Pediatr *65*, 557-560.

Harrell, J. C., Prat, A., Parker, J. S., Fan, C., He, X., Carey, L., Anders, C., Ewend, M., and Perou, C. M. (2012). Genomic analysis identifies unique signatures predictive of brain, lung, and liver relapse. Breast Cancer Res Treat *132*, 523-535.

Hauet, T., Yao, Z. X., Bose, H. S., Wall, C. T., Han, Z., Li, W., Hales, D. B., Miller, W. L., Culty, M., and Papadopoulos, V. (2005). Peripheral-type benzodiazepine receptor-mediated action of steroidogenic acute regulatory protein on cholesterol entry into leydig cell mitochondria. Mol Endocrinol *19*, 540-554.

He, B. P., Wang, J. J., Zhang, X., Wu, Y., Wang, M., Bay, B. H., and Chang, A. Y. (2006). Differential reactions of microglia to brain metastasis of lung cancer. Mol Med *12*, 161-170.

Heiba, S., Kolker, D., Ong, L., Sharma, S., Travis, A., Teodorescu, V., Ellozy, S., Kostakoglu, L., Savitch, I., and Machac, J. (2013). Dual-isotope SPECT/CT impact on hospitalized patients with suspected diabetic foot infection: saving limbs, lives, and resources. Nucl Med Commun *34*, 877-884.

Herx, L. M., and Yong, V. W. (2001). Interleukin-1 beta is required for the early evolution of reactive astrogliosis following CNS lesion. J Neuropathol Exp Neurol *60*, 961-971.

Hicks, R. J., and Hofman, M. S. (2012). Is there still a role for SPECT-CT in oncology in the PET-CT era? Nat Rev Clin Oncol *9*, 712-720.

Hijnen, N. M., de Vries, A., Nicolay, K., and Grull, H. (2012). Dual-isotope 111In/177Lu SPECT imaging as a tool in molecular imaging tracer design. Contrast Media Mol Imaging *7*, 214-222.

Hiratsuka, S., Watanabe, A., Aburatani, H., and Maru, Y. (2006). Tumour-mediated upregulation of chemoattractants and recruitment of myeloid cells predetermines lung metastasis. Nat Cell Biol *8*, 1369-1375.

Hirsch, J. D., Beyer, C. F., Malkowitz, L., Beer, B., and Blume, A. J. (1989). Mitochondrial benzodiazepine receptors mediate inhibition of mitochondrial respiratory control. Mol Pharmacol *35*, 157-163.

Hirsch, T., Decaudin, D., Susin, S. A., Marchetti, P., Larochette, N., Resche-Rigon, M., and Kroemer, G. (1998). PK11195, a ligand of the mitochondrial benzodiazepine receptor, facilitates the induction of apoptosis and reverses Bcl-2-mediated cytoprotection. Exp Cell Res *241*, 426-434.

Hu, X., Zhao, Y., He, X., Li, J., Wang, T., Zhou, W., Wan, D., Wang, H., and Gu, J. (2008). Ciliary neurotrophic factor receptor alpha subunit-modulated multiple downstream signaling pathways in hepatic cancer cell lines and their biological implications. Hepatology *47*, 1298-1308.

Huang, H. C., Huang, C. Y., Lin-Shiau, S. Y., and Lin, J. K. (2009). Ursolic acid inhibits IL-1beta or TNF-alpha-induced C6 glioma invasion through suppressing the association ZIP/p62 with PKC-zeta and downregulating the MMP-9 expression. Mol Carcinog *48*, 517-531.

Irusen, E., Matthews, J. G., Takahashi, A., Barnes, P. J., Chung, K. F., and Adcock, I. M. (2002). p38 Mitogen-activated protein kinase-induced glucocorticoid receptor phosphorylation reduces its activity: role in steroid-insensitive asthma. J Allergy Clin Immunol *109*, 649-657.

Ishida, T., Wang, X., Shimizu, T., Nawata, K., and Kiwada, H. (2007). PEGylated liposomes elicit an anti-PEG IgM response in a T cell-independent manner. J Control Release *122*, 349-355.

Izraely, S., Sagi-Assif, O., Klein, A., Meshel, T., Tsarfaty, G., Pasmanik-Chor, M., Nahmias, C., Couraud, P. O., Ateh, E., Bryant, J. L.*, et al.* (2012). The metastatic microenvironment: brain-residing melanoma metastasis and dormant micrometastasis. Int J Cancer *131*, 1071-1082.

Jadhav, S., Bochner, B. S., and Konstantopoulos, K. (2001). Hydrodynamic shear regulates the kinetics and receptor specificity of polymorphonuclear leukocyte-colon carcinoma cell adhesive interactions. J Immunol *167*, 5986-5993.

Jana, M., Anderson, J. A., Saha, R. N., Liu, X., and Pahan, K. (2005). Regulation of inducible nitric oxide synthase in proinflammatory cytokine-stimulated human primary astrocytes. Free Radic Biol Med *38*, 655-664.

Jang, S., Kelley, K. W., and Johnson, R. W. (2008). Luteolin reduces IL-6 production in microglia by inhibiting JNK phosphorylation and activation of AP-1. Proc Natl Acad Sci U S A *105*, 7534-7539.

Johansson, A., Engler, H., Blomquist, G., Scott, B., Wall, A., Aquilonius, S. M., Langstrom, B., and Askmark, H. (2007). Evidence for astrocytosis in ALS demonstrated by [11C](L)-deprenyl-D2 PET. J Neurol Sci *255*, 17-22.

Kahn, M. A., Ellison, J. A., Chang, R. P., Speight, G. J., and de Vellis, J. (1997). CNTF induces GFAP in a S-100 alpha brain cell population: the pattern of CNTF-alpha R suggests an indirect mode of action. Brain Res Dev Brain Res *98*, 221-233.

Kannan, R., Chakrabarti, R., Tang, D., Kim, K. J., and Kaplowitz, N. (2000). GSH transport in human cerebrovascular endothelial cells and human astrocytes: evidence for luminal localization of Na+-dependent GSH transport in HCEC. Brain Res *852*, 374-382.

Kannan, R., Kuhlenkamp, J. F., Jeandidier, E., Trinh, H., Ookhtens, M., and Kaplowitz, N. (1990). Evidence for carrier-mediated transport of glutathione across the blood-brain barrier in the rat. J Clin Invest *85*, 2009-2013.

Kaplan, R. N., Riba, R. D., Zacharoulis, S., Bramley, A. H., Vincent, L., Costa, C., MacDonald, D. D., Jin, D. K., Shido, K., Kerns, S. A.*, et al.* (2005). VEGFR1-positive haematopoietic bone marrow progenitors initiate the pre-metastatic niche. Nature *438*, 820-827.

Karimi-Abdolrezaee, S., and Billakanti, R. (2012). Reactive astrogliosis after spinal cord injury-beneficial and detrimental effects. Mol Neurobiol *46*, 251-264.

Karpuk, N., Burkovetskaya, M., and Kielian, T. (2012). Neuroinflammation alters voltage-dependent conductance in striatal astrocytes. J Neurophysiol *108*, 112-123.

Kasuya, Y., Abe, Y., Hama, H., Sakurai, T., Asada, S., Masaki, T., and Goto, K. (1994). Endothelin-1 activates mitogen-activated protein kinases through two independent signalling pathways in rat astrocytes. Biochem Biophys Res Commun *204*, 1325-1333.

Katz, A. M., Amankulor, N. M., Pitter, K., Helmy, K., Squatrito, M., and Holland, E. C. (2012). Astrocyte-specific expression patterns associated with the PDGF-induced glioma microenvironment. PLoS One *7*, e32453.

Kaye, A. H., Morstyn, G., Gardner, I., and Pyke, K. (1986). Development of a xenograft glioma model in mouse brain. Cancer Res *46*, 1367-1373.

Khuon, S., Liang, L., Dettman, R. W., Sporn, P. H., Wysolmerski, R. B., and Chew, T. L. (2010). Myosin light chain kinase mediates transcellular intravasation of breast cancer cells through the underlying endothelial cells: a three-dimensional FRET study. J Cell Sci *123*, 431-440.

Kienast, Y., von Baumgarten, L., Fuhrmann, M., Klinkert, W. E., Goldbrunner, R., Herms, J., and Winkler, F. (2010). Real-time imaging reveals the single steps of brain metastasis formation. Nat Med *16*, 116-122.

Kilian, M., Gregor, J. I., Heukamp, I., Hanel, M., Ahlgrimm, M., Schimke, I., Kristiansen, G., Ommer, A., Walz, M. K., Jacobi, C. A., and Wenger, F. A. (2006). Matrix metalloproteinase inhibitor RO 28-2653 decreases liver metastasis by reduction of MMP-2 and MMP-9 concentration in BOP-induced ductal pancreatic cancer in Syrian Hamsters: inhibition of matrix metalloproteinases in pancreatic cancer. Prostaglandins Leukot Essent Fatty Acids *75*, 429-434.

Kim, H. J., and Magrane, J. (2011). Isolation and culture of neurons and astrocytes from the mouse brain cortex. Methods Mol Biol *793*, 63-75.

Kim, K. Y., Kim, M. Y., Choi, H. S., Jin, B. K., Kim, S. U., and Lee, Y. B. (2002). Thrombin induces IL-10 production in microglia as a negative feedback regulator of TNF-alpha release. Neuroreport *13*, 849-852.

Kim, L. S., Huang, S., Lu, W., Lev, D. C., and Price, J. E. (2004a). Vascular endothelial growth factor expression promotes the growth of breast cancer brain metastases in nude mice. Clinical & experimental metastasis *21*, 107-118.

Kim, S. H., Lee, J. E., Yang, S. H., and Lee, S. W. (2013). Induction of cytokines and growth factors by rapamycin in the microenvironment of brain metastases of lung cancer. Oncol Lett *5*, 953-958.

Kim, S. J., Kim, J. S., Park, E. S., Lee, J. S., Lin, Q., Langley, R. R., Maya, M., He, J., Kim, S. W., Weihua, Z.*, et al.* (2011). Astrocytes upregulate survival genes in tumor cells and induce protection from chemotherapy. Neoplasia *13*, 286-298.

Kim, Y. S., Park, J. S., Jee, Y. K., and Lee, K. Y. (2004b). Dexamethasone inhibits TRAIL- and anti-cancer drugs-induced cell death in A549 cells through inducing NF-kappaB-independent cIAP2 expression. Cancer Res Treat *36*, 330-337.

Kohler, S., Ullrich, S., Richter, U., and Schumacher, U. (2010). E-/P-selectins and colon carcinoma metastasis: first in vivo evidence for their crucial role in a clinically relevant model of spontaneous metastasis formation in the lung. Br J Cancer *102*, 602-609.

Kozuka, N., Itofusa, R., Kudo, Y., and Morita, M. (2005). Lipopolysaccharide and proinflammatory cytokines require different astrocyte states to induce nitric oxide production. J Neurosci Res *82*, 717-728.

Krady, J. K., Lin, H. W., Liberto, C. M., Basu, A., Kremlev, S. G., and Levison, S. W. (2008). Ciliary neurotrophic factor and interleukin-6 differentially activate microglia. J Neurosci Res *86*, 1538-1547.

Kraft, J. C., Freeling, J. P., Wang, Z., and Ho, R. J. (2014). Emerging research and clinical development trends of liposome and lipid nanoparticle drug delivery systems. J Pharm Sci *103*, 29-52.

Kreisl, W. C., Jenko, K. J., Hines, C. S., Hyoung Lyoo, C., Corona, W., Morse, C. L., Zoghbi, S. S., Hyde, T., Kleinman, J. E., Pike, V. W.*, et al.* (2012). A genetic polymorphism for translocator protein 18 kDa affects both in vitro and in vivo radioligand binding in human brain to this putative biomarker of neuroinflammation. J Cereb Blood Flow Metab.

Kreutzberg, G. W. (1996). Microglia: a sensor for pathological events in the CNS. Trends Neurosci *19*, 312-318.

Kumar, A., Muzik, O., Shandal, V., Chugani, D., Chakraborty, P., and Chugani, H. T. (2012). Evaluation of age-related changes in translocator protein (TSPO) in human brain using (11)C-[R]-PK11195 PET. J Neuroinflammation *9*, 232.

Lai, F., Fadda, A. M., and Sinico, C. (2013). Liposomes for brain delivery. Expert Opin Drug Deliv *10*, 1003-1022.

Langley, R. R., Fan, D., Guo, L., Zhang, C., Lin, Q., Brantley, E. C., McCarty, J. H., and Fidler, I. J. (2009). Generation of an immortalized astrocyte cell line from H-2Kb-tsA58 mice to study the role of astrocytes in brain metastasis. Int J Oncol *35*, 665-672.

LaVail, M. M., Unoki, K., Yasumura, D., Matthes, M. T., Yancopoulos, G. D., and Steinberg, R. H. (1992). Multiple growth factors, cytokines, and neurotrophins rescue photoreceptors from the damaging effects of constant light. Proc Natl Acad Sci U S A *89*, 11249-11253.

Lavisse, S., Guillermier, M., Herard, A. S., Petit, F., Delahaye, M., Van Camp, N., Ben Haim, L., Lebon, V., Remy, P., Dolle, F.*, et al.* (2012). Reactive Astrocytes Overexpress TSPO and Are Detected by TSPO Positron Emission Tomography Imaging. J Neurosci *32*, 10809-10818.

Le, D. M., Besson, A., Fogg, D. K., Choi, K. S., Waisman, D. M., Goodyer, C. G., Rewcastle, B., and Yong, V. W. (2003). Exploitation of astrocytes by glioma cells to facilitate invasiveness: a mechanism involving matrix metalloproteinase-2 and the urokinase-type plasminogen activator-plasmin cascade. J Neurosci *23*, 4034-4043.

Le Fur, G., Vaucher, N., Perrier, M. L., Flamier, A., Benavides, J., Renault, C., Dubroeucq, M. C., Gueremy, C., and Uzan, A. (1983). Differentiation between two ligands for peripheral benzodiazepine binding sites, [3H]RO5-4864 and [3H]PK 11195, by thermodynamic studies. Life sciences *33*, 449-457.

Leaver, S. G., Cui, Q., Plant, G. W., Arulpragasam, A., Hisheh, S., Verhaagen, J., and Harvey, A. R. (2006). AAV-mediated expression of CNTF promotes long-term

survival and regeneration of adult rat retinal ganglion cells. Gene Ther *13*, 1328-1341.

Lee, H. W., Seol, H. J., Choi, Y. L., Ju, H. J., Joo, K. M., Ko, Y. H., Lee, J. I., and Nam, D. H. (2012). Genomic copy number alterations associated with the early brain metastasis of non-small cell lung cancer. Int J Oncol *41*, 2013-2020.

Lee, J., French, B., Morgan, T., and French, S. W. (2014). The liver is populated by a broad spectrum of markers for macrophages. In alcoholic hepatitis the macrophages are M1 and M2. Exp Mol Pathol *96*, 118-125.

Lee, S. C., Dickson, D. W., Liu, W., and Brosnan, C. F. (1993). Induction of nitric oxide synthase activity in human astrocytes by interleukin-1 beta and interferon-gamma. J Neuroimmunol *46*, 19-24.

Lehre, K. P., Levy, L. M., Ottersen, O. P., Storm-Mathisen, J., and Danbolt, N. C. (1995). Differential expression of two glial glutamate transporters in the rat brain: quantitative and immunocytochemical observations. J Neurosci *15*, 1835-1853.
Leibinger, M., Andreadaki, A., Diekmann, H., and Fischer, D. (2013). Neuronal STAT3 activation is essential for CNTF- and inflammatory stimulation-induced CNS axon regeneration. Cell Death Dis *4*, e805.

Lepekhin, E. A., Eliasson, C., Berthold, C. H., Berezin, V., Bock, E., and Pekny, M. (2001). Intermediate filaments regulate astrocyte motility. J Neurochem *79*, 617-625.

Levison, S. W., Ducceschi, M. H., Young, G. M., and Wood, T. L. (1996). Acute exposure to CNTF in vivo induces multiple components of reactive gliosis. Exp Neurol *141*, 256-268.

Levison, S. W., Hudgins, S. N., and Crawford, J. L. (1998). Ciliary neurotrophic factor stimulates nuclear hypertrophy and increases the GFAP content of cultured astrocytes. Brain Res *803*, 189-193.

Levison, S. W., Jiang, F. J., Stoltzfus, O. K., and Ducceschi, M. H. (2000). IL-6-type cytokines enhance epidermal growth factor-stimulated astrocyte proliferation. Glia *32*, 328-337.

Lewis, K. M., Harford-Wright, E., Vink, R., and Ghabriel, M. N. (2013). NK1 receptor antagonists and dexamethasone as anticancer agents in vitro and in a model of brain tumours secondary to breast cancer. Anticancer Drugs *24*, 344-354.

Leybaert, L., Paemeleire, K., Strahonja, A., and Sanderson, M. J. (1998). Inositol-trisphosphate-dependent intercellular calcium signaling in and between astrocytes and endothelial cells. Glia *24*, 398-407.

Li, J., Li, J. P., Zhang, X., Lu, Z., Yu, S. P., and Wei, L. (2012a). Expression of heparanase in vascular cells and astrocytes of the mouse brain after focal cerebral ischemia. Brain Res *1433*, 137-144.

Li, L. M., Kilbourn, R. G., Adams, J., and Fidler, I. J. (1991). Role of nitric oxide in lysis of tumor cells by cytokine-activated endothelial cells. Cancer Res *51*, 2531-2535.

Li, T., Bourgeois, J. P., Celli, S., Glacial, F., Le Sourd, A. M., Mecheri, S., Weksler, B., Romero, I., Couraud, P. O., Rougeon, F., and Lafaye, P. (2012b). Cell-penetrating anti-GFAP VHH and corresponding fluorescent fusion protein VHH-GFP spontaneously cross the blood-brain barrier and specifically recognize astrocytes: application to brain imaging. FASEB J.

Lieberman, A., LeBrun, Y., Glass, P., Goodgold, A., Lux, W., Wise, A., and Ransohoff, J. (1977). Use of high dose corticosteroids in patients with inoperable brain tumours. J Neurol Neurosurg Psychiatry *40*, 678-682.

Lin, E. Y. (2010). Linking inflammation to tumorigenesis in colon: Stat3, a double-edged sword? Cell Cycle *9*, 2485-2486.

Lin, Q., Balasubramanian, K., Fan, D., Kim, S. J., Guo, L., Wang, H., Bar-Eli, M., Aldape, K. D., and Fidler, I. J. (2010). Reactive astrocytes protect melanoma cells from chemotherapy by sequestering intracellular calcium through gap junction communication channels. Neoplasia *12*, 748-754.

Lin, R. C., Matesic, D. F., Marvin, M., McKay, R. D., and Brustle, O. (1995). Re-expression of the intermediate filament nestin in reactive astrocytes. Neurobiol Dis *2*, 79-85.

Liu, H., Kato, Y., Erzinger, S. A., Kiriakova, G. M., Qian, Y., Palmieri, D., Steeg, P. S., and Price, J. E. (2012). The role of MMP-1 in breast cancer growth and metastasis to the brain in a xenograft model. BMC Cancer *12*, 583.

Liu, W. L., Lee, Y. H., Tsai, S. Y., Hsu, C. Y., Sun, Y. Y., Yang, L. Y., Tsai, S. H., and Yang, W. C. (2008). Methylprednisolone inhibits the expression of glial fibrillary acidic protein and chondroitin sulfate proteoglycans in reactivated astrocytes. Glia *56*, 1390-1400.

Liu, Y., Kosaka, A., Ikeura, M., Kohanbash, G., Fellows-Mayle, W., Snyder, L. A., and Okada, H. (2013). Premetastatic soil and prevention of breast cancer brain metastasis. Neuro-oncology *15*, 891-903.

Lorger, M., and Felding-Habermann, B. (2010). Capturing changes in the brain microenvironment during initial steps of breast cancer brain metastasis. Am J Pathol *176*, 2958-2971.

Lovatt, D., Sonnewald, U., Waagepetersen, H. S., Schousboe, A., He, W., Lin, J. H., Han, X., Takano, T., Wang, S., Sim, F. J.*, et al.* (2007). The transcriptome and metabolic

gene signature of protoplasmic astrocytes in the adult murine cortex. J Neurosci *27*, 12255-12266.

Lu, X., and Kang, Y. (2010). Hypoxia and hypoxia-inducible factors: master regulators of metastasis. Clin Cancer Res *16*, 5928-5935.

Lyra, M., and Ploussi, A. (2011). Filtering in SPECT Image Reconstruction. Int J Biomed Imaging *2011*, 693795.

Mantovani, A., Sozzani, S., Locati, M., Allavena, P., and Sica, A. (2002). Macrophage polarization: tumor-associated macrophages as a paradigm for polarized M2 mononuclear phagocytes. Trends Immunol *23*, 549-555.

Marchetti, D., Li, J., and Shen, R. (2000). Astrocytes contribute to the brain-metastatic specificity of melanoma cells by producing heparanase. Cancer Res *60*, 4767-4770.

Marchetti, D., and Nicolson, G. L. (2001). Human heparanase: a molecular determinant of brain metastasis. Adv Enzyme Regul *41*, 343-359.

Marlin, S. D., and Springer, T. A. (1987). Purified intercellular adhesion molecule-1 (ICAM-1) is a ligand for lymphocyte function-associated antigen 1 (LFA-1). Cell *51*, 813-819.

Mattner, F., Staykova, M., Berghofer, P., Wong, H. J., Fordham, S., Callaghan, P., Jackson, T., Pham, T., Gregoire, M. C., Zahra, D*., et al.* (2013). Central Nervous System Expression and PET Imaging of the Translocator Protein in Relapsing-Remitting Experimental Autoimmune Encephalomyelitis. Journal of nuclear medicine : official publication, Society of Nuclear Medicine.

McAllister, M. S., Krizanac-Bengez, L., Macchia, F., Naftalin, R. J., Pedley, K. C., Mayberg, M. R., Marroni, M., Leaman, S., Stanness, K. A., and Janigro, D. (2001).

Mechanisms of glucose transport at the blood-brain barrier: an in vitro study. Brain Res *904*, 20-30.

McKeon, R. J., Jurynec, M. J., and Buck, C. R. (1999). The chondroitin sulfate proteoglycans neurocan and phosphacan are expressed by reactive astrocytes in the chronic CNS glial scar. J Neurosci *19*, 10778-10788.

Mendes, O., Kim, H. T., Lungu, G., and Stoica, G. (2007). MMP2 role in breast cancer brain metastasis development and its regulation by TIMP2 and ERK1/2. Clinical & experimental metastasis *24*, 341-351.

Mendes, O., Kim, H. T., and Stoica, G. (2005). Expression of MMP2, MMP9 and MMP3 in breast cancer brain metastasis in a rat model. Clinical & experimental metastasis *22*, 237-246.

Metselaar, J. M., van den Berg, W. B., Holthuysen, A. E., Wauben, M. H., Storm, G., and van Lent, P. L. (2004). Liposomal targeting of glucocorticoids to synovial lining cells strongly increases therapeutic benefit in collagen type II arthritis. Ann Rheum Dis *63*, 348-353.

Metselaar, J. M., Wauben, M. H., Wagenaar-Hilbers, J. P., Boerman, O. C., and Storm, G. (2003). Complete remission of experimental arthritis by joint targeting of glucocorticoids with long-circulating liposomes. Arthritis Rheum *48*, 2059-2066.

Miller, R. H., and Raff, M. C. (1984). Fibrous and protoplasmic astrocytes are biochemically and developmentally distinct. J Neurosci *4*, 585-592.

Minn, A. J., Gupta, G. P., Siegel, P. M., Bos, P. D., Shu, W., Giri, D. D., Viale, A., Olshen, A. B., Gerald, W. L., and Massague, J. (2005). Genes that mediate breast cancer metastasis to lung. Nature *436*, 518-524.

Mitri, Z., Constantine, T., and O'Regan, R. (2012). The HER2 Receptor in Breast Cancer: Pathophysiology, Clinical Use, and New Advances in Therapy. Chemother Res Pract *2012*, 743193.

Mittoux, V., Ouary, S., Monville, C., Lisovoski, F., Poyot, T., Conde, F., Escartin, C., Robichon, R., Brouillet, E., Peschanski, M., and Hantraye, P. (2002). Corticostriatopallidal neuroprotection by adenovirus-mediated ciliary neurotrophic factor gene transfer in a rat model of progressive striatal degeneration. J Neurosci *22*, 4478-4486.

Montero-Melendez, T., and Perretti, M. (2014). Gapdh Gene Expression Is Modulated by Inflammatory Arthritis and Is not Suitable for qPCR Normalization. Inflammation.

Moroz, M. A., Huang, R., Kochetkov, T., Shi, W., Thaler, H., de Stanchina, E., Gamez, I., Ryan, R. P., and Blasberg, R. G. (2011). Comparison of corticotropin-releasing factor, dexamethasone, and temozolomide: treatment efficacy and toxicity in U87 and C6 intracranial gliomas. Clin Cancer Res *17*, 3282-3292.

Moynagh, P. N., Williams, D. C., and O'Neill, L. A. (1993). Interleukin-1 activates transcription factor NF kappa B in glial cells. Biochem J *294 (Pt 2)*, 343-347.

Moynagh, P. N., Williams, D. C., and O'Neill, L. A. (1994). Activation of NF-kappa B and induction of vascular cell adhesion molecule-1 and intracellular adhesion molecule-1 expression in human glial cells by IL-1. Modulation by antioxidants. J Immunol *153*, 2681-2690.

Murata, J., Ricciardi-Castagnoli, P., Dessous L'Eglise Mange, P., Martin, F., and Juillerat-Jeanneret, L. (1997). Microglial cells induce cytotoxic effects toward colon carcinoma cells: measurement of tumor cytotoxicity with a gamma-glutamyl transpeptidase assay. Int J Cancer *70*, 169-174.

Murray, G. I., Duncan, M. E., O'Neil, P., McKay, J. A., Melvin, W. T., and Fothergill, J. E. (1998). Matrix metalloproteinase-1 is associated with poor prognosis in oesophageal cancer. J Pathol *185*, 256-261.

Murray, G. I., Duncan, M. E., O'Neil, P., Melvin, W. T., and Fothergill, J. E. (1996). Matrix metalloproteinase-1 is associated with poor prognosis in colorectal cancer. Nat Med *2*, 461-462.

Myer, D. J., Gurkoff, G. G., Lee, S. M., Hovda, D. A., and Sofroniew, M. V. (2006). Essential protective roles of reactive astrocytes in traumatic brain injury. Brain *129*, 2761-2772.

Naglich, J. G., Jure-Kunkel, M., Gupta, E., Fargnoli, J., Henderson, A. J., Lewin, A. C., Talbott, R., Baxter, A., Bird, J., Savopoulos, R.*, et al.* (2001). Inhibition of angiogenesis and metastasis in two murine models by the matrix metalloproteinase inhibitor, BMS-275291. Cancer Res *61*, 8480-8485.

Nduom, E. K., Yang, C., Merrill, M. J., Zhuang, Z., and Lonser, R. R. (2013). Characterization of the blood-brain barrier of metastatic and primary malignant neoplasms. J Neurosurg.

Neman, J., Choy, C., Kowolik, C. M., Anderson, A., Duenas, V. J., Waliany, S., Chen, B. T., Chen, M. Y., and Jandial, R. (2013). Co-evolution of breast-to-brain metastasis and neural progenitor cells. Clinical & experimental metastasis.

Newton, R. (2000). Molecular mechanisms of glucocorticoid action: what is important? Thorax *55*, 603-613.

Nielsen, N. M., Rostgaard, K., Rasmussen, S., Koch-Henriksen, N., Storm, H. H., Melbye, M., and Hjalgrim, H. (2006). Cancer risk among patients with multiple sclerosis: a population-based register study. Int J Cancer *118*, 979-984.

Nishimoto, N., Miyasaka, N., Yamamoto, K., Kawai, S., Takeuchi, T., and Azuma, J. (2009). Long-term safety and efficacy of tocilizumab, an anti-IL-6 receptor monoclonal antibody, in monotherapy, in patients with rheumatoid arthritis (the STREAM study): evidence of safety and efficacy in a 5-year extension study. Ann Rheum Dis *68*, 1580-1584.

Nishimura, K., Nonomura, N., Satoh, E., Harada, Y., Nakayama, M., Tokizane, T., Fukui, T., Ono, Y., Inoue, H., Shin, M.*, et al.* (2001). Potential mechanism for the effects of dexamethasone on growth of androgen-independent prostate cancer. J Natl Cancer Inst *93*, 1739-1746.

Nishizuka, I., Ishikawa, T., Hamaguchi, Y., Kamiyama, M., Ichikawa, Y., Kadota, K., Miki, R., Tomaru, Y., Mizuno, Y., Tominaga, N.*, et al.* (2002). Analysis of gene expression involved in brain metastasis from breast cancer using cDNA microarray. Breast Cancer *9*, 26-32.

Nkansah, M. K., Tzeng, S. Y., Holdt, A. M., and Lavik, E. B. (2008). Poly(lactic-co-glycolic acid) nanospheres and microspheres for short- and long-term delivery of bioactive ciliary neurotrophic factor. Biotechnol Bioeng *100*, 1010-1019.

Noda, M., Yamakawa, Y., Matsunaga, N., Naoe, S., Jodoi, T., Yamafuji, M., Akimoto, N., Teramoto, N., Fujita, K., Ohdo, S., and Iguchi, H. (2012). IL-6 Receptor Is a Possible Target against Growth of Metastasized Lung Tumor Cells in the Brain. Int J Mol Sci *14*, 515-526.

Ogris, M., Brunner, S., Schuller, S., Kircheis, R., and Wagner, E. (1999). PEGylated DNA/transferrin-PEI complexes: reduced interaction with blood components, extended circulation in blood and potential for systemic gene delivery. Gene Ther *6*, 595-605.

Oka, S., and Arita, H. (1991). Inflammatory factors stimulate expression of group II phospholipase A2 in rat cultured astrocytes. Two distinct pathways of the gene expression. J Biol Chem *266*, 9956-9960.

Okahara, H., Yagita, H., Miyake, K., and Okumura, K. (1994). Involvement of very late activation antigen 4 (VLA-4) and vascular cell adhesion molecule 1 (VCAM-1) in tumor necrosis factor alpha enhancement of experimental metastasis. Cancer Res *54*, 3233-3236.

Onder, T. T., Gupta, P. B., Mani, S. A., Yang, J., Lander, E. S., and Weinberg, R. A. (2008). Loss of E-cadherin promotes metastasis via multiple downstream transcriptional pathways. Cancer Res *68*, 3645-3654.

Owen, D. R., Gunn, R. N., Rabiner, E. A., Bennacef, I., Fujita, M., Kreisl, W. C., Innis, R. B., Pike, V. W., Reynolds, R., Matthews, P. M., and Parker, C. A. (2011). Mixed-affinity binding in humans with 18-kDa translocator protein ligands. Journal of nuclear medicine : official publication, Society of Nuclear Medicine *52*, 24-32.

Paku, S., Dome, B., Toth, R., and Timar, J. (2000). Organ-specificity of the extravasation process: an ultrastructural study. Clinical & experimental metastasis *18*, 481-492.

Papadopoulos, V., Amri, H., Boujrad, N., Cascio, C., Culty, M., Garnier, M., Hardwick, M., Li, H., Vidic, B., Brown, A. S.*, et al.* (1997). Peripheral benzodiazepine receptor in cholesterol transport and steroidogenesis. Steroids *62*, 21-28.

Pardridge, W. M. (1998). CNS drug design based on principles of blood-brain barrier transport. J Neurochem *70*, 1781-1792.

Park, E. S., Kim, S. J., Kim, S. W., Yoon, S. L., Leem, S. H., Kim, S. B., Kim, S. M., Park, Y. Y., Cheong, J. H., Woo, H. G.*, et al.* (2011). Cross-species hybridization of microarrays for studying tumor transcriptome of brain metastasis. Proc Natl Acad Sci U S A *108*, 17456-17461.

Patchell, R. A. (2003). The management of brain metastases. Cancer Treat Rev *29*, 533-540.

Pellerin, L., and Magistretti, P. J. (1994). Glutamate uptake into astrocytes stimulates aerobic glycolysis: a mechanism coupling neuronal activity to glucose utilization. Proc Natl Acad Sci U S A *91*, 10625-10629.

Pellerin, L., and Magistretti, P. J. (1997). Glutamate uptake stimulates Na+,K+-ATPase activity in astrocytes via activation of a distinct subunit highly sensitive to ouabain. J Neurochem *69*, 2132-2137.

Perea, G., and Araque, A. (2005). Properties of synaptically evoked astrocyte calcium signal reveal synaptic information processing by astrocytes. J Neurosci *25*, 2192-2203.

Perea, G., Navarrete, M., and Araque, A. (2009). Tripartite synapses: astrocytes process and control synaptic information. Trends Neurosci *32*, 421-431.

Perry, V. H. (2004). The influence of systemic inflammation on inflammation in the brain: implications for chronic neurodegenerative disease. Brain Behav Immun *18*, 407-413.

Piette, C., Deprez, M., Roger, T., Noel, A., Foidart, J. M., and Munaut, C. (2009). The dexamethasone-induced inhibition of proliferation, migration, and invasion in glioma cell lines is antagonized by macrophage migration inhibitory factor (MIF) and can be enhanced by specific MIF inhibitors. J Biol Chem *284*, 32483-32492.

Pipili-Synetos, E., Papageorgiou, A., Sakkoula, E., Sotiropoulou, G., Fotsis, T., Karakiulakis, G., and Maragoudakis, M. E. (1995). Inhibition of angiogenesis, tumour growth and metastasis by the NO-releasing vasodilators, isosorbide mononitrate and dinitrate. Br J Pharmacol *116*, 1829-1834.

Powell, E. M., and Geller, H. M. (1999). Dissection of astrocyte-mediated cues in neuronal guidance and process extension. Glia *26*, 73-83.

Pukrop, T., Dehghani, F., Chuang, H. N., Lohaus, R., Bayanga, K., Heermann, S., Regen, T., Van Rossum, D., Klemm, F., Schulz, M.*, et al.* (2010). Microglia promote colonization of brain tissue by breast cancer cells in a Wnt-dependent way. Glia *58*, 1477-1489.

Rahmim, A., and Zaidi, H. (2008). PET versus SPECT: strengths, limitations and challenges. Nucl Med Commun *29*, 193-207.

Ramakrishna, R., and Rostomily, R. (2013). Seed, soil, and beyond: The basic biology of brain metastasis. Surgical neurology international *4*, S256-264.

Reiss, Y., Hoch, G., Deutsch, U., and Engelhardt, B. (1998). T cell interaction with ICAM-1-deficient endothelium in vitro: essential role for ICAM-1 and ICAM-2 in transendothelial migration of T cells. Eur J Immunol *28*, 3086-3099.

Renfrow, J. J., and Lesser, G. J. (2013). Molecular Subtyping of Brain Metastases and Implications for Therapy. Curr Treat Options Oncol.

Reske, S. N., and Kotzerke, J. (2001). FDG-PET for clinical use. Results of the 3rd German Interdisciplinary Consensus Conference, "Onko-PET III", 21 July and 19 September 2000. Eur J Nucl Med *28*, 1707-1723.

Reynolds, A., Hanani, R., Hibbs, D., Damont, A., Da Pozzo, E., Selleri, S., Dolle, F., Martini, C., and Kassiou, M. (2010). Pyrazolo[1,5-a]pyrimidine acetamides: 4-Phenyl alkyl ether derivatives as potent ligands for the 18 kDa translocator protein (TSPO). Bioorg Med Chem Lett *20*, 5799-5802.

Rissanen, E., Virta, J. R., Paavilainen, T., Tuisku, J., Helin, S., Luoto, P., Parkkola, R., Rinne, J. O., and Airas, L. (2013). Adenosine A2A receptors in secondary progressive multiple sclerosis: a [(11)C]TMSX brain PET study. J Cereb Blood Flow Metab *33*, 1394-1401.

Rizzo, A., Pallone, F., Monteleone, G., and Fantini, M. C. (2011). Intestinal inflammation and colorectal cancer: a double-edged sword? World J Gastroenterol *17*, 3092-3100.

Rungta, R. L., Choi, H. B., Lin, P. J., Ko, R. W., Ashby, D., Nair, J., Manoharan, M., Cullis, P. R., and Macvicar, B. A. (2013). Lipid Nanoparticle Delivery of siRNA to Silence Neuronal Gene Expression in the Brain. Mol Ther Nucleic Acids *2*, e136.

Saito, N., Hatori, T., Murata, N., Zhang, Z. A., Ishikawa, F., Nonaka, H., Iwabuchi, S., and Samejima, H. (2007). A double three-step theory of brain metastasis in mice: the role of the pia mater and matrix metalloproteinases. Neuropathol Appl Neurobiol *33*, 288-298.

Salani, D., Rosano, L., Di Castro, V., Spinella, F., Venuti, A., Padley, R. J., Nicotra, M. R., Natali, P. G., and Bagnato, A. (2002). ABT-627, a potent endothelin receptor A antagonist, inhibits ovarian carcinoma growth in vitro. Clin Sci (Lond) *103 Suppl 48*, 318S-321S.

Samdani, A. F., Kuchner, E. B., Rhines, L., Adamson, D. C., Lawson, C., Tyler, B., Brem, H., Dawson, V. L., and Dawson, T. M. (2004). Astroglia induce cytotoxic effects on brain tumors via a nitric oxide-dependent pathway both in vitro and in vivo. Neurosurgery *54*, 1231-1237; discussion 1237-1238.

Santillo, A. F., Gambini, J. P., Lannfelt, L., Langstrom, B., Ulla-Marja, L., Kilander, L., and Engler, H. (2011). In vivo imaging of astrocytosis in Alzheimer's disease: an (1)(1)C-L-deuteriodeprenyl and PIB PET study. Eur J Nucl Med Mol Imaging *38*, 2202-2208.

Sceneay, J., Smyth, M. J., and Moller, A. (2013). The pre-metastatic niche: finding common ground. Cancer Metastasis Rev.

Schmitt, K. R., Kern, C., Berger, F., Ullrich, O., Hendrix, S., and Abdul-Khaliq, H. (2006). Methylprednisolone attenuates hypothermia- and rewarming-induced cytotoxicity and IL-6 release in isolated primary astrocytes, neurons and BV-2 microglia cells. Neurosci Lett *404*, 309-314.

Schuster, B., Kovaleva, M., Sun, Y., Regenhard, P., Matthews, V., Grotzinger, J., Rose-John, S., and Kallen, K. J. (2003). Signaling of human ciliary neurotrophic factor (CNTF) revisited. The interleukin-6 receptor can serve as an alpha-receptor for CTNF. J Biol Chem *278*, 9528-9535.

Seike, T., Fujita, K., Yamakawa, Y., Kido, M. A., Takiguchi, S., Teramoto, N., Iguchi, H., and Noda, M. (2011). Interaction between lung cancer cells and astrocytes via specific inflammatory cytokines in the microenvironment of brain metastasis. Clinical & experimental metastasis *28*, 13-25.

Serrano-Pozo, A., Gomez-Isla, T., Growdon, J. H., Frosch, M. P., and Hyman, B. T. (2013). A phenotypic change but not proliferation underlies glial responses in Alzheimer disease. Am J Pathol *182*, 2332-2344.

Serres, S., Martin, C. J., Sarmiento Soto, M., Bristow, C., O'Brien, E. R., Connell, J. J., Khrapitchev, A. A., and Sibson, N. R. (2014). Structural and functional effects of metastases in rat brain determined by multimodal MRI. Int J Cancer *134*, 885-896.

Serres, S., Raffard, G., Franconi, J. M., and Merle, M. (2008). Close coupling between astrocytic and neuronal metabolisms to fulfill anaplerotic and energy needs in the rat brain. J Cereb Blood Flow Metab *28*, 712-724.

Serres, S., Soto, M. S., Hamilton, A., McAteer, M. A., Carbonell, W. S., Robson, M. D., Ansorge, O., Khrapitchev, A., Bristow, C., Balathasan, L.*, et al.* (2012). Molecular MRI enables early and sensitive detection of brain metastases. Proc Natl Acad Sci U S A *109*, 6674-6679.

Shinonaga, M., Chang, C. C., Suzuki, N., Sato, M., and Kuwabara, T. (1988). Immunohistological evaluation of macrophage infiltrates in brain tumors. Correlation with peritumoral edema. J Neurosurg *68*, 259-265.

Sibson, N. R., Blamire, A. M., Bernades-Silva, M., Laurent, S., Boutry, S., Muller, R. N., Styles, P., and Anthony, D. C. (2004). MRI detection of early endothelial activation in brain inflammation. Magn Reson Med *51*, 248-252.

Sibson, N. R., Blamire, A. M., Perry, V. H., Gauldie, J., Styles, P., and Anthony, D. C. (2002). TNF-alpha reduces cerebral blood volume and disrupts tissue homeostasis via an endothelin- and TNFR2-dependent pathway. Brain *125*, 2446-2459.

Sibson, N. R., Lowe, J. P., Blamire, A. M., Martin, M. J., Obrenovitch, T. P., and Anthony, D. C. (2008). Acute astrocyte activation in brain detected by MRI: new insights into T(1) hypointensity. J Cereb Blood Flow Metab *28*, 621-632.

Siegel, R., Naishadham, D., and Jemal, A. (2012). Cancer statistics, 2012. CA Cancer J Clin *62*, 10-29.

Simmons, M. L., and Murphy, S. (1992). Induction of nitric oxide synthase in glial cells. J Neurochem *59*, 897-905.

Singh, S., and Gupta, A. K. (2011). Nitric oxide: role in tumour biology and iNOS/NO-based anticancer therapies. Cancer chemotherapy and pharmacology *67*, 1211-1224.

Sofroniew, M. V. (2009). Molecular dissection of reactive astrogliosis and glial scar formation. Trends Neurosci *32*, 638-647.

Sofroniew, M. V., and Vinters, H. V. (2010). Astrocytes: biology and pathology. Acta Neuropathol *119*, 7-35.

Solinas, G., Marchesi, F., Garlanda, C., Mantovani, A., and Allavena, P. (2010). Inflammation-mediated promotion of invasion and metastasis. Cancer Metastasis Rev *29*, 243-248.

Solum, N. O. (1975). Proceedings: Effects of bovine factor VIII-related protein on human platelets and isolated human platelet membranes. Thromb Diath Haemorrh *34*, 594-595.

Som, P., Atkins, H. L., Bandoypadhyay, D., Fowler, J. S., MacGregor, R. R., Matsui, K., Oster, Z. H., Sacker, D. F., Shiue, C. Y., Turner, H.*, et al.* (1980). A fluorinated glucose analog, 2-fluoro-2-deoxy-D-glucose (F-18): nontoxic tracer for rapid tumor detection. Journal of nuclear medicine : official publication, Society of Nuclear Medicine *21*, 670-675.

Soto, M. S., Serres, S., Anthony, D. C., and Sibson, N. R. (2013). Functional role of endothelial adhesion molecules in the early stages of brain metastasis. Neuro-oncology.

Sparacio, S. M., Zhang, Y., Vilcek, J., and Benveniste, E. N. (1992). Cytokine regulation of interleukin-6 gene expression in astrocytes involves activation of an NF-kappa B-like nuclear protein. J Neuroimmunol *39*, 231-242.

Spinella, F., Rosano, L., Di Castro, V., Nicotra, M. R., Natali, P. G., and Bagnato, A. (2003). Endothelin-1 decreases gap junctional intercellular communication by inducing phosphorylation of connexin 43 in human ovarian carcinoma cells. J Biol Chem *278*, 41294-41301.

Squires, R. F., and Brastrup, C. (1977). Benzodiazepine receptors in rat brain. Nature *266*, 732-734.

Stewart, P. A., Hayakawa, K., Farrell, C. L., and Del Maestro, R. F. (1987). Quantitative study of microvessel ultrastructure in human peritumoral brain tissue. Evidence for a blood-brain barrier defect. J Neurosurg *67*, 697-705.

Stolt, C. C., Lommes, P., Sock, E., Chaboissier, M. C., Schedl, A., and Wegner, M. (2003). The Sox9 transcription factor determines glial fate choice in the developing spinal cord. Genes Dev *17*, 1677-1689.

Suesca, E., Alejo, J. L., Bolanos, N. I., Ocampo, J., Leidy, C., and Gonzalez, J. M. (2013). Sulfocerebrosides upregulate liposome uptake in human astrocytes without inducing a proinflammatory response. Cytometry A *83*, 627-635.

Sur, P., Sribnick, E. A., Patel, S. J., Ray, S. K., and Banik, N. L. (2005). Dexamethasone decreases temozolomide-induced apoptosis in human gliobastoma T98G cells. Glia *50*, 160-167.

Takahashi, H., Matsumoto, H., Kumon, Y., Ohnishi, T., Freeman, C., Imai, Y., and Tanaka, J. (2007). Expression of heparanase in nestin-positive reactive astrocytes in ischemic lesions of rat brain after transient middle cerebral artery occlusion. Neurosci Lett *417*, 250-254.

Takai, E., Tsukimoto, M., Harada, H., Sawada, K., Moriyama, Y., and Kojima, S. (2012). Autocrine regulation of TGF-beta1-induced cell migration by exocytosis of ATP and activation of P2 receptors in human lung cancer cells. J Cell Sci *125*, 5051-5060.

Tang, D., Hight, M. R., McKinley, E. T., Fu, A., Buck, J. R., Smith, R. A., Tantawy, M. N., Peterson, T. E., Colvin, D. C., Ansari, M. S.*, et al.* (2012). Quantitative preclinical imaging of TSPO expression in glioma using N,N-diethyl-2-(2-(4-(2-18F-fluoroethoxy)phenyl)-5,7-dimethylpyrazolo[1,5-a]pyrimi din-3-yl)acetamide. Journal of nuclear medicine : official publication, Society of Nuclear Medicine *53*, 287-294.

Tang, Y., Shah, K., Messerli, S. M., Snyder, E., Breakefield, X., and Weissleder, R. (2003). In vivo tracking of neural progenitor cell migration to glioblastomas. Hum Gene Ther *14*, 1247-1254.

Tateishi, N., Mori, T., Kagamiishi, Y., Satoh, S., Katsube, N., Morikawa, E., Morimoto, T., Matsui, T., and Asano, T. (2002). Astrocytic activation and delayed infarct expansion after permanent focal ischemia in rats. Part II: suppression of astrocytic activation by a novel agent (R)-(-)-2-propyloctanoic acid (ONO-2506) leads to mitigation of delayed infarct expansion and early improvement of neurologic deficits. J Cereb Blood Flow Metab *22*, 723-734.

Tewson, T. J., Welch, M. J., and Raichle, M. E. (1978). [18F]-labeled 3-deoxy-3-fluoro-D-glucose: synthesis and preliminary biodistribution data. Journal of nuclear medicine : official publication, Society of Nuclear Medicine *19*, 1339-1345.

Thomsen, R., Daugaard, T. F., Holm, I. E., and Nielsen, A. L. (2013). Alternative mRNA Splicing from the Glial Fibrillary Acidic Protein (GFAP) Gene Generates Isoforms with Distinct Subcellular mRNA Localization Patterns in Astrocytes. PLoS One *8*, e72110.

Trapani, A., Palazzo, C., de Candia, M., Lasorsa, F. M., and Trapani, G. (2013). Targeting of the translocator protein 18 kDa (TSPO): a valuable approach for nuclear and optical imaging of activated microglia. Bioconjug Chem *24*, 1415-1428.

Turkheimer, F. E., Edison, P., Pavese, N., Roncaroli, F., Anderson, A. N., Hammers, A., Gerhard, A., Hinz, R., Tai, Y. F., and Brooks, D. J. (2007). Reference and target region modeling of [11C]-(R)-PK11195 brain studies. Journal of nuclear medicine : official publication, Society of Nuclear Medicine *48*, 158-167.

Ullian, E. M., Sapperstein, S. K., Christopherson, K. S., and Barres, B. A. (2001). Control of synapse number by glia. Science *291*, 657-661.

Vandesompele, J., De Preter, K., Pattyn, F., Poppe, B., Van Roy, N., De Paepe, A., and Speleman, F. (2002). Accurate normalization of real-time quantitative RT-PCR data by geometric averaging of multiple internal control genes. Genome Biol *3*, RESEARCH0034.

Vandevyver, S., Dejager, L., Tuckermann, J., and Libert, C. (2013). New insights into the anti-inflammatory mechanisms of glucocorticoids: an emerging role for glucocorticoid-receptor-mediated transactivation. Endocrinology *154*, 993-1007.

Vasdev, N., Green, D. E., Vines, D. C., McLarty, K., McCormick, P. N., Moran, M. D., Houle, S., Wilson, A. A., and Reilly, R. M. (2013). Positron-Emission Tomography Imaging of the TSPO with [(18)F]FEPPA in a Preclinical Breast Cancer Model. Cancer Biother Radiopharm *28*, 254-259.

Vecht, C. J. (1998). Clinical management of brain metastasis. J Neurol *245*, 127-131.

Versijpt, J. J., Dumont, F., Van Laere, K. J., Decoo, D., Santens, P., Audenaert, K., Achten, E., Slegers, G., Dierckx, R. A., and Korf, J. (2003). Assessment of neuroinflammation and microglial activation in Alzheimer's disease with radiolabelled PK11195 and single photon emission computed tomography. A pilot study. Eur Neurol *50*, 39-47.

Villeneuve, J., Galarneau, H., Beaudet, M. J., Tremblay, P., Chernomoretz, A., and Vallieres, L. (2008). Reduced glioma growth following dexamethasone or anti-angiopoietin 2 treatment. Brain Pathol *18*, 401-414.

Vleminckx, K., Vakaet, L., Jr., Mareel, M., Fiers, W., and van Roy, F. (1991). Genetic manipulation of E-cadherin expression by epithelial tumor cells reveals an invasion suppressor role. Cell *66*, 107-119.

Voronov, E., Shouval, D. S., Krelin, Y., Cagnano, E., Benharroch, D., Iwakura, Y., Dinarello, C. A., and Apte, R. N. (2003). IL-1 is required for tumor invasiveness and angiogenesis. Proc Natl Acad Sci U S A *100*, 2645-2650.

Wadsworth, H., Jones, P. A., Chau, W. F., Durrant, C., Fouladi, N., Passmore, J., O'Shea, D., Wynn, D., Morisson-Iveson, V., Ewan, A.*, et al.* (2012). [(1)(8)F]GE-180: a novel fluorine-18 labelled PET tracer for imaging Translocator protein 18 kDa (TSPO). Bioorg Med Chem Lett *22*, 1308-1313.

Wadt, K. A., Larsen, C. M., Andersen, H. U., Nielsen, K., Karlsen, A. E., and Mandrup-Poulsen, T. (1998). Ciliary neurotrophic factor potentiates the beta-cell inhibitory effect of IL-1beta in rat pancreatic islets associated with increased nitric oxide synthesis and increased expression of inducible nitric oxide synthase. Diabetes *47*, 1602-1608.

Wang, H., Pullambhatla, M., Guilarte, T. R., Mease, R. C., and Pomper, M. G. (2009). Synthesis of [(125)I]iodoDPA-713: a new probe for imaging inflammation. Biochem Biophys Res Commun *389*, 80-83.

Wang, L., Cossette, S. M., Rarick, K. R., Gershan, J., Dwinell, M. B., Harder, D. R., and Ramchandran, R. (2013). Astrocytes directly influence tumor cell invasion and metastasis in vivo. PLoS One *8*, e80933.

Wang, W., Wyckoff, J. B., Frohlich, V. C., Oleynikov, Y., Huttelmaier, S., Zavadil, J., Cermak, L., Bottinger, E. P., Singer, R. H., White, J. G.*, et al.* (2002). Single cell behavior in metastatic primary mammary tumors correlated with gene expression patterns revealed by molecular profiling. Cancer Res *62*, 6278-6288.

Weinstein, D. E., Shelanski, M. L., and Liem, R. K. (1991). Suppression by antisense mRNA demonstrates a requirement for the glial fibrillary acidic protein in the formation of stable astrocytic processes in response to neurons. J Cell Biol *112*, 1205-1213.

Wickstrom, T., Clarke, A., Gausemel, I., Horn, E., Jorgensen, K., Khan, I., Mantzilas, D., Rajanayagam, T., In 't Veld, D. J., and Trigg, W. (2014). The development of an automated and GMP compliant FASTlab Synthesis of [(18) F]GE-180; a radiotracer for imaging translocator protein (TSPO). J Labelled Comp Radiopharm *57*, 42-48.

Wilhelm, I., Molnar, J., Fazakas, C., Hasko, J., and Krizbai, I. A. (2013). Role of the blood-brain barrier in the formation of brain metastases. Int J Mol Sci *14*, 1383-1411.

Winkeler, A., Boisgard, R., Awde, A. R., Dubois, A., Theze, B., Zheng, J., Ciobanu, L., Dolle, F., Viel, T., Jacobs, A. H., and Tavitian, B. (2012). The translocator protein ligand [(1)(8)F]DPA-714 images glioma and activated microglia in vivo. Eur J Nucl Med Mol Imaging *39*, 811-823.

Winkler, F., Kienast, Y., Fuhrmann, M., Von Baumgarten, L., Burgold, S., Mitteregger, G., Kretzschmar, H., and Herms, J. (2009). Imaging glioma cell invasion in vivo reveals mechanisms of dissemination and peritumoral angiogenesis. Glia *57*, 1306-1315.

Winter, C. G., Saotome, Y., Levison, S. W., and Hirsh, D. (1995). A role for ciliary neurotrophic factor as an inducer of reactive gliosis, the glial response to central nervous system injury. Proc Natl Acad Sci U S A *92*, 5865-5869.

Wolff, J. E., Guerin, C., Laterra, J., Bressler, J., Indurti, R. R., Brem, H., and Goldstein, G. W. (1993). Dexamethasone reduces vascular density and plasminogen activator activity in 9L rat brain tumors. Brain Res *604*, 79-85.

Wu, X., and Gallo, K. A. (2013). The 18-kDa translocator protein (TSPO) disrupts mammary epithelial morphogenesis and promotes breast cancer cell migration. PLoS One *8*, e71258.

Wu, Y., Liu, R. G., and Zhou, J. P. (2006). Effect of ciliary neurotrophic factor on activation of astrocytes in vitro. Neurosci Bull *22*, 315-322.

Wu, Y. J., Muldoon, L. L., Gahramanov, S., Kraemer, D. F., Marshall, D. J., and Neuwelt, E. A. (2012). Targeting alphaV-integrins decreased metastasis and increased survival in a nude rat breast cancer brain metastasis model. J Neurooncol *110*, 27-36.

Wyatt, S. K., Manning, H. C., Bai, M., Bailey, S. N., Gallant, P., Ma, G., McIntosh, L., and Bornhop, D. J. (2010). Molecular imaging of the translocator protein (TSPO) in a pre-clinical model of breast cancer. Mol Imaging Biol *12*, 349-358.

Wyatt, S. K., Manning, H. C., Bai, M., Ehtesham, M., Mapara, K. Y., Thompson, R. C., and Bornhop, D. J. (2012). Preclinical molecular imaging of the translocator protein (TSPO) in a metastases model based on breast cancer xenografts propagated in the murine brain. Curr Mol Med *12*, 458-466.

Wyss-Coray, T., and Mucke, L. (2002). Inflammation in neurodegenerative disease--a double-edged sword. Neuron *35*, 419-432.

Xing, F., Kobayashi, A., Okuda, H., Watabe, M., Pai, S. K., Pandey, P. R., Hirota, S., Wilber, A., Mo, Y. Y., Moore, B. E.*, et al.* (2013). Reactive astrocytes promote the metastatic growth of breast cancer stem-like cells by activating Notch signalling in brain. EMBO Mol Med *5*, 384-396.

Xue, W., Cojocaru, R. I., Dudley, V. J., Brooks, M., Swaroop, A., and Sarthy, V. P. (2011). Ciliary neurotrophic factor induces genes associated with inflammation and gliosis in the retina: a gene profiling study of flow-sorted, Muller cells. PLoS One *6*, e20326.

Yanagawa, H., Kawano, T., Haku, T., Yano, S., Maniwa, K., and Sone, S. (1996). Palliative steroid therapy and serum interleukin-6 levels in a patient with lung cancer. J Pain Symptom Manage *12*, 195-198.

Yanagisawa, M., Kurihara, H., Kimura, S., Tomobe, Y., Kobayashi, M., Mitsui, Y., Yazaki, Y., Goto, K., and Masaki, T. (1988). A novel potent vasoconstrictor peptide produced by vascular endothelial cells. Nature *332*, 411-415.

Yang, Q., Ma, Y., Zhao, Y., She, Z., Wang, L., Li, J., Wang, C., and Deng, Y. (2013). Accelerated drug release and clearance of PEGylated epirubicin liposomes following repeated injections: a new challenge for sequential low-dose chemotherapy. Int J Nanomedicine *8*, 1257-1268.

Yoneda, T., Williams, P. J., Hiraga, T., Niewolna, M., and Nishimura, R. (2001). A bone-seeking clone exhibits different biological properties from the MDA-MB-231 parental human breast cancer cells and a brain-seeking clone in vivo and in vitro. J Bone Miner Res *16*, 1486-1495.

Young, J. D., Lawrence, A. J., MacLean, A. G., Leung, B. P., McInnes, I. B., Canas, B., Pappin, D. J., and Stevenson, R. D. (1999). Thymosin beta 4 sulfoxide is an anti-inflammatory agent generated by monocytes in the presence of glucocorticoids. Nat Med *5*, 1424-1427.

Yu, J. A., Sadaria, M. R., Meng, X., Mitra, S., Ao, L., Fullerton, D. A., and Weyant, M. J. (2012). Lung cancer cell invasion and expression of intercellular adhesion molecule-1 (ICAM-1) are attenuated by secretory phospholipase A(2) inhibition. J Thorac Cardiovasc Surg *143*, 405-411.

Zamanian, J. L., Xu, L., Foo, L. C., Nouri, N., Zhou, L., Giffard, R. G., and Barres, B. A. (2012). Genomic analysis of reactive astrogliosis. J Neurosci *32*, 6391-6410.

Zen, M., Canova, M., Campana, C., Bettio, S., Nalotto, L., Rampudda, M., Ramonda, R., Iaccarino, L., and Doria, A. (2011). The kaleidoscope of glucorticoid effects on immune system. Autoimmun Rev *10*, 305-310.

Zhang, C., Beckermann, B., Kallifatidis, G., Liu, Z., Rittgen, W., Edler, L., Buchler, P., Debatin, K. M., Buchler, M. W., Friess, H., and Herr, I. (2006). Corticosteroids induce chemotherapy resistance in the majority of tumour cells from bone, brain, breast, cervix, melanoma and neuroblastoma. Int J Oncol *29*, 1295-1301.

Zhang, L., Sullivan, P. S., Goodman, J. C., Gunaratne, P. H., and Marchetti, D. (2011). MicroRNA-1258 suppresses breast cancer brain metastasis by targeting heparanase. Cancer Res *71*, 645-654.

Zhang, L., Zhao, W., Li, B., Alkon, D. L., Barker, J. L., Chang, Y. H., Wu, M., and Rubinow, D. R. (2000). TNF-alpha induced over-expression of GFAP is associated with MAPKs. Neuroreport *11*, 409-412.

Zhang, M., and Olsson, Y. (1995). Reactions of astrocytes and microglial cells around hematogenous metastases of the human brain. Expression of endothelin-like immunoreactivity in reactive astrocytes and activation of microglial cells. J Neurol Sci *134*, 26-32.

Zhang, R. D., Price, J. E., Fujimaki, T., Bucana, C. D., and Fidler, I. J. (1992). Differential permeability of the blood-brain barrier in experimental brain metastases produced by human neoplasms implanted into nude mice. Am J Pathol *141*, 1115-1124.

Zhang, X., Zhang, W., Cao, W. D., Cheng, G., Liu, B., and Cheng, J. (2012). A review of current management of brain metastases. Ann Surg Oncol *19*, 1043-1050.

Zhuo, L., Sun, B., Zhang, C. L., Fine, A., Chiu, S. Y., and Messing, A. (1997). Live astrocytes visualized by green fluorescent protein in transgenic mice. Dev Biol *187*, 36-42.

Zlokovic, B. V., Mackic, J. B., McComb, J. G., Weiss, M. H., Kaplowitz, N., and Kannan, R. (1994). Evidence for transcapillary transport of reduced glutathione in vascular perfused guinea-pig brain. Biochem Biophys Res Commun *201*, 402-408.

Zucker, S., and Cao, J. (2009). Selective matrix metalloproteinase (MMP) inhibitors in cancer therapy: ready for prime time? Cancer Biol Ther *8*, 2371-2373.